UNIVERSITÄT DUISBURG ESSEN

Offen im Denken

Electrophoretic Deposition of Laser-generated Platinum- and Platinum-Alloy Nanoparticles onto Neural Electrode Surfaces

Dissertation

by

Vaijayanthi Ramesh

for the degree of
Doctor of Natural Sciences
– Dr. rer. nat. –

University of Duisburg-Essen
Institute of Technical Chemistry I
2023

DOI: 10.17185/duepublico/81286
URN: urn:nbn:de:hbz:465-20231201-094318-5

This thesis was prepared from March 2019 to May 2022 in the research group of Prof. Dr.-Ing. Stephan Barcikowski, Institute of Technical Chemistry I at the University of Duisburg-Essen.

Referees:

Prof. Dr.-Ing. Stephan Barcikowski
University of Duisburg-Essen

Prof. Dr.-Ing. Karsten Seidl
University of Duisburg-Essen

Chairman:

Prof. Dr. Georg Jansen
University of Duisburg-Essen

Oral Examination Date: 27.11.2023

The process is more important than the results. If you take care of the process, you will get the results.

M S Dhoni

Acknowledgements

First and foremost, I would like to thank every person I interacted with during my thesis, who directly or indirectly taught me many lessons, that will remain useful in the upcoming walks of my life.

I would like to extend my sincere gratitude to Prof. Barcikowski, for providing me with the opportunity of a PhD thesis under his supervision. Thanks a lot for many fruitful discussions, support, and faith in my opinions and for providing me with numerous worthy opportunities. At the end of every one of our discussions, I walked out with new-found knowledge, for which I am always grateful.

My sincere thanks go to Prof. Dr.-Ing. Karsten Seidl for accepting to be my second reviewer. Thanks for holding regular meetings and for your insights in shaping my thesis. Your valuable technical inputs played a role in improving this thesis' quality.

Christoph Rehbock, I would like to extend a big thanks to you for the project supervision. Thanks for being friendly, which allowed me to express my ideas without hesitation. Thanks a lot for being supportive and extremely flexible with your time, especially during the last months of my thesis. I will always be grateful for the patience you had with me and I learned many valuable insights from you.

A special thanks to Jurij Jakobi for the constant support, and the numerous student introductions you provided for me. Many thanks for supporting in measuring HR-TEM, XRF, and TEM. I would like to extend my thanks to René Streubel for all the laser safety introductions to my students and for helping me with technical drawings for the chamber design. Friedrich Waag, thanks a lot for your time, guidance, and patience with every question I posed, especially during the stressful final days of your thesis. I would like to thank Florian de Kock for measuring XRD and for all the friendly interactions. I thank Tobias Bessel for sharing his technical expertise with me, especially during the early phases of my thesis. A warm gratitude to all the other alumni and current TC I members, who have helped me with various things during my period here.

I would like to thank the German Research Foundation (DFG) for funding my thesis work. A hearty thanks to Brian Giera and John Karnes (affiliated to the Lawrence Livermore National Laboratory), for their fruitful collaboration. You both were extremely helpful in times of need and always treated me like a peer by looking forward to my opinions and ideas. I also thank you for the readiness you both displayed in exploring new questions. I also thank Brendan Thompson for designing a wonderful cover art for one of my publications. My sincere thanks to Prof. Joachim K. Krauss, Prof. Kerstin Schwabe, and Dr. Svilen Angelov from the Medical College of Hannover for their collaboration.

A very special thanks go to all my students, who substantially contributed to shaping this thesis: Johannes Wolter, Barbara Urbano, Anne Krause, Mena-Alexander Kraeenbring, Nadine Stratmann, Viktor Schaufler, and Joman Barakeh. I would like to thank David Koehler and Hanna Martin for all the experimental support and the long tedious hours spent in front of the lasers. Nathan Bradshaw, thank you for choosing my project and helping me a great deal to pave the way for my research stay.

I would like to thank Tobias Bochmann and Kateryna Loza for the exhausting weekly hours spent measuring the SEM of my wires. I thank Dr. Marcus Hildebrandt and Dr. Wael Ali for the AFM measurements. I thank Bernd Walkenfort and Dr. Mike Hasenberg (from the IMCES) for the SEM measurements of tissue sections. I thank the ICAN colleagues: Dr. Ulrich Hagemann for the XPS measurements and Dr. Steffen Franzka for the AFM measurements. I thank Dr. Ricardo A. Martínez Hincapié (from the MPI) and Stefan Kilian for their support in electrochemical measurements. I thank the workshop colleagues: Marcus Adamczak for preparing cables for EPD and Marcel Zilken for preparing various Teflon chambers. I sincerely thank my TC II friends, Philip Jahn, and Sebastian Buchholz, for their support with the freeze dryer and incubator.

I cannot be more grateful to Prof. Dr. Uwe Karst and Ilona Nordhorn (from the University of Münster), who readily responded to my request and accepted to measure the tissue samples in their lab at a very crucial and short notice. Thanks for the discussions and insights you both provided on the results obtained.

My time in Essen would not have been merrier without the people with whom I shared my office: Tobias Bessel, Sandra Zwiehoff, Michael Willeke, Tina Friedenauer, Farbod Riahi, Ruksan Nadarajah, and Jacob Johny. Many thanks for the wonderful memories and the countless eat-outs, ice creams, cakes, and coffee breaks.

Lastly, I would like to thank Sriram and Shashank, who always helped me remain sane in those stressful final phases of the thesis. Thanks for the support and for refilling my spirits. Sriram, thanks for the CAD drawings, proofreading, constructive criticisms, and constant emotional support. I am ever grateful and proud to have you both in my life.

Abstract

Platinum-based neural electrodes are used for implantation in the brain for recording neuronal activity and for acute or chronic neural stimulation, such as deep brain stimulation (DBS). For diseases like Parkinson's, epilepsy, depression, deafness, spinal cord injuries, blindness, advanced tremors, etc., there is no complete cure. Therefore, to reduce the severity of the symptoms and to improve the patient's quality of life, DBS is often performed. Although neural electrodes have been clinically used for a long time now, there are some drawbacks such as the increase in electrode impedance (Z) due to gliosis formation that reduces the efficacy of the electrodes to record or stimulate the neurons. Due to increasing Z, higher currents are required for better stimulation, which consequently reduces the battery life of the pulse generator. To eliminate these challenges faced by neurosurgeons, research has been carried out by modifying the surface topography using various methods to increase the electrochemical surface area (ECSA) and thereby reducing the Z. Various surface modification techniques have been employed for this purpose: chemical modifications, laser patterning, electrodeposition, vapor deposition, self-assembly, etc. One of the rising techniques is the electrophoretic deposition (EPD) of laser-generated ligand-free nanoparticles (NPs) onto platinum (Pt) electrode surfaces. It is one of the most versatile and simple methods without requiring complex equipment or processing tools. By the application of external electric fields, the colloidal NPs dispersed in water are subjected to a movement towards the oppositely charged electrode, on which the deposition takes place. The deposition output can be easily modified by simply adjusting the process parameters like time, field strength, solvent concentration, etc. Previously, our group focused on optimizing the EPD parameters of PtNP deposition on 2D flat targets. Varying diameters of these spherical NPs were coated on neural electrodes and their in vivo behavior for a period of three weeks was investigated. In this work, the established 2D EPD parameters were further optimized to obtain a parameter set for 3D neural electrode targets that produce homogeneous, sub-monolayer depositions. When comparing direct current (DC) and pulsed DC (PDC) fields, the latter produced homogeneous deposits decreasing the Z. To investigate the solvent influence on the deposits, ethanol-water mixtures were used for dispersing PtNPs, in which the 30% ethanol-water ratio produced a seven-fold increase in ECSA and a significant decrease in Z. Investigations were also carried out by coating PtW and PtIr alloy NPs, that are commonly seen in the base material composition of neural electrodes. In comparison to pure Pt, the Pt90Ir10 combination resulted in a significant decrease in the Z. Subsequently, the PtNP-coated neural electrodes were implanted into the subthalamic nucleus of rats and stimulated for a period of four weeks. It was observed that the PDC coatings could lower and stabilize the in vivo Z. Finally, to study the applicability of PDC-coated neural electrodes in the real world, a systematic investigation of their mechanical stability was performed confirming their suitability in clinical applications. Therefore, it was demonstrated that the EPD of laser-generated ligand-free colloidal PtNPs on neural electrode surfaces is an exciting and time-saving approach to efficiently modify the implant surfaces and enhance their performances.

Zusammenfassung

Neuroelektroden auf Platin (Pt) werden zur Implantation in das Gehirn für die Aufzeichnung der neuronalen Aktivität und für die akute/chronische Nervenstimulation, wie die tiefe Hirnstimulation (DBS), verwendet. Für Krankheiten wie Parkinson, Epilepsie, Depression, Taubheit, Blindheit, Rückenmarksverletzungen, Zittern usw. gibt es keine vollständige Heilung. Um die Schwere der Symptome zu verringern und die Lebensqualität der Patienten zu verbessern, wird daher häufig eine DBS durchgeführt. Obwohl Neuroelektroden schon seit langem klinisch eingesetzt werden, gibt es einige Nachteile, wie z. B. die Erhöhung der Elektrodenimpedanz (Z) aufgrund der Gliosebildung, die die Wirksamkeit der Elektroden bei der Stimulation der Neuronen verringert. Aufgrund der Zunahme von Z sind für eine bessere Stimulation höhere Ströme erforderlich, was die Lebensdauer der Batterie des Impulsgenerators verkürzt. Um diese Herausforderungen für die Neurochirurgen zu beseitigen, wurde die Oberflächentopographie mit verschiedenen Methoden modifiziert, um die elektrochemische Oberfläche (ECSA) zu vergrößern und dadurch Z zu verringern. Zu diesem Zweck wurden verschiedene Oberflächenmodifizierungsverfahren eingesetzt: chemische Modifikationen, Laserstrukturierung, Elektrodeposition, Dampfabscheidung, Selbstmontage usw. Eine der aufkommenden Techniken ist die elektrophoretische Abscheidung (EPD) von lasergenerierten ligandenfreien Nanopartikeln (NPs) auf Pt-Elektrodenoberflächen. Es handelt sich um eine der vielseitigsten & einfachsten Methoden, die keine komplexen Geräte oder Verarbeitungswerkzeuge erfordert. Durch Anlegen äußerer elektrischer Felder werden die in Wasser dispergierten kolloidalen Nanopartikel in Richtung der entgegengesetzt geladenen Elektrode bewegt, auf der die Abscheidung erfolgt. Die Abscheidungsleistung lässt sich durch einfache Anpassung der Prozessparameter wie Zeit, Feldstärke, Lösungsmittelkonzentration usw. leicht verändern. In der Vergangenheit hat sich unsere Gruppe auf die Optimierung der EPD-Parameter für die Abscheidung von PtNP auf 2D-Targets konzentriert. Diese sphärischen NPs mit unterschiedlichen Durchmessern wurden auf Neuroelektroden aufgebracht und ihr In-vivo-Verhalten über einen Zeitraum von 3 Wochen untersucht. In dieser Arbeit wurden die etablierten 2D-EPD-Parameter weiter optimiert, um einen Parametersatz für neurale 3D-Elektroden-Targets zu erhalten, der homogene, submonolagige Ablagerungen erzeugt. Um den Einfluss von Lösungsmitteln auf die Ablagerungen zu untersuchen, wurden Ethanol-Wasser-Gemische zur Dispergierung von PtNPs verwendet, wobei das 30%-ige Ethanol-Wasser-Verhältnis zu einer 7-fachen Erhöhung der ECSA und einer signifikanten Verringerung von Z führte. Die Untersuchungen wurden auch durch die Beschichtung von PtW- und PtIr-Legierungs-NPs durchgeführt, die häufig in der Basismaterialzusammensetzung Neuroelektroden vorkommen. Im Vergleich zu reinem Pt führte die Pt90Ir10-Kombination zu einer signifikanten Verringerung des Z. Anschließend wurden die mit PtNP beschichteten Neuroelektroden in den Nucleus subthalamicus von Ratten implantiert & über 4 Wochen stimuliert. Es wurde festgestellt, dass die PDC-Beschichtungen den Z-Wert in vivo senken & stabilisieren konnten. Schließlich, die Anwendbarkeit von PDC-beschichteten Neuroelektroden in der Praxis zu untersuchen, wurde eine systematische Prüfung ihrer mechanischen Stabilität durchgeführt, die ihre Eignung für klinische Anwendungen bestätigt. Es konnte daher gezeigt werden, dass die EPD von lasergenerierten PtNPs auf Neuroelektrodenoberflächen ein interessanter und zeitsparender Ansatz ist, um die Implantatoberflächen effizient zu modifizieren und ihre Leistung zu verbessern.

Contents

1 Introduction

Patients suffering from Parkinson's disease (PD) are characterized by a range of motor symptoms such as clinically progressive tremors, bradykinesia, rigidity, disturbances of the synaptic function, and so on[1]. Although there is no 100% cure for this major geriatric disease, the conventional treatments include the administration of drugs. In this disease, the dopamine levels needed for proper neurotransmission get depleted and hence do not readily cross the blood-brain barrier. Because of this, drugs that mimic the functioning of dopamine are administered, such as levodopa or synthetic dopamines. Levodopa is one of the most commonly administered ones, which gets decarboxylated into dopamine and works beneficially within the striatum. However, for a visible effect, large amounts of levodopa have to be administered, which then causes adverse effects once the drug crosses the blood-brain barrier[2]. Additionally, long-term administration of levodopa causes severe dyskinesia, combined with unpredictable periods of loss of mobility. The drugs are also only effective during the initial diagnosis phase. At the later stages of the disease, increased dosage would be required causing more undesirable effects for the patients[1,3].

To bypass the negative effects of drugs in the treatment of PD, deep brain stimulation (DBS) was introduced. With time, DBS has evolved as an important treatment for PD[4]. Although thalamic stimulation was initially predominant, the lack of its effect on other motor symptoms curtailed its application[5,6]. Nowadays, subthalamic nucleus (STN) stimulation is one of the most popular application sites for DBS of PD. Numerous studies are showing the advantageous benefits of DBS for the treatment of PD. DBS was able to improvise an extensive range of PD symptoms including, but not limited to, dystonia, drug-induced dyskinesia, and motor fluctuations[7]. However, there are still improvements needed with the electrode quality used for DBS. Essentially, the electrodes that are being implanted should act as a capacitor to store electric current and thereby avoid local tissue damage. A smooth-surfaced electrode poses the limitation of having less current flow. If the voltage is increased to increase the current flow, there is a high risk of tissue damage[8]. Therefore, to deliver higher currents without increasing the voltage, and to make the electrode act as a capacitor, the electrochemical surface area (ECSA) can be increased by employing surface modifications.

There is a wide range of surface modifications being performed on neural electrodes. To amplify the functioning of both neural stimulation- and recording-electrodes, surface patterning or coating is done[9]. Although nanocoatings based on carbon nanotubes, polymers, silicon, quantum dots, diamond, etc. are widely investigated, modifying the surfaces using materials that are minimally different from the base material is much preferred to avoid complications and rejections during manufacturing and certification[10,11]. Besides coating, the formation of metal nanostructures on the surfaces to reduce the impedance is performed, such as nanopillars[12], nanoflakes[13], nanorods[14], etc. Various methods of surface modifications are in use: nanoscale patterning, vapor deposition, self-assembly, electrodeposition, electrophoretic deposition, layer-by-layer deposition, etc., that are reviewed in detail in section 2.

Among them, the electrophoretic deposition (EPD) of conductive metal nanoparticles (NPs) produced by laser ablation in liquids (LAL) is an interesting surface modification method, in which

our working group specializes. EPD is a versatile and low-cost coating technique[15] in which particles dispersed in a suspension are coated onto target electrode surfaces under the influence of an external electric field[16]. This colloidal processing technique was discovered as early as the 1800s but only found its way into industrial processing in the 1990s for ceramic preparation[17]. It requires a simple experimental setup, with a chamber filled with precursor particles suspended in a liquid. Two electrodes (working and counter) are inserted into the chamber and connected to the two ends of the electric field generator[18]. Due to the influence of an applied electric field, the colloidal particles move toward the working electrode and deposit on them. On the other hand, LAL is a well-established method for generating NPs, where metal targets can be ablated using high-power laser beams inside a liquid environment, resulting in pure colloidal NPs without the need for the addition of ligands[19].

To study the EPD of charged metal NPs, our group investigated the electrophoretic mobility of the laser-generated NPs in water using particle scattering velocimetry. Au and PtIr NPs were observed and it was found that the electrophoretic velocity of the particles could be tuned by varying the electric field strength[20]. Further investigations were performed using PtIr alloy NPs to determine any changes in their stoichiometry and eventually their potential usage in the surface structuring on PtIr neural electrodes. It was observed that upon EPD, the coating and the substrate demonstrated the same chemical compositions[21]. Following, the influence of contact angle[22] and stabilizer ligands[23] during the EPD of NPs were studied. It was observed that the electrophoretic velocity and electric field strength had a linear relationship for laser-generated ligand-free NPs, making them a superior choice for process controlling and scaling[23]. Even a continuous direct-current (DC) EPD process was presented that could produce high deposition throughputs[24]. After the studies on fundamentals, there were works on the nanostructuring of neural electrodes by depositing 10 nm and 50 nm sized NPs and performing short-term in vitro and in vivo stimulations in rat models (in collaboration with the working group of Prof. Krauss/Prof. Schwabe, MHH). It was observed that the 10 nm particles produced a stable impedance in vivo[25]. To further optimize the coating procedure on flat 2D substrates, various parameters such as impedance, electric field strength, surface coverage, ECSA, and surface oxidation were studied[26].

However, when this thesis began, there were still unknowns on the EPD of laser-generated NPs that were to be addressed, as this working group is the only one focusing on this topic. Previous works optimized this process for 2D surfaces but not for 3D microelectrode targets. Therefore, there was an urgent need to deeply probe this technique. This is because, compared to the other existing methods the EPD is a simple and versatile way to modify electrode surfaces. It can be applied to any target shape and size using a minimal experimental setup. The simplicity with which the process parameters can be modified also makes this technique preferable. Furthermore, the coatings generated by EPD are unique by possessing mechanical stability, in vivo transferability, the material match between the electrode and the coating, and having no ligand contaminations in the precursors. Preliminary experiments with coated 3D neural electrodes showed an increased in vitro impedance, however, in vivo impedance decreased and the values did not fluctuate throughout the testing period. A systematic investigation of EPD on 3D targets was missing to find the link between synthesis parameters, coating process, and electrochemical readouts (both in vitro and in vivo). Therefore in

this thesis, a new set of coating parameters for 3D targets were established by varying the applied electric field and the solvent compositions. More clinically relevant readouts such as electrochemical impedance spectroscopy (EIS) and cyclic voltammetry (CV) were established. Previously, the impedance was measured only at a single frequency value (200 Hz). Improvised, well-characterized, and relatively homogeneous coatings were transferred onto real-time neural microelectrodes and analyzed the long-term in vitro and in vivo impedances through stimulation experiments. Furthermore, to make this EPD process clinically applicable, the mechanical stability of the produced coatings was systematically verified to determine their delamination characteristics. The workflow of the thesis is presented in Figure 1 below.

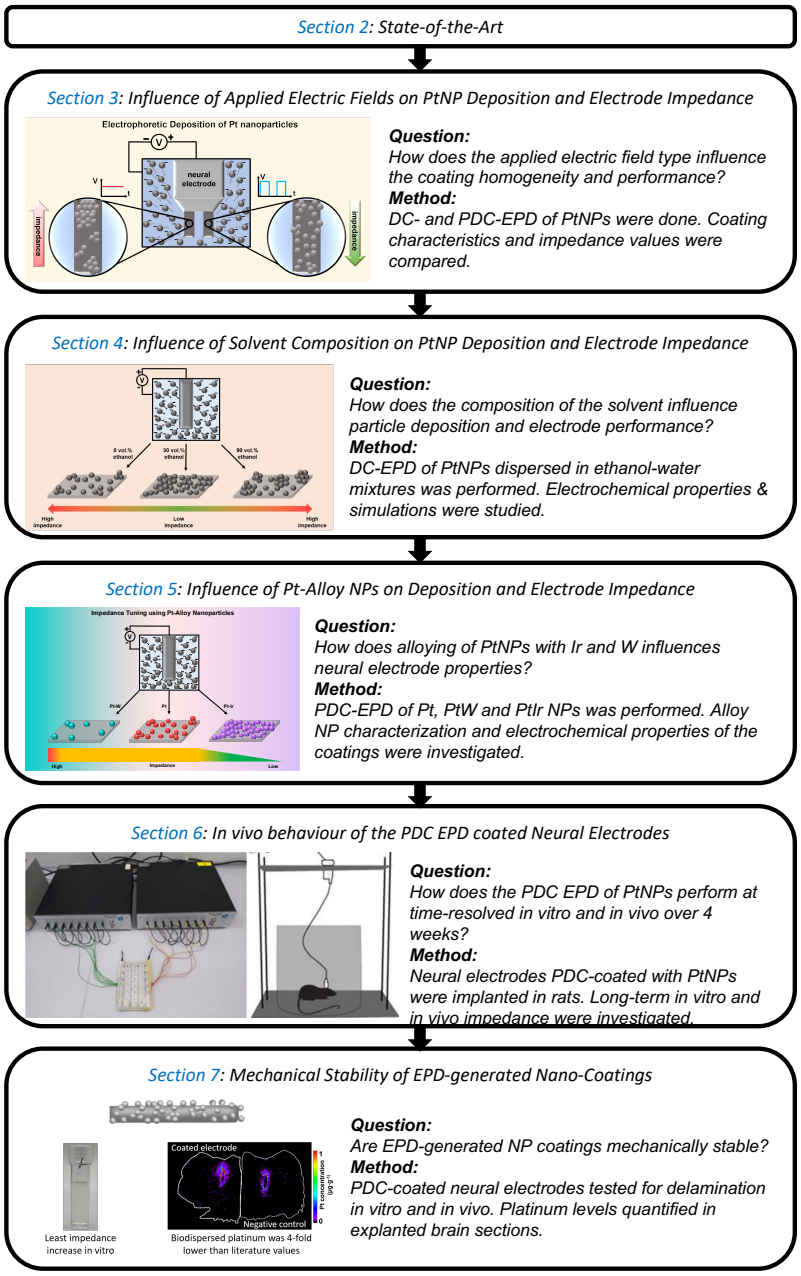

Figure 1: Workflow diagram of the thesis. The influence of the applied electric field, solvent composition, and coating materials on neural electrode properties was systematically studied. Clinical applicability was investigated through in vivo implantation and mechanical stability studies.

Upon discussing the state-of-the-art in section 2, the above-mentioned objectives of this thesis are discussed in detailed topics as below. Section 3 shows a systematic investigation of the EPD process performed on 3D neural electrodes, by comparing DC and PDC fields. The ligand-free colloidal PtNPs generated by LAL and LFL with a narrow size distribution averaging a diameter of 10 nm were used. The mass of NPs deposited on the wire samples was determined using UV-Vis extinction spectroscopy, and the topography of the coated surfaces was examined using SEM. Numerical simulations (in collaboration with the working group of Dr. Giera, LLNL) were performed to determine the overlapping behavior of NPs in each of the applied fields and finally, the impedances (in collaboration with the working group of Prof. Krauss/Prof. Schwabe, MHH) of DC- and PDC-coated electrodes were compared.

In section 4, the influence of the solvent composition used during EPD on the deposition behavior of NPs was studied. The laser-generated PtNPs which were ablated in Milli-Q water were mixed with increasing concentrations of ethanol, from 30% to 90% in steps of 10%. These NPs in ethanol-water mixtures were coated onto electrode wire surfaces using DC-EPD. Using numerical simulations (in collaboration with the working group of Dr. Giera, LLNL), the coordination numbers for each variant were determined and they were correlated to their surface coverage properties. The ECSA and CSC values of the variants were determined using electrochemical measurements. Finally using EIS measurements, the impedances of the samples were measured.

Section 5 details the influence of Pt-based alloy NPs on the neural impedance reduction upon depositing them onto electrode surfaces. The neural electrodes were coated using Pt-, Pt90W10-, Pt50W50-, and Pt90Ir10 NPs. The surface topography was analyzed using SEM. The electrochemical parameters such as ECSA and capacitance were measured using cyclic voltammetry (CV) and the electrode impedance was measured using electrochemical impedance spectroscopy (EIS). Pt90Ir10 was found to be the best among the tested alloy combinations to increase the ECSA and thereby significantly decrease the electrode impedance.

In section 6, the long-term in vitro and in vivo stimulation of PtNP-coated electrodes was performed in rat models (in collaboration with the working group of Prof. Krauss/Prof. Schwabe, MHH), and the influence of surface modification on the electrode behavior was studied. For in vivo testing, the coated and reference electrodes were implanted into the STN of rat models. As controls, uncoated samples, and samples immersed in NP colloids without the application of an external electric field were considered. PDC-coated neural electrodes were able to decrease impedance in vitro, and the in vivo impedance remained stable throughout the 4-week stimulation period.

Finally, in section 7, the mechanical stability of the nano-coatings in both in vitro and in vivo environments was investigated. After challenging the coated samples with mechanical stresses generated from simulated brain environments, adhesion, and ultrasonication, their electrochemical parameters such as ECSA, capacitance, and impedance were measured as mentioned before, and compared to the uncoated/untreated controls to understand how stable the EPD coatings are in subject to the stresses that might occur clinically. In simulated brain environments, there was very little delamination of the coatings and the impedance of the electrode remained highly unaffected. The unrealistic harsh stresses created by the adhesion test or ultrasonication were able to delaminate

the coatings thereby significantly increasing the electrode impedance. Additionally, the levels of PtNP remains in the explanted brain sections were highly below any relevant toxicological limits (in collaboration with the working group of Prof. Karst, University of Münster). This section demonstrates the clinical applicability of PtNP EPD coatings on neural electrode surfaces.

2 State of the Art

Unpublished review article under preparation:

A State-of-the-Art Review on Neural Electrode Nano-Coatings

Vaijayanthi Ramesh[1], Christoph Rehbock[1] and Stephan Barcikowski[1,*]

[1] Institute of Technical Chemistry I, University of Duisburg-Essen and Center for Nanointegration Duisburg-Essen (CENIDE), Essen, Germany

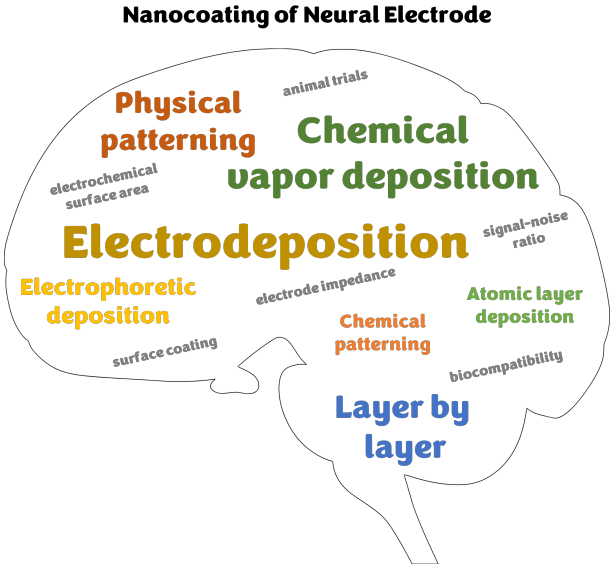

Summary:

A detailed introduction to this doctoral work is provided in the previous section. The major objective of this thesis is to develop 3D EPD parameters for coating laser-generated nanoparticles onto neural microelectrode surfaces, and thereby influence their in vitro and in vivo impedances. In the forthcoming section, the state-of-the-art review of the various nano-coating techniques performed on neural electrode surfaces with the aid of electric current, vacuum, patterning, and layer-by-layer depositions is presented.

Author Contributions:

Design, literature research, illustrations, and writing of the review were done by VR. CR and SB supervised and obtained funding for the work.

A State-of-the-Art Review on Neural Electrode Nano-Coatings

Vaijayanthi Ramesh[1], Christoph Rehbock[1] and Stephan Barcikowski[1,*]

[1] Technical Chemistry I, University of Duisburg-Essen and Center for Nanointegration Duisburg-Essen (CENIDE), Universitaetsstr. 7, 45141 Essen, Germany.

Abstract

Neural electrodes are chronically implanted for the purpose of stimulation and recording of brain activity for treating various neurological disorders. Among others, the increase in impedance with time hinders the implant's efficiency in delivering electric currents. If the current provided is increased to lower the impedance, it could lead to necrosis and consequently become unsafe for the patients. Additionally, scar tissue formations around the implant surface could lead to implant rejection. Therefore, researchers have established surface modification techniques to improve biocompatibility and for better transfer of electric currents. In this paper, the types of nanocoating methods available for neural electrode surface modifications will be reviewed in terms of their effectiveness and room for improvement.

1 Introduction

Neural electrodes are frequently used for the modulation of neuronal activities in order to alleviate the symptoms of various diseases[1]. Neural implants are increasingly used for auditory treatments[2,3], deep brain stimulation[4,5,6], visual prosthesis[7], functional electrical stimulation of spinal cord[8] and many more. Various materials are being employed for manufacturing these electrodes, including metal microwires, MEMS-based silicon, nanomaterials, conductive polymers, and carbon-based materials[9]. Conventional neural electrodes are made of metals such as platinum (Pt), gold (Au), or platinum-iridium (PtIr) that are highly biocompatible[10,11]. Among them, Pt is historically known to be the preferred material for fabricating neural prostheses[10,12] because of its excellent electrochemical stability and corrosion resistance properties[13]. From the biomedical perspective, Pt is preferred due to its inert nature towards biological environments[14,15]. With developing technological advancements in the field of neuroprosthesis, the world is moving towards implant miniaturization[16,17,18,19]. However, such miniaturization is difficult to achieve using pure metallic substrates such as Pt, as it has an electrochemical charge injection capacity (CIC) of only 20-150 $\mu C/cm^2$[20,21]. This CIC is inadequate for a high-density safe charge injection at therapeutic levels. To overcome such difficulties, geometrically small-sized electrodes with high electrochemical surface area (ECSA) are desired. Therefore, researchers investigated surface modifications on neural electrode surfaces in order to improve the electrode's electrochemical properties.

Miniaturized neural implants were found to have numerous advantages among which is the flexibility to probe neuronal activity either from the peripheral nerves or from neurons deep inside

the brain[22]. These neural implants can be used for recording neuronal activities or stimulating the deep brain for the treatment of various applications such as in the treatment of epilepsy and Parkinson's, in brain-machine interfaces, or for restoration of hearing, vision, walking, and grasping abilities. In addition, the smaller the sizes of neural implants are, the lesser their foreign body response and implant rejection after the procedure[12]. However, as the impedance (Z) of the electrodes is inversely proportional to the geometrical surface area (GSA), there is a great practical difficulty in applying smaller-sized electrodes. On the other hand, larger-sized electrodes possess high Z levels which do not help in safe neural stimulation, as high potentials exceeding the safe voltage limits of the tissues would be required to adequately stimulate the neurons. However, by roughening the surfaces of small-sized electrodes, the Z problem could be overcome. For about two decades, there have been various studies carried out on the electrochemical surface modifications of implantable electrdoes[23]. With advancements in nanotechnology, the recent trend towards surface structuring is at the nanoscale level, which proves to enclose great potential inside it.

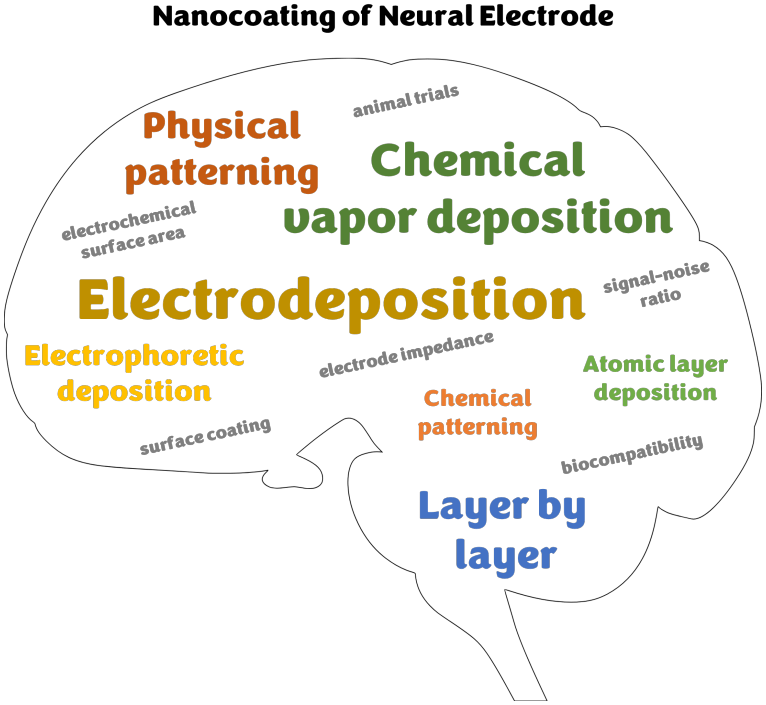

Figure 1: Schematic diagram showing neural electrode nanocoating methods

To date, many reviews have been published from around the world on state-of-the-art neural electrode surface modifications. A review of neural recording electrode types, current trends in recording, and technical challenges is presented by Patil and Thakor[24]. A review on nanomaterials and nanotechnology to improve electrode-tissue compatibility and biological tolerance is provided by Scaini and Ballerini[25]. Neural interface challenges and the nanomaterials used for neural electrodes are reviewed by Fairfield[26]. The current state of neural interfacing, the use of nanomaterials, and nanocolloids for biocompatibility and nanostructuring are reviewed by Timko et al[23]. Systemically delivered nanoparticle coatings and blood-brain barrier interfacing are reviewed by Young et al[27]. Nanomaterials, nanostructured devices, and implanted devices for better neural interfacing are reviewed by Zeng et al[28]. Current status of biomaterials for neural tissue interfacing, technology for

electrode fabrication and nanomaterials used for neural electrodes are reviewed by Wang et al [29]. Finally, Argueta-Robles et al. have published a review on organic coatings for neural interfaces and tissue engineering [1]. However, to our knowledge, there are no reviews published exclusively on the nanoscale coating methods used for modifying the electrode surfaces. The aim of this review is to provide a state-of-the-art compilation of current methodologies to generate nanocoatings on neural electrode surfaces to improve their performance efficiencies. Figure 1 shows an overview schematic representation of this review. The literature search was mainly carried out on the platforms of Google Scholar and Web of Science by using keywords such as "neural electrode coating", "nanocoating neural electrode", "electrodeposition neural electrodes nano", "vapor deposition neural electrodes nano", etc. The review discusses nanoscale coating methods performed on neural electrodes and is divided into four sections on the basis of how the coatings are produced: via electric current, via vacuum, via nanoscale patterning, and via layer-by-layer. Finally, we present our views on the future prospects in the field of neural electrode coatings.

2 Nano-Coatings aided by Electric Current

Due to advances in nanotechnology, biomaterials, and biomedical technology, various electric current-based nano-coatings and structuring on neural electrode surfaces are performed to improve their electrochemical properties [30]. Nanoscale coatings developed with the help of electric current are low-cost and eco-friendly methods to produce a variety of 2D and 3D surface depositions. The techniques can be broadly classified into two variants: electrodeposition and electrophoretic deposition (EPD) [31].

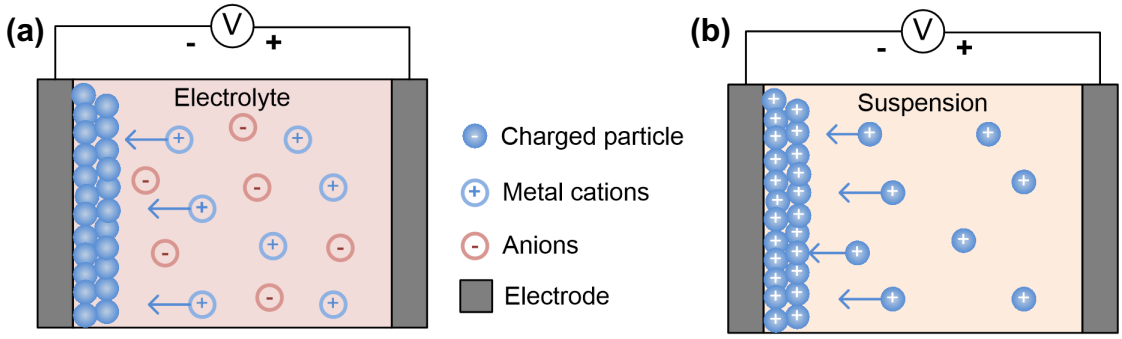

Figure 2: Schematic representation of (a) Electrodeposition and (b) Electrophoretic deposition [32].

2.1 Electrodeposition

The electrochemical phenomena associated with the reduction or deposition of electroactive substances onto the cathode surfaces form the basic principle of the electrodeposition method [30,33]. Generally, the electrodeposition process consists of an electrochemical cell inside which a conductive substrate is used as a working electrode, a Pt wire as a counter electrode, and Ag/AgCl or saturated calomel electrode (SCE) serves as the reference electrode (Figure 2a). The cell is filled with the

desired precursor solution to be deposited and the deposition occurs due to chemical bonding[34]. In literature, this coating method is synonymously referred to using various terms, such as electroplating, electrochemical deposition, electrochemical polymerization, etc.

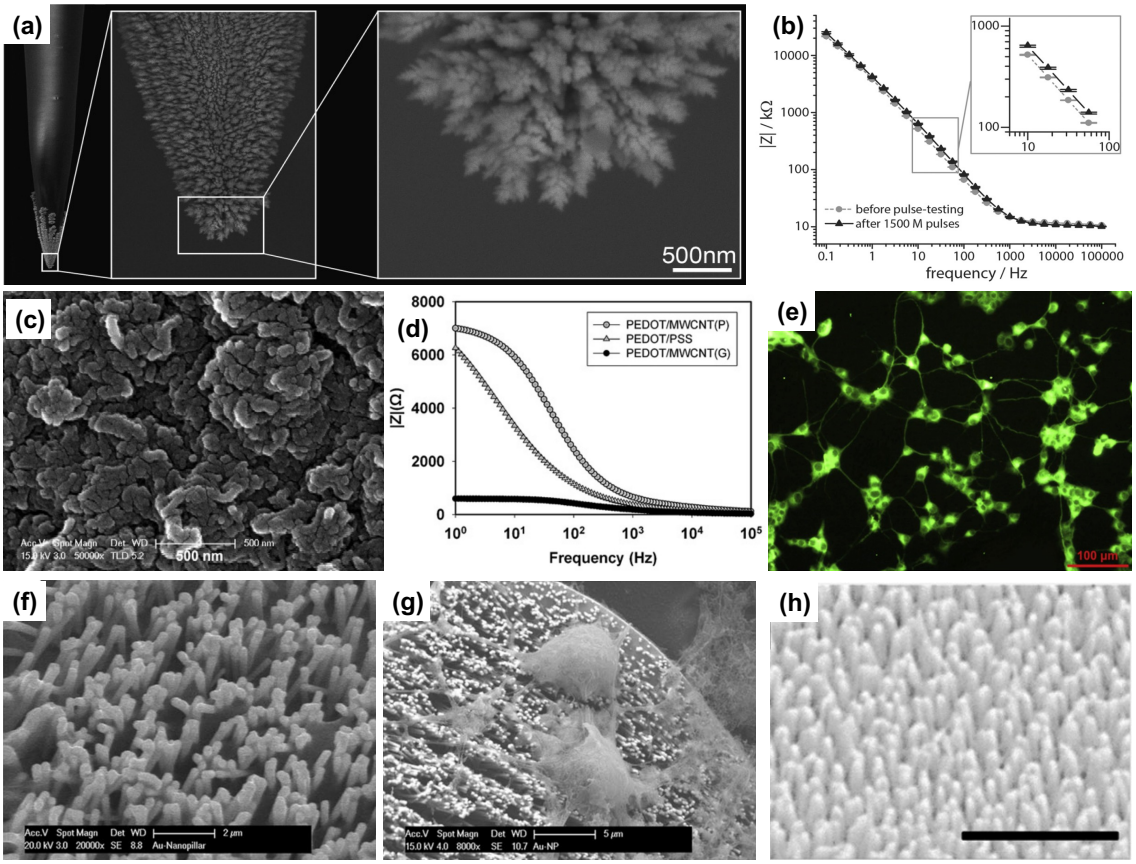

Figure 3: Neural electrode nano-coatings using Electrodeposition: (a) SEM images of conical-shaped microelectrodes coated with Pt Nanograss (scale bar: 500 nm), (b) Impedance spectra showing electrochemical stability of (a)[22] (c) SEM image (scale bar: 500 nm), (d) impedance spectra and (e) ß-III tubulin-stained PC12 cells (scale bar: 100 μm) on electrodeposited PEDOT:CNT films[35], (f) SEM images of Au nanopillars on neural microelectrodes showing morphology (scale bar: 2 μm) and (g) cell adhesion (scale bar: 5 μm)[36] (h) SEM image of electrodeposited Pt nanorods (scale bar: 2 μm)[37].

Brüggemann et al. developed gold nanopillars using the template-assisted electrodeposition technique. The gold nanopillars produced were around 300-400 nm in height, and 60 nm in diameter and were freestanding. After surface modification, neuronal signal recordings performed on cultured live HL-1 cells demonstrated enhanced SNR and low Z[38]. Boehler and co-workers published several works on electrochemical modification of the surfaces of neural microelectrodes using nanostructured platinum. In 2015, using a simple electrodeposition process, they developed Pt nanograss coatings on smooth Pt microelectrodes which substantially increased the ECSA and lowered the Z by a factor of 60 compared to the unmodified counterparts[39]. In 2017, they investigated the mechanical and electrochemical stability of their nanocoatings by inducing mechanical stress due to insertion in neural tissue and by performing long-term stimulation by applying over 240 million biphasic pulses.

As a result, they demonstrated exceptional mechanical and electrochemical stability of these nanoPt coatings[40]. In 2020, they further optimized the nanoPt coating process and additionally investigated the coating's in vitro and in vivo behaviors. When the SH-SY5Y cell line was cultured on the nanoPt coatings, they showed cell proliferation, and no signs of cell death were observed. After 5-week implantation in mouse models, the coatings could produce high-quality recordings with high SNR (which directly relates to a low Z) and further the durability of the coatings in vivo[22]. In another study gold nanoflakes were produced on microelectrode arrays by electrodeposition, demonstrating lower Z and improved cell-chip coupling[41]. Tan et al. produced ultra-thin nanoporous gold films on neural microelectrode surfaces via electrodeposition and these surfaces were found to be highly biocompatible by aiding the growth of microglia cells[42].

With the aim of making inorganic surfaces more biocompatible and thereby reducing the possibility of implant rejection, polymer nanocomposites are also increasingly studied. Zhou et al. deposited multi-walled carbon nanotubes (CNT) and poly(3,4-ethylenedioxythiophene) (PEDOT) nanocomposite coatings via electrodeposition on neural electrode surfaces and observed an enhancement in their electrochemical properties and an increase in cell adhesion and neurite outgrowth[35]. Similarly, when PEDOT/CNT coatings were electrodeposited on Pt microelectrodes, the Z values decreased both in vitro and in vivo. There was significantly less neuronal cell damage and the inflammatory response of the cells was also found to be lowered[43]. Even though Pt black coatings were commonly agreed to be undesired for neural electrode coatings due to toxicity, delamination, etc., the nano Pt black coatings developed by electrodeposition for treating facial paralysis were found to be superior to Pt black in morphology, functionality, electrical excitation of the orbicularis oculi muscle and mechanical stability[44]. Figure 3 shows representative nanocoatings performed via electrodeposition and Table 1 shows a consolidated list of studies utilizing electrodeposition as a coating technique for neural electrode nanocoatings. As mentioned before, the electrodeposition range of techniques is the most commonly used way to produce nanocoatings on neural electrode surfaces to date. Since the method is highly versatile, multiple studies on coating electrode surfaces for various other applications including the treatment of facial paralysis[44], recording of striatal dopamine levels[45], soft electronics[46], etc. have been published. However, the main drawback of this method is that only conductive precursors (organic or inorganic) can be used for depositions, narrowing the possibility of developing novel materials.

2.2 Electrophoretic Deposition

EPD is a colloidal processing technique, initially performed on depositing ceramic particles on substrates, which quickly spread onto depositing various materials. In this method, colloidal particles dispersed in a liquid migrate towards an oppositely charged electrode and get deposited there, in the presence of an electric field (Figure 2b). EPD was first observed by a Russian scientist called Ruess in 1808 when he saw movements of clay particles dispersed in water when the electric field was applied. However, a proper practical application was carried out only in 1933 by depositing thoria particles on a platinum electron beam cathode[47]. EPD is generally categorized into two types: cathodic and anodic EPD, based on the electrode on which the deposition is targeted (Figure 4a).

In cathodic EPD the particles are positively charged, and in anodic EPD the particles are negatively charged. The major advantages of EPD include, but are not limited to, short processing times, the requirement of simple apparatus, the possibility to apply various target shapes and sizes, etc. The method also offers easy control of the deposit morphology by adjusting the electric field potential or the deposition time[47,48]. Generally, the EPD process is influenced by its suspension parameters and physical parameters (like the electric field, time, etc.). As suspension parameters, the particle size, conductivity, viscosity, zeta potential, etc. play a major role[49,50,51,52]. As physical parameters, the deposition rate, applied voltage, and suspension concentration are deemed important[53,54,47].

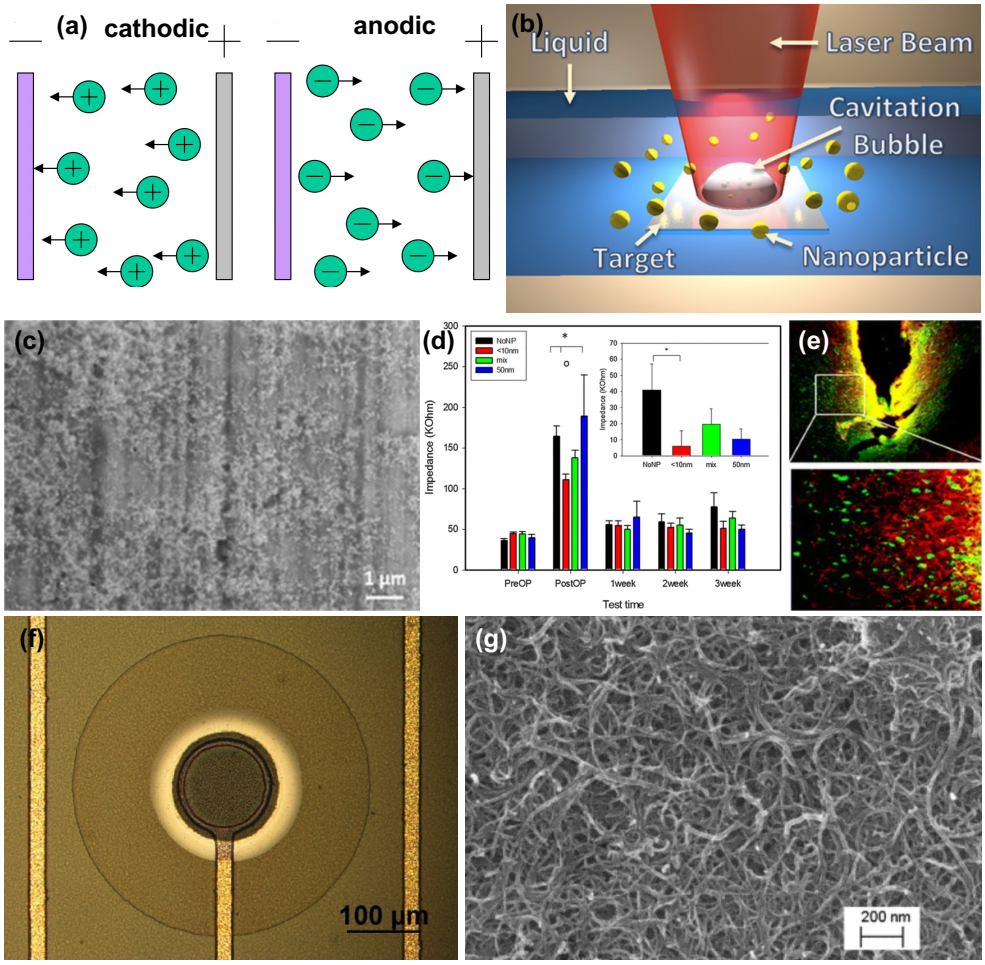

Figure 4: Neural electrode nano-coatings using EPD: (a) Schematic representation of two EPD types[47], (b) Schematic representation of NP generation using LAL mechanism[55], (c,d,e) SEM image, impedance values and immunohistological analysis of PtNP-coated PtIr microelectrodes in rat models[56], and (f,g) Flexible microelectrode array electrophoretically coated using multi-walled CNTs showing the coating morphology[57].

Although EPD is famous in ceramics processing, in the last decade it has begun to see its applications in the nanostructuring of neural electrode surfaces. For example, ligand-free colloidal NPs that are produced by a well-established laser processing technique called laser ablation in liquids (LAL) have been frequently electrophoretically deposited onto neural electrode surfaces to modify their electrochemical properties. In LAL, a metal precursor target is placed inside a liquid environment

and ablated via pulsed laser beams[58]. The generated NPs are partially oxidized on their surfaces, and hence have a negative surface charge. These negatively charged particles repel each other, automatically forming a stable colloid[59], eliminating the need for the addition of external stabilizing ligands[60]. In principle, when a laser beam interacts with the metal target in a liquid environment, a plasma plume is formed (typically for tens of ns up to few μs), containing the ablated particles[55]. The plasma plume grows in size, inducing a shockwave into the surrounding liquid leading to the formation of a cavitation bubble. This bubble expands and subsequently collapses dispersing the generated NPs into the liquid[55,58] (Figure 4b). However, the exact mechanism of particle formation in LAL is still under investigation and it is not the focus of this work[61,55,62]. Barcikowski and co-workers focussed their research on the EPD of laser-generated NPs onto neural electrode surfaces with the aim of reducing the electrode impedance via nanostructuring. After investigating the fundamentals of these charged NPs on EPD, they performed coatings on neural microsized electrodes to study the tuning of electrochemical properties. They determined the proportional relationship between electrophoretic mobility of Au- and PtIr-NPs and applied electric field strength[63]. The chemical composition of the developed coating remained unchanged even when coated with PtIr alloy NPs on PtIr electrode substrates[64]. The influence of ligands[53] and contact angle[65] on the electrode performance was further investigated and found that the presence of ligands in the suspension decreased the deposition rate due to shielding effects and that the contact angle was inversely proportional to the field strength and deposition time. One of the main advantages of such a linear correlation between electrophoretic mobility and field strength is the ability to better scale the process using ligand-free NPs. They were also able to establish continuous EPD chambers for high throughput[58] and optimize the EPD parameters using 2D surfaces by correlating the major neural electrode parameters such as impedance, ECSA, surface oxidation, and contact angle[59]. Furthermore, the EPD of laser-generated PtNPs (10 nm and 50 nm sizes) was performed on real-time 3D neural microelectrodes. These coated electrodes were tested for impedance performance in short-term both in vitro (in saline solution) and in vivo (implanting the electrodes in the STN of rat models). Upon stimulation, they found that the 10 nm sized PtNPs were able to achieve stable in vivo impedances in comparison to the 50 nm sized particles and uncoated electrodes[56]. A few other research groups are also starting to investigate this coating technique at nanoscale levels. For example, Winkin et al. performed EPD of multi-walled CNTs on flexible microelectrode arrays for increasing their ECSA and charge transfer capacities[57]. The application of EPD for nanostructuring neural electrode surfaces is a relatively new area that is slowly gaining interest among researchers.

Table 1: List of neural electrode surface modification studies with the aid of electric current

Type	Application	Reported functionality enhancement
Electrodeposition		
Gold nanoflakes[41]	Neural stimulation & recording electrodes	low Z, high cell-chip coupling
Gold nanograins[66]	Neuroelectronic interfaces	low Z, low RMS noise, ideal CIC
PEDOT:PPy nanotubes[67]	Neural stimulation microelectrodes	low Z, high CSC, no delamination, intact dorsal root ganglions
amino-functionalized CNTs[68]	Neural stimulation microelectrodes	91% low Z, high CSC, high CIC, high electrochemical stability
PEDOT:PSS: CNT nanocomposite[69]	Neural recording microelectrodes	increases recording stability over time
CNT:PPy nanocomposite[70]	Neural recording microelectrodes	significantly low Z and high SNR
Gold NPs[45]	Striatal dopamine recording electrodes	increased recording quality
Gold nanopillars[36]	Neural stimulation & recording electrodes	low Z, high neuronal adhesion
AuPt NPs[71]	Neural recording microelectrodes	low Z, low background noise, high SNR
TiO_2:Au nanowires[46]	stretchable neural recording electrode	high density chronic neural recording
Pt nanograss[39]	Neural stimulation microelectrode	high ECSA, 60x low Z
NanoPt[40]	Neural stimulation microelectrode	high mechanical and electrochemical stability
NanoPt[22]	Neural stimulation microelectrodes	high in vitro and in vivo biocompatibility
Au nanopillars[38]	Neural recording electrodes	high SNR, low Z

Nanoporous Au films[42]	Neural stimulation & recording microelectrode	high biocompatibility
CNT:PEDOT[35]	Neural stimulation & recording electrode	high performance, high biocompatibility
PEDOT:CNT[43]	Neural stimulation microelectrodes	low Z in vitro and in vivo, low inflammatory response
Nano Pt-black[44]	Facial paralysis stimulation microelectrode	high performance, high stability
Pt nanorods[37]	Neural recording electrode	high biocompatibility, record broadband of neuronal signals, high SNR
Au nanowires[72]	Electrochemical electrodes	high CSC, high ECSA, high capacitance
CNTs[73]	Neural stimulation electrode	low Z, high charge transfer
DCDPGYIGSR: PPy[74]	Neural recording probes	high in vivo recording performance
PEDOT:PSS[75]	Neural recording electrodes	high SNR, high long-term biocompatibility
PEDOT:CNT[76]	Electrocorticogram microelectrode	high ECSA, low Z, high conductivity
FeNi microactuators[77]	flexible magnetic microelectrodes	minimal neuronal cell loss, great promise for electrical interfacing
EPD		
AuNPs & PtIr NPs[63]	Neural stimulation electrodes	potential applicability for enhancing neural electrode properties
PtIr NPs[64]	Neural stimulation electrodes	matching chemical composition between coating and base material aiding biocompatibility
PtNPs[56]	Neural stimulation electrodes	low Z in vitro, stable in vivo impedance with 10 nm particles

PtNPs[59]	Neural stimulation and recording electrodes	Optimized EPD parameters to select desirable electrochemical outputs
CNTs[57]	flexible stimulation microelectrode arrays	enhanced ECSA and charge transfer capacity
PtNPs[78]	Neural stimulation and recording electrodes	in vitro impedance reduction due to electric field influence
PtNPs[79]	Neural stimulation and recording electrodes	in vitro impedance reduction due to solvent influence
PtNPs[80]	Neural stimulation and recording electrodes	improved mechanical stability in vitro and in vivo

3 Nano-Coatings aided by Vacuum

Vapor deposition is a coating technique in which materials in a vapor state undergo condensation, chemical reaction, or conversion to form a solid thin layer over a substrate[81]. The most common form of vapor deposition extensively researched to improve neural electrode surface properties is chemical vapor deposition (CVD). One variant of CVD is the atomic layer deposition (ALD), where gaseous precursors are introduced into the reaction chamber to enable depositions via chemical surface reactions[82] is also sometimes applied.

In CVD, a solid material is deposited from a vapor via chemical reactions occurring on or near a normally heated substrate. Microfabrication processes widely use CVD to deposit materials in various forms. Here, the material to be deposited is in vapor form that is allowed to react or decompose on the substrate in a vacuum chamber under elevated temperatures[83]. Ansaldo et. al performed in situ deposition of carbon nanotubes (CNTs) on microelectrodes via CVD. It was shown that the CVD-CNT-coated microelectrodes remained stable in their electrochemical properties even after 1 year of storage, proving to be a good choice for long-term implantation. Additionally, they were also able to record single unit neural signal[84]. Low-temperature CVD was experimented with to directly synthesize CNTs on flexible electrode substrates and was found to decrease the electrode impedance and improve the charge injection capacity, additionally showing in vitro biocompatibility for a period of 16 days[85].

Besides CNTs, the CVD method is also employed for depositing polymers onto neural electrode surfaces. O'Shaughnessy et al. deposited thin films of polytrivinyltrimethylcyclotrisiloxane (p(V_3D_3)) via initiated CVD on neural probes and observed no degradation for over 2.5 years under stimulated implant conditions[86]. Plasma-enhanced CVD was used to produce titanium nitride nanowires at low temperatures, which possessed high capacitance indicating an increase in the ECSA and good electrochemical stability[87]. In situ, fluffy growth of CNTs was produced on microelectrode surfaces

using CVD to obtain a significant reduction in the microelectrode impedance and their charge transfer capacity[88]. In addition, various nanoscale pillars, arrays, sheets, wires, etc. were deposited via CVD onto electrode surfaces to improve their performance. One study even investigated the nanoporous gold surfaces formed via ALD on neural electrodes to improve the neuron-electrode coupling, increase neuronal surface coverage, and decrease the scar tissue formation[89]. Most of the above studies generally demonstrate an inclination towards using simple, fast, and less harsh processing steps of the precursors for modifying the implant surfaces. Figure 5 shows exemplary images of nano-coatings developed using CVD on neural electrode surfaces and Table 2 provides a list of investigations carried out using CVD or its variant, ALD.

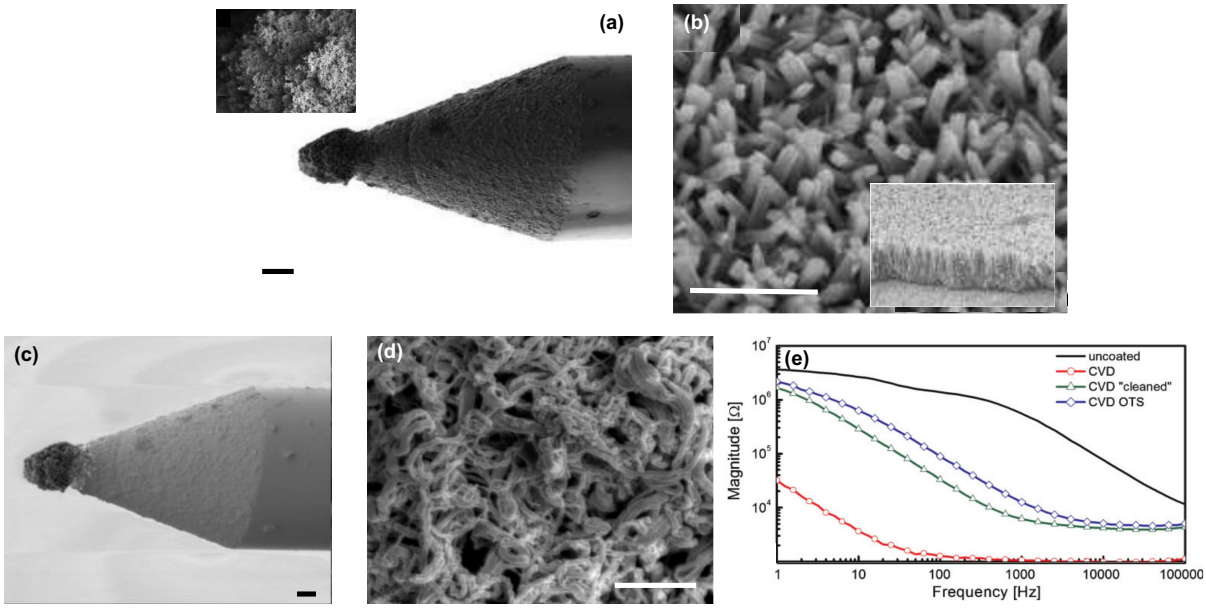

Figure 5: Neural electrode nano-coatings using CVD: (a) SEM images of microelectrodes coated with CNTs[84] (Inset showing a magnified image of the tip; scale bar: 20 μm). (b) SEM images of titanium dioxide nanorods grown at low temperatures[87] (Inset image showing different nucleation layers; scale bar: 2 μm). (c,d) CNT coatings at different magnifications developed on the tips of intracortical neural recording electrodes[88] (scale bars: 10 μm and 1 μm, respectively). (e) Electrochemical impedance spectra of CNT-coated electrode from (c), showing least impedance after CVD-CNT coating[88].

Table 2: List of implantable electrode surface modifications using CVD technique

Type	**Application**	**Reported functionality enhancement**
CNT[84]	Neural recording microelectrodes	long shelf-life, record single unit neural signal

CNT [85]	flexible stimulation electrodes	low Z, high CIC, high in vitro biocompatibility
Thin p(V_3D_3) films [86]	Neural stimulation electrodes	long-term stability
TiN nanowires [87]	Neural stimulation electrodes	high capacitance, high ECSA, high electrochemical stability
Fluffy CNT [88]	Neural stimulation microelectrodes	significantly low Z, high charge transfer capacity
CNT nanopillars [90]	Neural stimulation electrodes	high CIC
Vertically-aligned CNF arrays [91]	Neural stimulation electrodes	low Z, high biocompatibility and mechanical stability
CNT sheets and yarns [92]	Neural stimulation & recording electrode	high biocompatibility with increased neuronal growth and fibroblast migration
Vertically-aligned CNF [93]	Neural recording electrodes	enable dual-mode recording, high spatial resolution
Si nanowires [94]	Neural stimulation electrodes	enables delivery of biomolecules to guide neuronal progenitor growth
Si nanowires [95]	Implantable electrodes	potential tool for studying intra- and intercellular biological processes
Nitrogen-doped nanocrystalline diamond [96]	Retinal prosthesis	high performance, non-cytotoxic
Nanoporous Au [89]	Neural stimulation electrodes	high neuron-electrode coupling, low scar tissue formation

4 Nano-Coatings aided by Patterning

Extensive research has been carried out in studying the electrode performance and biocompatibility characteristics of neural electrodes by forming patterns on their surfaces. These patterns can be formed either via physical or chemical means. Physical methods involve topographical patterning using well-known lithography techniques or creating surface roughness using plasma. The two main

lithography techniques used to create nanocoatings on neural electrodes are photolithography and electron beam lithography. Photolithography is a process of generating patterns using photoresists that achieves high product resolution and also produces a variety of intricate planar designs[97]. Electron beam lithography generates nanoscale patterns by directly writing on resist layers with focused electron beams[98]. On the other hand, chemical patterning usually involves the self-assembly of monolayers, directly grown patterns, etc.

Ryu et al. fabricated ZnO nanowires by hydrothermally growing them on 3D neural microelectrode surfaces. The electrode array was flexible which due to the nanowire patterning showed increased ECSA, flexibility, and neural signal transduction efficiency. Upon in vivo signal recording, the modified electrodes showed high SNR and a significant reduction in electrical interference noise harmonics proving their efficiencies in both recording and stimulation capabilities[99]. In order to study the cell proliferation and attachment of neuronal cells on electrode surfaces various chemical patterning has been carried out using hydrocarbons[100], polyethylene glycol[101,102,103], oligoethylene glycol[102,103,104] and mannitol[105]. These patternings have been proven useful in cell inhibition immediately after implantation to reduce or avoid implant rejection due to scar formations. On the other hand, hydrophilic cell adhesive coatings were also produced using chemical patterns by depositing polylysine[106,107], laminin[108], collagen[109] and so on. Such chemical patterns guided the growth of neurons. Wyart et al. patterned cell-adhesive polylysine on which the neurite growth was guided[107]. It was observed that the neurons were viable up to 17 days and both inhibitory and excitatory neurons were interconnectedly present with functional synapses. Au nanowires were produced on neural electrode surfaces by evaporation-induced self-assembly, inducing cell growth along the direction of the nanowires[110].

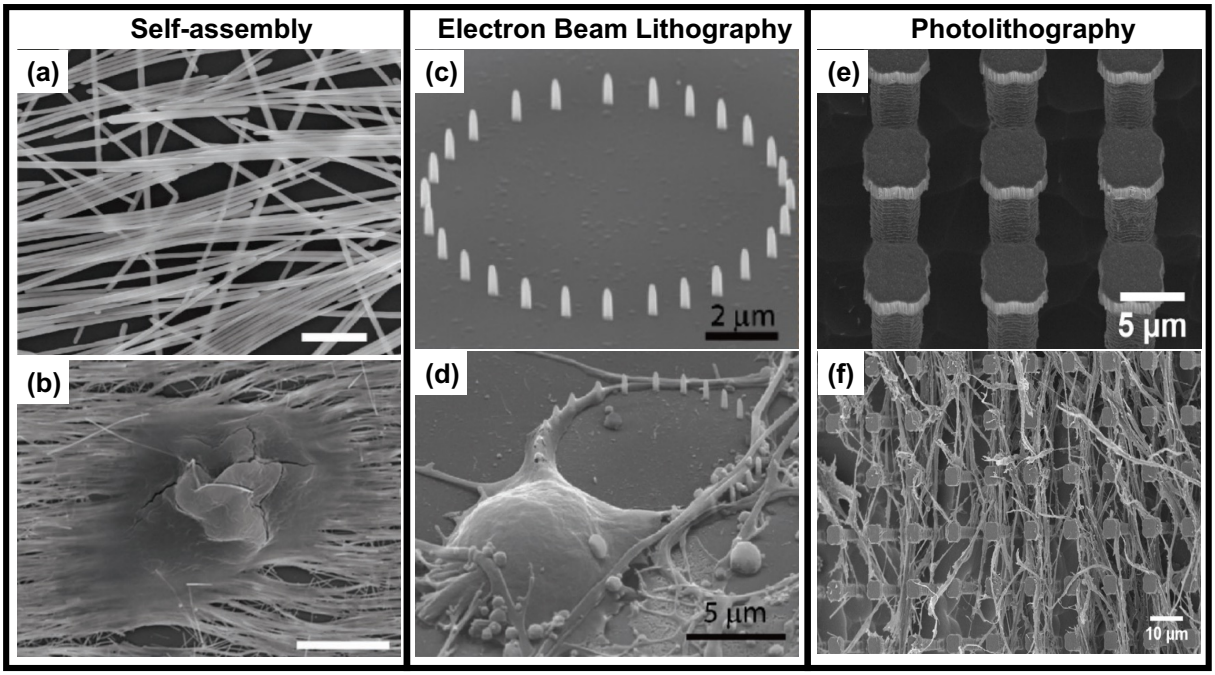

Figure 6: Neural electrode nano-structuring via patterning: (a,b) SEM images of bundled assembly of Ag nanowires and growth of neuronal cell on it (scale bars: 500 nm and 5 μm, respectively)[110] (c,d) SEM images of ring-shaped Pt nanopillars produced on microelectrode substrates using EBL showing the directional growth of neuron around the pattern (scale bars: 2 μm and 5 μm, respectively)[111] (e,f) Nanocrystalline diamond arrays produced using photolithography to aid directional growth of neuronal cells (scale bars: 5 μm and 10 μm, respectively)[112].

On the other hand, physical patterning focuses more on patterning of the electrode topography to enable surface roughness thereby promoting enhanced performances. Free-standing vertically aligned CNF arrays were produced to create a brush-like matrix for neuronal cell growth. These nanopatterned arrays demonstrated a highly potential system for localized stimulation and neuromodulation[113]. Dalby and co-workers produced regularly patterned nano pits using electron beam lithography (EBL) on silica[114] and PMMA[115] substrates and observed that in comparison to the plain unpatterned substrates, the patterned counterparts allowed the downregulation of cell adhesion, which might later influence in the scar tissue formation. In another study, PEDOT and PPy polymer materials were assembled on polystyrene substrates to form aligned nanofibres demonstrating higher electrochemical stability than the ones without PEDOT[116]. Flexible Au nanorods were produced using photolithography on microelectrode surfaces, which lowered the Z by 25 times[117]. Nanoscale surface roughness was created on neural interfaces using plasma treatments, to lower Z, increase the SNR, and recording quality[118]. Vertical Pt nanopillars were produced on electrode surfaces via EBL for pinning the neuron to place and improving their growth[111]. Not only neural electrodes but also cochlear implant surfaces were modified via photolithography using nanocrystalline diamonds[112]. The study demonstrated that the human and murine inner-ear ganglion neurites and neural progenitor cells attached to the patterned surfaces without the need for extracellular matrix coatings. It increased cell adhesion and growth along the nail-head-shaped pillars in an orderly manner[112]. Fig-

ure 6 shows a few neural electrode surfaces modified using nanoscale patterning and Table 3 enlists surface modifications performed on implant surfaces via patterning.

Table 3: List of implant surface modification studies via nanoscale patterning

Type	Application	Reported functionality enhancement
Self-assembly		
ZnO nanowires[99]	Neural recording electrodes	high ECSA, high SNR, flexibility, efficient signal transduction
Cell-adhesive polylysine[106,107]	Neural stimulation electrodes	high biocompatibility
Au nanowires[110]	Neural stimulation electrodes	induced cell growth
Nanoporous Au films[119]	Neural recording electrodes	low Z, high SNR
Vertical Si nanowires[120]	Neural stimulation electrodes	improved cell adhesion, proliferation & electrical properties
Vertically aligned CNF[113]	Neural stimulation electrode	localized stimulation and neuromodulation
PEDOT:PPy nanofibres[116]	Neural stimulation electrodes	high electrochemical stability
Plasma exfoliation		
Nanoroughness[118]	Neural recording electrodes	low Z, high SNR
Graphene oxide nanoroughness[121]	Neural stimulation electrodes	inert neuron-interfacing modification
EBL		
Nanopits[114,115]	Neural stimulation electrodes	low cell adhesion and scar tissue formation
Verticle Pt nanopillars[111]	Neural stimulation electrodes	ordered growth of neurons

Nanowires[122]	Neural recording electrodes	robust electronic properties, real-time monitoring
GaP nanowires[123]	Neural recording electrode	high quality in vitro recording
Si nanowires[124]	Neural stimulation & recording electrodes	scalable stimulation and recording
Photolithography		
Flexible Au nanorods[117]	Neural stimulation microelectrodes	25x low Z
Nanocrystalline diamonds[112]	Cochlear implants	increased cell growth

5 Nano-Coatings aided by Multilayer Depositions

Layer-by-Layer (LbL) techniques are considered to be universally applicable for depositing a spectrum of materials on substrates for various applications. LbL generates ultrathin films on solid supports by alternate exposure to positive and negative species with spontaneous deposition of the oppositely charged ions[125]. LbL utilizes mild operating conditions, a simple experimental setup, and in spite provides a high degree of structural control over the depositions produced. It facilitates combining organic and inorganic materials for coating and helps to accurately control the coating thickness by simply adjusting the number of layers deposited. LbL is considered to be a versatile method to produce multifunctional coatings at nanoscale level[126]. Many times, neural electrode surfaces were found to be modified using the LbL technique to improve their surface properties. Zhang et al. demonstrated that the LbL assembly of gold nanoparticles (AuNPs) on microelectrodes produced a more than a three-fold reduction in impedance and an order-of-magnitude increase in charge storage capacity[127]. Jan and co-workers employed in LbL of multi-walled CNTs[128] and single-walled CNTs[129] to improve the neural electrode biocompatibility. Using multi-walled CNTs, they were able to deposit CNTs in conjunction with polyelectrolytes in nanometer thickness and found that the LbL CNT-polyelectrolyte coating competes with traditional coatings in terms of the electrode's electrochemical properties[128]. CNTs are known to behave as supercapacitors[130,131], which became an added advantage for their depositions. When single-walled CNTs were deposited with polyelectrolytes via LbL, the mouse embryonic neural stem cells readily differentiated into neurons, astrocytes, and oligodendrocytes indicating high biocompatibility[129]. Single-walled CNTs were also deposited via LbL to improve the electrical conductivity of neural electrodes and to stimulate excitable neuronal cells[132]. Figure 7 shows a few neural electrode surfaces modified using nanoscale LbL and Table 4 enlists surface modifications performed on implant surfaces via LbL. Although LbL is considered versatile, for nanocoatings on neural electrode surfaces mainly CNTs and very few nanoparticles have been investigated so far.

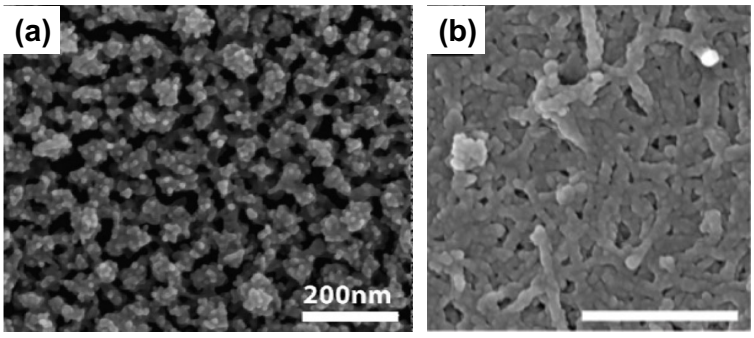

Figure 7: Neural electrode nano-structuring via LbL: (a) SEM images of AuNP LbL (scale bar: 200 nm)[127] (b) SEM image of PEDOT:CNT LbL (scale bar: 500 nm)[128].

Table 4: List of implant surface modification studies via Layer-by-Layer depositions

Type	Application	Advantages
AuNPs[127]	Neural stimulation microelectrodes	3x reduced Z, high CSC
PEM:Multi-walled CNT[128]	Neural stimulation electrodes	high electrochemical properties
PEM:Single-walled CNT[129]	Neural stimulation electrodes	high biocompatibility
PEM:Single-walled CNT[132]	Neural stimulation electrodes	high conductivity and stimulation capability

6 Conclusion and Future Perspectives

Using implantable neural electrodes for stimulation and recording of neuronal activity is a common way of intervention towards symptom-relieving treatments of numerous neurological disorders. In order to enhance therapeutic efficiency, these miniaturized electrodes are increasingly modified on their surfaces using biocompatible nanomaterials. For such coating purposes, a few of the conventional industrial coating methods have been adapted in research. In Table 5, an overview of the comparison of different coating techniques is presented.

Table 5: Comparison of the different Nano-coating Methods

Coating Method	**Reproducibility**	**Structural flexibility**	**Functionality enhancement**	**Potential scalability**	**Real-world transferability**
Electrodeposition	High	High	High	High	High
EPD of NPs	Low	High	Medium	High	Medium-Low
CVD	High	Medium-High	Medium	High	Medium-High
Nanopatterns	Medium	Low	Medium-High	Low	Low
LbL	High	High	Medium	High	Low

In this literature analysis, it has been revealed that a wide range of nanoscale coating methods can be used to modify neural electrode surfaces in order to improve their efficiency. Among them, the electrodeposition method shows the highest level of promise in terms of coating stability, reproducibility, surface variations, industrial scalability, and performance enhancement. This is mainly due to the sheer volume of research done using this long-existing conventional method and its applicability to various materials ranging from metals to degradable polymers. The second desirable approach could be CVD which is again highly researched. It produces reproducible coatings and can be applied to different electrode shapes and sizes. As it is already industrially applied, the real-world transferability of the coatings produced should not be a problem. However, this method seems to be limited to carbon-based materials in the neural electrode applications which limits its application with novel emerging materials like degradable polymer combinations. The reproducibility and scalability of the coatings produced via nanopatterning are rarely reported. Additionally, the mechanical stability of such coatings should be further investigated if they are to be clinically used. LbL coatings are newly emerging in neural electrode surface modifications and hence further research is necessary to have a concrete perspective on these coatings. Similarly, the EPD of laser-generated NPs is also an emerging technique for this application. EPD looks attractive as it already offers structural flexibility and ease of scaling up industrially. However, to industrialize and clinically apply these coatings, further research on reproducibility and in vivo performances is required. Due to advancements in NP productions, various material combinations could also be tried to find the best combinations for neural electrode performance enhancement. Until today, only the electrodeposition method offers such material flexibility in the nanoscale. Communities in industry and academia should strive to bring more research into improvising the electrode performance that can eventually be even applied beyond neural electrodes. The shelf-life and electrochemical stability of the coatings are highly important.

During long-term applications, the coating should not delaminate inside the body or the material being used cannot corrode. That said, a huge step has to be taken to transform all of these research findings into a real-world market. Manufacturers have to think about upgrading the coatings so that they can satisfy more than one requirement at the same time.

References

[1] Ulises A Aregueta-Robles, Andrew J Woolley, Laura A Poole-Warren, Nigel H Lovell, and Rylie A Green. Organic electrode coatings for next-generation neural interfaces. *Frontiers in neuroengineering*, 7:15, 2014.

[2] Douglas B McCreery and Steven R Otto. Cochlear nucleus auditory prostheses. In *Auditory Prostheses: New Horizons*, pages 179–205. Springer, 2011.

[3] Robert V Shannon. Advances in auditory prostheses. *Current opinion in neurology*, 25(1):61, 2012.

[4] Joel S Perlmutter and Jonathan W Mink. Deep brain stimulation. *Annu. Rev. Neurosci.*, 29:229–257, 2006.

[5] Andres M Lozano and Nir Lipsman. Probing and regulating dysfunctional circuits using deep brain stimulation. *Neuron*, 77(3):406–424, 2013.

[6] DM Andrade, D Zumsteg, C Hamani, MMDMF Hodaie, S Sarkissian, AM Lozano, and RA Wennberg. Long-term follow-up of patients with thalamic deep brain stimulation for epilepsy. *Neurology*, 66(10):1571–1573, 2006.

[7] Robert K Shepherd, Mohit N Shivdasani, David AX Nayagam, Christopher E Williams, and Peter J Blamey. Visual prostheses for the blind. *Trends in biotechnology*, 31(10):562–571, 2013.

[8] Jennifer L Collinger, Stephen Foldes, Tim M Bruns, Brian Wodlinger, Robert Gaunt, and Douglas J Weber. Neuroprosthetic technology for individuals with spinal cord injury. *The journal of spinal cord medicine*, 36(4):258–272, 2013.

[9] Nan Wu, Shu Wan, Shi Su, Haizhou Huang, Guangbin Dou, and Litao Sun. Electrode materials for brain–machine interface: A review. *InfoMat*, 3(11):1174–1194, 2021.

[10] SB Brummer, LS Robblee, and FT Hambrecht. Criteria for selecting electrodes for electrical stimulation: theoretical and practical considerations. *Annals of the New York Academy of Sciences*, 405:159–171, 1983.

[11] Leslie A Geddes and R Roeder. Criteria for the selection of materials for implanted electrodes. *Annals of biomedical engineering*, 31(7):879, 2003.

[12] Stuart F Cogan. Neural stimulation and recording electrodes. *Annu. Rev. Biomed. Eng.*, 10:275–309, 2008.

[13] Robert L White and Thomas J Gross. An evaluation of the resistance to electrolysis of metals for use in biostimulation microprobes. *IEEE Transactions on Biomedical Engineering*, (6):487–490, 1974.

[14] DR Merrill. Bikson m, jefferys jg. *Electrical stimulation of excitable tissue: design of efficacious and safe protocols. J Neurosci Methods*, 141:171–198, 2005.

[15] Vadim S Polikov, Patrick A Tresco, and William M Reichert. Response of brain tissue to chronically implanted neural electrodes. *Journal of neuroscience methods*, 148(1):1–18, 2005.

[16] Yasuhide Nakayama and Takehisa Matsuda. Surface microarchitectural design in biomedical applications: preparation of microporous polymer surfaces by an excimer laser ablation technique. *Journal of biomedical materials research*, 29(10):1295–1301, 1995.

[17] Karen C Cheung. Implantable microscale neural interfaces. *Biomedical microdevices*, 9:923–938, 2007.

[18] BA Wester, RH Lee, and MC LaPlaca. Development and characterization of in vivo flexible electrodes compatible with large tissue displacements. *Journal of neural engineering*, 6(2):024002, 2009.

[19] M Schuettler, S Stiess, BV King, and GJ Suaning. Fabrication of implantable microelectrode arrays by laser cutting of silicone rubber and platinum foil. *Journal of neural engineering*, 2(1):S121, 2005.

[20] TL Rose and LS Robblee. Electrical stimulation with pt electrodes. viii. electrochemically safe charge injection limits with 0.2 ms pulses (neuronal application). *IEEE Transactions on Biomedical Engineering*, 37(11):1118–1120, 1990.

[21] Rylie A Green, Hamza Toor, Christopher Dodds, and Nigel H Lovell. Variation in performance of platinum electrodes with size and surface roughness. *Sensors and Materials*, 24(4):165–180, 2012.

[22] Christian Boehler, Diego M Vieira, Ulrich Egert, and Maria Asplund. Nanopt—a nanostructured electrode coating for neural recording and microstimulation. *ACS applied materials & interfaces*, 12(13):14855–14865, 2020.

[23] NA Kotov and JO Winter. Clements ip, jan e. *Timko BP, Campidelli S, Pathak S, Mazzatenta A, Lieber CM, Prato M, Bellamkonda RV. Nanomaterials for neural interfaces. Advanced Materials*, 21(40):3970–4004, 2009.

[24] Anoop C Patil and Nitish V Thakor. Implantable neurotechnologies: a review of micro-and nanoelectrodes for neural recording. *Medical & biological engineering & computing*, 54:23–44, 2016.

[25] Denis Scaini and Laura Ballerini. Nanomaterials at the neural interface. *Current opinion in neurobiology*, 50:50–55, 2018.

[26] Jessamyn A Fairfield. Nanostructured materials for neural electrical interfaces. *Advanced Functional Materials*, 28(12):1701145, 2018.

[27] Ashlyn T Young, Neil Cornwell, and Michael A Daniele. Neuro-nano interfaces: Utilizing nanocoatings and nanoparticles to enable next-generation electrophysiological recording, neural stimulation, and biochemical modulation. *Advanced functional materials*, 28(12):1700239, 2018.

[28] Qi Zeng, Xiaojian Li, Shiyun Zhang, Chunshan Deng, and Tianzhun Wu. Think big, see small—a review of nanomaterials for neural interfaces. *Nano Select*, 3(5):903–918, 2022.

[29] Mian Wang, Gujie Mi, Di Shi, Nicole Bassous, Daniel Hickey, and Thomas J Webster. Nanotechnology and nanomaterials for improving neural interfaces. *Advanced Functional Materials*, 28(12):1700905, 2018.

[30] Farzad Nasirpouri, Katayoon Alipour, Farhad Daneshvar, and Mohammad-Reza Sanaeian. Electrodeposition of anticorrosion nanocoatings. In *Corrosion Protection at the Nanoscale*, pages 473–497. Elsevier, 2020.

[31] Nur Ubaidah Saidin, Kok Kuan Ying, and Ng Inn Khuan. Electrodeposition: principles, applications and methods. 2011.

[32] L Santos, JP Neto, Ana Crespo, Pedro Baião, P Barquinha, L Pereira, R Martins, and E Fortunato. Electrodeposition of wo3 nanoparticles for sensing applications. *Electroplating of nanostructures*, pages 1–22, 2015.

[33] PK Kannan, Sushmita Chaudhari, Suhash Ranjan Dey, et al. Progress in development of czts for solar photovoltaics applications. 2022.

[34] Mehmood Shahid, Suresh Sagadevan, Waqar Ahmed, Yiqiang Zhan, and Pakorn Opaprakasit. Metal oxides for optoelectronic and photonic applications: A general introduction. In *Metal Oxides for Optoelectronics and Optics-Based Medical Applications*, pages 3–31. Elsevier, 2022.

[35] Haihan Zhou, Xuan Cheng, Li Rao, Tao Li, and Yanwen Y Duan. Poly (3, 4-ethylenedioxythiophene)/multiwall carbon nanotube composite coatings for improving the stability of microelectrodes in neural prostheses applications. *Acta biomaterialia*, 9(5):6439–6449, 2013.

[36] Christoph Nick, Sebastian Quednau, Reza Sarwar, HF Schlaak, and Christiane Thielemann. High aspect ratio gold nanopillars on microelectrodes for neural interfaces. *Microsystem technologies*, 20:1849–1857, 2014.

[37] Mehran Ganji, Angelique C Paulk, Jimmy C Yang, Nasim W Vahidi, Sang Heon Lee, Ren Liu, Lorraine Hossain, Ezequiel M Arneodo, Martin Thunemann, Michiko Shigyo, et al. Selective formation of porous pt nanorods for highly electrochemically efficient neural electrode interfaces. *Nano letters*, 19(9):6244–6254, 2019.

[38] Dorothea Brüggemann, Bernhard Wolfrum, Vanessa Maybeck, Yulia Mourzina, Michael Jansen, and Andreas Offenhäusser. Nanostructured gold microelectrodes for extracellular recording from electrogenic cells. *Nanotechnology*, 22(26):265104, 2011.

[39] C Boehler, T Stieglitz, and M Asplund. Nanostructured platinum grass enables superior impedance reduction for neural microelectrodes. *Biomaterials*, 67:346–353, 2015.

[40] Christian Boehler, F Oberueber, Thomas Stieglitz, and Maria Asplund. Nanostructured platinum as an electrochemically and mechanically stable electrode coating. In *2017 39th Annual International Conference of the IEEE Engineering in Medicine and Biology Society (EMBC)*, pages 1058–1061. IEEE, 2017.

[41] Ju-Hyun Kim, Gyumin Kang, Yoonkey Nam, and Yang-Kyu Choi. Surface-modified microelectrode array with flake nanostructure for neural recording and stimulation. *Nanotechnology*, 21(8):085303, 2010.

[42] Yih Horng Tan, Shana E Terrill, Geeta S Paranjape, Keith J Stine, and Michael R Nichols. The influence of gold surface texture on microglia morphology and activation. *Biomaterials science*, 2(1):110–120, 2014.

[43] Christi L Kolarcik, Kasey Catt, Erika Rost, Ingrid N Albrecht, Dennis Bourbeau, Zhanhong Du, Takashi DY Kozai, Xiliang Luo, Douglas J Weber, and X Tracy Cui. Evaluation of poly (3, 4-ethylenedioxythiophene)/carbon nanotube neural electrode coatings for stimulation in the dorsal root ganglion. *Journal of neural engineering*, 12(1):016008, 2014.

[44] Y Zhang, KY Li, C Jin, YT Wang, L Geng, YJ Sun, HC Tian, JQ Liu, and XJ Jin. Comparative studies on the implantation of nano platinum black and pure platinum electrodes in the rabbit orbicularis oculi muscle. *The Journal of Laryngology & Otology*, 128(8):679–689, 2014.

[45] Tien-Chun Tsai, Chun-Xian Guo, Huan-Zhang Han, Yu-Ting Li, Ying-Zu Huang, Chang-Ming Li, and Jia-Jin Jason Chen. Microelectrodes with gold nanoparticles and self-assembled monolayers for in vivo recording of striatal dopamine. *Analyst*, 137(12):2813–2820, 2012.

[46] Klas Tybrandt, Dion Khodagholy, Bernd Dielacher, Flurin Stauffer, Aline F Renz, György Buzsáki, and János Vörös. High-density stretchable electrode grids for chronic neural recording. *Advanced Materials*, 30(15):1706520, 2018.

[47] Laxmidhar Besra and Meilin Liu. A review on fundamentals and applications of electrophoretic deposition (epd). *Progress in materials science*, 52(1):1–61, 2007.

[48] L Besra, T Uchikoshi, TS Suzuki, and Y Sakka. Application of constant current pulse to suppress bubble incorporation and control deposit morphology during aqueous electrophoretic deposition (epd). *Journal of the European Ceramic Society*, 29(10):1837–1845, 2009.

[49] WD Ristenpart, Ilhan A Aksay, and DA Saville. Electrically driven flow near a colloidal particle close to an electrode with a faradaic current. *Langmuir*, 23(7):4071–4080, 2007.

[50] Laxmidhar Besra, Tetsuo Uchikoshi, Tohru S Suzuki, and Yoshio Sakka. Bubble-free aqueous electrophoretic deposition (epd) by pulse-potential application. *Journal of the American Ceramic Society*, 91(10):3154–3159, 2008.

[51] B Ferrari and R Moreno. Electrophoretic deposition of aqueous alumina slips. *Journal of the European Ceramic Society*, 17(4):549–556, 1997.

[52] Laxmidhar Besra, Tetsuo Uchikoshi, Tohru Suzuki, and Yoshio Sakka. Pulsed-dc electrophoretic deposition (epd) of aqueous alumina suspension for controlling bubble incorporation and deposit microstructure. In *Key Engineering Materials*, volume 412, pages 39–44. Trans Tech Publ, 2009.

[53] Carmen Streich, Sven Koenen, Marco Lelle, Kalina Peneva, and Stephan Barcikowski. Influence of ligands in metal nanoparticle electrophoresis for the fabrication of biofunctional coatings. *Applied Surface Science*, 348:92–99, 2015.

[54] Yoshihiro Hirata, Akihiko Nishimoto, and Yoshimi Ishihara. Forming of alumina powder by electrophoretic deposition. *Journal of The Ceramic Society of Japan*, 99(1146):108–113, 1991.

[55] Dongshi Zhang, Bilal Gokce, and Stephan Barcikowski. Laser synthesis and processing of colloids: fundamentals and applications. *Chemical reviews*, 117(5):3990–4103, 2017.

[56] Svilen D Angelov, Sven Koenen, Jurij Jakobi, Hans E Heissler, Mesbah Alam, Kerstin Schwabe, Stephan Barcikowski, and Joachim K Krauss. Electrophoretic deposition of ligand-free platinum nanoparticles on neural electrodes affects their impedance in vitro and in vivo with no negative effect on reactive gliosis. *Journal of nanobiotechnology*, 14(1):1–11, 2016.

[57] N Winkin, U Gierth, W Mokwa, and M Schneider. Nanomaterial-modified flexible microelectrode array by electrophoretic deposition of carbon nanotubes. *Biochip Tissue Chip*, 6(115):2153–0777, 2016.

[58] Sven Koenen, René Streubel, Jurij Jakobi, Kerstin Schwabe, Joachim K Krauss, and Stephan Barcikowski. Continuous electrophoretic deposition and electrophoretic mobility of ligand-free, metal nanoparticles in liquid flow. *Journal of The Electrochemical Society*, 162(4):D174, 2015.

[59] Sven Koenen, Christoph Rehbock, Hans E Heissler, Svilen D Angelov, Kerstin Schwabe, Joachim K Krauss, and Stephan Barcikowski. Optimizing in vitro impedance and physicochemical properties of neural electrodes by electrophoretic deposition of pt nanoparticles. *ChemPhysChem*, 18(9):1108–1117, 2017.

[60] S Barcikowski, V Amendola, M Lau, G Marzun, C Rehbock, S Reichenberger, D Zhang, and B Gökce. Handbook of laser synthesis & processing of colloids, 2019.

[61] M DellAglio, Rosalba Gaudiuso, O De Pascale, and Alessandro De Giacomo. Mechanisms and processes of pulsed laser ablation in liquids during nanoparticle production. *Applied Surface Science*, 348:4–9, 2015.

[62] F Taccogna, M Dell'Aglio, M Rutigliano, G Valenza, and A De Giacomo. On the growth mechanism of nanoparticles in plasma during pulsed laser ablation in liquids. *Plasma Sources Science and Technology*, 26(4):045002, 2017.

[63] Ana Menendez-Manjon, Jurij Jakobi, Kerstin Schwabe, Joachim K Krauss, and Stephan Barcikowski. Mobility of nanoparticles generated by femtosecond laser ablation in liquids and its application to surface patterning. *JLMN-Journal of Laser Micro/Nanoengineering*, 4(2):95–99, 2009.

[64] Jurij Jakobi, Ana Menéndez-Manjón, Venkata Sai Kiran Chakravadhanula, Lorenz Kienle, Philipp Wagener, and Stephan Barcikowski. Stoichiometry of alloy nanoparticles from laser ablation of ptir in acetone and their electrophoretic deposition on ptir electrodes. *Nanotechnology*, 22(14):145601, 2011.

[65] Alexander Heinemann, Sven Koenen, Kerstin Schwabe, Christoph Rehbock, and Stephan Barcikowski. How electrophoretic deposition with ligand-free platinum nanoparticles affects contact angle. In *Key engineering materials*, volume 654, pages 218–223. Trans Tech Publ, 2015.

[66] Raeyoung Kim, Nari Hong, and Yoonkey Nam. Gold nanograin microelectrodes for neuroelectronic interfaces. *Biotechnology journal*, 8(2):206–214, 2013.

[67] Mohammad Reza Abidian, Joseph M Corey, Daryl R Kipke, and David C Martin. Conducting-polymer nanotubes improve electrical properties, mechanical adhesion, neural attachment, and neurite outgrowth of neural electrodes. *small*, 6(3):421–429, 2010.

[68] Haihan Zhou, Tanyuan Wang, and Yanwen Y Duan. A simple method for amino-functionalization of carbon nanotubes and electrodeposition to modify neural microelectrodes. *Journal of Electroanalytical Chemistry*, 688:69–75, 2013.

[69] Elisa Castagnola, Emma Maggiolini, Luca Ceseracciu, Francesca Ciarpella, Elena Zucchini, Sara De Faveri, Luciano Fadiga, and Davide Ricci. phema encapsulated pedot-pss-cnt microsphere microelectrodes for recording single unit activity in the brain. *Frontiers in Neuroscience*, 10:151, 2016.

[70] Gytis Baranauskas, Emma Maggiolini, Elisa Castagnola, Alberto Ansaldo, Alberto Mazzoni, Gian Nicola Angotzi, Alessandro Vato, Davide Ricci, Stefano Panzeri, and Luciano Fadiga. Carbon nanotube composite coating of neural microelectrodes preferentially improves the multiunit signal-to-noise ratio. *Journal of neural engineering*, 8(6):066013, 2011.

[71] Zongya Zhao, Ruxue Gong, Liang Zheng, and Jue Wang. In vivo neural recording and electrochemical performance of microelectrode arrays modified by rough-surfaced aupt alloy nanoparticles with nanoporosity. *Sensors*, 16(11):1851, 2016.

[72] Hideyuki Nakanishi, Ikuo Kikuta, Satoshi Teraji, Tomohisa Norisuye, and Qui Tran-Cong-Miyata. Effects of nanowire length on charge transport in vertically aligned gold nanowire array electrodes. *Langmuir*, 34(51):15674–15680, 2018.

[73] Edward W Keefer, Barry R Botterman, Mario I Romero, Andrew F Rossi, and Guenter W Gross. Carbon nanotube coating improves neuronal recordings. *Nature nanotechnology*, 3(7):434–439, 2008.

[74] Xinyan Cui, James Wiler, Marta Dzaman, Richard A Altschuler, and David C Martin. In vivo studies of polypyrrole/peptide coated neural probes. *Biomaterials*, 24(5):777–787, 2003.

[75] Valentina Castagnola, Emeline Descamps, Aurélie Lecestre, Lionel Dahan, Jessica Remaud, Lionel G Nowak, and Christian Bergaud. Parylene-based flexible neural probes with pedot coated surface for brain stimulation and recording. *Biosensors and Bioelectronics*, 67:450–457, 2015.

[76] Elisa Castagnola, Alberto Ansaldo, Emma Maggiolini, Gian Nicola Angotzi, Miran Skrap, Davide Ricci, and Luciano Fadiga. Biologically compatible neural interface to safely couple nanocoated electrodes to the surface of the brain. *ACS nano*, 7(5):3887–3895, 2013.

[77] Lei Gao, Jinfen Wang, Shouliang Guan, Mingde Du, Kun Wu, Ke Xu, Liang Zou, Huihui Tian, and Ying Fang. Magnetic actuation of flexible microelectrode arrays for neural activity recordings. *Nano letters*, 19(11):8032–8039, 2019.

[78] Vaijayanthi Ramesh, Christoph Rehbock, Brian Giera, John J Karnes, Jean-Baptiste Forien, Svilen D Angelov, Kerstin Schwabe, Joachim K Krauss, and Stephan Barcikowski. Comparing direct and pulsed-direct current electrophoretic deposition on neural electrodes: deposition mechanism and functional influence. *Langmuir*, 37(32):9724–9734, 2021.

[79] Vaijayanthi Ramesh, Brian Giera, John J Karnes, Nadine Stratmann, Viktor Schaufler, Yao Li, Christoph Rehbock, and Stephan Barcikowski. Solvent composition during electrophoretic deposition of platinum nanoparticles on neural electrode surfaces influences their electrochemical behavior. *Journal of the Electrochemical Society*, 169(LLNL-JRNL-826684), 2022.

[80] Vaijayanthi Ramesh, Nadine Stratmann, Viktor Schaufler, Svilen D Angelov, Ilona D Nordhorn, Hans E Heissler, Ricardo Martínez-Hincapié, Viktor Čolić, Christoph Rehbock, Kerstin Schwabe, et al. Mechanical stability of nano-coatings on clinically applicable electrodes, generated by electrophoretic deposition. *Advanced Healthcare Materials*, 11(23):2102637, 2022.

[81] Ajit Behera, P Mallick, and SS Mohapatra. Nanocoatings for anticorrosion: An introduction. In *Corrosion protection at the nanoscale*, pages 227–243. Elsevier, 2020.

[82] Swapnil L Sonawane, Prakash K Labhane, and Gunvant H Sonawane. Carbon-based nanocomposite membranes for water purification. In *Handbook of Nanomaterials for Wastewater Treatment*, pages 555–574. Elsevier, 2021.

[83] Yasir Beeran Pottathara, Yves Grohens, Vanja Kokol, Nandakumar Kalarikkal, and Sabu Thomas. Synthesis and processing of emerging two-dimensional nanomaterials. In *Nanomaterials synthesis*, pages 1–25. Elsevier, 2019.

[84] Alberto Ansaldo, Elisa Castagnola, Emma Maggiolini, Luciano Fadiga, and Davide Ricci. Superior electrochemical performance of carbon nanotubes directly grown on sharp microelectrodes. *ACS nano*, 5(3):2206–2214, 2011.

[85] Yung-Chan Chen, Hui-Lin Hsu, Yu-Tao Lee, Huan-Chieh Su, Shiang-Jie Yen, Chang-Hsiao Chen, Wei-Lun Hsu, Tri-Rung Yew, Shih-Rung Yeh, Da-Jeng Yao, et al. An active, flexible carbon nanotube microelectrode array for recording electrocorticograms. *Journal of neural engineering*, 8(3):034001, 2011.

[86] WS O'shaughnessy, SK Murthy, DJ Edell, and KK Gleason. Stable biopassive insulation synthesized by initiated chemical vapor deposition of poly (1, 3, 5-trivinyltrimethylcyclotrisiloxane). *Biomacromolecules*, 8(8):2564–2570, 2007.

[87] Roaa Sait, Sridhar Govindarajan, and Richard Cross. Nitridation of optimised tio2 nanorods through pecvd towards neural electrode application. *Materialia*, 4:127–138, 2018.

[88] Elisa Castagnola, Alberto Ansaldo, Luciano Fadiga, and Davide Ricci. Chemical vapour deposited carbon nanotube coated microelectrodes for intracortical neural recording. *physica status solidi (b)*, 247(11-12):2703–2707, 2010.

[89] Christopher AR Chapman, Hao Chen, Marianna Stamou, Juergen Biener, Monika M Biener, Pamela J Lein, and Erkin Seker. Nanoporous gold as a neural interface coating: effects of topography, surface chemistry, and feature size. *ACS applied materials & interfaces*, 7(13):7093–7100, 2015.

[90] Ke Wang, Harvey A Fishman, Hongjie Dai, and James S Harris. Neural stimulation with a carbon nanotube microelectrode array. *Nano letters*, 6(9):2043–2048, 2006.

[91] TD Barbara Nguyen-Vu, Hua Chen, Alan M Cassell, Russell Andrews, Meyya Meyyappan, and Jun Li. Vertically aligned carbon nanofiber arrays: an advance toward electrical–neural interfaces. *Small*, 2(1):89–94, 2006.

[92] Pedro Galvan-Garcia, Edward W Keefer, Fan Yang, Mei Zhang, Shaoli Fang, Anvar A Zakhidov, Ray H Baughman, and Mario I Romero. Robust cell migration and neuronal growth on pristine carbon nanotube sheets and yarns. *Journal of Biomaterials Science, Polymer Edition*, 18(10):1245–1261, 2007.

[93] Zhe Yu, Timothy E McKnight, M Nance Ericson, Anatoli V Melechko, Michael L Simpson, and Barclay Morrison. Vertically aligned carbon nanofiber neural chip for interfacing with neurological system. In *2010 IEEE International Conference on Nano/Molecular Medicine and Engineering*, pages 188–191. IEEE, 2010.

[94] Alex K Shalek, Jacob T Robinson, Ethan S Karp, Jin Seok Lee, Dae-Ro Ahn, Myung-Han Yoon, Amy Sutton, Marsela Jorgolli, Rona S Gertner, Taranjit S Gujral, et al. Vertical silicon nanowires as a universal platform for delivering biomolecules into living cells. *Proceedings of the National Academy of Sciences*, 107(5):1870–1875, 2010.

[95] Woong Kim, Jennifer K Ng, Miki E Kunitake, Bruce R Conklin, and Peidong Yang. Interfacing silicon nanowires with mammalian cells. *Journal of the American Chemical Society*, 129(23):7228–7229, 2007.

[96] Kumaravelu Ganesan, David J Garrett, Arman Ahnood, Mohit N Shivdasani, Wei Tong, Ann M Turnley, Kate Fox, Hamish Meffin, and Steven Prawer. An all-diamond, hermetic electrical feedthrough array for a retinal prosthesis. *Biomaterials*, 35(3):908–915, 2014.

[97] Mohamed Ismail Ma, Raghavendra Babu Bb, Arivanandhan Ma, and Jayavel Ra. Rapidly emerging aspects & future r&d directions for supercapacitor. *Smart Supercapacitors: Fundamentals, Structures, and Applications*, page 137, 2022.

[98] Shaurya Prakash and Junghoon Yeom. *Nanofluidics and microfluidics: systems and applications*. William Andrew, 2014.

[99] Mingyu Ryu, Jae Hoon Yang, Yumi Ahn, Minkyung Sim, Kyung Hwa Lee, Kyungsoo Kim, Taeju Lee, Seung-Jun Yoo, So Yeun Kim, Cheil Moon, et al. Enhancement of interface characteristics of neural probe based on graphene, zno nanowires, and conducting polymer pedot. *ACS applied materials & interfaces*, 9(12):10577–10586, 2017.

[100] JM Corey, BC Wheeler, and GJ Brewer. Micrometer resolution silane-based patterning of hippocampal neurons: critical variables in photoresist and laser ablation processes for substrate fabrication. *IEEE transactions on Biomedical Engineering*, 43(9):944–955, 1996.

[101] Christopher R Jenney and James M Anderson. Effects of surface-coupled polyethylene oxide on human macrophage adhesion and foreign body giant cell formation in vitro. *Journal of biomedical materials research*, 44(2):206–216, 1999.

[102] Emanuele Ostuni, Robert G Chapman, R Erik Holmlin, Shuichi Takayama, and George M Whitesides. A survey of structure- property relationships of surfaces that resist the adsorption of protein. *Langmuir*, 17(18):5605–5620, 2001.

[103] Rahul Singhvi, Amit Kumar, Gabriel P Lopez, Gregory N Stephanopoulos, Daniel IC Wang, George M Whitesides, and Donald E Ingber. Engineering cell shape and function. *Science*, 264(5159):696–698, 1994.

[104] Emanuele Ostuni, Bartosz A Grzybowski, Milan Mrksich, Carmichael S Roberts, and George M Whitesides. Adsorption of proteins to hydrophobic sites on mixed self-assembled monolayers. *Langmuir*, 19(5):1861–1872, 2003.

[105] Yan-Yeung Luk, Mihoko Kato, and Milan Mrksich. Self-assembled monolayers of alkanethiolates presenting mannitol groups are inert to protein adsorption and cell attachment. *Langmuir*, 16(24):9604–9608, 2000.

[106] Tingting Zhang, Jackie L Stilwell, Daniele Gerion, Lianghao Ding, Omeed Elboudwarej, Patrick A Cooke, Joe W Gray, A Paul Alivisatos, and Fanqing Frank Chen. Cellular effect

of high doses of silica-coated quantum dot profiled with high throughput gene expression analysis and high content cellomics measurements. *Nano letters*, 6(4):800–808, 2006.

[107] Claire Wyart, Christophe Ybert, Laurent Bourdieu, Catherine Herr, Christelle Prinz, and Didier Chatenay. Constrained synaptic connectivity in functional mammalian neuronal networks grown on patterned surfaces. *Journal of neuroscience methods*, 117(2):123–131, 2002.

[108] L Kam, W Shain, JN Turner, and R Bizios. Axonal outgrowth of hippocampal neurons on micro-scale networks of polylysine-conjugated laminin. *Biomaterials*, 22(10):1049–1054, 2001.

[109] Stephan Rohr, Regula Flückiger-Labrada, and Jan P Kucera. Photolithographically defined deposition of attachment factors as a versatile method for patterning the growth of different cell types in culture. *Pflügers Archiv*, 446:125–132, 2003.

[110] Zhen Zhang, Yu Fu, Wei Yu, Xiaoyun Qin, Zhenjie Xue, Yan Liu, Dan Luo, Cong Yan, Xiaohua Sun, and Tie Wang. Dynamically regulated ag nanowire arrays for detecting molecular information of substrate-induced stretched cell growth. *Advanced Materials*, 28(43):9589–9595, 2016.

[111] Chong Xie, Lindsey Hanson, Wenjun Xie, Ziliang Lin, Bianxiao Cui, and Yi Cui. Noninvasive neuron pinning with nanopillar arrays. *Nano letters*, 10(10):4020–4024, 2010.

[112] Yixiao Cai, Fredrik Edin, Zhe Jin, Andrei Alexsson, Olafur Gudjonsson, Wei Liu, Helge Rask-Andersen, Mikael Karlsson, and Hao Li. Strategy towards independent electrical stimulation from cochlear implants: Guided auditory neuron growth on topographically modified nanocrystalline diamond. *Acta biomaterialia*, 31:211–220, 2016.

[113] TD Barbara Nguyen-Vu, Hua Chen, Alan M Cassell, Russell J Andrews, M Meyyappan, and Jun Li. Vertically aligned carbon nanofiber architecture as a multifunctional 3-d neural electrical interface. *IEEE Transactions on Biomedical Engineering*, 54(6):1121–1128, 2007.

[114] Matthew J Dalby, Nikolaj Gadegaard, Mathis O Riehle, Chris DW Wilkinson, and Adam SG Curtis. Investigating filopodia sensing using arrays of defined nano-pits down to 35 nm diameter in size. *The international journal of biochemistry & cell biology*, 36(10):2005–2015, 2004.

[115] Matthew J Dalby, Manus JP Biggs, Nikolaj Gadegaard, Gabriela Kalna, Chris DW Wilkinson, and Adam SG Curtis. Nanotopographical stimulation of mechanotransduction and changes in interphase centromere positioning. *Journal of cellular biochemistry*, 100(2):326–338, 2007.

[116] Junyan Yang and David C Martin. Microporous conducting polymers on neural microelectrode arrays: I electrochemical deposition. *Sensors and actuators B: Chemical*, 101(1-2):133–142, 2004.

[117] Hong-Bo Zhou, Gang Li, Xiao-Na Sun, Zhuang-Hui Zhu, Qing-Hui Jin, Jian-Long Zhao, and Qiu-Shi Ren. Integration of au nanorods with flexible thin-film microelectrode arrays for improved neural interfaces. *Journal of microelectromechanical systems*, 18(1):88–96, 2009.

[118] T Chung, JQ Wang, J Wang, B Cao, Y Li, and SW Pang. Electrode modifications to lower electrode impedance and improve neural signal recording sensitivity. *Journal of neural engineering*, 12(5):056018, 2015.

[119] Erkin Seker, Yevgeny Berdichevsky, Matthew R Begley, Michael L Reed, Kevin J Staley, and Martin L Yarmush. The fabrication of low-impedance nanoporous gold multiple-electrode arrays for neural electrophysiology studies. *Nanotechnology*, 21(12):125504, 2010.

[120] Parvaneh Mokarian-Tabari, Catalina Vallejo-Giraldo, Marc Fernandez-Yague, Cian Cummins, Michael A Morris, and Manus JP Biggs. Nanoscale neuroelectrode modification via sub-20 nm silicon nanowires through self-assembly of block copolymers. *Journal of Materials Science: Materials in Medicine*, 26:1–5, 2015.

[121] Alessandra Fabbro, Denis Scaini, Veronica Leon, Ester Vázquez, Giada Cellot, Giulia Privitera, Lucia Lombardi, Felice Torrisi, Flavia Tomarchio, Francesco Bonaccorso, et al. Graphene-based interfaces do not alter target nerve cells. *ACS nano*, 10(1):615–623, 2016.

[122] Bozhi Tian, Jia Liu, Tal Dvir, Lihua Jin, Jonathan H Tsui, Quan Qing, Zhigang Suo, Robert Langer, Daniel S Kohane, and Charles M Lieber. Macroporous nanowire nanoelectronic scaffolds for synthetic tissues. *Nature materials*, 11(11):986–994, 2012.

[123] Dmitry B Suyatin, Lars Wallman, Jonas Thelin, Christelle N Prinz, Henrik Jörntell, Lars Samuelson, Lars Montelius, and Jens Schouenborg. Nanowire-based electrode for acute in vivo neural recordings in the brain. *PLoS One*, 8(2):e56673, 2013.

[124] Robinson JT Jorgolli M Shalek AK and MH Yoon. Gertner rs park h. vertical nanowire electrode arrays as a scalable platform for intracellular interfacing to neuronal circuits. *Nat. Nanotechnol*, 7:180–184, 2012.

[125] Deepak Rawtani and Yadvendra K Agrawal. Emerging strategies and applications of layer-by-layer self-assembly. *Nanobiomedicine*, 1:8, 2014.

[126] Sudhanshu Srivastava and Nicholas A Kotov. Composite layer-by-layer (lbl) assembly with inorganic nanoparticles and nanowires. *Accounts of chemical research*, 41(12):1831–1841, 2008.

[127] Huanan Zhang, Jimmy Shih, Jian Zhu, and Nicholas A Kotov. Layered nanocomposites from gold nanoparticles for neural prosthetic devices. *Nano letters*, 12(7):3391–3398, 2012.

[128] Edward Jan, Jeffrey L Hendricks, Vincent Husaini, Sarah M Richardson-Burns, Andrew Sereno, David C Martin, and Nicholas A Kotov. Layered carbon nanotube-polyelectrolyte electrodes outperform traditional neural interface materials. *Nano letters*, 9(12):4012–4018, 2009.

[129] Edward Jan and Nicholas A Kotov. Successful differentiation of mouse neural stem cells on layer-by-layer assembled single-walled carbon nanotube composite. *Nano letters*, 7(5):1123–1128, 2007.

[130] Kay Hyeok An, Won Seok Kim, Young Soo Park, Young Chul Choi, Seung Mi Lee, Dong Chul Chung, Dong Jae Bae, Seong Chu Lim, and Young Hee Lee. Supercapacitors using single-walled carbon nanotube electrodes. *Advanced Materials*, 13(7):497–500, 2001.

[131] DN Futaba, K Hata, T Yamada, T Hiraoka, and Y Haramizu. Y. kakudate, o. tanaike, h. hatori, m. yumura, s. iijima. *Nat. Mater*, 5:987, 2006.

[132] Muhammed K Gheith, Todd C Pappas, Anton V Liopo, Vladimir A Sinani, Bong Sup Shim, Massoud Motamedi, James P Wicksted, and Nicholas A Kotov. Stimulation of neural cells by lateral currents in conductive layer-by-layer films of single-walled carbon nanotubes. *Advanced Materials*, 18(22):2975–2979, 2006.

3 Influence of EPD Applied Electric Fields on the Platinum Nanoparticle Deposition

Published in Langmuir 37 (2021) 9724-9734

Comparing Direct and Pulsed-Direct Current Electrophoretic Deposition on Neural Electrodes: Deposition Mechanism and Functional Influence

Vaijayanthi Ramesh[1], Christoph Rehbock[1], Brian Giera[2], John J. Karnes[2], Jean-Baptiste Forien[2], Svilen D. Angelov[3], Kerstin Schwabe[3], Joachim K. Krauss[3], and Stephan Barcikowski[1,*]

[1] Institute of Technical Chemistry I, University of Duisburg-Essen and Center for Nanointegration Duisburg-Essen (CENIDE), Essen, Germany

[2] Center for Engineered Materials and Manufacturing, Lawrence Livermore National Laboratory, California, USA

[3] Department of Neurosurgery, Hannover Medical School, Hannover, Germany

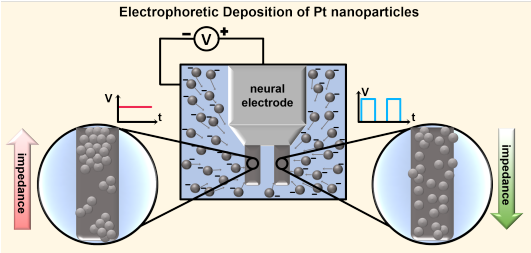

Summary:

The established 2D EPD parameters such as electric field strength, electric field type, deposition time, and colloid concentrations were varied and further optimized for them to be appropriate on 3D surfaces through preliminary experiments. However, a systematic investigation of the parameter comparison was required to determine its influence on the impedance tuning. Therefore in this section, the EPD of laser-generated PtNPs using DC- and PDC-fields were studied. It was observed that the PDC EPD produced more homogeneously distributed depositions of PtNPs on 3D neural electrodes compared to the DC EPD. The electroosmotic- and electrohydrodynamic flows were believed to govern the aggregation of NPs on the surfaces. The electrode impedance was measured in vitro, and a significant lowering was observed for PDC samples.

Author contributions:

Design of experiments and studies on EPD of NPs on 3D surfaces including their characterization were performed by VR. Numerical simulation experiments and data curation were done by BG and JJK. The impedance measurements on coated electrodes were performed by SDA. The original manuscript draft was prepared by VR. The review and editing of the manuscript were carried out by VR, CR, BG, JJK, SDA, KS, JKK, and SB. SB and CR designed the study, and supervised and promoted the collaboration between the institutions.

LANGMUIR

pubs.acs.org/Langmuir Article

Comparing Direct and Pulsed-Direct Current Electrophoretic Deposition on Neural Electrodes: Deposition Mechanism and Functional Influence

Vaijayanthi Ramesh, Christoph Rehbock, Brian Giera, John J. Karnes, Jean-Baptiste Forien, Svilen D. Angelov, Kerstin Schwabe, Joachim K. Krauss, and Stephan Barcikowski*

Cite This: *Langmuir* 2021, 37, 9724–9734 Read Online

ACCESS | Metrics & More | Article Recommendations | Supporting Information

ABSTRACT: Electrophoretic deposition (EPD) of platinum nanoparticles (PtNPs) on platinum–iridium (Pt–Ir) neural electrode surfaces is a promising strategy to tune the impedance of electrodes implanted for deep brain stimulation in various neurological disorders such as advanced Parkinson's disease and dystonia. However, previous results are contradicting as impedance reduction was observed on flat samples while in three-dimensional (3D) structures, an increase in impedance was observed. Hence, defined correlations between coating properties and impedance are to date not fully understood. In this work, the influence of direct current (DC) and pulsed-DC electric fields on NP deposition is systematically compared and clear correlations between surface coating homogeneity and *in vitro* impedance are established. The ligand-free NPs were synthesized via pulsed laser processing in liquid, yielding monomodal particle size distributions, verified by analytical disk centrifugation (ADC). Deposits formed were quantified by UV–vis supernatant analysis and further characterized by scanning electron microscopy (SEM) with semiautomated interparticle distance analyses. Our findings reveal that pulsed-DC electric fields yield more ordered surface coatings with a lower abundance of particle assemblates, while DC fields produce coatings with more pronounced aggregation. Impedance measurements further highlight that impedance of the corresponding electrodes is significantly reduced in the case of more ordered coatings realized by pulsed-DC depositions. We attribute this phenomenon to the higher active surface area of the adsorbed NPs in homogeneous coatings and the reduced particle–electrode electrical contact in NP assemblates. These results provide insight for the efficient EPD of bare metal NPs on micron-sized surfaces for biomedical applications in neuroscience and correlate coating homogeneity with *in vitro* functionality.

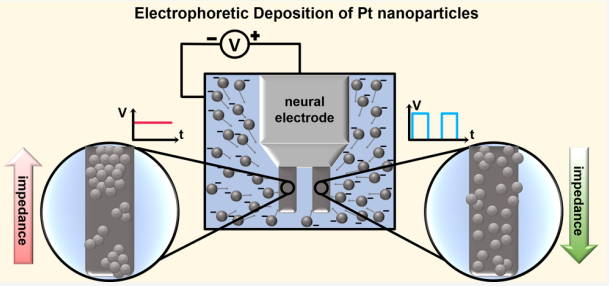

INTRODUCTION

Electrophoretic deposition (EPD) is the process wherein charged colloidal particles accumulate on target surfaces due to an external electric field.[1−5] EPD is a versatile technique, benefiting from simple experimental setups and relatively rapid deposition of thick coatings on arbitrarily complex targets[6−8] and also sub-monolayer coatings.[9] EPD was first performed nearly a century ago, depositing thoria particles onto platinum (Pt) surfaces,[2] and since has been used in a wide range of applications. EPD is central to processing advanced ceramics,[6,10] oxygen sensing devices,[11] biomaterials,[12] energy storage devices,[13] electrophoretic displays,[14] and various other fields. Biomedical applications for EPD include carbon nanotube coatings and antibacterial coatings for implants,[15] coatings on drug delivery systems,[16] biosensors,[17] etc. Metal nanoparticles (NPs) deposited through EPD on various surfaces are used in the fields of catalysis,[18] memory devices and semiconductors,[19] and solar cells.[20] In this context, the EPD of metal NPs can also be applied to implants such as neural electrodes.[9,21,22] Deep brain stimulation delivering electrical pulses to the thalamus and various basal ganglia nuclei via implanted electrodes has become an established treatment option for movement disorders such as Parkinson's disease.[23] To improve their long-term efficiency and to avoid impedance increase over time, the electrodes' surface properties can be improved using sub-monolayer NP depositions.[22] In particular, electrochemically active surface area, impedance, and wettability of the surfaces can be controlled by the EPD of PtNPs on Pt electrodes.[9] Ongoing efforts to improve the neural electrode efficiency by surface modification include increasing the surface roughness by laser patterning,[24,25] application of porous coatings,[26,27] and deposition of "nano-

Received: April 20, 2021
Revised: July 25, 2021
Published: August 6, 2021

https://doi.org/10.1021/acs.langmuir.1c01081
Langmuir 2021, 37, 9724–9734

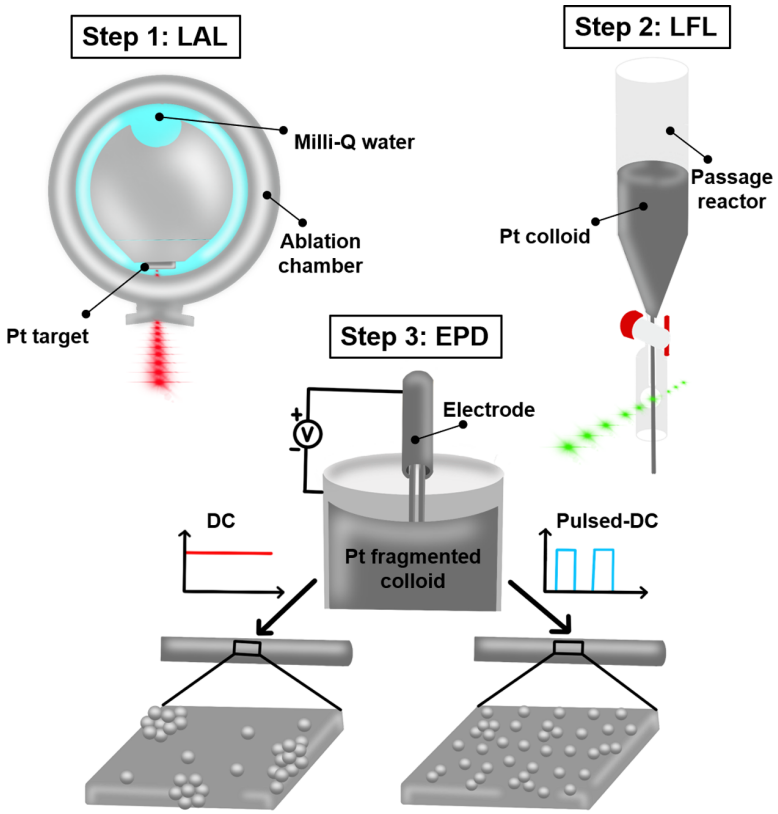

Figure 1. Schematic representation of the experimental workflow.

grass"[28] or "nanorods"[29] on the electrode surface. However, most of these designs involve dissimilar substrate and coating materials, which could pose difficulties during regulatory approval for testing in human patients.[26] Additionally, these manufacturing processes involve multiple stages, which increases the production time.[27,29] EPD stands out, production-wise, offering a relatively simple setup, fast production cycles, and batch processing of electrodes.

Although EPD is a straightforward technique requiring only a colloidal suspension and a working electrode, the properties of the final deposit may be tuned to benefit the application. These properties depend strongly on the interplay between system parameters like colloid concentration, deposition time, electric field strength, deposition media composition, and field variation.[7,8] Neirinck et al. and Hirata et al. found that the EPD yield of alumina powders was directly proportional to the deposition time.[30,31] Doungdaw et al. performed EPD with different suspension concentrations and found that the deposit weight increased with highly concentrated suspension at higher voltages and deposition times.[32] Acevedo-Peña et al. found that the TiO_2 deposit thickness scaled with the applied electric field and concluded that the applied field has a greater influence on the deposit formation compared to the other parameters.[33] These relationships were experimentally verified by Sarkar and Nicholson, where they have implicated an agreement between the experimental data and the existing theory.[34]

Direct current (DC) EPD usually produces thick inhomogeneous deposits, presumably due to water electrolysis and the evolution of hydrogen bubbles near the target electrode.[6,10] Uchikoshi et al. circumvent these issues using palladium electrodes that readily absorb evolved hydrogen gas, thereby increasing coating homogeneity.[10] Besra et al. used pulsed-DC to produce bubble-free deposits and carried out EPD in organic media to obtain high-quality deposits.[2,6,7] Furthermore, it is widely known that in aqueous EPD, electrohydrodynamic (EHD)[5] and electroosmotic flows (EOF)[4] at the surface−solvent interface affect NP deposition and favor the formation of NP assemblates. One way to circumvent this mechanism is the utilization of alternating current (AC) or pulsed-DC fields during EPD. In the case of pulsed-DC fields cycling, the pulses on and off may resuspend deposited particles during the off state and deposit them at different locations during the subsequent on state, resulting in more homogeneous deposits.[35] Although organic EPD media are preferred in certain applications, the availability and environmental compatibility of water, especially for biomedical applications, makes it the most sought-after solvent.[2] Therefore, to use water as a solvent and at the same time avoid the discrepancies mentioned earlier, AC and pulsed-DC fields could be used.[3] However, such effects were mostly studied in microparticle suspensions yielding deposits in the microgram range.[6,7,33,36−38] Therefore, it would be highly interesting to study the effects of DC and pulsed-DC fields on an NP scale producing sub-monolayer coverages.

To the best of our knowledge, the effect of applied electric fields in metal-on-metal EPD systems for implant coatings has been far less investigated. Our own previous work examined the impedance of Pt neural stimulation electrodes coated with PtNPs via DC-EPD. Sub-monolayer NP coverage was observed, which helped to increase the activity of the surface through deposition of oxidized and highly charged particles;[9]

https://doi.org/10.1021/acs.langmuir.1c01081
Langmuir 2021, 37, 9724−9734

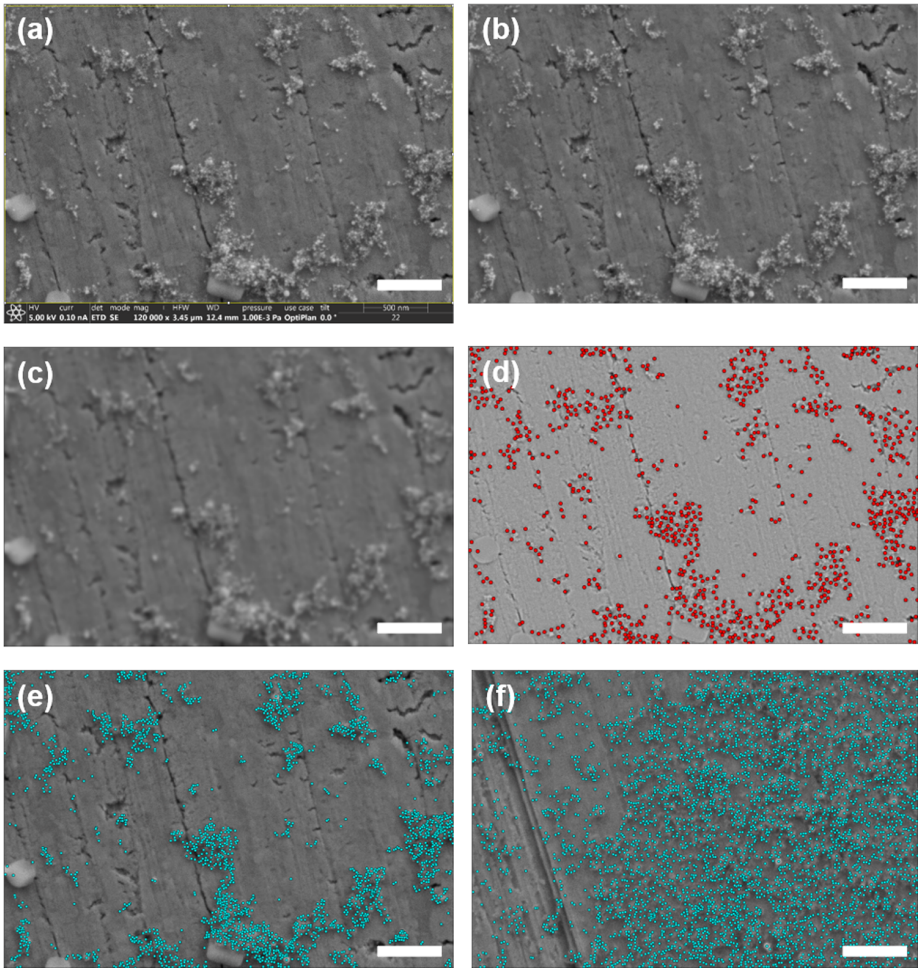

Figure 2. Sequence of processing steps to find the coordinates of particles by denoizing a ROI (yellow selection in (a)) via (b) median and (c) Gaussian filtering. (d) ImageJ's *Find Maxima* function is applied to the result of dividing (b) by (c) to find the particles (red dots). Experts rectify false-positives and false-negatives near cracks/scratches in the electrode and dense clusters, respectively, to locate particle coordinates (cyan) in (e) DC and (f) pulsed-DC experiments. Scale bar: 500 nm. (Please note that (a–e) represent the same image to illustrate the image analysis process while (f) constitutes a different example of an image analyzed by the same approach.)

however, their measured impedance values revealed contradicting results.[22] While PtNPs deposited on Pt-sputtered flat targets revealed a reduction of impedance with increasing particle surface coverage, these results were not transferable to three-dimensional (3D) electrodes. Here impedance increased *in vitro*, while it remained stable under *in vivo* conditions.[9,22] Hence, a systematic investigation of the EPD process for 3D electrodes has not been done to date and is presented in this work (see Figure 1), with emphasis on the differences between DC and pulsed-DC depositions for metal–metal NP EPD with sub-monolayer coverage in an aqueous medium.

MATERIALS AND METHODS

Nanoparticle Generation. Ligand-free PtNPs were synthesized by pulsed laser ablation in liquid (LAL)[39] of a platinum target (10 × 10 × 1 mm^3) in ultrapure water using an Nd:YAG laser (Ekspla, Atlantic series, 10 ps, 1064 nm, 9.6 mJ, 100 kHz) by means of a custom-made ablation chamber (described elsewhere in more detail[21,22]) for 5 min yielding about 500 μg/mL colloid mass concentration. The laser beam was focused using an F-theta lens (f = 113 mm) and directed onto the target using a galvoscanner (Scan Lab, SCANcube 10) scanning a 6 mm spiral pattern. The ablated colloidal PtNPs acted as educt for the pulsed laser fragmentation in liquid (LFL) process performed in a custom-made passage reactor (described in detail elsewhere[40]). The passage reactor was filled with educt colloid and fragmented using a nanosecond laser (Innolas, Spitlight, 9 ns, 532 nm, 84 mJ, 100 Hz, 1.5 J/cm^2). The fragmented colloids were used for EPD after dilution to a concentration of about 100 μg/mL using ultrapure water and adjustment to a pH of 11. The ionic strength of the colloids was 0.035 × 10^{-3} mol/L, equivalent to a Debye screening length of 52 nm in DLVO-based particle interaction models.

The absorbance of PtNPs was measured by a UV–vis extinction spectrometer (Thermo Scientific, Evolution 201) in the wavelength range of 190–900 nm using a quartz cuvette with a path length of 10 mm. The hydrodynamic diameter of the colloids was determined using an analytical disk centrifuge (ADC, CPS Instrument DC 24000 UHR) at 22 000 rpm. The measurement was based on sedimentation of particles through a sucrose sugar gradient and their time-dependent detection at 405 nm. Dispersion states of PtNPs were characterized from the obtained UV–vis spectra using an approach pioneered by Furlong et al.,[41] which is well established for laser-generated colloids (for Pt[42] and CoFeOx[43]). Furlong slopes (S) were determined using eq 1, where A represents the absorbance and λ represents the wavelength range from UV–vis spectroscopy measurements.

https://doi.org/10.1021/acs.langmuir.1c01081
Langmuir 2021, 37, 9724–9734

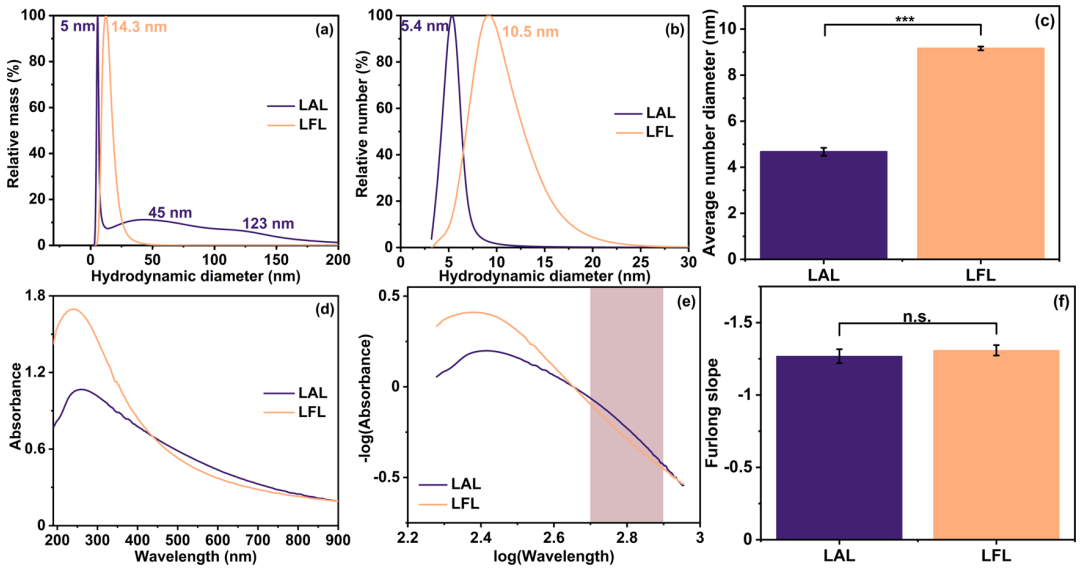

Figure 3. (a) Peak-normalized hydrodynamic weight distribution of PtNPs after LAL and LFL; (b) peak-normalized hydrodynamic number distribution of PtNPs after LAL and LFL; (c) average-number peak diameters before and after LFL (N = 5, p = 0.05); (d) UV−vis absorbance spectra of LAL and LFL Pt colloids; (e) Furlong curves derived by plotting −log(absorbance) vs log(wavelength) from the UV−vis data; and (f) average Furlong slope values of LAL and LFL colloids showing no significant change in particle size in both the groups (N = 5, α = 0.05).

$$S = \frac{-d \log A}{d \log \lambda} \quad (1)$$

The corresponding UV−vis spectra were normalized to 450 nm and −log(normalized absorbance) vs log(wavelength) was plotted to obtain the Furlong curves (Figure S4). These curves were linearly fitted for the x-axis values between 2.7 and 2.9 (corresponding to a wavelength range of 500−800 nm) and their slope values were determined. The obtained Furlong slope values give an indirect insight on the size changes occurring in the colloids, where the slope change is indirectly proportional to the particle size change (the S value of an ideal Rayleigh scattered particle would be −4 according to the formula, $I \propto \lambda^{-4}$).

Electrophoretic Deposition. Neural electrodes were prepared by the parallel assembly of two PTFE-isolated platinum−iridium (Pt−Ir, 90:10) wires (Science Products GmbH, Germany) having a diameter of 0.055 mm at a distance of about 0.25 mm and inserted into a hollow stainless steel tube cut from 24G syringe needle. Electrical contacts were established by soldering plug pins to the ends of the wires. The electrodes were precleaned by immersion in 65% nitric acid for 15 min, followed by rinsing with distilled water. EPD onto these samples was carried out using a custom-made EPD chamber (described in ref 9) and application of either DC or pulsed-DC electric fields. The positive pole of the power supply was connected to the electrodes and the negative pole to the surrounding metal ring (acting as a counter electrode). The chamber was filled with 600 μL of Pt colloid (with a ζ-potential of −62 mV and pH of 11), which was then deposited onto the Pt−Ir samples. DC depositions were carried out at 5 V/cm for 5 min and pulsed-DC depositions at 5 V/cm, 1 μs period, and 50% duty cycle for 10 min. The colloid was magnetically stirred during deposition to avoid particle sedimentation. It is to be noted that the above-mentioned EPD parameters were preoptimized by varying the electric field strength, deposition time, colloid concentration, and pH. After coating, the supernatant was characterized using UV−vis spectroscopy to determine the deposited mass and Furlong slopes. Here, we quantified the area under the curve (AUC) in a spectral range from 190 to 900 nm and used Pt colloids with known mass concentrations for calibration (Figure S3). Furlong slopes of supernatant colloid were calculated to detect particle size changes after EPD. Scanning electron microscopy (SEM, Thermo Fisher Scientific, Apreo S LoVac) images of coated and uncoated Pt−Ir samples were collected (operating voltage: 5 kV) and further analyzed to quantify the spatial distribution of deposited particles.

Impedance Measurements. *In vitro* impedance measurements on electrodes, before and after coating with DC and pulsed-DC fields, were performed by immersing the electrodes into 0.9% NaCl electrolyte solution and applying a sinusoidal voltage of 200 mV p−p (circuit diagram explained previously in ref 22). The voltage drop across the resistor was amplified and the impedance across the electrode was calculated using Ohm's law. Measurements were performed at a single frequency of 200 Hz (as this frequency value closely resembles the clinical stimulation value of 130−180 Hz[23]). As a control group, the samples immersed in Milli-Q water (without particles) and exposed to the corresponding pulsed-DC field were measured. Short-term *in vitro* stimulation was performed to test whether impedance values remain stable. One-way analysis of variance (ANOVA) statistical evaluations was performed on the data followed by Tukey's test. The p-value was set to 0.05, and the obtained probability values less than the set p-value were considered to be statistically significant.

Particle Coordinates and SEM Image Analyses. To extract particle x−y coordinates from SEM images, we developed and implemented a semiautomated procedure using the open-sourced image analysis software ImageJ[44] and in-house code. This semi-automated protocol locates the centers of deposited particles and calculates the center−center distances between each possible pair of particles. Subsequently, the nearest-neighbor (NN) distances and local particle arrangements ($g(r)$) were analyzed. Figure 2 shows each step of this algorithm. We first crop out instrumentation overlay and several pixels from the edge of the 16-bit images to eliminate artifacts. The edge regions are 3−5 pixels wide and colored yellow (Figure 2a). Although small, we found that removal of these edges is critical for the success of later steps. This trimmed region of interest (ROI) is then used to generate two new images. First, the ROI is processed with a two-pixel radius median filter that removes noise while preserving the edge features by replacing each pixel with the median value of the neighboring pixels (Figure 2b). A second image is generated by applying a Gaussian blur filter to the original trimmed ROI. This filter uses a Gaussian smoothing function with a standard deviation of 10 pixels; the results of this filtering are shown in Figure 2c. We then divide the median filtered image by the Gaussian blur filtered image to

https://doi.org/10.1021/acs.langmuir.1c01081
Langmuir 2021, 37, 9724−9734

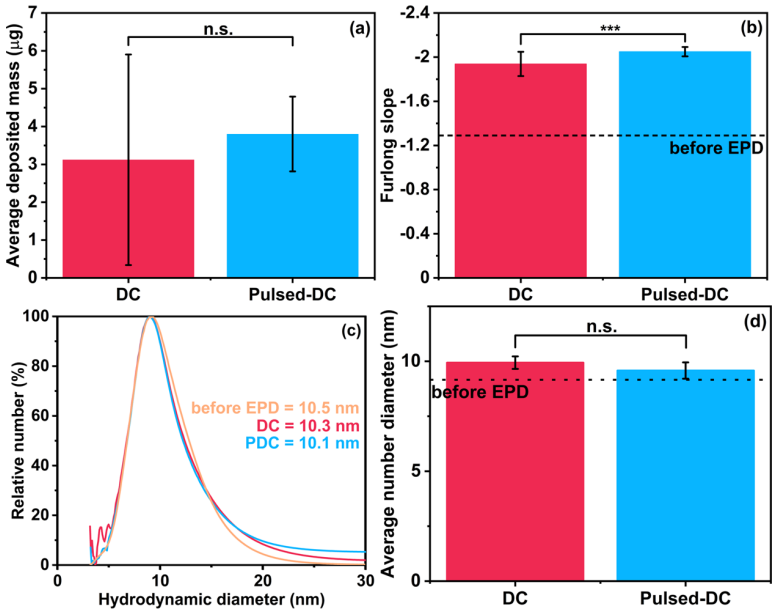

Figure 4. (a) Average deposited mass of NPs on electrode surfaces via DC and pulsed-DC depositions (N = 15, p = 0.05); (b) Furlong slopes of the supernatant colloid before (dashed line) and after EPD (N = 15, p = 0.05); (c) peak-normalized hydrodynamic number distribution of the supernatant colloid after DC and pulsed-DC-EPD; and (d) average-number peak diameters of the supernatant colloids before (dashed line) and after EPD (N = 5, α = 0.05).

enhance edge detection and apply ImageJ's *Find Maxima* function to the result in Figure 2d using prominence values between 0.15 and 0.2.

Of the three parameters governing this algorithm (i.e., median radius, Gaussian blur standard deviation, and prominence), prominence is the most sensitive and sets the "shoulder length" of pixel intensity contours. We chose a value that minimizes the amount of false-positives, which typically cluster around defects in the substrate (e.g., scratches) present in the SEM images. We then manually inspect the algorithm's output as in Figure 2d to correct any false-positive or false-negative before recording the list of particle coordinates. Figure 2e,f shows the final particle coordinates of DC and pulsed-DC experiments, as determined by experts. We also explored ImageJ's machine learning implementation that performs a tertiary classification that prompts a user for regions of (1) particles, (2) background, and (3) scratches. However, for our SEM images, this approach did not generalize across all of our images nor sufficiently reduce false-positive/negative particle detection to eliminate the need for manual inspection. ImageJ software then exports the positions of all detected particles as a list of x−y coordinates.

RESULTS AND DISCUSSION

To reduce the impedance of neural electrodes, we deposited colloidal PtNPs obtained from the laser-based synthesis in solution onto Pt−Ir surfaces. Since Angelov et al. found that 10 nm particles stabilized *in vivo* impedance values more than their counterparts with larger diameters,[22] we used ∼10 nm particles in this study. Figure 3 shows the size distributions of colloids measured via ADC and absorption spectra measured using UV−vis spectroscopy.

In ADC, the LAL-generated colloids (Figure 3a) showed peaks at 5, 45, and 120 nm diameters. Such multimodal particle size distributions were previously observed by Nichols et al., ablating Pt in water at a wavelength of 355 nm.[45] Shih et al. explained based on computational studies during ablation of a silver target placed in water that multimodal size distributions are closely linked to early-stage formation mechanisms in LAL and are hence often found experimentally.[46] Therefore, pulsed LFL was subsequently performed to obtain a monomodal size distribution of about 10 nm as shown in mass (Figure 3a) and number-weighted (Figure 3b) distributions. Laser fragmentation of noble-metal colloids usually results in diameters less than 10 nm;[40,47] however, in such studies, the educt concentrations were 7.5,[47] 10,[48] or 130−170 μg/mL,[42] which are considerably lower than our educt concentration of ∼500 μg/mL. In such highly concentrated colloids, particle growth could occur in the form of coalescence or Ostwald ripening.[42] Coalescence is the growth of particles caused by diffusion due to bombardment,[49] whereas Ostwald ripening is the dissolution of one particle and redepositing on a larger particle, inducing growth.[50,51] Jendrzej et al. showed the growth of ligand-free PtNPs stored at room temperatures and suggested that storing the colloids at lower temperatures might prevent their growth.[42] Therefore, our samples were stored at temperatures around 10 °C and we could show that there was no significant growth in particle sizes even after 2 months of storage (Figure S2). As a result, the shift in peak diameter value of the smallest mode from 5 nm after LAL to 10 nm after LFL is attributed to an overlap between the original 5 nm particles (which would be unaffected by the laser pulse due to their low extinction coefficients[52]) mixed with the fragmented products of the larger particles in Figure 3b,c.

Figure 3d shows the UV−vis absorbance of colloids after LAL and LFL. The absorbance peak at 250 nm is derived from Pt^+ complexes and can be correlated with the surface oxidation of PtNPs due to laser ablation in deionized water.[9,45] Since LFL colloids have a higher absorbance peak than LAL colloids, it implies increased surface oxidation, which, in turn, increases the surface charges around NPs, making them more electrostatically stable and resistant to ripening.[48] Furlong slopes of the colloids in Figure 3e were determined by best fit for the slope of a −log(UV−vis absorbance) vs log(wavelength) plot and give an indirect measure of particle size change in colloidal systems. Interestingly, Furlong slopes are stable during the

https://doi.org/10.1021/acs.langmuir.1c01081
Langmuir 2021, 37, 9724−9734

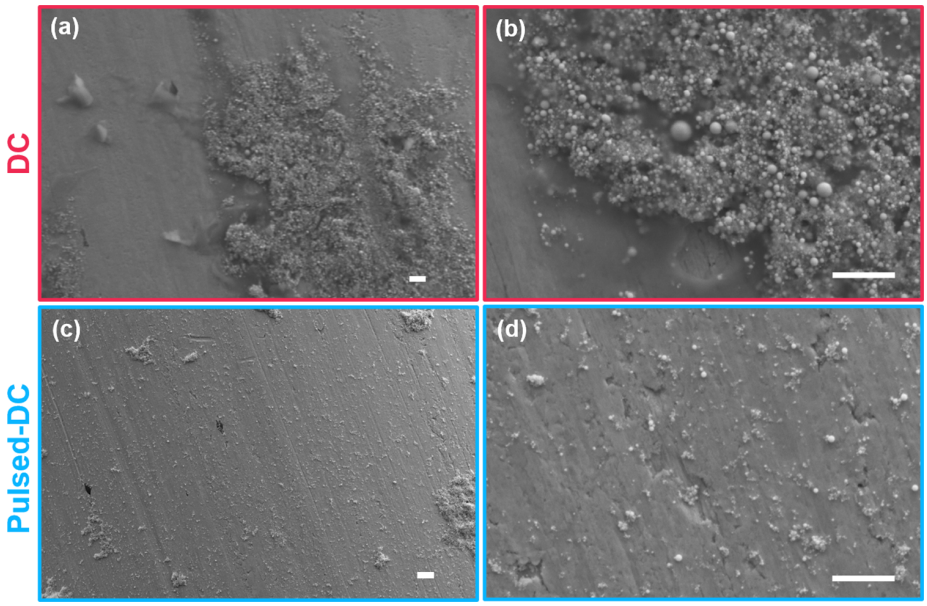

Figure 5. SEM images of PtNPs deposited on Pt−Ir samples using (a, b) DC and (c, d) pulsed-DC electric fields showing deposition behavior at (a, c) lower and (b, d) higher magnifications. Scale bar: 500 nm.

fragmentation process, which seems to indicate no pronounced changes in the aggregation state due to the fragmentation process.

EPD is commonly used for depositing powders, ceramic particles, etc.[53] Due to the large surface area of targets and the need for thick deposit coverage, the yield obtained is in the scale of micrograms or more and measured directly by weighing the target.[6,33,38] However, in the case of NP depositions producing a sub-monolayer coverage on relatively much smaller surface areas, weighing the targets is an unsuitable assessment method. Therefore, indirect yield determinations using UV−vis spectroscopy measurements have been performed in this work. To study the impact of the applied electric field on the used Pt colloids, the supernatants after EPD were analyzed.

Figure 4a compares the average deposited mass of NPs after EPD in DC and pulsed-DC fields. Depositions in DC fields show a slightly reduced yield compared to those in pulsed-DC fields. Notably, error bars are considerably higher in DC-based deposition in contrast to pulsed-DC, which seems to indicate a low reproducibility of the procedure when DC fields are used (SEM images supporting the statement are shown in Figure S5). Although deposition under pulsed-DC fields is more reproducible than DC fields (indicated by smaller error bar), the difference in the total deposited masses is statistically insignificant. Absolute Furlong slope values of the supernatants after EPD in Figure 4b increase for both DC and pulsed-DC supernatants, indicating a narrowed distribution, i.e., colloidal nanoparticles have reduced amount of hydrodynamic aggregates or agglomerates after the EPD procedure was applied. This effect was significantly higher in pulsed-DC than in DC supernatants. However, ADC measurements of the supernatants in Figure 4c,d do not exhibit a significant difference in the hydrodynamic number-weighted diameters between the groups, confirming that particle sizes do not change during the EPD process. As Furlong slope results are contradictory to the more reliable ADC measurements (Furlong slopes are indirectly derived data taken from UV−vis spectra after data processing and are prone to errors), we conclude that particle size does not significantly change during EPD and that the deposition process is not size-dependent, a finding in accordance with the literature.[21]

Most of the EPD literature focuses on producing deposit yields in milligram scale or more whose efficiencies are evaluated by deposit yield and their quality (crack-free or bubble-free depositions).[6,7,33,36−38] However, to influence the impedance of stimulation electrodes, sub-monolayer PtNP depositions with rough surface textures and increased surface area are more relevant than the yield or defect-free deposits.

Figure 5 shows SEM images of PtNP deposits formed by DC (a, b) and pulsed-DC (c, d) fields. DC-EPD produces highly non reproducible clustered deposits, whereas pulsed-DC produces fairly distributed deposits with minimal clusters (see also Figure S5). Even though both depositions take place in an aqueous medium, the deposition mechanism here is assumed to be influenced by applied electric fields, leading to highly clustered and sparsely clustered depositions. It is well known from the literature that during EPD in aqueous media, field-induced flows such as EOF and EHD play major roles in the way particles are deposited.[1,3,5,30] The EOF results from the movement of polar liquids under the influence of external electric field and EHD originates due to the interaction of electric field and electric double layer near the target electrode.[3] Therefore, when a particle comes near the electrode surface, it is already under the influence of an applied electric field plus the flows induced by it.[3] Both EOF and EHD act simultaneously superimposed on each other,[54] pushing the subsequent incoming particles to attach near the first particle, thus resulting in cluster formations. Because of the accumulating surface charges, these clusters tend to attract more particles and hence grow faster. In DC-EPD, the applied field is constant and hence EOF and EHD continuously act on the particles to create large amounts of clusters. However, in pulsed-DC-EPD, the applied field is discontinuous and hence relaxes the particles from external influences during the off state. During this time, weakly bound particles in the clusters

https://doi.org/10.1021/acs.langmuir.1c01081
Langmuir 2021, 37, 9724−9734

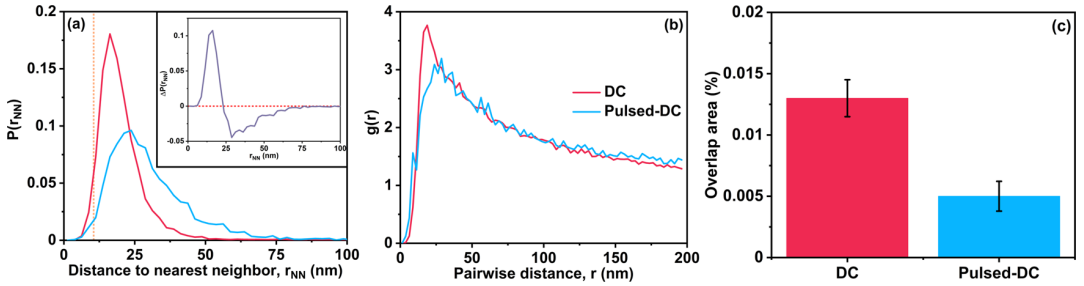

Figure 6. Relative positions of maxima at (a) nearest-neighbor distributions (orange dotted line: average particle diameter of 10 nm, corresponding to the minimum possible r_{NN} found when two neighboring particles are in direct contact) and the inset shows their difference (red dotted line guides the eye to zero value); (b) RDFs averaged from three DC and six pulsed-DC (legend) SEM images reveal particles are more closely spaced when deposited using DC fields and (c) the average percentage of the image where there is particle overlap because particle stacking is negligible in both pulsed-DC and DC.

break off and resuspend into the solution. When the field is switched on, these resuspended particles are deposited directly on the electrode surfaces instead of a cluster, thus producing distributed deposits over time.[1,3,5,30]

Therefore, the mechanisms studied for microparticles might also hold true for ligand-free charged metal NPs because the deposition of these particles is different when different electric fields are applied. In addition, as higher frequencies induce better ordering,[55] the frequency of 1 MHz used in our experiments further aided better ordering of the PtNPs during pulsed-DC-EPD. We can explain this further in terms of diffusive motion that occurs when the pulsed-DC field is off. For our system, we calculate the diffusion constant to be[56,57]

$$\mathcal{D} = \frac{k_B T}{3\pi\mu d_p} C_c = 5.2 \times 10^{-11}\ \mathrm{m^2/s} \tag{2}$$

where d_p is the particle diameter, T is the solvent temperature, μ is the viscosity, k_B is the Boltzmann's constant, and C_c = 1.063 is the slip correction factor.[56] During the time the field is off $t_{field\text{-}off}$ = 500 ns, the average distance particles diffusively migrate, $\delta = \sqrt{6 t_{field-off}\mathcal{D}}$, is 12 nm. Notably, at these conditions, this migration distance is on the order of the particle diameter, i.e., $\delta \approx d_p$. Thus, the 1 MHz field frequency allows for significant diffusive particle motion to occur, reducing the propensity for particles to aggregate into clusters. This implies there is an upper limit to the pulsed-DC frequency (or equivalently lower limit to $t_{field\text{-}off}$) in which clustering may occur with pulsed-DC-EPD. Based on the diffusion arguments, we posit that aggregation may occur when the diffusion distance is less than the particle size. That is

$$\left(\frac{\delta}{d_p} \equiv \sqrt{\frac{2k_B T C_c t_{field-off}}{\pi\mu d_p^3}}\right) \ll 1 \tag{3}$$

. A series of different duty cycles were implemented as controls to check the validity of eq 3 (see Section S5), and it was found that cluster formation occurred in cases where $\delta/d_p \ll 1$ and also when $t_{field\text{-}on}/t_{field\text{-}off}$ = 1. Further investigation is required to determine whether or not clusters are formed in case the deposition time is higher than the diffusion time, i.e., $t_{field\text{-}on} > t_{field\text{-}off}$.

To evaluate particle spacing in the deposits, we extract particle coordinates from SEM images using our semi-automated algorithm described in Figure 2. Figure 6 shows quantitative comparisons between DC and pulsed-DC deposits that are the result of averaging three DC and six pulsed-DC SEM images, each with a sample area of ~3450 × 3420 nm^2. Figure 6a shows probability histograms of particles' nearest-neighbor distances and the inset highlights the difference between these curves. Nearest-neighbor (NN) histograms are generated by calculating the pairwise distances r between a reference particle i and every other detected particle j using center−center distances. The minimum i−j distance is stored as r_{NN} and this calculation is repeated for every possible reference particle i. The collection of NN distances are presented as probability distributions $P(r_{NN})$ [where $\int_0^\infty P(r_{NN})\, dr_{NN} = 1$] in Figure 6a. The minimum center−center distance in this distribution, indicating particles touching each other (orange dotted line in Figure 6a), is represented by the mean particle diameter and is assumed to be 10 nm. These histograms reveal that DC particles are more closely spaced at ~37.5 nm vs ~42.5 nm for particles created with pulsed-DC. Furthermore, the distribution and inset in Figure 6a is broader for pulsed-DC than for pure DC fields, indicating that particles deposited under DC conditions are arranged in denser clusters. This quantitative result is consistent with the SEM images in Figure 5a,b that show deposits in DC fields comprised of clustered particles.

The same set of particle coordinates measured from SEM images is used to compute two-dimensional (2D) radial distribution functions (RDF) of the deposited particles at the surface, $g(r)$ in Figure 6b. The RDF is calculated as

$$g(r) = \frac{1}{\eta_c}\left\langle \sum_{n=1}^{N} \delta(r - r_n) \right\rangle \tag{4}$$

where r_n is the distance between atom centers i and j, δ is the Kronecker delta, η_c is a normalization factor proportional to the number of particles in a ring with radius r at average particle density ρ, and the ensemble average is collected over all N deposited particles and all possible reference particles i. In practice, the 2D RDF is calculated as nested annuli centered at equally spaced r with finite width dr that defines the RDF's resolution. Here, the RDF may be interpreted as the likelihood of finding a neighboring particle at a distance r from any given reference particle of reference within the deposit. This value is normalized by the average (bulk) density of particles in a given image so that $g(r) > 1$ indicates some greater-than-average local density and $\lim_{r\to\infty} g(r) = 1$.

The curves in Figure 6b represent averages collected over all particles detected in each set of SEM images. Like the

https://doi.org/10.1021/acs.langmuir.1c01081
Langmuir 2021, 37, 9724−9734

histograms in Figure 6a, the $g(r)$ show that particles in deposits created with pure DC fields are more closely spaced compared with that in deposits produced in pulsed-DC fields. Additionally, the $g(r)$ also contains information about the local ordering of the particles. The smaller peak of the pulsed-DC depositions is due to a more diffused local arrangement of particles around the central reference particle. A Boltzmann inversion of the $g(r)$ in Figure 6b provides insight into interparticle interactions near the electrode via the effective potential of mean force[58]

$$w_{\text{at-electrode}} = -k_B T \ln(g(r)) \quad (5)$$

Extracting this thermodynamic information from an ensemble of positional data may assist in the validation or development of related EPD computer simulations and theoretical models. Since this approach reports $g(r)$ of deposited particles at the electrode, eq 5 reveals particle−particle interactions exclusively near the wall. Unlike the bulk colloid−colloid interactions that are traditionally modeled with the DLVO potential, near-electrode interactions may be influenced by (at least) EOF and/or EHD that can influence ordering between particles. Admittedly, without performing this analysis on a greater number of SEM images, the $g(r)$ curves in Figure 6b are not well converged. However, this method of collecting SEM images and locating particle coordinates with the semiautomated algorithm is scalable. Analyses like those shown in Figure 6 can be performed over large SEM image sets to measure empirically derived $w_{\text{at-electrode}}$ and improve the EPD modeling efforts. Structural information from the interactions among particles within the first layer of particles captured by $w_{\text{at-electrode}}$ is crucial to understanding how subsequently deposited particles are arranged in multilayer deposits. In addition to the gained physical insights, such models could expedite optimization of EPD processing conditions to tune impedance values of the resulting deposits.

This approach and the results of Figure 6 are limited to 2D deposits such as ours. Particles occluded within 3D clusters skew the analysis in Figure 6a,b. Configurations where small particles touch or particles sit atop each other contribute to nonzero values in $P(r_{NN} < d_p)$ and $g(r < d_p)$. We quantify the amount of particle occlusion in our SEM images in Figure 6c. We first compute the theoretical coverage assuming no overlap, $N\pi d_p^2/4$. We then compute the total area within a 5 nm radius of every particle, ensuring not to double count regions between particles. We then report the difference of these areal coverage metrics, normalized by the total area of the SEM image to determine the percentage of particle overlap in each image. In both DC and pulsed-DC, the percentage of estimated overlap is negligible as expected for our system. However, the larger values for the DC depositions provide another indication that particles arrange into denser configurations than in pulsed-DC.

Deep brain stimulation has been used in over 160 000 patients for various neurological and other conditions like chronic pain, psychiatric diseases, and eating disorders.[59,60] While there has been tremendous progress, drainage of battery source due to increasing impedance of the stimulation circuitry is still an unresolved problem.[22,61] We assume that by increasing the active surface area of electrodes, electric discharge efficiency could be increased, thereby reducing the impedance. Here, changes in the geometric surface area through sub-monolayer deposition are minimal (0.03% increase) and cannot fully account for pronounced changes in impedance. Previous studies conducted with 2D targets highlight that the oxidation state and electrochemical potential of laser fabricated PtNPs significantly enhanced the active surface area.[9] Hence, it is not the geometric surface area increase but the surface activity increase that drives changes in impedance. Therefore, in addition to 2D image analysis, sub-monolayer PtNPs were deposited on 21 Pt−Ir electrode surfaces. Electrodes were coated using DC and pulsed-DC electric fields along with a control group coated using the vehicle medium (here, Milli-Q water) and their impedance was determined. The electrode impedance constitutes a functional readout and helps to elucidate whether there is a correlation between deposit quality and electrophysiological properties.

Figure 7 shows the average impedance values of the electrode samples. It can be seen that the DC-EPD samples

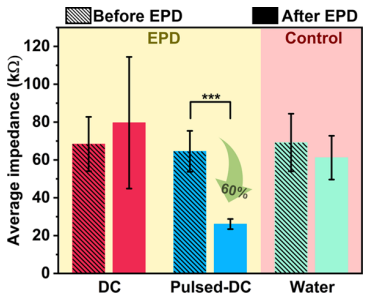

Figure 7. Average impedance values of neural stimulation electrodes before and after EPD via DC, pulsed-DC fields, and control group (N = 7, α = 0.05), showing a significant decrease in impedance when pulsed-DC fields were used.

show no significant change in their impedance before and after coating. As clustering happens more often in an aqueous DC-EPD, the surfaces are only partially covered and result in an inefficient increase in active surface area. Furthermore, such large clusters may cause insufficient electrical contact, with the electrode surface overshadowing the positive effects of more active NPs in lower layers of the deposit. As a result, a further deposition and the corresponding increase of surface area hardly influence the impedance after DC deposition. This finding is in good accordance with our previous results, where impedance even increased after DC-EPD *in vitro*.[22] Similar trend can be seen in the case of water-coated control samples, which is naturally expected. In the case of pulsed-DC samples, a statistically significant ($p \leq 0.05$) lowering of the impedance values after EPD can be observed. Higher level of ordering results in lesser cluster formations and more accessible active surface area. Here, more single particles cover the electrode surface, facilitating the total active surface area to increase and eventually their impedance values to decrease.

CONCLUSIONS

Neural electrode impedance, i.e., during deep brain stimulation or neural electrode recording, is an important factor influencing the electrostimulation efficiency and neural recording quality. When impedance is kept low, it not only improves the charge transfer but also reduces the need for frequent battery source replacement surgeries. One approach in this context is to increase the active surface area of electrodes through the introduction of nanoroughness on the surfaces, which is made possible by the EPD of PtNPs. In this work, we examined to what extent the DC-EPD and pulsed-DC-EPD electric fields affect the coating properties. We observed a more homogeneous coating in the case of pulsed-DC-EPD. We also

https://doi.org/10.1021/acs.langmuir.1c01081
Langmuir 2021, 37, 9724−9734

pose a simple mathematical equation, eq 3, as a way to identify parameter space where rough coatings could arise in pulsed-DC systems. A quantitative analysis of SEM images yielded nearest-neighbor histograms and radial distribution functions of nanoparticle deposits. These functions reveal that particles are arranged into denser clusters when deposited under pure DC fields in comparison to pulsed-DC fields. Furthermore, such an analysis, when performed at a large scale, offers a way to measure intercolloidal potentials that describe the near-wall effects in sub-monolayer EPD deposits. Particle-based EPD models could incorporate these empirically derived potentials to offer additional physical insights into the connection between the colloidal ordering and the resulting impedance of neural electrode coatings. The electrode samples coated with pulsed-DC showed a significant decrease in their impedance values, which remained stable throughout the stimulation period. The experiment also confirms that impedance remains unaltered for DC-EPD. Future experimental and simulation studies continue to pursue a deeper understanding of the effect of colloid composition on particle deposition. Additionally, we confirm that the homogeneous coatings prepared by pulsed-DC-EPD enhance biomedical device performance with long-term *in vitro* and *in vivo* stimulation experiments.

■ ASSOCIATED CONTENT

Supporting Information

The Supporting Information is available free of charge at https://pubs.acs.org/doi/10.1021/acs.langmuir.1c01081.

Additional details regarding PtNP size distributions, particle growth, yield after EPD, Furlong slope calculations, SEM images showing coating reproducibility, and control experiments on particle coordinate analysis (PDF)

■ AUTHOR INFORMATION

Corresponding Author

Stephan Barcikowski − *Technical Chemistry I, Center for Nanointegration Duisburg-Essen (CENIDE), University of Duisburg-Essen, 45141 Essen, Germany;* orcid.org/0000-0002-9739-7272; Email: stephan.barcikowski@uni-due.de

Authors

Vaijayanthi Ramesh − *Technical Chemistry I, Center for Nanointegration Duisburg-Essen (CENIDE), University of Duisburg-Essen, 45141 Essen, Germany;* orcid.org/0000-0003-4753-5064

Christoph Rehbock − *Technical Chemistry I, Center for Nanointegration Duisburg-Essen (CENIDE), University of Duisburg-Essen, 45141 Essen, Germany;* orcid.org/0000-0002-4708-5246

Brian Giera − *Center for Engineered Materials and Manufacturing, Lawrence Livermore National Laboratory, Livermore, California 94550, United States;* orcid.org/0000-0001-6543-7498

John J. Karnes − *Center for Engineered Materials and Manufacturing, Lawrence Livermore National Laboratory, Livermore, California 94550, United States;* orcid.org/0000-0002-2917-8406

Jean-Baptiste Forien − *Center for Engineered Materials and Manufacturing, Lawrence Livermore National Laboratory, Livermore, California 94550, United States*

Svilen D. Angelov − *Department of Neurosurgery, Hannover Medical School, 30625 Hannover, Germany*

Kerstin Schwabe − *Department of Neurosurgery, Hannover Medical School, 30625 Hannover, Germany*

Joachim K. Krauss − *Department of Neurosurgery, Hannover Medical School, 30625 Hannover, Germany*

Complete contact information is available at: https://pubs.acs.org/10.1021/acs.langmuir.1c01081

Notes

The authors declare no competing financial interest.

■ ACKNOWLEDGMENTS

The authors gratefully acknowledge the German Research Foundation (DFG) for their financial support under the Project Number BA 3580/24-1, and B.G. thanks DFG for Mercator Fellowship. This work was performed in part under the auspices of the U.S. Department of Energy by Lawrence Livermore National Laboratory under Contract DE-AC52-07-NA27344, LLNL-JRNL-820981. The authors also thank Tobias Bochmann for the SEM measurements and Prof. Elliott for helpful thoughts on $g(r)$.

■ REFERENCES

(1) Böhmer, M. In situ observation of 2-dimensional clustering during electrophoretic deposition. *Langmuir* **1996**, *12*, 5747−5750.

(2) Besra, L.; Liu, M. A review on fundamentals and applications of electrophoretic deposition (EPD). *Prog. Mater. Sci.* **2007**, *52*, 1−61.

(3) Neirinck, B.; Van der Biest, O.; Vleugels, J. A current opinion on electrophoretic deposition in pulsed and alternating fields. *J. Phys. Chem. B* **2013**, *117*, 1516−1526.

(4) Solomentsev, Y.; Böhmer, M.; Anderson, J. L. Particle clustering and pattern formation during electrophoretic deposition: a hydrodynamic model. *Langmuir* **1997**, *13*, 6058−6068.

(5) Ristenpart, W.; Aksay, I. A.; Saville, D. Electrohydrodynamic flow around a colloidal particle near an electrode with an oscillating potential. *J. Fluid Mech.* **2007**, *575*, 83.

(6) Besra, L.; Uchikoshi, T.; Suzuki, T. S.; Sakka, Y. Bubble-Free Aqueous Electrophoretic Deposition (EPD) by Pulse-Potential Application. *J. Am. Ceram. Soc.* **2008**, *91*, 3154−3159.

(7) Besra, L.; Uchikoshi, T.; Suzuki, T.; Sakka, Y. Pulsed-DC electrophoretic deposition (EPD) of aqueous alumina suspension for controlling bubble incorporation and deposit microstructure. *Key Eng. Mater.* **2009**, 39−44.

(8) Naim, M. N.; Kuwata, M.; Kamiya, H.; Lenggoro, I. W. Deposition of TiO_2 nanoparticles in surfactant-containing aqueous suspension by a pulsed DC charging-mode electrophoresis. *J. Ceram. Soc. Jpn.* **2009**, *117*, 127−132.

(9) Koenen, S.; Rehbock, C.; Heissler, H. E.; Angelov, S. D.; Schwabe, K.; Krauss, J. K.; Barcikowski, S. Optimizing in Vitro Impedance and Physico-Chemical Properties of Neural Electrodes by Electrophoretic Deposition of Pt Nanoparticles. *ChemPhysChem* **2017**, *18*, 1108−1117.

(10) Uchikoshi, T.; Ozawa, K.; Hatton, B. D.; Sakka, Y. Dense, bubble-free ceramic deposits from aqueous suspensions by electrophoretic deposition. *J. Mater. Res.* **2001**, *16*, 321−324.

(11) Caproni, E.; Gouvea, D.; Muccillo, R. Yttria-stabilized zirconia closed end tubes prepared by electrophoretic deposition. *Ceram. Int.* **2011**, *37*, 273−277.

(12) Avcu, E.; Baştan, F. E.; Abdullah, H. Z.; Rehman, M. A. U.; Avcu, Y. Y.; Boccaccini, A. R. Electrophoretic deposition of chitosan-based composite coatings for biomedical applications: A review. *Prog. Mater. Sci.* **2019**, *103*, 69−108.

(13) Ye, L.; Wen, K.; Zhang, Z.; Yang, F.; Liang, Y.; Lv, W.; Lin, Y.; Gu, J.; Dickerson, J. H.; He, W. Highly efficient materials assembly via

electrophoretic deposition for electrochemical energy conversion and storage devices. *Adv. Energy Mater.* **2016**, *6*, No. 1502018.
(14) Bukosky, S. C.; Hammons, J. A.; Giera, B.; Lee, E.; Han, J.; Freyman, M. C.; Ivanovskaya, A.; Krauter, K. G.; Kuntz, J. D.; Worsley, M. A.; et al. Correlating dynamic microstructure to observed color in electrophoretic displays via in situ small-angle x-ray scattering. *Phys. Rev. Mater.* **2020**, *4*, No. 075802.
(15) Atiq Ur Rehman, M.; Chen, Q.; Braem, A.; Shaffer, M. S.; Boccaccini, A. R. Electrophoretic deposition of carbon nanotubes: recent progress and remaining challenges. *Int. Mater. Rev.* **2020**, 1−30.
(16) Akhtar, M. A.; Hadzhieva, Z.; Dlouhy, I.; Boccaccini, A. R. Electrophoretic deposition and characterization of functional coatings based on an antibacterial gallium (III)-chitosan complex. *Coatings* **2020**, *10*, No. 483.
(17) Szklarska, M.; Łosiewicz, B.; Dercz, G.; Maszybrocka, J.; Rams-Baron, M.; Stach, S. Electrophoretic deposition of chitosan coatings on the Ti15Mo biomedical alloy from a citric acid solution. *RSC Adv.* **2020**, *10*, 13386−13393.
(18) Szydło, A.; Goossen, J.-D.; Linte, C.; Uphoff, H.; Bredol, M. Preparation of platinum-based electrocatalytic layers from catalyst dispersions with adjusted colloidal stability via a pulsed electrophoretic deposition method. *Mater. Chem. Phys.* **2020**, *242*, No. 122532.
(19) Zhang, C.; Li, H.; Su, Y.; Zhang, Q.; Li, Y.; Lu, J. Controllable and versatile electrophoretic deposition technology for monolithic organic memory devices. *ACS Appl. Mater. Interfaces* **2020**, *12*, 15482−15490.
(20) Guo, W.; Liu, B. Liquid-phase pulsed laser ablation and electrophoretic deposition for chalcopyrite thin-film solar cell application. *ACS Appl. Mater. Interfaces* **2012**, *4*, 7036−7042.
(21) Koenen, S.; Streubel, R.; Jakobi, J.; Schwabe, K.; Krauss, J. K.; Barcikowski, S. Continuous electrophoretic deposition and electrophoretic mobility of ligand-free, metal nanoparticles in liquid flow. *J. Electrochem. Soc.* **2015**, *162*, D174.
(22) Angelov, S. D.; Koenen, S.; Jakobi, J.; Heissler, H. E.; Alam, M.; Schwabe, K.; Barcikowski, S.; Krauss, J. K. Electrophoretic deposition of ligand-free platinum nanoparticles on neural electrodes affects their impedance in vitro and in vivo with no negative effect on reactive gliosis. *J. Nanobiotechnol.* **2016**, *14*, No. 3.
(23) Groiss, S.; Wojtecki, L.; Südmeyer, M.; Schnitzler, A. Deep brain stimulation in Parkinsonas disease. *Ther. Adv. Neurol. Disord.* **2009**, *2*, 379−391.
(24) Green, R. A.; Toor, H.; Dodds, C.; Lovell, N. H. Variation in performance of platinum electrodes with size and surface roughness. *Sens. Mater.* **2012**, *24*, 165−180.
(25) Green, R.; Matteucci, P.; Dodds, C.; Palmer, J.; Dueck, W.; Hassarati, R.; Byrnes-Preston, P.; Lovell, N.; Suaning, G. Laser patterning of platinum electrodes for safe neurostimulation. *J. Neural Eng.* **2014**, *11*, No. 056017.
(26) Leber, M.; Bhandari, R.; Mize, J.; Warren, D.; Shandhi, M.; Solzbacher, F.; Negi, S. Long term performance of porous platinum coated neural electrodes. *Biomed. Microdevices* **2017**, *19*, No. 62.
(27) Persson, J.; Danielsen, N.; Wallman, L. Porous silicon as a neural electrode material. *J. Biomater. Sci., Polym. Ed.* **2007**, *18*, 1301−1308.
(28) Boehler, C.; Stieglitz, T.; Asplund, M. Nanostructured platinum grass enables superior impedance reduction for neural microelectrodes. *Biomaterials* **2015**, *67*, 346−353.
(29) Ganji, M.; Paulk, A. C.; Yang, J. C.; Vahidi, N. W.; Lee, S. H.; Liu, R.; Hossain, L.; Arneodo, E. M.; Thunemann, M.; Shigyo, M.; et al. Selective formation of porous Pt nanorods for highly electrochemically efficient neural electrode interfaces. *Nano Lett.* **2019**, *19*, 6244−6254.
(30) Neirinck, B.; Fransaer, J.; Van der Biest, O.; Vleugels, J. Aqueous electrophoretic deposition in asymmetric AC electric fields (AC−EPD). *Electrochem. Commun.* **2009**, *11*, 57−60.
(31) Hirata, Y.; Nishimoto, A.; Ishihara, Y. Forming of alumina powder by electrophoretic deposition. *J. Ceram. Soc. Jpn.* **1991**, *99*, 108−113.
(32) Doungdaw, S.; Uchikoshi, T.; Noguchi, Y.; Eamchotchawalit, C.; Sakka, Y. Electrophoretic deposition of lead zirconate titanate (PZT) powder from ethanol suspension prepared with phosphate ester. *Sci. Technol. Adv. Mater.* **2005**, *6*, 927.
(33) Acevedo-Peña, P.; González, I. TiO_2 photoanodes prepared by cathodic electrophoretic deposition in 2-propanol: effect of the electric field and deposition time. *J. Solid State Electrochem.* **2013**, *17*, 519−526.
(34) Sarkar, P.; Nicholson, P. S. Electrophoretic deposition (EPD): mechanisms, kinetics, and application to ceramics. *J. Am. Ceram. Soc.* **1996**, *79*, 1987−2002.
(35) Naim, M. N.; Iijima, M.; Sasaki, K.; Kuwata, M.; Kamiya, H.; Lenggoro, I. W. Electrical-driven disaggregation of the two-dimensional assembly of colloidal polymer particles under pulse DC charging. *Adv. Powder Technol.* **2010**, *21*, 534−541.
(36) Besra, L.; Uchikoshi, T.; Suzuki, T.; Sakka, Y. Application of constant current pulse to suppress bubble incorporation and control deposit morphology during aqueous electrophoretic deposition (EPD). *J. Eur. Ceram. Soc.* **2009**, *29*, 1837−1845.
(37) Besra, L.; Uchikoshi, T.; Suzuki, T. S.; Sakka, Y. Experimental verification of pH localization mechanism of particle consolidation at the electrode/solution interface and its application to pulsed DC electrophoretic deposition (EPD). *J. Eur. Ceram. Soc.* **2010**, *30*, 1187−1193.
(38) Anné, G.; Vanmeensel, K.; Neirinck, B.; Van der Biest, O.; Vleugels, J. Ketone-amine based suspensions for electrophoretic deposition of Al_2O_3 and ZrO_2. *J. Eur. Ceram. Soc.* **2006**, *26*, 3531−3537.
(39) Zhang, D.; Gökce, B.; Barcikowski, S. Laser synthesis and processing of colloids: fundamentals and applications. *Chem. Rev.* **2017**, *117*, 3990−4103.
(40) Lau, M.; Barcikowski, S. Quantification of mass-specific laser energy input converted into particle properties during picosecond pulsed laser fragmentation of zinc oxide and boron carbide in liquids. *Appl. Surf. Sci.* **2015**, *348*, 22−29.
(41) Furlong, D. N.; Launikonis, A.; Sasse, W. H.; Sanders, J. V. Colloidal platinum sols. Preparation, characterization and stability towards salt. *J. Chem. Soc., Faraday Trans. 1* **1984**, *80*, 571−588.
(42) Jendrzej, S.; Gökce, B.; Amendola, V.; Barcikowski, S. Barrierless growth of precursor-free, ultrafast laser-fragmented noble metal nanoparticles by colloidal atom clusters-A kinetic in situ study. *J. Colloid Interface Sci.* **2016**, *463*, 299−307.
(43) Waag, F.; Li, Y.; Ziefuß, A. R.; Bertin, E.; Kamp, M.; Duppel, V.; Marzun, G.; Kienle, L.; Barcikowski, S.; Gökce, B. Kinetically-controlled laser-synthesis of colloidal high-entropy alloy nanoparticles. *RSC Adv.* **2019**, *9*, 18547−18558.
(44) Schneider, C. A.; Rasband, W. S.; Eliceiri, K. W. NIH Image to ImageJ: 25 years of image analysis. *Nat. Methods* **2012**, *9*, 671−675.
(45) Nichols, W. T.; Sasaki, T.; Koshizaki, N. Laser ablation of a platinum target in water. III. Laser-induced reactions. *J. Appl. Phys.* **2006**, *100*, No. 114913.
(46) Shih, C.-Y.; Streubel, R.; Heberle, J.; Letzel, A.; Shugaev, M. V.; Wu, C.; Schmidt, M.; Gökce, B.; Barcikowski, S.; Zhigilei, L. V. Two mechanisms of nanoparticle generation in picosecond laser ablation in liquids: The origin of the bimodal size distribution. *Nanoscale* **2018**, *10*, 6900−6910.
(47) Ziefuß, A. R.; Reichenberger, S.; Rehbock, C.; Chakraborty, I.; Gharib, M.; Parak, W. J.; Barcikowski, S. Laser fragmentation of colloidal gold nanoparticles with high-intensity nanosecond pulses is driven by a single-step fragmentation mechanism with a defined educt particle-size threshold. *J. Phys. Chem. C* **2018**, *122*, 22125−22136.
(48) Lau, M.; Haxhiaj, I.; Wagener, P.; Intartaglia, R.; Brandi, F.; Nakamura, J.; Barcikowski, S. Ligand-free gold atom clusters adsorbed on graphene nano sheets generated by oxidative laser fragmentation in water. *Chem. Phys. Lett.* **2014**, *610*−*611*, 256−260.
(49) Ribeiro, C.; Lee, E. J.; Longo, E.; Leite, E. R. A kinetic model to describe nanocrystal growth by the oriented attachment mechanism. *ChemPhysChem* **2005**, *6*, 690−696.

https://doi.org/10.1021/acs.langmuir.1c01081
Langmuir 2021, 37, 9724−9734

(50) Taylor, P. Ostwald ripening in emulsions. *Adv. Colloid Interface Sci.* **1998**, *75*, 107−163.
(51) Simonsen, S. B.; Chorkendorff, I.; Dahl, S.; Skoglundh, M.; Sehested, J.; Helveg, S. Ostwald ripening in a Pt/SiO_2 model catalyst studied by in situ TEM. *J. Catal.* **2011**, *281*, 147−155.
(52) Ziefuß, A. R.; Barcikowski, S.; Rehbock, C. Synergism between Specific Halide Anions and pH Effects during Nanosecond Laser Fragmentation of Ligand-Free Gold Nanoparticles. *Langmuir* **2019**, *35*, 6630−6639.
(53) Heavens, S. Electrophoretic Deposition as a Processing Route for Ceramics. In *Advanced Ceramic Processing and Technology*; Noyes Publications: 1990; Vol. *1*, pp 255−283.
(54) Ristenpart, W.; Aksay, I. A.; Saville, D. Electrically driven flow near a colloidal particle close to an electrode with a faradaic current. *Langmuir* **2007**, *23*, 4071−4080.
(55) Song, M.-G.; Bishop, K. J.; Pinchuk, A. O.; Kowalczyk, B.; Grzybowski, B. A. Formation of dense nanoparticle monolayers mediated by alternating current electric fields and electrohydrodynamic flows. *J. Phys. Chem. C* **2010**, *114*, 8800−8805.
(56) Liu, D.-L. *Developments in Surface Contamination and Cleaning*; Elsevier, 2010; pp 1−56.
(57) *Physics of the Human Body − The Properties of Water (PHYS 304 Lecture Notes), Spring 2003*; University of Virginia, USA. http://galileo.phys.virginia.edu/classes/304/
(58) McQuarrie, D. *Statistical Mechanics*; University Science Books, 2000; *1*, p 694.
(59) Lozano, A. M.; Lipsman, N.; Bergman, H.; Brown, P.; Chabardes, S.; Chang, J. W.; Matthews, K.; McIntyre, C. C.; Schlaepfer, T. E.; Schulder, M.; et al. Deep brain stimulation: current challenges and future directions. *Nat. Rev. Neurol.* **2019**, *15*, 148−160.
(60) Harmsen, I. E.; Elias, G. J.; Beyn, M. E.; Boutet, A.; Pancholi, A.; Germann, J.; Mansouri, A.; Lozano, C. S.; Lozano, A. M. Clinical trials for deep brain stimulation: current state of affairs. *Brain Stimul.* **2020**, *13*, 378−385.
(61) Krauss, J. K.; Lipsman, N.; Aziz, T.; Boutet, A.; Brown, P.; Chang, J. W.; Davidson, B.; Grill, W. M.; Hariz, M. I.; Horn, A.; et al. Technology of deep brain stimulation: current status and future directions. *Nat. Rev. Neurol.* **2021**, *17*, 75−87.

https://doi.org/10.1021/acs.langmuir.1c01081
Langmuir 2021, 37, 9724−9734

4 Influence of EPD Solvent Composition on the Platinum Nanoparticle deposition

Published in The Journal of Electrochemical Society (2022) 169 022504

Electrophoretic Deposition of Platinum Nanoparticles using Ethanol-Water Mixtures Significantly Reduces Neural Electrode Impedance

Vaijayanthi Ramesh[1], Brian Giera[2], John J. Karnes[2], Nadine Stratmann[1], Viktor Schaufler[1], Yao Li[1], Christoph Rehbock[1], and Stephan Barcikowski[1,*]

[1] Institute of Technical Chemistry I, University of Duisburg-Essen and Center for Nanointegration Duisburg-Essen (CENIDE), Essen, Germany

[2] Center for Engineered Materials and Manufacturing, Lawrence Livermore National Laboratory, California, USA

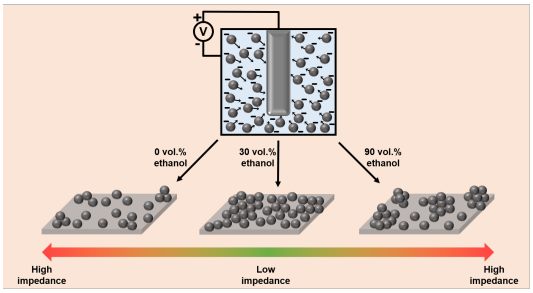

Summary:

In the previous section, the influence of physical parameters involved in the EPD process (applied electric field) on the deposition mechanism was investigated. However, the question of the influence of solvent composition on the homogeneity of the coatings was still open. Therefore, the upcoming section investigates the influence of the solvent medium used for the coating on the NP deposition. The EPD of laser-generated PtNPs dispersed in varying concentrations of ethanol-water mixtures is performed and the most homogeneous surface coverage was obtained at 30 vol.% ethanol concentration. A systematic electrochemical characterization was performed using CV and EIS. At 30 vol.% ethanol, the ECSA increased by 7-fold and the electrode impedance decreased significantly. An increased coating quality with increasing ethanol concentration could be due to the reduction in water splitting and bubble formation, and with very high ethanol concentration, particle assemblages are formed due to higher viscosity. The above observations are complemented by mesoscale multiparticle computational simulations.

Author contributions:

Design and supervision of the experiments on EPD of NPs using various ethanol-water mixtures including their characterization were performed by VR. Data collection was carried out by NS and VS. Numerical simulation experiments and their data curation were done by BG and JJK. The original manuscript draft was prepared by VR. The review and editing of the manuscript were carried out by VR, CR, BG, JJK, and SB. SB and CR designed the study, and supervised and promoted the collaboration between the institutions.

Journal of The Electrochemical Society, 2022 **169** 022504
1945-7111/2022/169(2)/022504/9/$40.00 © 2022 The Electrochemical Society ("ECS"). Published on behalf of ECS by IOP Publishing Limited

Electrophoretic Deposition of Platinum Nanoparticles using Ethanol-Water Mixtures Significantly Reduces Neural Electrode Impedance

Vaijayanthi Ramesh,[1] Brian Giera,[2] John J. Karnes,[2] Nadine Stratmann,[1] Viktor Schaufler,[1] Yao Li,[1] Christoph Rehbock,[1] and Stephan Barcikowski[1,z]

[1]*Institute of Technical Chemistry I, University of Duisburg-Essen and Center for Nanointegration Duisburg-Essen (CENIDE), 45141 Essen, Germany*
[2]*Center for Engineered Materials and Manufacturing, Lawrence Livermore National Laboratory, 94550 California, United States of America*

Platinum electrodes are critical components in many biomedical devices, an important example being implantable neural stimulation or recording electrodes. However, upon implantation, scar tissue forms around the electrode surface, causing unwanted deterioration of the electrical contact. We demonstrate that sub-monolayer coatings of platinum nanoparticles (PtNPs) applied to 3D neural electrodes by electrophoretic deposition (EPD) can enhance the electrode's active surface area and significantly lower its impedance. In this work we use ethanol-water mixtures as the EPD solvent, in contrast to our previous studies carried out in water. We show that EPD coating in 30 vol.% ethanol improves the device's electrochemical performance. Computational mesoscale multiparticle simulations were for the first time applied to PtNP-on-Pt EPD, revealing correlations between ethanol concentration, electrochemical properties, and coating homogeneity. Thereto, this optimum ethanol concentration (30 vol.%) balances two opposing trends: (i) the addition of ethanol reduces water splitting and gas bubble formation, which benefits surface coverage, and (ii) increased viscosity and reduced permittivity occur at high ethanol concentrations, which impair the coating quality and favoring clustering. A seven-fold increase in active surface area and significantly reduced in vitro impedance of the nano-modified neural stimulation electrode surfaces highlight the influence of ethanol-water mixtures in PtNP EPD.
 [DOI: 10.1149/1945-7111/ac51f8]

Manuscript submitted November 12, 2021; revised manuscript received January 18, 2022. Published February 11, 2022.

Supplementary material for this article is available online

Electrodes made of platinum (Pt) are of high relevance in various applications such as gas diffusion electrodes for fuel cells,[1,2,3] sensor electrodes (in electrochemical detection of glucose,[4–6] pH,[7,8] dissolved oxygen,[9] etc.), neural stimulation[10–13] or recording implants,[14–16] retinal implants,[17–19] cochlear implants,[20,21] in vitro monitoring of electrogenic cells,[22] dye sensitized solar cells[23–25] and many more. Pt is preferred in biomedicine[26] and electrocatalysis[27] because of its biocompatible and corrosion-resistant nature. In all applications, the most important electrode parameters to be optimized are the electrochemical surface area (ECSA) and electrochemical impedance (Z)—the key readouts to study their electrochemical behavior.[28–30] In electrocatalytic applications of Pt electrodes like the fuel cells, a high ECSA of Pt plays a major role in fuel conversion rates resulting in high power outputs.[3] In biomedical stimulation and recording applications, Z plays a vital role, where a low Z corresponds to a high charge injection capacity (CIC) of the electrodes, yielding efficient stimulations. Furthermore, in most of the electrochemical analyses, parameters like ECSA, Z, CIC and charge storage capacity (CSC) are all interdependent.[31–33]

The design of Pt and Pt-based electrodes as neural stimulators and signal recorders is an important and established research field.[34,35] An ideal high-performance neural electrode should preferably possess high CIC, ECSA, signal-to-noise ratio, and low Z.[36] Theoretically, Pt microelectrodes can inject a charge of 300–350 μC cm^{-2}; in practice they inject only around 100 μC cm^{-2}, reducing the stimulation efficiency.[26] This is because, in vivo, the cathodal stimulation range is limited to between 0 and −0.6 V (vs Ag/AgCl) to avoid water electrolysis.[26,37] Increasing the geometrical surface areas (GSA) would be a suitable way to achieve a low Z, nevertheless such designs would suffer from a decreased implantation feasibility due to bigger sizes. Hence, researchers have been increasing the ECSA of electrodes through different kinds of surface modifications with an aim to decrease Z. Until now, various metallic, semiconducting, carbon-based and polymer-based materials have been used to structure the surfaces of neural electrodes.[38] Poly(3,4-ethylenedioxythiophene) (PEDOT) was electrodeposited onto Pt electrodes insulated in PDMS[39] or polyimide[40] and was found to increase the CIC and decrease Z by 95%, respectively. Pt black was ultrasonically electroplated onto Pt microelectrodes, which reduced Z by 90% and increased the CSC. However, after mechanical durability tests, a significant increase of impedance up to 21% was found, indicating the impaired mechanical stability of these coatings.[36] In another study, Pt microelectrode arrays were platinized with Pt, increasing the ECSA of the recording area but also increasing Z in vivo.[41] Although promising, these systems suffer from serious drawbacks like delamination,[41] poor durability,[36] and require exhaustive regulatory procedures prior to clinical applications, particularly, when coating and electrode materials are dissimilar.[42]

Electrophoretic deposition (EPD) is the movement of charged colloidal particles under the influence of an applied electric field toward an oppositely charged electrode surface, and subsequent deposition of the particles onto this electrode.[43,44] EPD of laser-generated Pt nanoparticles (PtNPs) on Pt neural electrodes is a surface modification method that does not share the limitations mentioned above.[43] These laser-generated PtNPs are ligand-free, which prevents unwanted contamination of the surfaces and allows for well-controlled deposition since deposition rates scale linearly with time.[45] These particles are highly charged due to partial surface oxidation and ion adsorption, which improves particle mobility toward the target surfaces under an external electric field.[46] Another advantage of this approach is that the deposited particles and electrodes are of the same material, meaning that application of the coating would not affect biocompatibility[47] or hinder clinical approval. We previously reported a systematic direct-current (DC) EPD parameter optimization on 2D flat targets[46] and studied the in vivo performance of DC-EPD coated neuro stimulation electrodes in rats, finding that the coatings yielded more stable impedance values.[47] We also recently found that the morphology of PtNP deposition may be tuned by selecting either DC or pulsed-DC fields in aqueous media and studied the influence on neural electrode

[z]E-mail: stephan.barcikowski@uni-due.de

functionality. Here, the EPD mechanism, electric flows involved and the role of pulses during pulsed-DC EPD were discussed in a detailed manner. It has been observed that during DC-EPD thick, agglomerated deposits may be formed due to water electrolysis and gas bubble formation near the target surface.[48,49] Such stochastically nucleated deposits in aqueous medium are caused by electroosmotic and electrohydrodynamic flows that interact with colloidal particles and lead to aggregate formation.[43] On the other hand, it was observed that the pulsed-DC coatings resulted in more homogeneous and therefore more desirable deposits due to the pulsing, during which the loosely agglomerated particles tend to rearrange and deposit in a more orderly fashion.[43]

Until now, all published studies dealing with the deposition of laser-fabricated PtNPs on neural electrodes have been exclusively conducted in water.[43,46,47] It has been shown that EPD performance can greatly benefit from the utilization of alcohols or alcohol-water mixtures as solvents.[44,50] Hence in this work we aim to investigate using ethanol-water mixtures, to which extent the EPD solvent composition influences surface coverage and neural electrode's functionality. Electrochemical performance of the coated surfaces was examined via cyclic voltammetry (CV) and electrochemical impedance spectroscopy (EIS). In addition, computer simulations were used to deepen our understanding of particle deposition and link coating homogeneity to electrochemical performance (Fig. 1). Here, a mesoscale model was developed and applied to characterize sub-monolayer PtNP coverage electrophoretically deposited onto Pt substrates.

Materials and Methods

Nanoparticle synthesis.—Ligand-free PtNPs with an average hydrodynamic diameter of 10 nm and total mass concentration of about 500 μg/ml were synthesized in deionized water via laser processing in liquids using procedures and parameters previously described elsewhere.[43] In brief, a Pt bulk target ($10\times10\times1$ mm^3) was ablated in Milli-Q water using an Nd:YAG laser (Ekspla, Atlantic series, 10 ps, 1064 nm, 9.6 mJ, 100 kHz) followed by laser fragmentation in liquids (LFL) using a nanosecond laser (Innolas, Spitlight, 9 ns, 532 nm, 84 mJ, 100 Hz, 1.5 J cm^{-2}) to tune NP size distributions. Highly concentrated colloids directly obtained from synthesis in water were diluted to a concentration of about 100 μg/ml (confirmed via UV–Vis extinction spectroscopy) using corresponding ethanol-water mixtures, realizing the compositions of 0 vol.%, 10 vol.% through 90 vol.% (in steps of 20 vol.% of ethanol). The pH values of all the colloids (each of around 20 ml in volume) were adjusted to 11 using 10–20 μl of 0.1 M NaOH solution prior to EPD. UV-Vis absorbance spectra of Pt colloids before and after EPD were obtained using an UV–Vis extinction spectrometer (Evolution 201, Thermo Scientific) in the wavelength range of 190–900 nm using a quartz cuvette with 10 mm path length to determine the deposited mass of NPs on target surfaces (Fig. S1)[43]. The area under curve (AUC) between 190–900 nm spectral range was integrated and quantified against known mass concentrations of Pt colloids (Fig. S2).

Platinum-Iridium sample preparation.—PTFE coated Pt-Ir (90:10) wires of 76 μm diameter (Science Products GmbH, Germany) were used as coating substrates. The wires were cut into pieces having a length of 20 mm. The PTFE isolations were removed on either ends yielding about 4 mm of exposed wire. One end of the wires were soldered to an electrical contact pin and the other end was immersed into the colloid for deposition. The ends to be coated were washed thoroughly with ethanol prior to EPD.

Electrophoretic deposition.—Prepared Pt-Ir wires were coated via EPD using a custom-made chamber[46] and by applying DC electric fields. The previously synthesized PtNPs were dispersed in ethanol-water mixtures and used for deposition. The positive pole of the power supply was connected to the electrodes and the negative terminal to the surrounding metal counter electrode. The chamber was filled with 600 μl of the respective Pt colloid suspension, which was continuously mixed with a magnetic stirrer during deposition.

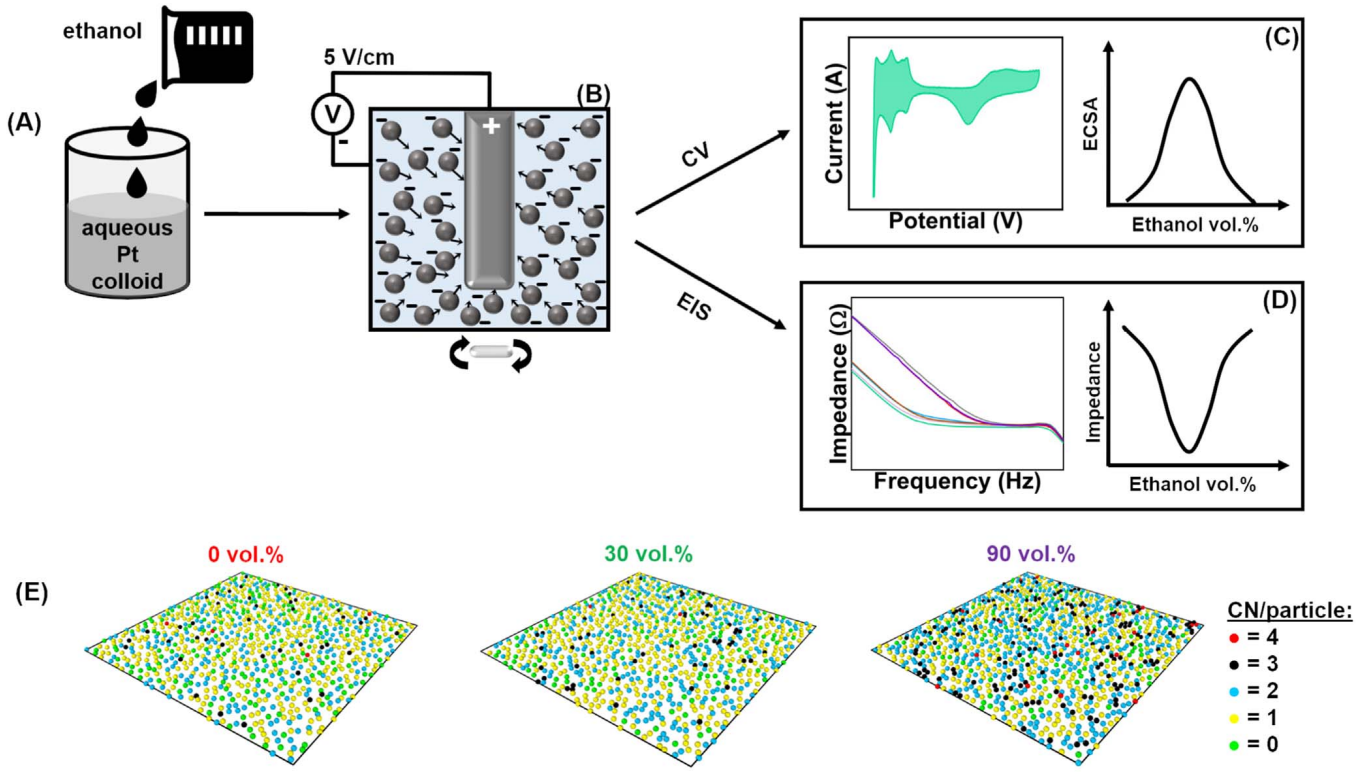

Figure 1. A schematic representation of the experimental workflow. (A) Ethanol mixed with aqueous PtNP colloids, (B) EPD of Pt-Ir wires, (C) CV measurements show a bell-shaped trend for ECSA, (D) EIS measurements reveal an inverted bell-shaped trend for *Z*, (E) Particle-based simulation snapshots, confirming higher levels of particle aggregation at 90 vol.% of ethanol.

EPD was carried out at 5 V/cm for 5 min during which the negatively charged PtNPs move toward the positively charged Pt surfaces and deposit onto their surfaces. The laser processing generally yields colloidal metal NPs with partial surface oxidation[46] as well as anion adsorption.[51] These two phenomena lead to a pH-dependent equilibrium between Pt-OH and Pt-O^- groups, which at alkaline pH lead to a pronounced negative surface charge.[52] Scanning electron microscopic images (SEM, Thermo Fisher Scientific, Apreo S LoVac; operating voltage: 5 kV) from the sides of Pt-Ir wires were obtained to analyze the deposit quality. Coated wires were mounted onto aluminum sample holders and electrical contact was established with conductive copper wires.

Electrochemical characterization.—To determine the electrochemical properties of the coated Pt-Ir wires, the samples were characterized using a three-electrode setup potentiostat (VersaSTAT 3F, AMETEK Scientific Instruments). A Pt wire was used as counter electrode and Ag/AgCl served as a reference electrode. Coated or uncoated Pt-Ir wires acted as working electrodes.

CV measurements were carried out in 1.0 M sulphuric acid solution. The vertex potentials were set between −0.2 and 1.2 V (vs RHE) and the scan rate was 0.2 V/s. Before measurements, the electrolyte was purged with nitrogen for 45 min and thereafter for 5 min between consecutive measurements. Twenty cycles were performed for each sample and the ECSA was calculated from the voltammogram using[53,54]

$$ECSA = Q_H/Q_a \qquad [1]$$

where Q_H is the charge associated with the hydrogen adsorption peak (refer Fig. 6) and Q_a is the theoretical charge density of polycrystalline Pt surface, 210 μ C cm^{-2}.[55–58] Alternatively, ECSA can also be calculated under consideration of PtNP mass loading for the purpose of roughness factor determination. Further information on this method can be found in the available at stacks.iop.org/JES/169/022504/mmediasupporting information Section S5.

Z measurements were performed in potentiostatic EIS mode in a frequency range from 1 Hz to 100 kHz by applying an AC_{rms} value of 10 mV and using 0.9% NaCl as the electrolyte (Fig. S3). The obtained data were plotted in Bode format (Z_{mag} vs frequency) and *Z* values at medically-relevant frequencies (150 Hz and 1 kHz) were examined. Additionally, the CSC was calculated via CV enlargement factor (integrating the AUC of one CV cycle,[59,60] Fig. S4).

Model details.—EPD simulations of the colloidal suspensions were performed using a 3D mesoscale multi-particle model described in detail elsewhere.[61,62] The model is formulated within the Molecular Dynamics framework and uses LAMMPS[63] to compute colloidal particle trajectories via Newtonian physics. The simulation is periodic in the *x*- and *y*-dimensions and bounded by a uniformly charged electrode located at $-z$. Colloid-colloid interactions are assumed to follow standard DLVO theory.[64,65] Since the colloids are ligand-free and highly mono-disperse, their steric interactions are well-described by van der Waals forces. Colloid-solvent interactions are stochastic and treated implicitly in a way that reproduces Stokes-Einstein diffusion.[66] For the simulated parameter sweep, all parameters like the system temperature *T* and ionic strength *I* are held constant except those that depend on the ethanol concentration: the relative dielectric constant ϵ_r, Debye length λ_D, and the effective charge on the colloid. The dielectric decreases with increasing ethanol concentration in a known empirical way.[67] This in turn changes the Debye length via

$$\lambda_D = \sqrt{\frac{\epsilon_r \epsilon_0 k_B T}{e^2 N_{Avogadro} I}} \qquad [2]$$

with vacuum permittivity ϵ_0, Boltzmann's constant k_B, Avogadro's number $N_{Avogadro}$, and elementary charge *e*. Thus, the characteristics length scale for electrostatic repulsion, λ_D, decreases as ethanol concentration increases. Simulations are initialized with randomized particle coordinates and deposited under an artificially high electric field of 5000 kV/m for 300 μs, equilibrated at appropriate experimental conditions, then resulting particle configurations are compared against each other over 900 μs of simulated time.

Statistical analysis.—All data points are presented as mean values ± standard deviation. Statistical analysis was performed in OriginLab (v. 2020b) software. One-way ANOVA statistical evaluations were performed on the data with Tukey's test as post-hoc comparison. The α value was set to 0.05, and the levels of statistical significance are represented as $*P \leqslant 0.05$, $**P \leqslant 0.01$, $***P \leqslant 0.001$ and $****P \leqslant 0.0001$.

Results and Discussion

To study the deposition mechanism in ethanol-water mixtures, Pt-Ir wires having the same geometry as that of the neural electrodes used for in vivo stimulations were coated with laser-generated PtNPs using DC EPD at 5 V/cm for 5 min. NP colloids in ethanol-water mixtures were prepared with different volumes of ethanol (0 vol.% (pure water), 10 vol.% through 90 vol.%, in steps of 20 vol.%) before deposition. In all the mixtures, the final Pt concentration was 100 μg/ml. Figure 2a shows the average mass deposited on the wires and Figs. 2b–d shows exemplary SEM images of sample surfaces coated with 0 vol.%, 30 vol.% and 90 vol.% of ethanol. An uncoated Pt-Ir surface is shown in Fig. S5a.

As we can see from Fig. 2(a), the mass deposited on samples increases with increasing ethanol concentration until it saturates at 50 vol.%. In general, the viscosity of water is less than that of ethanol.[68] Hence, when the quantity of ethanol increases, the viscosity of the suspension would also increase. According to Henry's equation,[66,44] the electrophoretic mobility of particles is inversely proportional to the suspension viscosity. Therefore, with increasing viscosity, the mobility of particles and hence the mass deposited on the surfaces should decrease. In our experiments, the deposited mass increases sharply until a certain value (50 vol.% of ethanol) and saturates for the samples that are coated with ethanol volumes higher than 50 vol.%. One explanation could be that at 50 vol.% or less, the beneficial effects from gas bubble reduction exceeds viscosity effects, however, after 50 vol.% the viscosity

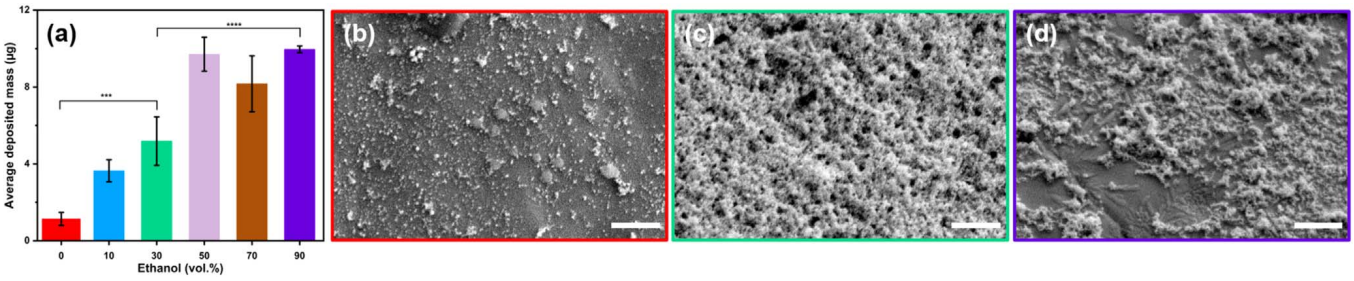

Figure 2. (a) Average deposited mass of PtNPs via DC EPD using increasing volume percentages of ethanol-water mixtures (N = 4, $\alpha = 0.05$); SEM images taken from the sides of Pt-Ir wires coated in (b) pure water, (c) 30 vol.% ethanol and (d) 90 vol.% ethanol. Scale bars are 500 nm.

becomes dominant and the curve saturates. Alternatively when ethanol concentration in water increases, the dielectric constant decreases,[67] thereby increasing the zeta potential.[69] This might also be a cause for higher levels of particle deposition at higher ethanol concentrations. Additionally, from the SEM images, we observe a qualitative influence of increasing ethanol volumes on the coating. The higher the viscosity (greater than 50 vol.%), the higher the inhomogeneity of the coating, displaying a more aggregated deposition (Figs. 2d and Fig. S5d). Sadeghi et al. studied the EPD of titania NPs in different alcohols and found that the EPD in highly viscous alcohols (like heptanol), produced non-uniform deposits with substantial amount of aggregates on the substrates.[50] This result corresponds with our observation, where at low viscosity the deposited mass was comparatively low (Figs. 2b, Fig. S5b), at intermediate viscosities of 30 vol.% (Fig. 2c) and 50 vol.% (Fig. S5c), the particles deposited with better uniformity and at higher viscosities, aggregated deposition was observed (Figs. 2d and S5d). The fact that low viscosity solvents produce homogeneous coatings, could be one of the reasons why this parameter remains as a desired suspension property during EPD.[44,70]

Since the qualitative SEM analysis suffers from poor statistics and inconclusive results, we performed particle-based numerical simulations to further analyze the impact of physical solvent parameters like viscosity and permittivity on coating quality. Experimental results by themselves make it difficult to elucidate the underlying mechanism, since they are produced by an overlap of inseparable physical effects. Main contributors to the indeterminate properties of the coatings would be: inhomogeneous electrode surface texture due to different deposition behaviors exhibited by the particles on edges (edge effect[46]), gas bubble formation due to water electrolysis (here, oxygen gas at the anode[71]) and solvent properties (viscosity, dielectric constants, etc.). Therefore, modeling studies were performed to separately evaluate the impact of liquid properties independent of the other effects.

Particle configurations within the simulated deposits are analyzed in order to discern how particle ordering changes with increasing ethanol concentration. The EPD model provides particle coordinates at each time step throughout the simulation. Particles are assigned randomized locations, deposited using an artificially high electric field, and then equilibrated under the experimental electric field before data is collected and analyzed. From these sets of deposits under experimental conditions, time-averaged measurements of the coordination number (CN) per particle and the radial distribution function (RDF)[43] are computed for each simulation. Figure 3a shows how the average CN of particles in the deposit increases with the ethanol concentration. Although this occurs over a narrow range (i.e. the maximum and minimum values are within 10%), the trend is readily apparent. At these conditions, the number of deposited particles and electrode area are equal, yielding surface coverage of 16.6% that is constant across all simulations. Thus, the trend in

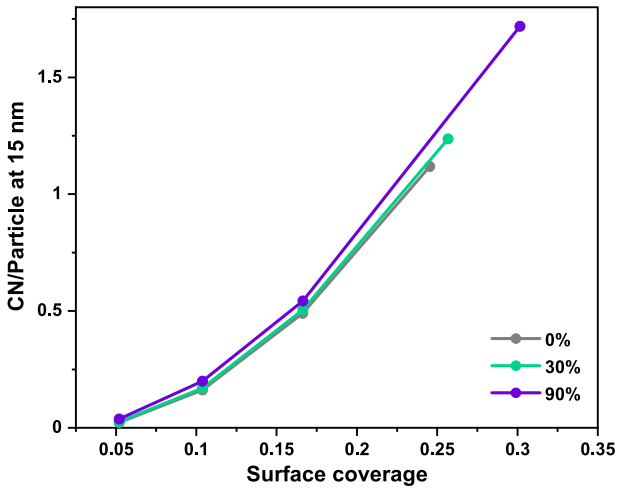

Figure 4. CN per particle as a function of surface coverage reveals an increased coverage with increasing ethanol concentrations, for a range of sub-monolayer packing densities. These subtle differences also match the trend revealed in Fig. 3.

Fig. 3(a) is due to the inter-particle interactions that allow for closer particle spacing at higher ethanol concentrations. As ethanol concentration increases, the relative permittivity and Debye length decrease, as shown in Figs. 3b and c, respectively. This reduces the range of electrostatic repulsion between colloids, allowing for a larger per-particle CN.

In accordance with the increasing particle CN, the RDFs ($g(r)$) reveal deposits formed in higher ethanol concentrations to exhibit particle configurations with a higher degree of ordering at short distances in Fig. S7. This is apparent in larger and non-monotonic RDF values at higher ethanol concentrations at short distances, i.e. $g_{90\%} > g_{0,30\%}$ for $r < 15$ nm. Since the sub-monolayer deposits in simulation contain the same number of particles, this is compensated with reduced probabilities of particles spaced at intermediate distances at higher ethanol concentrations $g_{90\%} < g_{0,30\%}$ for $15\ \text{nm} \leqslant r \leqslant 27\ \text{nm}$. Finally, as expected, all RDFs converge at far distances $g_{0,30,90\%}(r > 30\ \text{nm}) \rightarrow 1$. Since a Boltzmann inversion of the RDF yields the effective potential of mean force, these differences are also explained by smaller Debye lengths (and range of electrostatic repulsion) as ethanol concentration increases.

To explore the trends in Figs. 3 and S7 further, a parameter sweep was performed for simulations with a larger number of particles for select ethanol concentrations: 0%, 30%, and 90%. In Fig. 4, CN are computed from simulations in which all physical parameters were kept constant except the total number of particles. Since it is not guaranteed that all particles will deposit (and this is

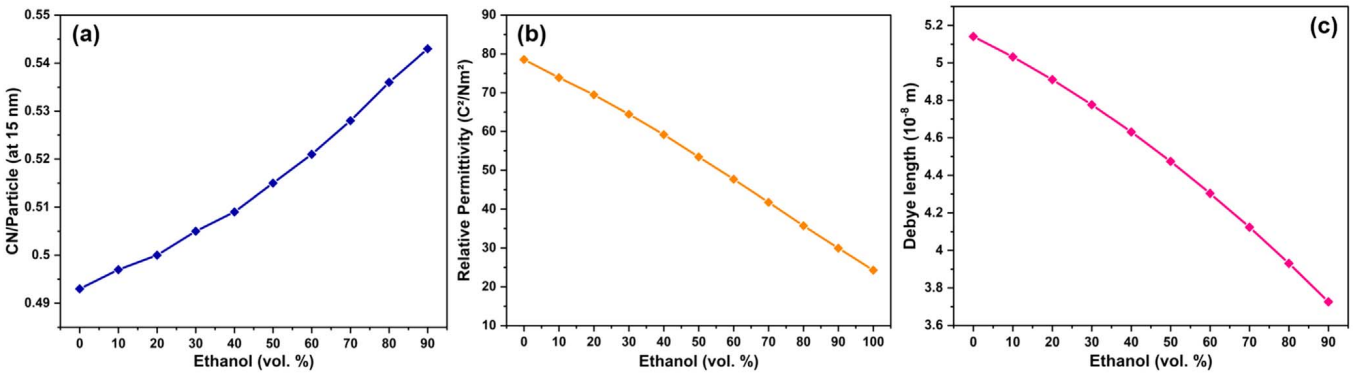

Figure 3. (a) Average CN per particle, computed at particle separation distances of 15 nm, increases with ethanol concentration, albeit over a tight range of values. Larger CNs per particle indicate an increasing degree of aggregation at higher ethanol concentrations. This is due to decreasing relative permittivity (b) and Debye lengths (c) over this range of ethanol concentrations, since the reduced range of electrostatic repulsion allows for closer particle spacing.

especially true at large particle loadings as described below), the surface coverage is not a programmable parameter. Nevertheless, the simulated range of surface coverage spans from 5% to 30%, with higher variability between simulations with more particles. As expected, the CN increases with surface coverage since the average spacing of particles decreases with increasing sub-monolayer deposit density. Furthermore, the CN increases with ethanol concentrations as shown in Fig. 3a and similarly increased local ordering can be seen in the radial distribution functions in Fig. S7. This behavior again can be explained by the decreasing Debye length with increasing ethanol concentration, shown quantitatively in Fig. 3b. Deposition differences with changing ethanol are subtle at surface coverages $\leqslant$16.6% but the trend appears more pronounced at larger surface coverage. Figure 5 shows simulation snapshots of the deposits taken from the highest particle loading for each ethanol concentration. The number of deposited particles and CN per particle can be seen to increase with ethanol concentration. Furthermore, a quantitative analysis of the CN distribution, Fig. 5d, shows how the majority of particles in 0% and 30% have CN = 1, which shifts to CN = 2 at 90%. Also, the number of uncoordinated particles, CN = 0, decreases with ethanol concentration.

The reduced repulsion at 90% ethanol (with the lowest simulated Debye length), produced the highest sub-monolayer packing—again because particles are able to arrange into denser configurations. It is worth noting that additional simulations were performed using a larger number of particles than shown here; however, simulated surface coverage values saturated at about 30%. This is because the collective inter-particle electrostatic repulsion from deposited particles is stronger than the electric field driving incoming particles toward the partially-coated electrode. Since more highly clustered deposits form in experiment, this suggests the model's assumptions (i.e. DLVO inter-particle physics and uniform electric fields) do not fully capture the system's physics when dense sub-monolayer deposits begin to form. For instance, it is possible that charge transfer between deposited particles and the electrode (not accounted for in the model), could reduce electrostatic repulsion and allow for more dense deposits. NP charge transfer has been reported in literature for laser-generated Pt[72] and Pd[73] NPs and other NP deposition systems.[74]

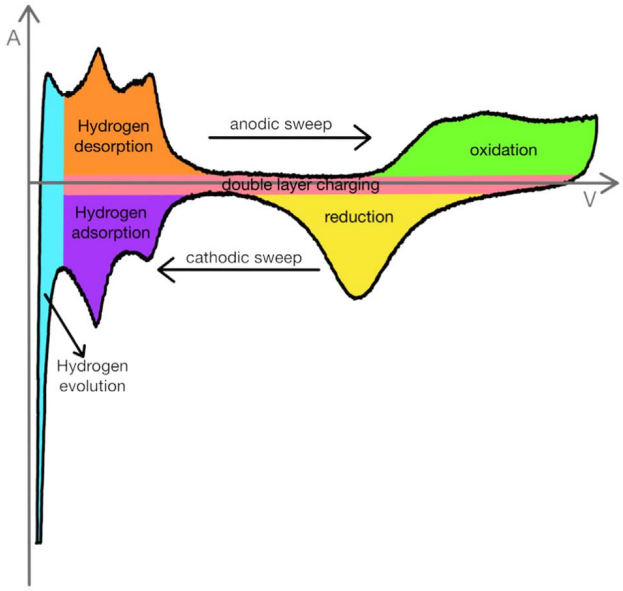

Figure 6. Schematic representation of a Pt voltammogram showing the processes occurring during one cycle in H_2SO_4 electrolyte.

As previously suggested, an impact of viscosity on coating homogeneity is observed. Higher ethanol concentration results in higher viscosity and lower dielectric constants. This eventually favors the formation of surface assemblages. These simulation results are in fair accordance with the experimental data where stronger assemblage formation was seen at higher ethanol concentrations. Based on this it may be concluded that physical solvent

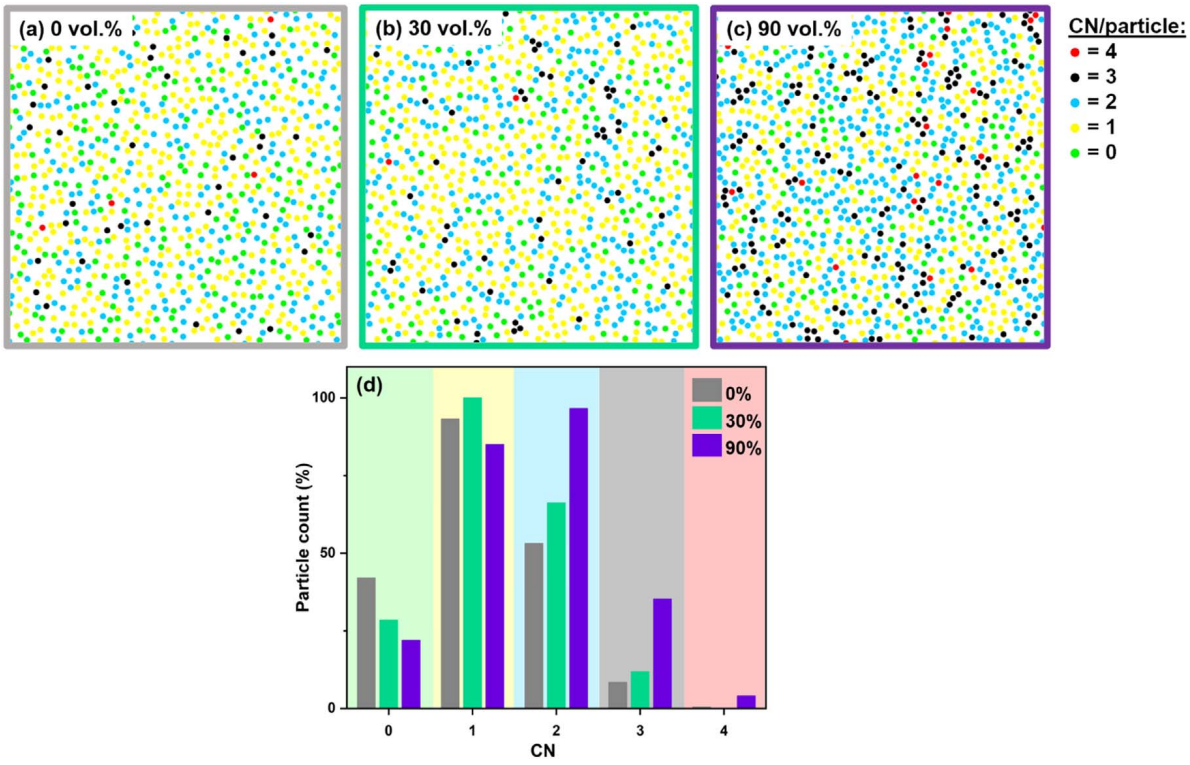

Figure 5. Snapshots of simulated deposits at the highest particle loading for (a) 0%, (b) 30% and (c) 90 % by volume ethanol concentration with particles colored according to the coordination number (legend). (d) The distribution of CN for these snapshots show how the peak in the CN shifts from 1 to 2 as ethanol concentration increases.

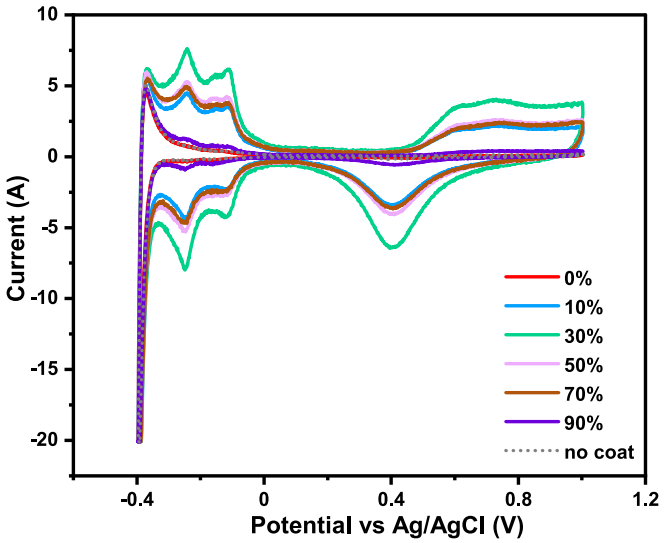

Figure 7. Exemplary cyclic voltammograms of Pt-Ir wires coated with PtNPs using increasing ethanol concentrations.

parameters like viscosity and dielectric constant are relevant contributors to coating quality during EPD. Furthermore, spherical NP surfaces possess larger surface areas compared to smooth and flat ones, however, it was recently estimated that the pure increase of GSA due to sub-monolayer NP deposition would have a negligible impact on the ECSA of the electrode.[43]

Therefore, upon revealing the correlation between ethanol concentration and coating homogeneity, we investigated how coating homogeneity, a strong function of solvent composition, would affect the electrochemical performance of PtNP coated samples. For this purpose CV (for determining ECSA) and EIS were performed. A typical cyclic voltammogram of Pt is shown in Fig. 6, illustrating the various processes taking place during an i–V sweep of a Pt electrode.[53,75,76–78]

CV of Pt in H_2SO_4 is one of the most commonly studied systems since it produces peaks characteristic of electrode-electrolyte interactions. When the anodic sweep (increasing potential in the positive direction) begins, hydrogen evolves and the evolved hydrogen atoms then desorb from the surface. This is followed by surface oxidation of Pt. When the potential is reversed (cathodic sweep), surface reduction occurs, followed by adsorption of hydrogen onto the Pt surface, thereby completing one i–V sweep.[75] It has been reported that one hydrogen atom is chemisorbed on each surface Pt atom (Pt:H = 1:1),[53,56] making the charge associated with hydrogen adsorption equivalent to the available ECSA of the electrodes. Therefore, for ECSA calculations, the area of the CV curve corresponding to the hydrogen adsorption charge is integrated (Fig. 6). In the double layer charging strip, the current remains constant and hence no electron transfer occurs.[75]

Cyclic voltammograms of DC-EPD coated Pt-Ir wires are shown in Fig. 7. The measurements were performed in a three-electrode potentiostat setup as explained before using 1.0 M H_2SO_4 as the electrolyte. Sulphuric acid produces stable Pt CV curves in comparison to other electrolytes.[75] CV of the coated samples were sweeped for 20 cycles until the curves stabilised,[78] and the 20th cycle was considered for evaluation. It was observed that the AUC increased for coatings with ethanol concentrations up to 30 vol.%, and then decreased gradually, while the 90 vol.% sample looked similar to that of an uncoated sample (dotted line in Fig. 7).

From the CV curves, ECSA was calculated by integrating the area associated with the charge of hydrogen adsorption on the surfaces and plotted against the different volume percentages of ethanol in colloid mixtures (Fig. 8a). An increasing trend in ECSA was seen until 30 vol.% after which it decreased. Please note that the ECSA may also be calculated under consideration of the GSA, with which roughness factor is calculated. Details on this procedure can be found in Section S5 of the supporting information, and the observed trends from both the calculation methods were similar. Average CSC values (Fig. 8b) of the samples were calculated by integrated AUC of one CV cycle and compared with increasing ethanol concentrations. ECSA and CSC are directly proportional to each other and the obtained results agree with the existing relationship,[36,57] with a significant ECSA increase by an enlargement factor of 7.

Impedance is the second critical parameter that dictates neural electrode functionality. Electrochemical impedances of the coated Pt-Ir wires were measured using a three-electrode potentiostat setup using 0.9% NaCl solution[47,79] as the electrolyte. A frequency range from 1 Hz to 100 kHz was measured (Fig. 9a). In medical practice, chronic deep brain stimulation uses frequencies between 130 and 180 Hz[80] and the neuronal action potentials are recorded at 1 kHz.[81] We selected these medically relevant frequencies of 150 Hz and 1 kHz and show Z versus volume percent ethanol for each in Figs. 9c and d. Therefore, at these frequencies, these Z versus solvent composition results represent stimulation and recording applications. From Figs. 9c and d, it is observed that the electrode Z decreased until it reached the statistically significant lowest value for 30 vol.% ethanol samples, and then increased again. For an optimum neural electrode performance, we wish to minimize Z in order to transfer electric charge to the tissues more efficiently. Additionally, the electrode Z decreases when ECSA increases.[82] Therefore, in both the frequencies (150 Hz and 1 kHz), the samples coated with 30 vol.% ethanol mixtures display effective results. These findings are in good accordance with the ECSA measurements and clearly indicate that EPD in a 30 vol.% ethanol solution yields the most favorable electrochemical properties of the electrode.

ECSA is a factor that increases when the minute surface areas of the electrodes are modified by the coating process. In this paper, spherical NPs are deposited onto surfaces, which increases the ECSA. Since it was discussed earlier that the GSA increase would have negligible impact on ECSA of the electrode,[43] it is highly probable that the higher chemical potential of the laser-fabricated PtNPs, which exhibit more surface defects and a substantial portion of oxidized surface atoms,[46,83] is the main contributor to the ECSA increase and Z decrease. Therefore, the functional readouts with an optimum of 30 vol.% ethanol are in good accordance with our previous prediction: more extensive and homogeneous coatings result in better preforming electrodes. Hence, at low ethanol quantities, the oxygen gas bubble formation reduces surface coverage and coating homogeneity, while at higher ethanol content, high viscosity favors the formation of aggregated coatings, as experimentally and theoretically observed. While the correlation of increasing functionality (significantly increased ECSA and decreased Z) with increasing coverage is straightforward and explains the increase of functionality at low ethanol concentrations well, the impact of assemblage formation and functionality is less straightforward. In this context, it has to be considered that in order to enable an efficient charge transfer between the surface-oxidized PtNPs (possessing high surface areas) and the electrode surface, an intensive contact (similar to a metallic bond) is necessary. However, when particles primarily deposit on other particles (as in assemblages), the GSA might increase but the bonding between the two particles is weaker than the ones between the electrode surface and the particles directly on it, giving insulating properties to the multilayers. As a consequence, electrical contact between the surface and the particle clusters would deteriorate, leading to an increased Z and reduced ECSA.

In accordance with our findings, use of ethanol for EPD has proven beneficial since it was shown to yield smooth and defect-free coatings.[44] Ethanol, when added to water in minimal quantities, reduces gas bubble evolution by water electrolysis.[84–86] However, this ”minimal” value depends on the system being used. In our case, different ethanol-water ratios (containing up to 90 vol.% of ethanol) were tested, and by trial-and-error approach it was observed that the

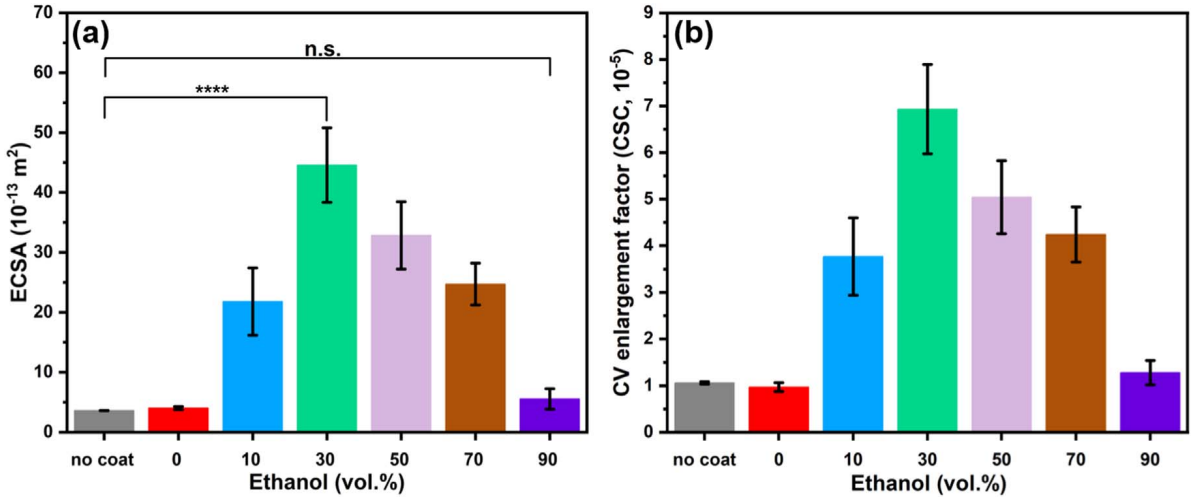

Figure 8. Average (a) ECSA (N = 4, $\alpha = 0.05$) and (b) CV enlargement factor (CSC) values (N = 4) of electrophoretically coated Pt-Ir wires with varying ethanol concentrations.

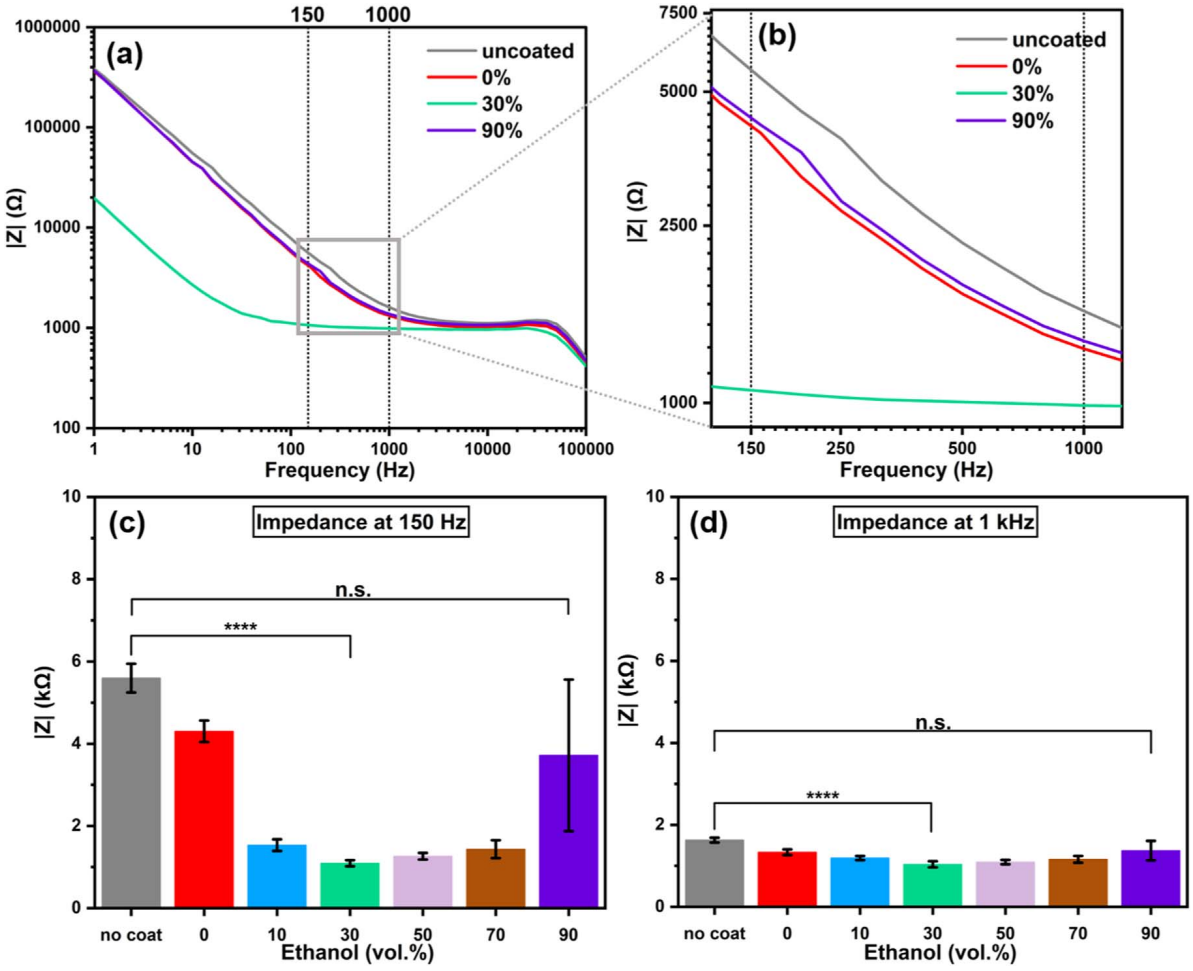

Figure 9. (a) EIS of Pt-Ir wires coated with PtNPs dispersed in 0 vol.%, 30 vol.% and 90 vol.% of ethanol mixtures. For comparison, the impedance spectrum of an uncoated wire is shown. (b) Enlarged image of (a) showing 150 Hz and 1 kHz reference lines. (c) Average impedance values of the samples at 150 Hz (N = 4, $\alpha = 0.05$). (d) Average impedance values of the samples at 1 kHz (N = 4, $\alpha = 0.05$).

most homogeneous coatings were obtained when a 30 vol.% ethanol and 70 vol.% water mixture was used.[86,87]

Conclusion

Electrochemistry of Pt electrodes greatly influence their performance in almost all applications, especially in neural stimulation and recording. Here, optimal performance is related to a high ECSA, high CSC and low *Z*. In this work, we demonstrate that the coating

of electrodes with laser-fabricated PtNPs via EPD is a suitable way to optimize and control their electrochemical properties. In contrast to all our previous works on EPD using aqueous medium, here we investigate the influence of solvent composition to optimize the EPD process of our system. We highlighted the influence of ethanol-water mixtures, which is frequently used in EPD studies. Our findings demonstrate that the solvent controls not only the surface coverage, but also the homogeneity of the deposits. Here, we find an optimum coating at an ethanol volume content of 30%, where the coatings are the most homogeneous. This finding can be attributed to two effects: (i) increasing coating quality with increasing ethanol concentration, hindering water splitting and gas bubble formation and (ii) the tendency to form particle assemblages in solvents with higher viscosity. We also demonstrated the utility of mesoscale computational simulations in elucidating the basic mechanisms of deposit formation in sub-monolayer EPD. Lastly, we have found interesting trends linking surface coating homogeneity with electrode functionality (significantly reduced impedance and an ECSA-increase by a factor of 7) which can pave the way toward optimization of electrode coating properties for applications in biomedicine.

Acknowledgments

We gratefully acknowledge the German Research Foundation (DFG) for their financial support under the project number BA 3580/24-1 and B.G. thanks DFG for Mercator Fellowship. This work was performed in part under the auspices of the U.S. Department of Energy by Lawrence Livermore National Laboratory under contract DE-AC52-07-NA27344, release number LLNL-JRNL-826684. V.R. thanks Tobias Bochmann (for the SEM measurements) and Johannes Wolter (for his support in the preliminary optimization experiments).

ORCID

Vaijayanthi Ramesh https://orcid.org/0000-0003-4753-5064
John J. Karnes https://orcid.org/0000-0002-2917-8406
Stephan Barcikowski https://orcid.org/0000-0002-9739-7272

References

1. J. Perez, E. Gonzalez, and E. Ticianelli, "Oxygen electrocatalysis on thin porous coating rotating platinum electrodes." *Electrochimica Acta*, **44**, 1329 (1998).
2. A. Feltham and M. Spiro, "Platinized platinum electrodes." *Chem. Rev.*, **71**, 177 (1971).
3. A. Kloke, F. von Stetten, R. Zengerle, and S. Kerzenmacher, "Strategies for the fabrication of porous platinum electrodes." *Adv. Mater.*, **23**, 4976 (2011).
4. Y. Y. Song, D. Zhang, W. Gao, and X. H. Xia, "Nonenzymatic glucose detection by using a three-dimensionally ordered, macroporous platinum template." *Chemistry—A European Journal*, **11**, 2177 (2005).
5. J. Yuan, K. Wang, and X. Xia, "Highly ordered platinum-nanotubule arrays for amperometric glucose sensing." *Adv. Funct. Mater.*, **15**, 803 (2005).
6. Y. J. Lee, D. J. Park, and J. Y. Park, "Fully packaged nonenzymatic glucose microsensors with nanoporous platinum electrodes for anti-fouling." *IEEE Sens. J.*, **8**, 1922 (2008).
7. J. Noh, S. Park, H. Boo, H. C. Kim, and T. D. Chung, "Nanoporous platinum solid-state reference electrode with layer-by-layer polyelectrolyte junction for pH sensing chip." *Lab Chip*, **11**, 664 (2011).
8. J. H. Han, S. Park, H. Boo, H. C. Kim, J. Noh, and T. D. Chung, "Solid-State Reference Electrode Based on Electrodeposited Nanoporous Platinum for Microchip." *Electroanalysis: An International Journal Devoted to Fundamental and Practical Aspects of Electroanalysis*, **19**, 786 (2007).
9. Y. J. Lee and J. Y. Park, "A Highly Miniaturized Dissolved Oxygen Sensor Using a Nanoporous Platinum Electrode Electroplated on Silicon." *J. Korean Phys. Soc.*, **58**, 1505 (2011).
10. A. Weremfo, P. Carter, D. B. Hibbert, and C. Zhao, "Investigating the interfacial properties of electrochemically roughened platinum electrodes for neural stimulation." *Langmuir*, **31**, 2593 (2015).
11. K. U. Sikder, M. N. Shivdasani, J. B. Fallon, P. Seligman, K. Ganesan, J. Villalobos, S. Prawer, and D. J. Garrett, "Electrically conducting diamond films grown on platinum foil for neural stimulation." *Journal of Neural Engineering*, **16**, 066002 (2019).
12. K. G. Shah, V. M. Tolosa, A. C. Tooker, S. H. Felix, and S. S. Pannu, "Improved chronic neural stimulation using high surface area platinum electrodes." *35th Annual International Conference of the IEEE Engineering in Medicine and Biology Society (EMBC)*1546 (2013).
13. C. Bodart, N. Rossetti, J. Hagler, P. Chevreau, D. Chhin, F. Soavi, S. B. Schougaard, F. Amzica, and F. Cicoira, "Electropolymerized poly (3,4-ethylenedioxythiophene)(PEDOT) coatings for implantable deep-brain-stimulating microelectrodes." *ACS Applied Materials & Interfaces*, **11**, 17226 (2019).
14. C. Boehler, D. M. Vieira, U. Egert, and M. Asplund, "NanoPtA nanostructured electrode coating for neural recording and microstimulation." *ACS Applied Materials & Interfaces*, **12**, 14855 (2020).
15. L. C. Wang, M. H. Wang, C. F. Ge, B. W. Ji, Z. J. Guo, X. L. Wang, B. Yang, C. Y. Li, and J. Q. Liu, "The use of a double-layer platinum black-conducting polymer coating for improvement of neural recording and mitigation of photoelectric artifact." *Biosensors and Bioelectronics*, **145**, 111661 (2019).
16. J. H. Bae, K. Kim, D. Han, and T. D. Chung, "Ultra Compact Nanoporous Platinum Coating Improves Neural Recording." *Electroanalysis*, **33**, 839.
17. L. Yue, V. Wuyyuru, A. Gonzalez-Calle, J. D. Dorn, and M. S. Humayun, "Retina-electrode interface properties and vision restoration by two generations of retinal prostheses in one patient–one in each eye." *Journal of Neural Engineering*, **17**, 026020 (2020).
18. R. Green, P. Matteucci, C. Dodds, J. Palmer, W. Dueck, R. Hassarati, P. Byrnes-Preston, N. Lovell, and G. Suaning, "Laser patterning of platinum electrodes for safe neurostimulation." *Journal of Neural Engineering*, **11**, 056017 (2014).
19. A. Barriga-Rivera, L. Bareket, J. Goding, U. A. Aregueta-Robles, and G. J. Suaning, "Visual prosthesis: interfacing stimulating electrodes with retinal neurons to restore vision." *Frontiers in Neuroscience*, **11**, 620 (2017).
20. K. Wissel, G. Brandes, N. Pütz, G. L. Angrisani, J. Thieleke, T. Lenarz, and M. Durisin, "Platinum corrosion products from electrode contacts of human cochlear implants induce cell death in cell culture models." *PLoS One*, **13**, e0196649 (2018).
21. C. D. Lee, E. M. Hudak, J. J. Whalen III, A. Petrossians, and J. D. Weiland, "Low-impedance, high surface area Pt-Ir electrodeposited on cochlear implant electrodes." *J. Electrochem. Soc.*, **165**, G3015 (2018).
22. W. Franks, I. Schenker, P. Schmutz, and A. Hierlemann, "Impedance characterization and modeling of electrodes for biomedical applications." *IEEE Transactions on Biomedical Engineering*, **52**, 1295 (2005).
23. M. K. Nazeeruddin, E. Baranoff, and M. Grätzel, "Dye-sensitized solar cells: A brief overview." *Solar energy*, **85**, 1172 (2011).
24. S. J. Cho and J. Ouyang, "Attachment of platinum nanoparticles to substrates by coating and polyol reduction of a platinum precursor." *The Journal of Physical Chemistry C*, **115**, 8519 (2011).
25. G. Calogero, P. Calandra, A. Irrera, A. Sinopoli, I. Citro, and G. Di Marco, "A new type of transparent and low cost counter-electrode based on platinum nanoparticles for dye-sensitized solar cells." *Energy & Environmental Science*, **4**, 1838 (2011).
26. S. F. Cogan, "Neural stimulation and recording electrodes." *Annual Reviews Biomedical Engineering*, **10**, 275 (2008).
27. R. J. Seymour, J. I. O'Farrelly, and L. C. Potter, *Platinum-group metals* (Wiley, Kirk-Othmer Encyclopedia of Chemical Technology) (2000).
28. S. Schlie-Wolter, A. Deiwick, E. Fadeeva, G. Paasche, T. Lenarz, and B. N. Chichkov, "Topography and coating of platinum improve the electrochemical properties and neuronal guidance." *ACS Applied Materials & Interfaces*, **5**, 1070 (2013).
29. D. F. Acevedo, H. J. Salavagione, A. F. Lasagni, E. Morallon, F. Mücklich, and C. Barbero, "Fabrication of highly ordered arrays of platinum nanoparticles using direct laser interference patterning." *ACS Applied Materials & Interfaces*, **1**, 549 (2009).
30. K. R. Knowles, C. C. Hanson, A. L. Fogel, B. Warhol, and D. A. Rider, "Layer-by-layer assembled multilayers of polyethylenimine-stabilized platinum nanoparticles and PEDOT:PSS as anodes for the methanol oxidation reaction." *ACS Applied Materials & Interfaces*, **4**, 3575 (2012).
31. H. Vara and J. E. Collazos-Castro, "Biofunctionalized conducting polymer/carbon microfiber electrodes for ultrasensitive neural recordings." *ACS Applied Materials & Interfaces*, **7**, 27016 (2015).
32. M. Ryu et al., "Enhancement of interface characteristics of neural probe based on graphene, ZnO nanowires, and conducting polymer PEDOT." *ACS Applied Materials & Interfaces*, **9**, 10577 (2017).
33. D. E. Arreaga-Salas, A. Avendaño-Bolívar, D. Simon, R. Reit, A. Garcia-Sandoval, R. L. Rennaker, and W. Voit, "Integration of high-charge-injection-capacity electrodes onto polymer softening neural interfaces." *ACS Applied Materials & Interfaces*, **7**, 26614.
34. M. Ferguson, D. Sharma, D. Ross, and F. Zhao, "A critical review of microelectrode arrays and strategies for improving neural interfaces." *Advanced Healthcare Materials*, **8**, 1900558 (2019).
35. S. Khan and G. Newaz, "A comprehensive review of surface modification for neural cell adhesion and patterning." *Journal of Biomedical Materials Research Part A*, **93**, 1209 (2010).
36. Y. F. Rui, J. Q. Liu, B. Yang, K. Y. Li, and C. S. Yang, "Parylene-based implantable platinum-black coated wire microelectrode for orbicularis oculi muscle electrical stimulation." *Biomedical microdevices*, **14**, 367 (2012).
37. T. Rose and L. Robblee, "Electrical stimulation with Pt electrodes. VIII. Electrochemically safe charge injection limits with 0.2 ms pulses (neuronal application)." *IEEE Transactions on Biomedical Engineering*, **37**, 1118 (1990).
38. J. A. Fairfield, "Nanostructured materials for neural electrical interfaces." *Adv. Funct. Mater.*, **28**, 1701145 (2018).
39. R. A. Green, R. T. Hassarati, L. Bouchinet, C. S. Lee, G. L. Cheong, F. Y. Jin, C. W. Dodds, G. J. Suaning, L. A. Poole-Warren, and N. H. Lovell, "Substrate dependent stability of conducting polymer coatings on medical electrodes." *Biomaterials*, **33**, 5875 (2012).
40. T. Boretius, M. Schuettler, and T. Stieglitz, "On the stability of poly-ethylenedioxythiopene as coating material for active neural implants." *Artificial organs*, **35**, 245 (2011).

41. A. Zátonyi, F. Fedor, Z. Borhegyi, and Z. Fekete, "In vitro and in vivo stability of black-platinum coatings on flexible, polymer microECoG arrays." *Journal of Neural Engineering*, **15**, 054003 (2018).
42. M. Leber, R. Bhandari, J. Mize, D. Warren, M. Shandhi, F. Solzbacher, and S. Negi, "Long term performance of porous platinum coated neural electrodes." *Biomedical microdevices*, **19**, 1 (2017).
43. V. Ramesh, C. Rehbock, B. Giera, J. J. Karnes, J. B. Forien, S. D. Angelov, K. Schwabe, J. K. Krauss, and S. Barcikowski, "Comparing Direct and Pulsed-Direct Current Electrophoretic Deposition on Neural Electrodes: Deposition Mechanism and Functional Influence." *Langmuir*, **37**, 9724 (2021).
44. L. Besra and M. Liu, *A review on fundamentals and applications of electrophoretic deposition (EPD) Progress in materials science*, **52**, 1 (2007).
45. C. Streich, S. Koenen, M. Lelle, K. Peneva, and S. Barcikowski, "Influence of ligands in metal nanoparticle electrophoresis for the fabrication of biofunctional coatings." *Appl. Surf. Sci.*, **348**, 92 (2015).
46. S. Koenen, C. Rehbock, H. E. Heissler, S. D. Angelov, K. Schwabe, J. K. Krauss, and S. Barcikowski, "Optimizing in Vitro Impedance and Physico-Chemical Properties of Neural Electrodes by Electrophoretic Deposition of Pt Nanoparticles." *ChemPhysChem*, **18**, 1108 (2017).
47. S. D. Angelov, S. Koenen, J. Jakobi, H. E. Heissler, M. Alam, K. Schwabe, S. Barcikowski, and J. K. Krauss, *Electrophoretic deposition of ligand-free platinum nanoparticles on neural electrodes affects their impedance in vitro and in vivo with no negative effect on reactive gliosis Journal of Nanobiotechnology*, **14**, 1 (2016).
48. L. Besra, T. Uchikoshi, T. S. Suzuki, and Y. Sakka, "Bubble-Free Aqueous Electrophoretic Deposition (EPD) by Pulse-Potential Application." *J. Am. Ceram. Soc.*, **91**, 3154 (2008).
49. T. Uchikoshi, K. Ozawa, B. D. Hatton, and Y. Sakka, "Dense, bubble-free ceramic deposits from aqueous suspensions by electrophoretic deposition." *J. Mater. Res.*, **16**, 321 (2001).
50. A. Sadeghi, T. Ebadzadeh, B. Raissi, and S. Ghashghaie, "Electrophoretic deposition of TiO_2 nanoparticles in viscous alcoholic media." *Ceramics International*, **39**, 7433 (2013).
51. C. Pfeiffer, C. Rehbock, D. Hühn, C. Carrillo-Carrion, D. J. de Aberasturi, V. Merk, S. Barcikowski, and W. J. Parak, "Interaction of colloidal nanoparticles with their local environment: the (ionic) nanoenvironment around nanoparticles is different from bulk and determines the physico-chemical properties of the nanoparticles." *Journal of The Royal Society Interface*, **11**, 20130931 (2014).
52. S. Barcikowski, V. Amendola, M. Lau, G. Marzun, C. Rehbock, S. Reichenberger, D. Zhang, and B. Gökce, *Handbook of Laser Synthesis & Processing of Colloids* (DuEPublico, Duisburg-Essen Publications online) (2019).
53. S. Campbell, J. Smith, G. Lloyd, F. Walsh, and T. Ralph, "Electrochemical and microscopic characterisation of platinum-coated perfluorosulfonic acid (Nafion 117) materials." *Analyst*, **123**, 1923 (1998).
54. E. P. Lee, Z. Peng, D. M. Cate, H. Yang, C. T. Campbell, and Y. Xia, "Growing Pt nanowires as a densely packed array on metal gauze." *J. Am. Chem. Soc.*, **129**, 10634 (2007).
55. A. Capon and R. Parsons, "The oxidation of formic acid at noble metal electrodes Part III. Intermediates and mechanism on platinum electrodes." *Journal of Electroanalytical Chemistry and Interfacial Electrochemistry*, **45**, 205 (1973).
56. S. Trasatti and O. Petrii, "Real surface area measurements in electrochemistry." *Journal of Electroanalytical Chemistry*, **327**, 353 (1992).
57. T. Boretius, T. Jurzinsky, C. Koehler, S. Kerzenmacher, H. Hillebrecht, and T. Stieglitz, "High-porous platinum electrodes for functional electrical stimulation."*Annual International Conference of the IEEE Engineering in Medicine and Biology Society*, pp.5404-5407 (2011).
58. D. W. Kumsa, N. Bhadra, E. M. Hudak, S. C. Kelley, D. F. Untereker, and J. T. Mortimer, "Electron transfer processes occurring on platinum neural stimulating electrodes: a tutorial on the i(Ve) profile." *Journal of Neural Engineering*, **13**, 052001 (2016).
59. C. Boehler, T. Stieglitz, and M. Asplund, "Nanostructured platinum grass enables superior impedance reduction for neural microelectrodes." *Biomaterials*, **67**, 346 (2015).
60. M. Ganji et al., "Selective formation of porous Pt nanorods for highly electro-chemically efficient neural electrode interfaces." *Nano Lett.*, **19**, 6244 (2019).
61. B. Giera, L. A. Zepeda-Ruiz, A. J. Pascall, and T. H. Weisgraber, *Mesoscale particle-based model of electrophoretic deposition Langmuir*, **33**, 652 (2017).
62. S. C. Bukosky, J. A. Hammons, B. Giera, E. Lee, J. Han, M. C. Freyman, A. Ivanovskaya, K. G. Krauter, J. D. Kuntz, M. A. Worsley, T. Y. J. Han, W. D. Ristenpart, and A. J. Pascall, "Correlating dynamic microstructure to observed color in electrophoretic displays via in situ small-angle x-ray scattering." *Phys. Rev. Materials*, **4**, 075802 (2020).
63. S. Plimpton, "Fast Parallel Algorithms for Short-Range Molecular-Dynamics." *J. Comput. Phys.*, **117**, 1 (1995).
64. B. Derjaguin and L. Landau, "The Theory of Stability of Highly Charged Lyophobic Sols and Coalescence of Highly Charged Particles in Electrolyte Solutions." *Acta Physicochim URSS*, **14**, 633 (1941).
65. E. Verwey and G. Overbeek, *Theory of the Stability of Lyophobic Colloids Elsevier*, **1**, 205 (1948).
66. B. Giera, L. A. Zepeda-Ruiz, A. J. Pascall, J. D. Kuntz, C. M. Spadaccini, and T. H. Weisgraber, *Mesoscale particle-based model of electrophoresis JES*, **162**, D3030 (2015).
67. J. Wyman, "The dielectric constant of mixtures of ethyl alcohol and water from-5 to 40 degrees." *J. Am. Chem. Soc.*, **53**, 3292 (1931).
68. Y. Tanaka, T. Yamamoto, Y. Satomi, H. Kubota, and T. Makita, *Specific volume and viscosity of ethanol-water mixtures under high pressure The Review of Physical Chemistry of Japan*, **47**, 12http://hdl.handle.net/2433/47042 (1977).
69. G. V. Lowry, R. J. Hill, S. Harper, A. F. Rawle, C. O. Hendren, F. Klaessig, Ul. f. Nobbmann, P. Sayre, and J. Rumble, "Guidance to improve the scientific value of zeta-potential measurements in nanoEHS." *Environmental Science: Nano*, **3**, 953 (2016).
70. B. Ferrari and R. Moreno, "Electrophoretic deposition of aqueous alumina slips." *J. Eur. Ceram. Soc.*, **17**, 549 (1997).
71. S. Hu, W. Li, H. Finklea, and X. Liu, "A review of electrophoretic deposition of metal oxides and its application in solid oxide fuel cells." *Adv. Colloid Interface Sci.*, **276**, 102102 (2020).
72. G. Marzun, C. Streich, S. Jendrzej, S. Barcikowski, and P. Wagener, "Adsorption of colloidal platinum nanoparticles to supports: charge transfer and effects of electrostatic and steric interactions." *Langmuir*, **30**, 11928 (2014).
73. X. Zhang, W. Ooki, Y. R. Kosaka, A. Okonogi, G. Marzun, P. Wagener, S. Barcikowski, T. Kondo, and J. Nakamura, "Effect of pH on the spontaneous synthesis of palladium nanoparticles on reduced graphene oxide." *Appl. Surf. Sci.*, **389**, 911 (2016).
74. M. A. Bratescu and N. Saito, "Charge doping of large-area graphene by gold-alloy nanoparticles." *The Journal of Physical Chemistry C*, **117**, 26804 (2013).
75. E. M. Hudak, D. W. Kumsa, H. B. Martin, and J. T. Mortimer, "Electron transfer processes occurring on platinum neural stimulating electrodes: calculated charge-storage capacities are inaccessible during applied stimulation." *Journal of Neural Engineering*, **14**, 046012 (2017).
76. A. Pazio, M. De Francesco, A. Cemmi, F. Cardellini, and L. Giorgi, *Comparison of High Surface Pt/C Catalysts by Cyclic Voltammetry J. of Power Source*, **105**, 13 (2002).
77. G. Jerkiewicz, G. Vatankhah, J. Lessard, M. P. Soriaga, and Y. S. Park, "Surface-oxide growth at platinum electrodes in aqueous H_2SO_4: Reexamination of its mechanism through combined cyclic-voltammetry, electrochemical quartz-crystal nanobalance, and Auger electron spectroscopy measurements." *Electrochimica Acta*, **49**, 1451 (2004).
78. D. Rand and R. Woods, "A study of the dissolution of platinum, palladium, rhodium and gold electrodes in 1 M sulphuric acid by cyclic voltammetry." *Journal of Electroanalytical Chemistry and Interfacial Electrochemistry*, **35**, 209 (1972).
79. K. Wang, L. Tian, T. Wang, Z. Zhang, X. Gao, L. Wu, B. Fu, and X. Liu, "Electrodeposition of alginate with PEDOT/PSS coated MWCNTs to make an interpenetrating conducting hydrogel for neural interface." *Composite Interfaces*, **26**, 27 (2019).
80. S. Groiss, L. Wojtecki, M. Südmeyer, and A. Schnitzler, "Deep brain stimulation in Parkinson's disease." *Therapeutic advances in neurological disorders*, **2**, 379 (2009).
81. N. Lago and A. Cester, "Flexible and organic neural interfaces: a review." *Applied Sciences*, **7**, 1292 (2017).
82. A. T. Young, N. Cornwell, and M. A. Daniele, "Neuro-Nano Interfaces: Utilizing Nano-Coatings and Nanoparticles to Enable Next-Generation Electrophysiological Recording, Neural Stimulation, and Biochemical Modulation." *Adv. Funct. Mater.*, **28**, 1700239 (2018).
83. S. Reichenberger, G. Marzun, M. Muhler, and S. Barcikowski, "Perspective of surfactant-free colloidal nanoparticles in heterogeneous catalysis." *ChemCatChem*, **11**, 4489 (2019).
84. M. Schäfer, L. Vogt, F. Raether, and D. Kurth, "Towards local deposition of particles by electrophoresis in dc electric fields in polar and nonpolar media and mixtures thereof." *Ceramics International*, **46**, 17857 (2020).
85. D. Kuscer, M. S. Bernardo, M. Z. Santo, and B. Malič, "Patterning of lead-zirconate-titanate thick-film structures by electrophoretic deposition from ethanol-based dispersions." *J. Eur. Ceram. Soc.*, **36**, 291 (2016).
86. L. E. C. Arias, "Electrophoretic deposition of organic/inorganic composite coatings on metallic substrates for bone replacement applications: mechanisms and development of new bioactive materials based on polysaccharides." *Ph.D. thesis*, Friedrich-Alexander-Universität Erlangen-Nürnberg (FAU) (2015).
87. Q. Chen, L. Cordero-Arias, J. A. Roether, S. Cabanas-Polo, S. Virtanen, and A. R. Boccaccini, "Alginate/Bioglass®composite coatings on stainless steel deposited by direct current and alternating current electrophoretic deposition." *Surf. Coat. Technol.*, **233**, 49 (2013).

5 Influence of Platinum Alloy Nanoparticle EPD on Neural Electrode Impedance Reduction

Unpublished results under submission:

Platinum-Iridium Alloy Nanoparticle Coatings Produced by Electrophoretic Deposition Reduce Impedance in 3D Neural Electrodes

Vaijayanthi Ramesh[1], Jacob Johny[1], Jurij Jakobi[1], Christoph Rehbock[1] and Stephan Barcikowski[1,*]

[1] Institute of Technical Chemistry I, University of Duisburg-Essen and Center for Nanointegration Duisburg-Essen (CENIDE), Essen, Germany

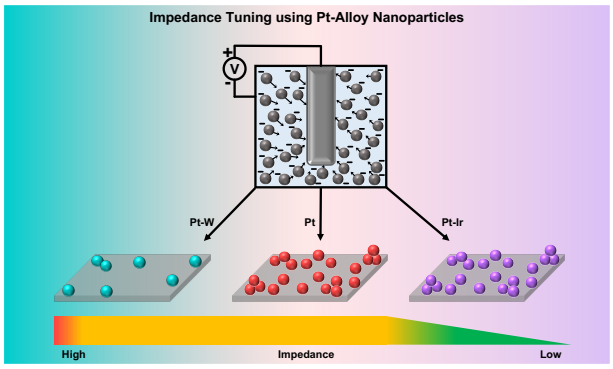

Summary:

Upon investigating the influence of applied electric field and solvent composition in the previous sections, the influence of Pt-based alloy NPs on the electrochemical properties of the electrodes was studied in the following using neural electrode-relevant materials. For this, the PtNPs were alloyed with Ir and W, which are the constituents of neural electrode materials and hence might minimally affect the clinical approval of the coatings. The results generated showed that the Pt90Ir10 alloy NP could significantly lower the impedance in comparison to the other combinations.

Author contributions:

Design and supervision of the experiments on EPD of NPs using various alloy materials including their characterization were performed by VR. HR-TEM measurements were performed by JJ and the XRD analysis was by JaJ. The original manuscript draft was prepared by VR. The review and editing of the manuscript were carried out by VR, CR, and SB. SB and CR designed the study and supervised and obtained funding support.

Platinum-Iridium Alloy Nanoparticle Coatings Produced by Electrophoretic Deposition Reduce Impedance in 3D Neural Electrodes

Vaijayanthi Ramesh[1], Jacob Johny[1], Jurij Jakobi[1], Christoph Rehbock[1] and Stephan Barcikowski[1,*]

[1] Technical Chemistry I, University of Duisburg-Essen and Center for Nanointegration Duisburg-Essen (CENIDE), Universitaetsstr. 7, 45141 Essen, Germany.

Abstract

Platinum-based neural electrodes frequently alloyed with Ir or W are routinely used for the treatment of neurological conditions like movement disorders. However, the performance of neural electrodes is hampered by impaired electrical contact of the electrode and tissue or physiological reactions that compromise long-term implant stability. Though there are multiple coating techniques available to address this issue, electrode, and base material often exhibit a compositional mismatch, which not only impairs mechanical stability but can also lead to toxicological side effects that limit clinical approval. In addition, it is known that iridium has beneficial electrophysiological properties. Hence, a coating with a composition closely matching the electrode base material, that is a Pt-Ir or Pt-W alloy depending on the electrode application, is in high demand. To this end we coated Pt wire electrodes with organic ligand-free electrostatically stabilized colloidal Pt90Ir10, Pt90W10, and Pt50W50 alloy nanoparticles (NPs) using electrophoretic deposition (EPD) with direct-current (DC) and pulsed-DC fields in aqueous medium. Pt coatings were utilized as controls. The generated alloy NPs exhibit a solid solution structure as evidenced by HR-TEM-EDX and XRD, though additional WO_x phases were identified in the Pt50W50 samples. Consequently, coating efficiency was also impaired in the presence of high W mass fractions in the alloy NPs. Characterization of the NP coatings by cyclic voltammetry and impedance spectroscopy yielded a significant reduction of the impedance in the Pt90Ir10 sample in comparison to the Pt control. The electrochemical surface area (ECSA) of the PtW alloy coatings, on the other hand, was significantly reduced. Based on these findings it may be concluded that alloying PtNPs in neural electrode coatings with low portions of Ir significantly improves the electrode's electrochemical performance, while the addition of W is less beneficial, probably due to the formation of oxide phases.

Keywords: Biomaterials, laser ablation in liquids, laser fragmentation in liquids, cyclic voltammetry, tungsten oxide, ligand-free nanoparticles, and surface charge.

1 Introduction

Neural electrodes made of noble metals like platinum (Pt) are often coated with Pt or platinum-based alloy micro- and nanostructures for the purpose of surface modification[1]. These coatings

are pseudocapacitive in nature, which means the charging and discharging process during neural stimulation is highly reversible, i.e., no unwanted chemical byproducts are formed [1,2]. Recent studies indicate that platinum-based alloy coatings possess better electrochemical properties than their Pt counterparts [3], and the most frequently applied alloy coating is platinum-iridium (PtIr) [4,5,3,6,7]. PtIr alloy was electrodeposited on cochlear implants, resulting in decreased impedance (Z), which could improve the sound quality and spectral resolution [4], significantly increased charge storage capacity (CSC), and decreased Z [6]. Cassar et al. electrodeposited Pt60Ir40 coatings onto commercially available 16-electrode microwire arrays, implanted them in Parkinson's rat models for 12 weeks, and tested them for single-unit recording capabilities. Their coated electrodes showed reduced Z, reduced noise, and increased signal-to-noise ratio [5]. Similarly, Petrossians and co-workers electrodeposited Pt60Ir40 coatings on Pt microelectrode arrays and investigated their performances. They observed an increased electrochemically active surface area (ECSA), more than two orders of magnitude decrease in Z, and an increase in capacitance of these coatings in comparison to a simple Pt coating [7,3]. It should be noted that in all of the above-mentioned studies, the PtIr coatings were produced directly from an electrolyte containing Pt and Ir salts. Furthermore, a few studies have also investigated the performance of tungsten (W) microwires for the purpose of neural recording. Prasad and co-workers implanted W microwire arrays into the cortex of rats and monitored their Z daily. They observed a continuous increase in the Z value during a 5-week period [8,9].

In this context, electrophoretic deposition (EPD) of laser-fabricated nanoparticles (NPs) is an attractive and simple technique to modify surfaces of different geometries. These purely electrostatically stabilized NPs are free from ligand contaminants and hence the deposition rate linearly increases with time, which allows excellent scaling of the deposition process [10,11]. Since laser-generated NPs are spherical in nature, they possess a high surface area-to-volume ratio, which could also help in the increase of ECSA. Previously, we performed EPD of PtNPs on 2D surfaces to optimize the process parameters [11] and investigated the *in vivo* functionality of EPD-coated neural electrodes by implanting them into the subthalamic nucleus of model rats [12]. In our more recent work, we compared the coating homogeneity and electrode performance of PtNP-coated neural electrodes by applying direct current (DC) and pulsed direct current (PDC) electric fields [13]. It was observed that due to the pulsation of the applied electric field in PDC-EPD, the homogeneity of the surface coatings increased in comparison to the ones coated using DC fields, which significantly decreased the electrode Z. To study the influence of solvent composition during EPD, we also examined the process in the presence of ethanol-water mixtures and observed a seven-fold increase in ECSA at an ethanol mass content of 30% [14]. To test the mechanical stability of the EPD-generated Pt-nanocoatings, in vivo and in vitro stability tests were performed and delamination in simulated brain environments was shown to be minimal. Furthermore, the Pt mass released into the explanted in vivo brain sections was four times lower in magnitude than those reported in Pt-nanotoxicity literature and the mechanical stability of the nanocoatings was high even after 4 weeks of in vivo stimulation [15]. Moreover, postoperative recovery and histological analysis revealed that NP coating did not affect glial reactions or neuronal cell count, showing that coating with NP $\leq$ 10 nm may improve electrode impedance stability without affecting biocompatibility [12].

In the present work, we systematically investigate the electrochemical performance of EPD-

coated neural electrodes using laser-generated Pt alloy NPs: Pt90W10, Pt50W50, and Pt90Ir10 (mole fractions). PtIr and PtW alloys were chosen as they are already frequently utilized as part of neural electrode base material and hence using the same elemental combinations for base material and coating could ease clinical approvals. In this context, we aim to evaluate whether the beneficial electrochemical features of PtIr coatings, previously reported in the case of electrodeposition from salt precursors are transferable to ligand-free PtIr NPs deposited on electrode surfaces. Furthermore, we aim to evaluate the performance of the underexplored PtW as a potential coating material. The colloidal alloy NPs were generated using laser processing in liquids using PtIr and PtW alloy target base materials and characterized using UV-Vis extinction spectroscopy, analytical disc centrifuge (ADC), high-resolution transmission electron microscopy (HR-TEM) and X-ray diffraction (XRD). EPD surface coatings were probed using scanning electron microscopy (SEM). The ECSA and CSC of the coated electrodes were measured using cyclic voltammetry (CV) and the Z values were measured using electrochemical impedance spectroscopy (EIS). Furthermore, the capacitances of coated electrodes were calculated by fitting the EIS data with an equivalent circuit (EC) model.

2 Materials and Methods

2.1 Preparation of ablation targets

For PtW NP synthesis, the corresponding ablation targets were produced by weighing, homogenizing, pressing, and heat-treating (in an argon atmosphere) the Pt and W micro powders (Alfa Aesar, Haverhill, USA). Two different Pt:W molar ratios were prepared, 90:10 and 50:50. The powders were homogenized using a mortar and pestle for 15 min before pressing the mixture at 200 MPa into circular targets of 10 mm diameter and 1 mm thickness. The targets were heat-treated in an argon atmosphere for 23 h at 900° C. A thin oxide layer formed on the heat-treated surfaces was later removed by sanding. For the synthesis of Pt and PtIr NPs, the commercially available ablation targets (10 $\times$ 10 $\times$ 1 mm) were utilized (Goodfellow GmbH, Hamburg, Germany).

2.2 Nanoparticle synthesis

Ligand-free NPs of Pt, Pt90W10, Pt50W50, and Pt90Ir10 were synthesized in deionized water via laser processing in liquids using procedures and parameters previously described elsewhere [13,14]. In brief, the metal targets were ablated in Milli-Q water and a self-designed stirred batch reactor with a volume of 30 mL using an Nd:YAG laser (Ekspla, Atlantic series, 10 ps, 1064 nm, 9.6 mJ, 100 kHz) followed by laser fragmentation in liquids (LFL) using a nanosecond laser (Innolas, Spitlight, 9 ns, 532 nm, 84 mJ, 100 Hz, 1.5 J/cm^2) to tune NP size distributions. Fragmentation was conducted in a cylindrical jet passage reactor [13]. Highly concentrated colloids obtained after LFL were diluted to a concentration of about 100 μg/ml (confirmed via UV-Vis extinction spectroscopy) using Milli-Q water. The pH values of all the colloids (each of around 20 ml in volume) were adjusted to 11 using 10-20 μl of 0.1 M NaOH solution prior to EPD.

2.3 Nanoparticle characterization

UV-Vis absorbance spectra of the colloids before and after EPD were obtained using a UV-Vis extinction spectrometer (Evolution 201, Thermo Scientific) in the wavelength range of 190–900 nm using a quartz cuvette with 10 mm path length to determine the deposited mass of NPs on target surfaces (Figure S4)[13]. The area under the curve (AUC) between 190–900 nm was integrated and quantified using calibration curves based on Pt and alloy colloids with known mass concentrations (Figure S5). The hydrodynamic diameters of the colloids were determined using an analytical disk centrifuge (ADC, CPS Instruments, DC 24000 UHR) at 22000 rpm. The measurement was based on the sedimentation of particles through a sucrose sugar gradient and photometric detection of different size fractions at 405 nm. The HR-TEM measurements were carried out with a Cs aberration-corrected HR TEM Jeol 2200F at 200 kV. For this, the samples were placed on Cu grids (300 mesh) with carbon supporting film. Additionally, EDX line scans were performed using a windowless 80 mm^2 SDD X-MaxN 80 TLE detector Oxford with 0.21 sr solid angle. The synthesized colloids were freeze-dried, homogeneously spread on silicon wafers and the phase analysis was performed using XRD (Bruker D8 Advance, Cu K_α radiation, $\lambda = 1.54$ Å; 40 kV, 40 mA) in the 2θ range of 10–90°.

2.4 Platinum-Iridium substrates

PTFE-coated Pt-Ir (90:10) wires of 76 μm diameter (Science Products GmbH, Germany) were used as coating substrates. The wires were cut into 20 mm long pieces. The PTFE isolations were removed on either end yielding about 4 mm of exposed wire. One end of the wires was soldered to an electrical plug pin and the other end was immersed into the NP colloid for deposition. The ends to be coated were washed thoroughly with ethanol prior to EPD.

2.5 Electrophoretic deposition

Pt-Ir wire electrodes were coated via EPD using a custom-made chamber[11] and by applying DC or PDC electric fields. The positive pole of the power supply was connected to the electrodes and the negative terminal was connected to the surrounding metal counter electrode. The chamber was filled with 600 μL of the respective Pt-based colloid and magnetically stirred during deposition to avoid sedimentation. DC depositions were carried out at 5 V/cm for 5 min and PDC depositions at 5 V/cm, 1 μs period, and 50% duty cycle for 10 min. Scanning electron microscopy equipped with energy dispersive X-ray analysis (SEM/EDX, Thermo Fisher Scientific, Apreo S LoVac; operating voltage: 5 kV) was used to analyze the deposit quality by mounting the wires onto aluminum sample holders and electrical contact was established using conductive copper wires.

2.6 Electrochemical characterization

To determine the electrochemical properties of the coated Pt-Ir wires, the samples were characterized using a three-electrode setup potentiostat (VersaSTAT 3F, AMETEK Scientific Instruments). A Pt

wire was used as a counter electrode and Ag/AgCl served as a reference electrode. Coated or uncoated Pt-Ir wires acted as working electrodes.

CV measurements were carried out in 1.0 M sulphuric acid solution. The vertex potentials were set between -0.2 and 1.2 V (vs RHE) and the scan rate was 0.2 V/s. Before measurements, the electrolyte was purged with nitrogen for 45 min and thereafter for 5 min between consecutive measurements. Twenty cycles were performed for each sample and the ECSA was calculated from the voltammogram using[16,17]

$$ECSA = Q_H/Q_a \tag{1}$$

where Q_H is the charge associated with the hydrogen adsorption peak and Q_a is the theoretical charge density of polycrystalline Pt surface, 210 μC/cm^2.[18,19,20,2]

Z measurements were performed in potentiostatic EIS mode in a frequency range from 1 Hz to 100 kHz by applying an AC$_{rms}$ value of 10 mV and using 0.9% NaCl as the electrolyte (Figure S3). The obtained data was plotted in Bode format (Z_{mag} vs frequency) and Z values at medically-relevant frequencies (150 Hz and 1 kHz) were examined. Additionally, the CSC was calculated via the CV enlargement factor (integrating the AUC of one CV cycle[21,22]).

2.7 Statistical analysis

All data points are presented as mean values $\pm$ standard deviation. Statistical analysis was performed in OriginLab (v. 2020b) software. One-way ANOVA statistical evaluations were performed on the data with Tukey's test as a post hoc comparison. The α value was set to 0.05, and the levels of statistical significance are represented as *$P \leq 0.05$, **$P \leq 0.01$, ***$P \leq 0.001$, and ****$P \leq 0.0001$.

3 Results and Discussion

To evaluate the performance of Pt alloy NP-coated neural electrodes, ligand-free colloidal Pt90W10, Pt50W50, and Pt90Ir10 NPs were synthesized using laser processing in liquids, as previously described[13]. The PtNPs were used as a reference.

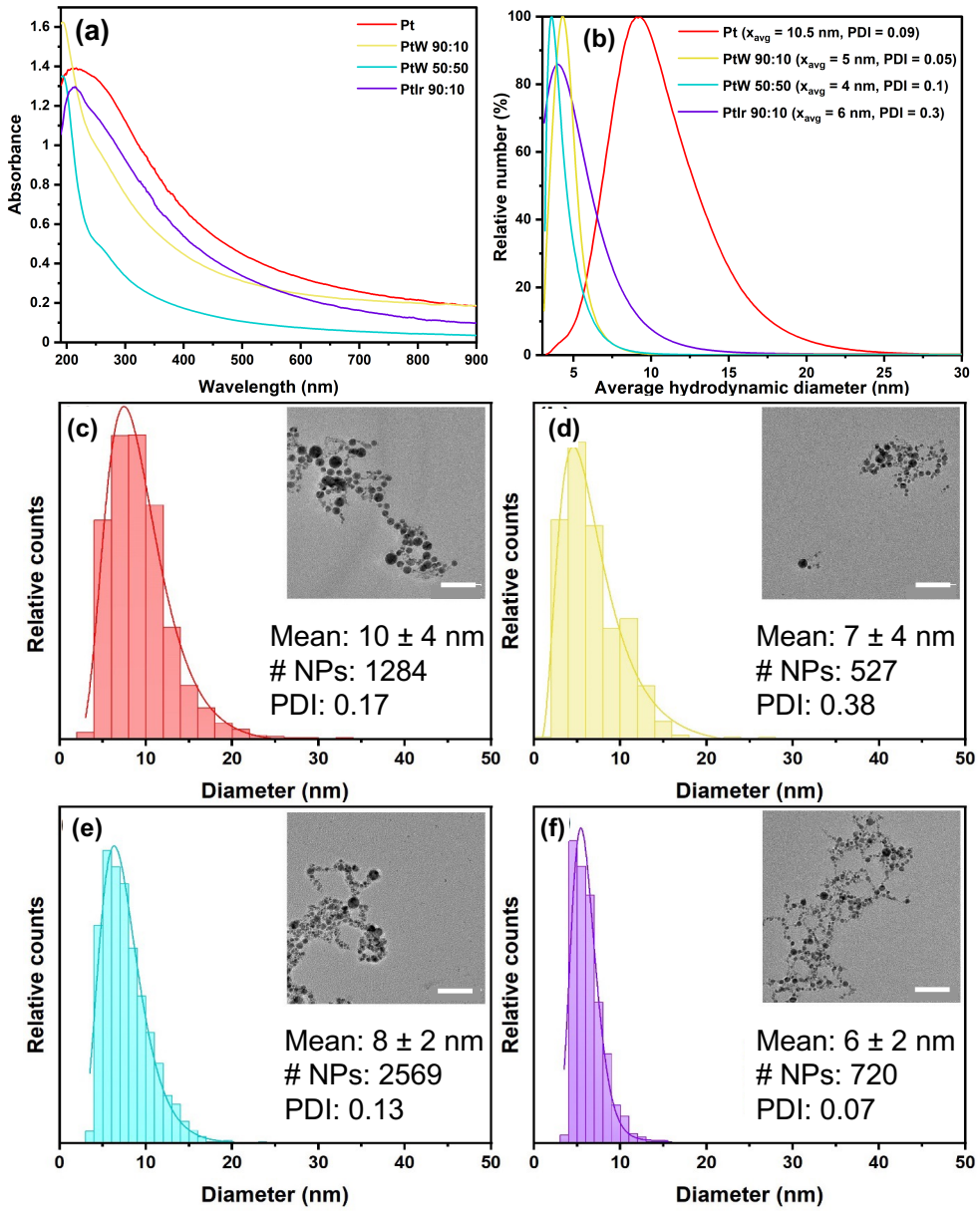

Figure 1: (a) UV-Vis extinction spectra of Pt & Pt alloy NPs. (b) Average hydrodynamic number-weighted particle size distribution of the synthesized NPs using ADC. Particle size distributions using TEM of (c) Pt (d) Pt90W10 (e) Pt50W50 & (f) Pt90Ir10 NPs by measuring the Feret diameter. Representative TEM images, mean diameter, number of measured NPs (# NPs), and polydispersity index (PDI) values are given as inserts. All scale bars in c) to f) are 50 nm.

Figure 1(a) shows the UV-Vis extinction spectra of the laser-generated alloy NPs. The characteristic Pt peak at around 220 nm could be observed. This absorbance peak is obtained from the Pt^{+} complexes and can be correlated with the surface oxidation of PtNPs due to laser ablation in water[11,23]. Since there is only 10 wt.% of W in Pt90W10 and Ir in Pt90Ir10 present, their characteristic peaks are hardly visible, which may also indicate successful alloying (please see below for structural analytics). On the other hand, in Pt50W50 colloid, a shoulder at around 300 nm could be seen, indicating the presence of WO_x or WO_3[24].

Size distributions of the laser-generated Pt, Pt90W10, Pt50W50, and Pt90Ir10 NPs obtained by measuring the Feret diameter of more than 500 NPs in each sample are depicted in Figure 1(c-f). All samples feature narrow size distributions with most particles in the range of 5-10 nm, irrespective of the elemental composition in the ablation targets. While pure PtNPs show the largest mean size of around 9.5 $\pm$ 3.9 nm, the alloy NPs of PtW and PtIr show a mean size of 7.6 $\pm$ 2.7 nm and 6 $\pm$ 1.6 nm, respectively. The PDI of the samples is in the range of 0.07 to 0.38, which indicates monodispersity of the samples[25,26,27]. The particle size distributions were further confirmed via ADC measurements and the trend displaying the largest mean diameter in Pt was confirmed (Figure 1(b) and Figure S3). Differences in the overall particle diameters between ADC and TEM are probably attributed to different measuring principles and the fact that ADC determines hydrodynamic diameters while Feret-diameters are derived from TEM. Often, laser ablation in liquids (LAL) leads to the formation of NPs with a broad size distribution due to the overlaying of different ablation mechanisms[28]. However, more narrow size distributions were obtained by consecutive LFL which leads to fragmentation of all particles exceeding a threshold diameter of around 10 nm[29,30]. In the present study, the synthesis of Pt and Pt-alloy NPs with similar average particle sizes was a mandatory prerequisite for the reasonable comparison of material-specific electrochemical properties.

For further confirmation of the composition of the laser-generated NPs, powder XRD was performed on dried Pt and Pt-alloy NP samples to determine their crystalline nature on a bulk scale. Figure 2(a) shows the powder XRD diffractograms of Pt, Pt90W10, Pt50W50, and Pt90Ir10 NPs within the 2θ region 10°-90°. As evident from the diffractograms, all samples exhibit major reflections at 2θ positions 39.7°, 46.2°, 67.5°, 81.3°, and 85.7°which corresponds to (111), (200), (220), (311), and (222) crystal planes of fcc-Pt, respectively. This indicates that Pt atoms provide the host platform for the unit cell formations in the alloy samples where W or Ir atoms are incorporated according to the elemental composition of the respective alloy. Other authors also reported similar XRD patterns for PtW NPs synthesized by the thermal decomposition of W and platinum carbonyl clusters under a controlled atmosphere[31] and PtIr NPs by a super hydride-ethanol reduction method[32].

The additional reflections observed in Pt50W50 NPs could be attributed to the tetragonal phase of WO_3 (JCPDS #89-1287) which could have been formed as a byproduct of the Pt50W50 alloy target in Milli-Q water as also indicated in the UV-Vis spectra (Figure 1a). However, the crystalline oxide phases were not detected in other compositions probably due to the much lower wt.% of W or Ir compared to Pt. Between the 2θ regions of 80°-88°of Pt90W10 NPs, major fcc reflections (311) can be observed. A shoulder reflection (222) of low intensity is observed at higher 2θ angles. Since Pt and W have similar atomic radii (approx. 0.139 nm[33,34]), the emergence of such a shoulder peak could not be attributed to the contraction of the unit cell and thus decrease in the lattice parameter due to the incorporation of W atom into the Pt unit cell. Instead, it might have resulted from a strain-induced contraction of the unit cell due to the alloy formation. When the W content in the ablation target was further increased from 10 wt.% to 50 wt.%, the double fcc reflections were merged and a single wider fcc reflection in the Pt50W50 in the 2θ range of 80°-88°is observed. This multiple fcc character is often observed in the case of laser ablation of binary alloy targets in liquids as previously reported for Co-Au[35] and Fe-Au[36] alloy NPs. However, it should be noted that in those cases, the multiple fcc phases were mainly attributed to the substitution of one element by

the other in the alloy which differs in their atomic radius thus leading to the increase or decrease of the unit cells. However, in general, the XRD analysis of the Pt and Pt-based alloys in the current study confirms the formation of the alloy phases due to the absence of individual crystalline metallic phases in the collected diffractograms. Rietveld refinement analysis would be required to further substantiate diffraction peak shifts by Pt alloying, which is beyond the scope of this work, in particular as HR-TEM-EDX studies have been carried out on the NPs.

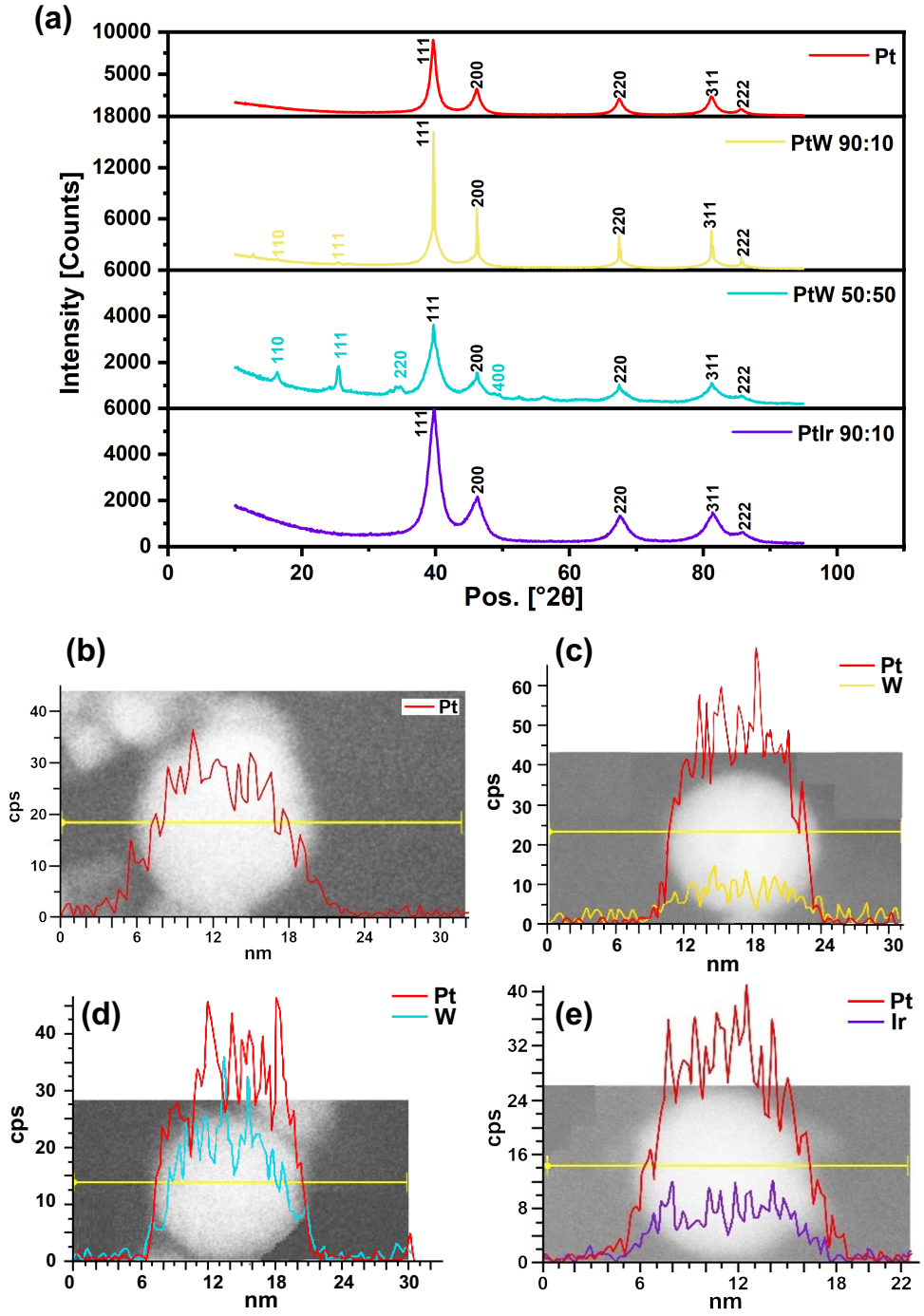

Figure 2: (a) XRD of Pt- and Pt-alloy NPs. EDX line-scan of single NPs obtained by laser processing in water (b) Pt, (c) Pt90W10, (d) Pt50W50, and (e) Pt90Ir10.

Figure 2(b-e) shows a single particle HR-TEM of the laser-generated NPs overlayed with their respective EDX line scans. All line scan results indicate a homogeneous elemental distribution within the NPs, which points to the formation of a solid solution structure. In line with these results, PtW[37] and PtIr[38] particles have already been reported to form homogeneous solid solutions in the literature. Additionally, the varying intensities of the W line scan in Figure 2(b) and (c) confirm the presence of alloy phases with different Pt:W elemental ratios. Therefore, we can assume that the synthesized Pt- and Pt-alloy NPs possess a solid solution structure with a homogeneous elemental distribution with expected ratios dictated by the composition of the respective alloy targets. However, the potential presence of amorphous oxide phases cannot be fully excluded based on these findings.

The NP colloids were diluted to a concentration of 100 μg/ml, adjusted to a pH of 11, and used for DC- (5 V/cm, 5 min) and PDC-EPD (5 V/cm, 1 μs period, 50% duty cycle, 10 min) on PtIr electrode surfaces, as previously described[13]. Since we show in our previous work that the PDC-EPD produces more homogeneous and reproducible deposits when compared to DC-EPD, only the results obtained from PDC-EPD are shown below. The results from DC-EPD are given in section S6 of the supporting information. Figure 3a summarizes the mass deposited on the wire electrodes determined by UV-Vis extinction spectroscopy. Here, we quantified the AUC in a spectral range from 190 to 900 nm and used Pt colloids with known mass concentrations for calibration (see also section S4 in supporting information). Figure 3b-e also displays representative SEM images to characterize coating morphology.

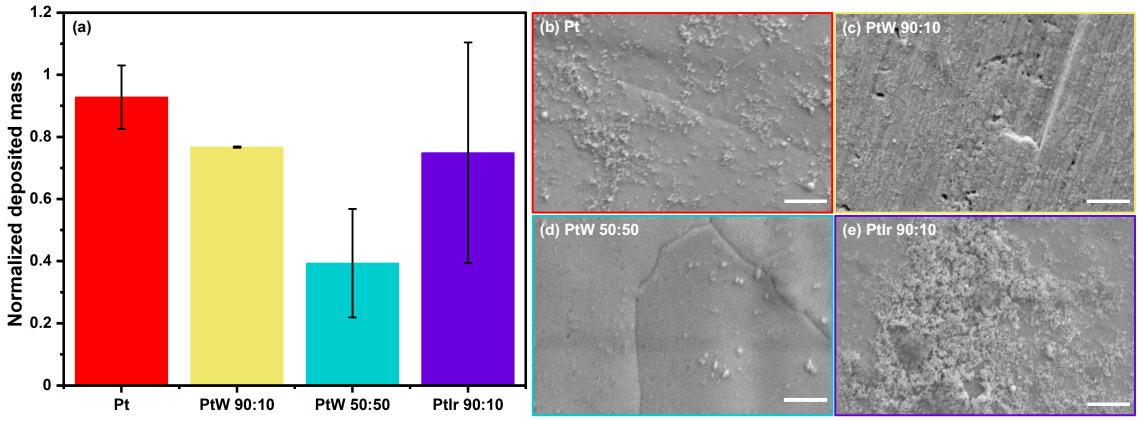

Figure 3: Electrophoretic deposition of Pt and Pt alloy NPs: (a) Normalized mass deposited on the neural electrode surfaces, and (b–e) Exemplary SEM images obtained from the sides of the coated samples after EPD using Pt and Pt alloy NPs. Scale bars are 500 nm.

It can be seen from Figure 3 that the deposition of Pt and PtIr NPs was evenly efficient. However, in the samples coated with Pt50W50 NPs, the mass deposition was lower, which could be a hint for a decreasing coating efficiency with increasing W content, a phenomenon probably correlated with the presence of WO_3 oxide phases (compare XRD and UV-Vis extinction spectroscopy results). Khoo et al. reported that the yield of electrophoretically deposited WO_3 nanorods produced a low yield due to the screening effect of oxide layers present on the nanorod surfaces[39]. Additionally, it has also been reported that the oxide layers influence and potentially weaken the negative surface charge of NPs (due to the voltage drop across the oxide layer). This goes along with a drop in

electrophoretic mobility, the driving force of EPD [40]. This kind of reduction in the particle mobility could be the reason why the Pt50W50-coated samples have lower deposition rates and consequently lower deposited mass, which may be directly proportional to the oxide layer thickness [39].

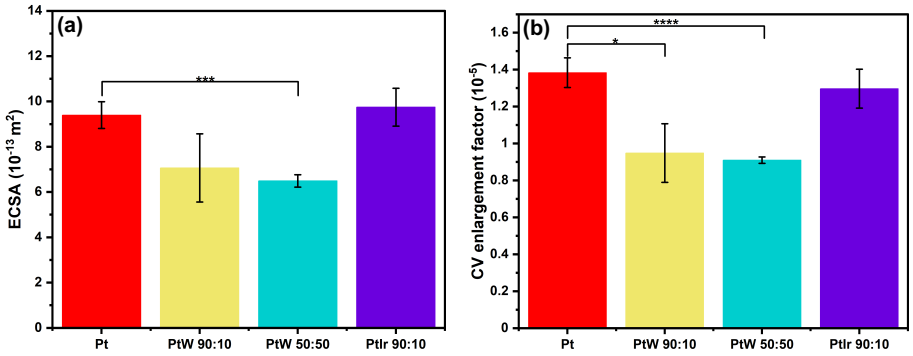

Figure 4: Cyclic voltammetry analysis on the coated electrodes: (a) Average ECSA values (N = 3, α = 0.05), and (b) Average CV enlargement factor (CSC) of the electrodes calculated by integrating the area under the curve of CV cycles (N = 3, α = 0.05).

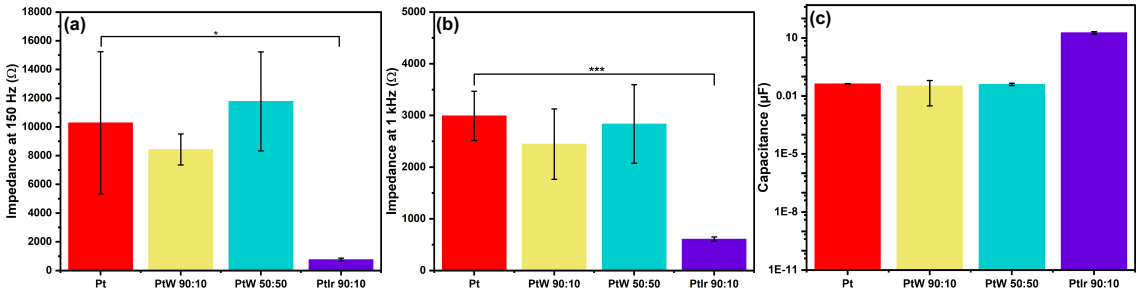

Figure 5: Electrochemical impedance analysis on the coated electrodes: (a) Average Z values at 150 Hz (N = 3, α = 0.05), (b) Average Z values at 1 kHz (N = 3, α = 0.05), and (c) Average capacitance values fitted with an EC model (N = 3, α = 0.05).

In neural stimulation electrode applications, the ECSA and Z values play an important role in determining electrode performances. Furthermore, the ECSA and capacitances are inversely proportional to the Z values [20,41]. From Figure 4(a) and Figure 4(b), it is obvious that the ECSA and CSC values of PtIr coatings are comparable with those of the Pt coatings. However, the ECSA of Pt50W50 coatings was significantly lower than that of the Pt samples. Additionally, the CSC values of both Pt90W10 and Pt50W50 were significantly lower than those of Pt-coated samples. The effect of PtIr coatings increasing the ECSA is however clearly visible in DC-EPD coatings (section S6). Although DC-EPD produces more aggregated deposits than PDC-EPD, the ability of PtIr to produce more sponge-like coatings [42,43] could have been the reason for such a highly visible difference in the values (Figure S8). On the other hand, the Z values of PtIr-coated electrodes were significantly lower than Pt-coated electrodes. The EIS spectrum of a representative PtIr sample was almost flat (Figure S6). Furthermore, the fitted capacitances of the PtIr electrodes were the highest among all four variants (Figure S6). This trend is also confirmed by the DC-EPD, where the effect is more pronounced. The reduced deposition rate of PtW NPs discussed above could be the reason for this kind of Z increase.

According to the available literature, both PtIr and PtW alloy materials were found to be non-toxic and biocompatible[44]. Using these alloy combinations would help in easing the market approvals as Ir and W are already used as additives in base materials for neural electrode manufacturing. In line with our observations, Petrossians et al. found a decreased Z and increased capacitance values of PtIr coatings in comparison to the ones performed using Pt[3]. Dalrymple et al. also found a significant increase in CSC and a significant decrease in Z under chronic in vivo settings of PtIr-coated cochlear implants[6]. In this context, the PtIr coatings were reported to possess an elevated electrochemical performance in comparison to smooth Pt controls. Here, it is also reported that Pt is more prone to corrosion during long-term stimulations, while PtIr can deliver consistent charges over longer periods indicating superior electrochemical stability[6,45,46,47]. On the other hand, there are very few studies using W to reduce the Z of neural electrodes[48]. Recently, a pilot study by Shuang et. al produced nanoporous W via chemical etching resulting in low Z and high conductivity, however, the main disadvantage is a lack of available research data in this field[49]. Also, W may be beneficial in reducing Z via chemical etching or similar methods, however, these effects could probably not be harvested in EPD coatings due to partial particle oxidation as reported above. Therefore, while the performance of PtW-NPs seems less beneficial for coatings of neural electrodes where a low Z and high ECSA are desired, the EPD coatings generated using PtIr NPs produce desirable electrochemical performance in neural electrodes compared to the pure Pt.

4 Conclusion

Neural electrodes are commonly made of Pt and Pt-based alloys containing W or Ir. As the electrical contact between electrode and tissue as well as the electrochemical or electrophysiological properties should be as good as possible, indicated by low impedance *in vitro* and *in vivo*, new methods for coating neural electrodes with metal and alloy NPs are in high demand. However, for future clinical approval of coated implantable electrodes, close elemental matches between the base material and coating are beneficial, which significantly limits the options for coating variants. Moreover, it is known that iridium and iridium alloys provide beneficial electrophysiological properties. To this end, we synthesized fully ligand-free, solid solution Pt90Ir10, Pr90W10, and Pt50W50 alloy NP colloids with mean diameters of 5 to 10 nm by laser processing in liquids and deposited those on commercial Pt electrodes utilizing the EPD technique. Electrodes were characterized for performance by evaluating their impedance (Z) and ECSA in correlation with the coatings. We could demonstrate that alloying Pt with only 10% Ir yielded an increase in the ECSA as well as a significant reduction of the impedance. The addition of W, on the other hand, proved to be less favorable. The PtW coatings were overall less homogeneous, potentially associated with the presence of oxide phases, which reduced ECSA and increased impedance. As Pt90Ir10 NP coatings by EPD were shown to be beneficial for neural electrode performance, consecutive steps should include more thorough investigations of this material system. Here a variation of the Pt:Ir ratio could be beneficial for further optimization of performance. Furthermore, an enhancement of the PtIr coating process should be performed as a follow-up investigation, utilizing e.g. ethanol-water mixtures which have been demonstrated to be beneficial for Pt[14], complemented by tests of mechanical stability[15] and

in vivo performance[12]. The PtW coatings on the other hand seem to be less beneficial for coating of neural electrodes where low Z values are desired, however, applications requiring high Z materials, e.g. for recording or sensing may benefit from the PtW-coated base materials.

5 Acknowledgement

The authors gratefully acknowledge the German Research Foundation (DFG) for their financial support (project BA 3580/24-1). VR thanks Joman Barakeh for data collection, Tobias Bochmann for SEM measurements, and Florian de Kock for XRD measurements.

References

[1] Stuart F Cogan. Neural stimulation and recording electrodes. *Annu. Rev. Biomed. Eng.*, 10:275–309, 2008.

[2] Doe W Kumsa, Narendra Bhadra, Eric M Hudak, Shawn C Kelley, Darrel F Untereker, and J Thomas Mortimer. Electron transfer processes occurring on platinum neural stimulating electrodes: a tutorial on the i (ve) profile. *Journal of neural engineering*, 13(5):052001, 2016.

[3] Artin Petrossians, John J Whalen III, James D Weiland, and Florian Mansfeld. Electrodeposition and characterization of thin-film platinum-iridium alloys for biological interfaces. *Journal of The Electrochemical Society*, 158(5):D269, 2011.

[4] Curtis D Lee, Eric M Hudak, John J Whalen III, Artin Petrossians, and James D Weiland. Low-impedance, high surface area pt-ir electrodeposited on cochlear implant electrodes. *Journal of The Electrochemical Society*, 165(12):G3015, 2018.

[5] Isaac R Cassar, Chunxiu Yu, Jaydeep Sambangi, Curtis D Lee, John J Whalen III, Artin Petrossians, and Warren M Grill. Electrodeposited platinum-iridium coating improves in vivo recording performance of chronically implanted microelectrode arrays. *Biomaterials*, 205:120–132, 2019.

[6] Ashley N Dalrymple, Mario Huynh, Bryony A Nayagam, Curtis D Lee, Greg R Weiland, Artin Petrossians, J John, James B Fallon, Robert K Shepherd, et al. Electrochemical and biological characterization of thin-film platinum-iridium alloy electrode coatings: a chronic in vivo study. *Journal of neural engineering*, 17(3):036012, 2020.

[7] Artin Petrossians, John J Whalen, James D Weiland, and Florian Mansfeld. Surface modification of neural stimulating/recording electrodes with high surface area platinum-iridium alloy coatings. In *2011 Annual International Conference of the IEEE Engineering in Medicine and Biology Society*, pages 3001–3004. IEEE, 2011.

[8] Abhishek Prasad, Qing-Shan Xue, Viswanath Sankar, Toshikazu Nishida, Gerry Shaw, Wolfgang J Streit, and Justin C Sanchez. Comprehensive characterization and failure modes of

tungsten microwire arrays in chronic neural implants. *Journal of neural engineering*, 9(5):056015, 2012.

[9] Abhishek Prasad and Justin C Sanchez. Quantifying long-term microelectrode array functionality using chronic in vivo impedance testing. *Journal of neural engineering*, 9(2):026028, 2012.

[10] Carmen Streich, Sven Koenen, Marco Lelle, Kalina Peneva, and Stephan Barcikowski. Influence of ligands in metal nanoparticle electrophoresis for the fabrication of biofunctional coatings. *Applied Surface Science*, 348:92–99, 2015.

[11] Sven Koenen, Christoph Rehbock, Hans E Heissler, Svilen D Angelov, Kerstin Schwabe, Joachim K Krauss, and Stephan Barcikowski. Optimizing in vitro impedance and physico-chemical properties of neural electrodes by electrophoretic deposition of pt nanoparticles. *ChemPhysChem*, 18(9):1108–1117, 2017.

[12] Svilen D Angelov, Sven Koenen, Jurij Jakobi, Hans E Heissler, Mesbah Alam, Kerstin Schwabe, Stephan Barcikowski, and Joachim K Krauss. Electrophoretic deposition of ligand-free platinum nanoparticles on neural electrodes affects their impedance in vitro and in vivo with no negative effect on reactive gliosis. *Journal of nanobiotechnology*, 14(1):1–11, 2016.

[13] Vaijayanthi Ramesh, Christoph Rehbock, Brian Giera, John J. Karnes, Jean-Baptiste Forien, Svilen D. Angelov, Kerstin Schwabe, Joachim K. Krauss, and Stephan Barcikowski. Comparing direct and pulsed-direct current electrophoretic deposition on neural electrodes: Deposition mechanism and functional influence. *Langmuir*, 37(32):9724–9734, 2021.

[14] Vaijayanthi Ramesh, Brian Giera, John J Karnes, Nadine Stratmann, Viktor Schaufler, Yao Li, Christoph Rehbock, and Stephan Barcikowski. Solvent composition during electrophoretic deposition of platinum nanoparticles on neural electrode surfaces influences their electrochemical behavior. *Journal of the Electrochemical Society*, 169(LLNL-JRNL-826684), 2022.

[15] Vaijayanthi Ramesh, Nadine Stratmann, Viktor Schaufler, Svilen D Angelov, Ilona D Nordhorn, Hans E Heissler, Ricardo Martínez-Hincapié, Viktor Čolić, Christoph Rehbock, Kerstin Schwabe, et al. Mechanical stability of nano-coatings on clinically applicable electrodes, generated by electrophoretic deposition. *Advanced Healthcare Materials*, page 2102637, 2022.

[16] SheelagháA Campbell, JamesáR Smith, GrongaráW Lloyd, FrankáC Walsh, ThomasáR Ralph, et al. Electrochemical and microscopic characterisation of platinum-coated perfluorosulfonic acid (nafion 117) materials. *Analyst*, 123(10):1923–1929, 1998.

[17] Eric P Lee, Zhenmeng Peng, David M Cate, Hong Yang, Charles T Campbell, and Younan Xia. Growing pt nanowires as a densely packed array on metal gauze. *Journal of the American chemical Society*, 129(35):10634–10635, 2007.

[18] Andrew Capon and Roger Parsons. The oxidation of formic acid at noble metal electrodes part iii. intermediates and mechanism on platinum electrodes. *Journal of Electroanalytical Chemistry and Interfacial Electrochemistry*, 45(2):205–231, 1973.

[19] S Trasatti and OA Petrii. Real surface area measurements in electrochemistry. *Journal of Electroanalytical Chemistry*, 327(1-2):353–376, 1992.

[20] Tim Boretius, Tilman Jurzinsky, Christian Koehler, Sven Kerzenmacher, Harald Hillebrecht, and Thomas Stieglitz. High-porous platinum electrodes for functional electrical stimulation. In *2011 Annual International Conference of the IEEE Engineering in Medicine and Biology Society*, pages 5404–5407. IEEE, 2011.

[21] C Boehler, T Stieglitz, and M Asplund. Nanostructured platinum grass enables superior impedance reduction for neural microelectrodes. *Biomaterials*, 67:346–353, 2015.

[22] Mehran Ganji, Angelique C Paulk, Jimmy C Yang, Nasim W Vahidi, Sang Heon Lee, Ren Liu, Lorraine Hossain, Ezequiel M Arneodo, Martin Thunemann, Michiko Shigyo, et al. Selective formation of porous pt nanorods for highly electrochemically efficient neural electrode interfaces. *Nano letters*, 19(9):6244–6254, 2019.

[23] William T Nichols, Takeshi Sasaki, and Naoto Koshizaki. Laser ablation of a platinum target in water. iii. laser-induced reactions. *Journal of applied physics*, 100(11):114911, 2006.

[24] Martin Schieder, Thomas Lunkenbein, Thomas Martin, Wolfgang Milius, Gudrun Auffermann, and Josef Breu. Hierarchically porous tungsten oxide nanotubes with crystalline walls made of the metastable orthorhombic polymorph. *Journal of Materials Chemistry A*, 1(2):381–387, 2013.

[25] S Barcikowski, V Amendola, M Lau, G Marzun, C Rehbock, S Reichenberger, D Zhang, and B Gökce. Handbook of laser synthesis & processing of colloids, 2019.

[26] Sagar S Rane and Phillip Choi. Polydispersity index: how accurately does it measure the breadth of the molecular weight distribution? *Chemistry of materials*, 17(4):926–926, 2005.

[27] Ulf Nobbmann and Ana Morfesis. Light scattering and nanoparticles. *Materials today*, 12(5):52–54, 2009.

[28] Cheng-Yu Shih, René Streubel, Johannes Heberle, Alexander Letzel, Maxim V Shugaev, Chengping Wu, Michael Schmidt, Bilal Gökce, Stephan Barcikowski, and Leonid V Zhigilei. Two mechanisms of nanoparticle generation in picosecond laser ablation in liquids: the origin of the bimodal size distribution. *Nanoscale*, 10(15):6900–6910, 2018.

[29] Ksenia Maximova, Andrei Aristov, Marc Sentis, and Andrei V Kabashin. Size-controllable synthesis of bare gold nanoparticles by femtosecond laser fragmentation in water. *Nanotechnology*, 26(6):065601, 2015.

[30] Anna R Ziefuß, Sven Reichenberger, Christoph Rehbock, Indranath Chakraborty, Mustafa Gharib, Wolfgang J Parak, and Stephan Barcikowski. Laser fragmentation of colloidal gold nanoparticles with high-intensity nanosecond pulses is driven by a single-step fragmentation mechanism with a defined educt particle-size threshold. *The Journal of Physical Chemistry C*, 122(38):22125–22136, 2018.

[31] Liufeng Xiong and Ting He. Synthesis and characterization of carbon supported ptw catalysts from carbonyl complexes for oxygen electroreduction. *Electrochemistry communications*, 8(10):1671–1676, 2006.

[32] Betül Sen, Ayşenur Aygun, Aysun Şavk, Mehmet Harbi Çalımlı, Mehmet Ferdi Fellah, and Fatih Sen. Composites of platinum-iridium alloy nanoparticles and graphene oxide for the dimethyl amine borane (dmab) dehydrogenation at ambient conditions: An experimental and density functional theory study. *Scientific Reports*, 9(1):1–12, 2019.

[33] J Hurly and PT Wedepohl. Optical properties of coloured platinum intermetallic compounds. *Journal of Materials Science*, 28:5648–5653, 1993.

[34] Dongdong Gu, Donghua Dai, Wenhua Chen, and Hongyu Chen. Selective laser melting additive manufacturing of hard-to-process tungsten-based alloy parts with novel crystalline growth morphology and enhanced performance. *Journal of Manufacturing Science and Engineering*, 138(8), 2016.

[35] Jacob Johny, Marius Kamp, Oleg Prymak, Anna Tymoczko, Ulf Wiedwald, Christoph Rehbock, Ulrich Schurmann, Radian Popescu, Dagmar Gerthsen, Lorenz Kienle, et al. Formation of co–au core–shell nanoparticles with thin gold shells and soft magnetic ε-cobalt cores ruled by thermodynamics and kinetics. *The Journal of Physical Chemistry C*, 125(17):9534–9549, 2021.

[36] Jacob Johny, Oleg Prymak, Marius Kamp, Florent Calvo, Se-Ho Kim, Anna Tymoczko, Ayman El-Zoka, Christoph Rehbock, Ulrich Schürmann, Baptiste Gault, et al. Multidimensional thermally-induced transformation of nest-structured complex au-fe nanoalloys towards equilibrium. *Nano Research*, 15(1):581–592, 2022.

[37] Daiya Kobayashi, Hirokazu Kobayashi, Kohei Kusada, Tomokazu Yamamoto, Takaaki Toriyama, Syo Matsumura, Shogo Kawaguchi, Yoshiki Kubota, Masaaki Haneda, Susan Meñez Aspera, et al. Boosting reverse water-gas shift reaction activity of pt nanoparticles through light doping of w. *Journal of Materials Chemistry A*, 9(28):15613–15617, 2021.

[38] Li Jiayan, Xie Ming, Yang Youcai, Zhang Jiming, Chen Yongtai, Liu Manmen, Wang Saibei, Hu Jieqiong, and Nin Ping. Effect of zr, mo and y adding on microstructure, mechanical and electrical properties of au-pd, pt-ir and pd-ru systems. *Rare Metal Materials and Engineering*, 42(10):2027–2033, 2013.

[39] Eugene Khoo, Pooi See Lee, and Jan Ma. Electrophoretic deposition (epd) of wo3 nanorods for electrochromic application. *Journal of the European Ceramic Society*, 30(5):1139–1144, 2010.

[40] Partho Sarkar and Patrick S Nicholson. Electrophoretic deposition (epd): mechanisms, kinetics, and application to ceramics. *Journal of the American Ceramic Society*, 79(8):1987–2002, 1996.

[41] Sharanya Arcot Desai, John D Rolston, Liang Guo, and Steve M Potter. Improving impedance of implantable microwire multi-electrode arrays by ultrasonic electroplating of durable platinum black. *Frontiers in neuroengineering*, 3:5, 2010.

[42] Kevin Wang, Chung-Chiun Liu, Dominique M Durand, et al. Flexible nerve stimulation electrode with iridium oxide sputtered on liquid crystal polymer. *IEEE transactions on biomedical engineering*, 56(1):6–14, 2009.

[43] Xian Wu, Weihua Pei, He Zhang, Yuanfang Chen, Xuhong Guo, Hongda Chen, and Shirong Wang. Sodium dodecyl sulfate doping pedot to enhance the performance of neural microelectrode. *Journal of Electroanalytical Chemistry*, 758:26–32, 2015.

[44] Anthony M Dymond, Lloyd E Kaechele, John M Jurist, and Paul H Crandall. Brain tissue reaction to some chronically implanted metals. *Journal of neurosurgery*, 33(5):574–580, 1970.

[45] Stuart F Cogan, Philip R Troyk, Julia Ehrlich, and Timothy D Plante. In vitro comparison of the charge-injection limits of activated iridium oxide (airof) and platinum-iridium microelectrodes. *IEEE Transactions on Biomedical Engineering*, 52(9):1612–1614, 2005.

[46] S Negi, R Bhandari, L Rieth, and F Solzbacher. In vitro comparison of sputtered iridium oxide and platinum-coated neural implantable microelectrode arrays. *Biomedical materials*, 5(1):015007, 2010.

[47] Ashley N Dalrymple, Mario Huynh, Ulises Aregueta Robles, Jason B Marroquin, Curtis D Lee, Artin Petrossians, John J Whalen, Dan Li, Helena C Parkington, John S Forsythe, et al. Electrochemical and mechanical performance of reduced graphene oxide, conductive hydrogel, and electrodeposited pt–ir coated electrodes: an active in vitro study. *Journal of neural engineering*, 17(1):016015, 2019.

[48] Emily Kolaya and Bonnie L Firestein. Deep brain stimulation: Challenges at the tissue-electrode interface and current solutions. *Biotechnology progress*, 37(5):e3179, 2021.

[49] Fei Shuang, Haokun Deng, Ashfaque B Shafique, Steve Marsh, David Treiman, Kostas Tsakalis, and Katerina E Aifantis. A first study on nanoporous tungsten recording electrodes for deep brain stimulation. *Materials Letters*, 260:126885, 2020.

6 Influence of Platinum Nanoparticle Coatings on the In vivo Behaviour of Neural Electrodes

Unpublished results under review:

Coating of neural electrodes with platinum nanoparticles reduces and stabilizes impedance in vitro and in vivo in a rat model

Svilen D. Angelov[1], Christoph Rehbock[2], Vaijayanthi Ramesh[2], Hans E. Heissler[1], Mesbah Alam[1], Stephan Barcikowski[2], Kerstin Schwabe[1,*] and Joachim K. Krauss[1]

[1] Department of Neurosurgery, Hannover Medical School, Carl-Neuberg-Str. 1, 30625 Hannover, Germany

[2] Institute of Technical Chemistry I, University of Duisburg-Essen and Center for Nanointegration Duisburg-Essen (CENIDE), Essen, Germany

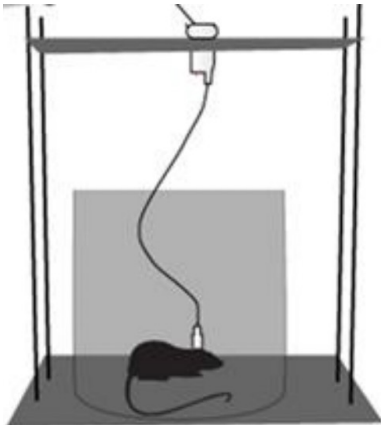

Summary:

From the previous sections, the PDC EPD was found to perform superior to the DC EPD coatings. However, the question still remains on the in vivo behavior of the PDC coatings in rat models. Therefore, neural electrodes were coated using PtNPs via PDC EPD, intracranially implanted into the STN of rats, and stimulated long-term to determine their in vitro and in vivo characteristics. It was observed that the coated electrodes reduce impedance in vitro and favor stimulation efficiency and may support the prolonged battery life of the pulse generator. The optimized PtNP coatings might also enhance the quality and durability of chronic recording and stimulation in patients.

Author contributions:

Design, implantation, and study of the in vitro and in vivo behavior of the nano-coated electrodes were carried out by SDA, HEH, and MA. The electrodes were electrophoretically deposited using PtNPs and the coating characterizations were performed by VR. The original manuscript draft was prepared by SDA and KS. The review and editing of the manuscript were carried out by SDA, CR, VR, HEH, MA, SB, KS, and JKK. JKK and KS designed the study, supervised, obtained funding support, and promoted collaborations between the institutions.

Coating of neural electrodes with platinum nanoparticles reduces and stabilizes impedance in vitro and in vivo in a rat model

Svilen D. Angelov[1], Christoph Rehbock[2], Vaijayanthi Ramesh[2], Hans E. Heissler[1], Mesbah Alam[1], Stephan Barcikowski[2], Kerstin Schwabe[1,*], Joachim K. Krauss[1]

[1] Department of Neurosurgery, Hannover Medical School, Carl-Neuberg-Str. 1, 30625 Hannover, Germany.

[2] Technical Chemistry I, University of Duisburg-Essen and Center for Nanointegration Duisburg-Essen (CENIDE), Universitaetsstr. 7, 45141 Essen, Germany.

Abstract

Background: Chronically implanted electrodes are used for neural recording and stimulation in the context of deep brain stimulation (DBS) for the treatment of various neurological disorders. The efficacy of stimulation critically depends on the stable impedance of the electrode contacts and reliable delivery of electric energy to the adjacent neuronal tissue.

Methods: Pulsed direct current (pulsed-DC) was applied to coat platinum-iridium electrodes through the process of electrophoretic deposition (EPD) using laser-generated platinum nanoparticle colloids (PtNPs). Electrodes that were immersed in the colloid without an electric field and uncoated electrodes served as controls. Before and after surface coating the impedance of the electrodes was measured. In the in vitro study, the electrodes were stimulated for weeks in a 0.9% NaCl solution and the electrode impedance was assessed. In the in vivo study, NP-coated electrodes were implanted in the left subthalamic nucleus (STN) of rats, the left STN received uncoated electrodes. After a recovery period of two weeks, the animals were subjected to four weeks of chronic stimulation, during which impedance measurements were conducted after each week of stimulation.

Results: Coating with PtNP resulted in a significant reduction in electrode impedance (p¡0.05), which remained lower than that of uncoated electrodes during in vitro stimulation for four weeks. After implantation intracranially in the STN, the electrodes coated with NP exhibited an initial increase in impedance, which subsequently declined to lower values during stimulation for four weeks. Electrodes coated with NP had a lower fluctuation of impedance during stimulation compared to uncoated electrodes in vitro and in vivo ($p < 0.05$).

Conclusions: Laser-generated PtNPs applied to electrodes by pulsed DC-EPD lead to constant lower electrode impedance during chronic stimulation. The more stable impedance may have the potential to enhance the performance of DBS systems during chronic use.

Keywords: Nanoparticles, Electrophoretic Deposition, Deep Brain Stimulation.

1 Introduction

Neural electrodes are implanted in the brain for the recording of neuronal activity and for elec-

trical stimulation both in acute and chronic settings[1]. In particular, deep brain stimulation (DBS) with the option of closed-loop adaptive stimulation has gained widespread attention[2,3]. The efficacy of the electrodes depends on the material properties which account for stabilization of the electrode impedance directly affecting electrical stimulation or recording. Approaches in this context are nanoscopic structuring by chemical surface modification techniques[4], laser-based patterning techniques[5], or deposition of nanoscale materials on the electrode surface by either sputtering of iridium oxide[6] or chemical reduction methods (platinum grass)[7,8,9]. These techniques reduce electrode impedance[8,10], although in vivo performance remains to be proved in long-term applications.

In addition, several alternative techniques for depositing nanoparticles onto electrodes are available, including methods such as physical vapor deposition (PVD), chemical vapor deposition (CVD), dip coating, and spin coating. However, the choice of deposition method depends on the specific requirements of the electrode-tissue interface and the desired performance characteristics. Laser-based NP deposition could be used to create specific electrode geometries or surface structures that improve the contact between the electrode and the neural tissue. The deposition of IrOx and Pt-grass deposition are aimed at enhancing the conductivity and stability of the electrode materials. The advantages of EPD for nanoparticle deposition on electrode surfaces can include uniformity, adhesion, tailored properties, thickness control, simplicity, and efficiency.

Electrophoretic deposition (EPD) is another well-established coating method for solids, based on the movement of charged colloidal particles in an electric field towards an oppositely-charged counter electrode, followed by controlled deposition of the particles on the surface. Next to industrial and energy applications, EPD is used to generate biomaterials, including neuro-electrodes[11]. In contrast to other modification methods, however, the EPD of laser-generated platinum nanoparticles (Pt-NP) on the surface of platinum-iridium (Pt-Ir) electrodes increased their impedance in vitro[12]. After intracranial implantation in a rat model, impedance was even further enhanced, temporarily. Nevertheless, this effect was lowest for electrodes coated with particles < 10 nm, which also showed the most stable impedance dynamics during stimulation for three weeks, while the impedance of the uncoated electrodes continued to increase over time.

Different from DC-EPD, during processing with pulsed DC EPD, the field is turned off 50% of the time, which counteracts electroosmotic and electrohydrodynamic forces and avoids the formation of assemblages[13]. Indeed, pulsed DC EPD yielded homogeneous coatings on Pt-Ir electrodes, while large assemblages dominated the DC-EPD-coated samples. Moreover, the pulsed DC coatings reduced the impedance in comparison to the uncoated and DC EPD-coated electrodes[14]. So far, the mechanical stability of pulsed DC EPD coatings has been verified in vitro and in vivo, thus supporting the clinical applicability of the designed coatings[15].

Here we examined whether the impedance of neural electrodes coated via pulsed DC EPD would change after intracranial implantation in rats, followed by four weeks of in vivo stimulation. These studies are complemented by four weeks of in vitro stimulation of NP-coated and uncoated electrodes in saline solution. From a fundamental viewpoint, these experiments will help to clarify how the impedance of electrodes changes in vivo based on the initially applied coating properties. Furthermore, these experiments may help to elucidate to which extent changes in impedance during

long-term in vivo trials depend on the properties of the electrode, the interactions with the brain tissue, the 130 Hz frequency stimulation, or a combination thereof.

2 Materials and Methods

2.1 Experimental Design

First, the impedance of bipolar electrodes was measured in vitro. Electrodes were coated via electrophoretic deposition using pulsed DC-generated electric fields or left uncoated. In the latter case, electrodes were dipped into the NP colloids in the absence of a directed external electric field. After that, impedance dynamics were studied during 4 weeks of electrostimulation in vitro and in vivo.

For the in vitro study, coated and uncoated control electrodes (n=8 each) were immersed in 0.9% NaCl solution, in separate wells of a standard 24-well cell culture plate with a modified lid with openings, fixators, and contacts for the electrodes (Figure 1). The electrodes were left unplugged for two weeks (to simulate the in vivo postoperative period); after that continuous electrostimulation was conducted for 4 weeks.

For the in vivo study, electrodes were bilaterally implanted in the STN of rats (n=8) with coated electrodes frequently implanted in the left hemisphere and uncoated in the right hemisphere for internal control. After two weeks of postoperative recovery, the animals received chronic stimulation for 4 weeks.

Impedance was assessed in vitro and in vivo after the 2 weeks recovery period and each stimulation week. At the end of the in vivo experiment, the rats were sacrificed, perfused with paraformaldehyde and the brains were histologically processed for Nissl staining.

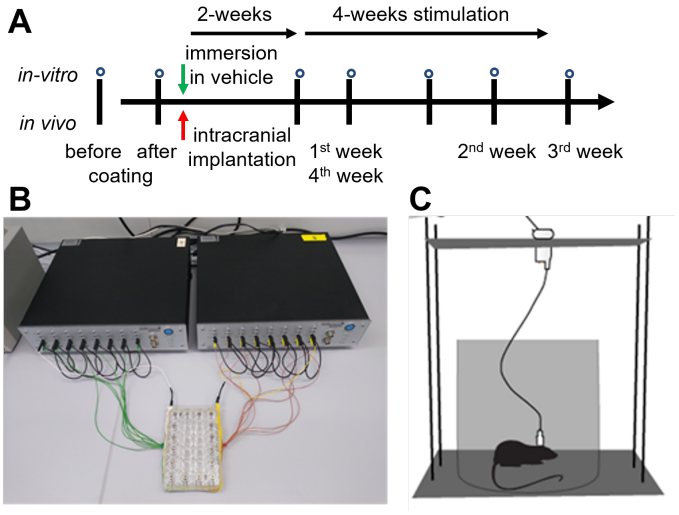

Figure 1: (A) Schematic representation of the in vitro/in vivo experiments with impedance measurements depicted as °. (B) For in vitro measures the electrodes were immersed in 0.9% NaCl in a stimulation chamber. (C) For in vivo measures, the rat's head stage was connected to the stimulation device, and impedance was measured in the awake, free-moving rat once a week.

2.2 Nanoparticle synthesis

PtNPs for the EPD coating process were fabricated by laser processing in liquids using a two-step procedure, including a process termed Laser ablation in Liquids (LAL) of a Pt target in water, yielding a polydisperse Pt colloid, and subsequent laser fragmentation in liquids (LFL) in a liquid jet reactor which leads to an efficient particle size reduction and a narrowing of the particle size distribution. Details on the synthesis process and further colloid characterization can be found here in our previous work[14].

2.3 Electrodes and Coating

Bipolar electrodes were made of two parallel Pt90Ir10 wires insulated with PTFE ($\phi = 0.0055$ with insulation; $\phi = 0.003$ uninsulated; Science-Products GmbH, Hofheim, Germany), placed in a 0.55 x 17 mm stainless steel tube cut from a 24G syringe needle. At the contact end, both wires were uninsulated leaving a 500 μm long bare surface with approximately 250 μm intercontact distance. Contact pins were soldered to the other end. The electrode tip was cleaned and conditioned before coating by immersing it in 65% nitric acid for 15 min. After that, it was rinsed thoroughly with distilled water.

The NPs were deposited on the neural electrode contact surface via EPD using pulsed DC electric fields, a procedure described in our previous work in more detail[14]. In short, pulsed DC fields (50% duty cycle, 1 μs period) with a field strength of 5 V/cm and a deposition time of 10 min were applied. The deposition was carried out in an aqueous solution at alkaline pH. In total, 16 samples were coated for in vitro and in vivo stimulation experiments. As controls, another 16 electrodes were immersed in the Pt colloids for 10 min without applying an electric field.

2.3.1 Impedance Measurement

The impedance of the electrodes was determined by applying Ohm's law at a single frequency of 200 Hz as previously described[12,14]. The electrodes were immersed in 0.9% NaCl and a sinusoidal test voltage (200 mV p-p) was applied to drive a current through the electrode and a serial-measurement-resistor (200 $\pm$ 1% Ω). This current is proportional to the voltage drop across the measurement resistor, which was fed into a precision differential amplifier (AMP01, Analog Devices, Inc., Norwood, MA, USA). The amplifier output voltage allowed the calculation of the current amplitude, and thus, by applying Ohm's law, the estimation of electrode impedance by the ratio of electrode voltage and current. The phase shift of the test voltage and current verified the existence of capacitive reactance. The above-described methodology was used for both in vitro and in vivo impedance measurements.

Notably, the first impedance measurement was done before coating, but after cleaning in 65% nitric acid for 15 min, to exclude changes induced by the cleaning procedure.

2.4 Animals

For the in vivo study male Sprague Dawley rats (n=8) were obtained from (Charles River Laboratories, Germany, as done before for other work of our group[12,14]). The rats were housed in groups of 3-4 in standard Macrolon Type IV cages (Techniplast, Hohenpeissenberg, Germany) under controlled environmental conditions (22°C, 14 h light/ 10 h dark cycle, lights on at 07:00 a.m.). Following the surgical procedure, each rat was kept in a standard Macrolon Type III cage. The rats were provided with laboratory rat chow and tap water.

The experimental protocols used in this study followed the national and international ethical guidelines, complied with the German Animal Welfare Act, and were approved by the local authorities (AZ 18/2837), including an animal ethics committee approval. This study was performed in accordance with the Animal Experiments Act guideline: Reporting of In Vivo Experiments (ARRIVE).

2.4.1 Surgery

For surgery, we used the procedure described before in our group[12,14]. The rats underwent intraperitoneally anaesthesia with chloral hydrate (360 mg/kg) and fixed into a stereotaxic frame. Additionally, a local anesthetic (2% prilocaine hydrochloride) was infiltrated into the surgical site. Following the initial incision and identification of the bregma point, a pair of burr holes were created on both sides directly above the desired targets. Subsequently, two bipolar electrodes were surgically inserted into the subthalamic nucleus (STN) at specific coordinates relative to the bregma: anteroposterior: -3.8 mm, mediolateral: $\pm$2.5 mm, dorsoventral: -8.0 mm. Additionally, the tooth bar was adjusted to a position of -3.3 mm. The electrodes and the socket were fixed to the skull with dental acrylic cement (Paladur, Heraeus Kulzer GmbH, Hanau, Germany). Four screws (1 x 2 mm) were wound to the skull as reinforcement. Antibiotics (marbofloxacin, 6.6 mg/kg) were applied for eight days subcutaneously, starting two days preoperatively. The analgetic carprofen (5 mg/kg) was subcutaneously injected intraoperatively and for the first two postoperative days.

2.4.2 Electrostimulation

Continuous electrical stimulation was applied via a cable that was bite-protected by a spring-like metal shield for the in vivo study. One side of the cable was connected to the socket on the skull, the other to a stimulation device (Multichannel Systems STG2008, Software: Mc-Stimulus II). A swivel (Plastics One Inc, Roanoke, VA, USA) in the stimulation line allowed free movement of the rat without twisting the cable. For electrical stimulation symmetric, bipolar, rectangular waves with a pulse width of 160 μs and frequency of 130 Hz were used. Stimulation parameters were controlled with an oscilloscope (Tektronix TDS2000C), as described in the authors' previous work[15].

For the in vivo study, the amplitude was experimentally determined to be 20% below the individual motor reaction threshold (e.g., contralateral paw movement). Each rat was single-housed in a standard Macrolon Type III cage during continuous stimulation. A slot in the lid allowed free movement of the animal with the cable attached. Before applying DBS in the STN, the individual

current intensity threshold for stimulation-induced side effects was determined. The reason for adjusting the stimulation intensity to 20% below the motor response level lies in the aim of finding a balance that maximizes therapeutic benefits while minimizing the occurrence of adverse effects. After adjusting the stimulation amplitude for each individual rat, the impedance was measured just after implantation and then weekly until the fourth week of stimulation. In our implantation rat model, the threshold was adjusted only once upon implantation, which is a potential limitation.

For the in vitro study the electrodes were immersed in physiological saline solution (0.9% NaCl) filled wells of a 24-well cell culture plate, used as a stimulation chamber. Electrodes were stimulated with a pulse amplitude of 200 μA.

2.4.3 Histology

After the end of the experiments, the implantation sites were histologically verified by referring to the atlas of Paxinos and Watson[16]. Rats were deeply anesthetized with an overdose of chloral hydrate and transcardially perfused with 4% paraformaldehyde solution. Following, the brains were extracted from the cranial cavity, placed in 30% sucrose/phosphate-buffered saline (PBS) solution for at least 12 h, and cut on a freezing microtome (coronal plane) with a section width of 40 μm in three series. To evaluate the localization, Nissl staining was employed, and the samples were observed under a light microscope (Zeiss, Göttingen, Germany). This procedure for verification of the electrode's position is routinely used in our group[12].

2.5 Statistical Analysis

For statistical evaluation of the impedance dynamics in vitro and in vivo, data was analyzed by one-way repeated measures ANOVA, followed by post hoc Tukey's test. In addition, the measures of all groups were compared after calculating the relative impedance to the preoperative measures, which were set at 100%. Thereafter, a two-way repeated measure (RM) ANOVA was applied with factors group and time. All tests were performed two-sided with $p < 0.05$ considered statistically significant.

3 Results

3.1 Characterization of nanoparticles and electrode coatings

A representative UV-Vis spectrum of the colloidal Pt nanoparticles shows Pt's typical broadband extinction behavior with a peak at 260 nm (Figure 2A), attributed to the presence of Pt-water complexes[17], indicating partial oxidation of the generated nanoparticles. Oxidation of Pt nanoparticles is commonly reported in laser synthesis of nanoparticles in liquids[18], which is the main reason for the negative surface charge (zeta potential) of the Pt colloids (data not shown here but reported in previous works[18,19]. The particle size distributions of the colloidal Pt nanoparticles analyzed by analytical disk centrifugation exhibit monodispersity with a median diameter of $\sim$10 nm (Figure 2B)

- the particle size that proved to be most efficient concerning impedance stabilization of neural electrodes in vivo in our previous work[12].

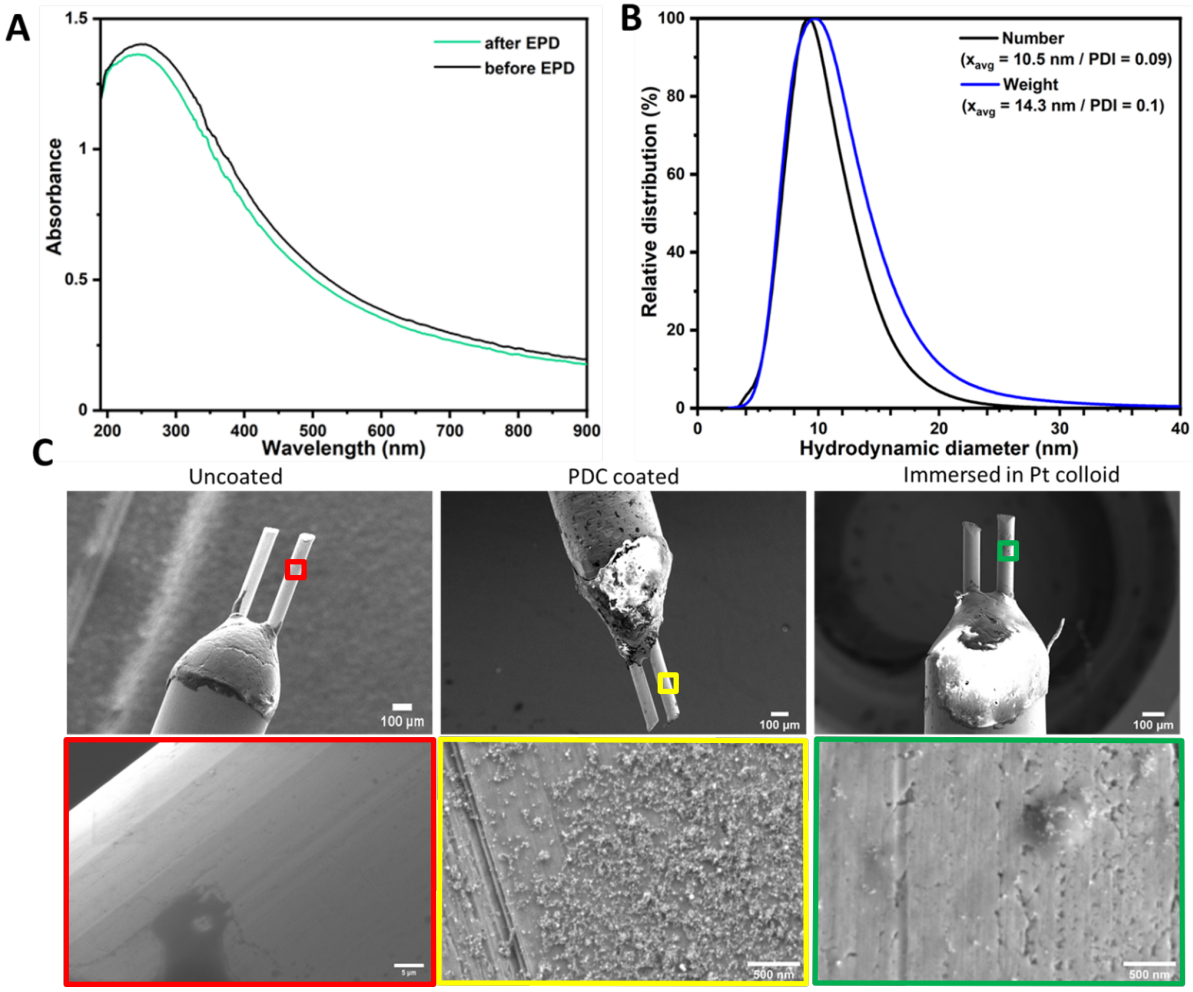

Figure 2: Characterization of colloidal nanoparticles and coated electrodes: (A) Representative UV-Vis extinction spectra of PtNP colloids before and after EPD coating, (B) Representative hydrodynamic particle size distribution of PtNP colloid, determined by analytical disk centrifugation. Mean values were determined from the median values of a log-normal fit of the corresponding distributions (PDI = Polydispersity index). (C) Representative SEM images (overview top row and higher magnification bottom row) of uncoated (left), pulsed DC coated (middle), and immersed (right) neural electrodes. The electrodes consist of two Pt metal tips which were coated by EPD. The red square roughly marks the area where the magnified images were taken, showing that coating was only found in the samples processed by Pulsed-DC EPD, while neither the uncoated electrode nor the one immersed in Pt colloid in the absence of an electric field displayed NP deposition.

The deposited mass of Pt was determined via analysis of UV-Vis spectra before and after the coating process (Figure 2A). Here, a reduction in absorbance is observable over the whole spectral range after coating, which indicates a loss of platinum mass in the colloid, indicating deposition on the electrodes. Quantification of the deposited mass was conducted using a calibration curve in which the area under the curve of the UV-Vis spectra in a spectral range of 190–900 nm was plotted

against known mass concentrations of reference Pt colloids (Figure S1 in the supporting information). The total deposited mass of Pt nanoparticles on the electrodes (mean and standard deviation of 16 samples) was 3.4 $\pm$ 0.8 μg. The coatings of the electrodes were further characterized by SEM analysis (Figure 2C). Here, homogeneous coatings were formed on the EPD-coated electrodes, with results similar to those reported previously upon utilization of pulsed DC EPD[14]. The immersed samples show minute particle deposition with very few particles sticking to the electrode surface. This finding indicates that the coating is formed due to the application of the electric field and not solely by adsorption from the solution. As expected, the control sample (not in contact with the Pt colloid) shows a smooth surface without nanoparticles.

3.2 Impedance in vitro

For the coated group, 7 electrodes were analyzed (one coated electrode broke during stimulation), and 8 electrodes for the control group. For the in vitro measurements, statistical analysis of the impedance of coated electrodes with one-way ANOVA showed a significant effect of coating ($F_{6,36}=34.375$, $p<0.001$). Post-hoc testing always revealed that NP-coating significantly reduced impedance after coating (all $p<0.001$), whereas dipping of control electrodes into the NP-colloid did not affect impedance. After immersion of the coated electrodes into the saline solution and stimulation for 4 weeks impedance in vitro was stable, whereas, in the control sample, the impedance varied to some extent (Figure 3A, white and black bars).

3.3 Impedance in vivo

Histological analysis showed that all NP-coated and uncoated electrodes ($n=8$, each) were placed in the STN of the left and right hemispheres. As one electrode of each group broke during the experiments, 7 electrodes could be used for statistical analysis of impedance measurements. Statistical analysis of the impedance of coated and uncoated electrodes over time with one-way ANOVA showed a significant effect in coated ($F_{6,36}=34.926$, $p<0.001$) and uncoated electrodes ($F_{6,36}=16.930$, $p<0.001$). Post-hoc testing revealed that NP-coating significantly reduced impedance ($p<0.001$) before implantation and during four weeks of stimulation (all $p<0.05$), whereas impedance two weeks after implantation was temporarily enhanced. Dipping of electrodes in NP-solution and intracranial implantation did not affect impedance. In contrast, during the first three weeks of stimulation, the impedance of uncoated electrodes was significantly reduced, compared to the impedance before and after dipping in NP-solution (all $p<0.05$).

3.4 Normalized data

For better comparability between the groups and to cancel out total impedance differences between individual groups of electrodes, all data was normalized by the impedance of the corresponding uncoated electrodes (white bars in Figure 3 A and B set as 100%). Comparison between all groups with data relative to the electrode's impedance before coating with two-way RM ANOVA showed

significant effects for the factor group ($F_{2,150}=15.345$, $p<0.001$), the factor time ($F_{6,150}=84.448$, $p<0.001$) and their interaction ($F_{18,150}=10.417$, $p<0.001$). Post-hoc comparison between groups showed that NP-coating significantly reduces impedance in electrodes applicable to both, in vitro and in vivo groups ($p<0.001$). After intracranial implantation, the impedance of NP-coated electrodes was increased, while no significant change was observable for the uncoated controls. In contrast, immersion in saline of both coated and uncoated electrodes led to reduced impedances. In total, this leads to an overall higher electrode impedance after in vivo intracranial implantation in comparison to saline-immersed electrodes in vitro ($p<0.05$). Nevertheless, the impedance of NP-coated electrodes was still reduced in comparison to their uncoated counterpart ($p<0.05$). During the four weeks of stimulation, the impedance of coated electrodes was reduced compared to uncoated electrodes for in vivo and in vitro approaches ($p<0.05$), an effect which did not reach the level of significance for intracranial implanted coated electrodes at week 2 and week 3 of stimulation ($p<0.1$; Figure 3C).

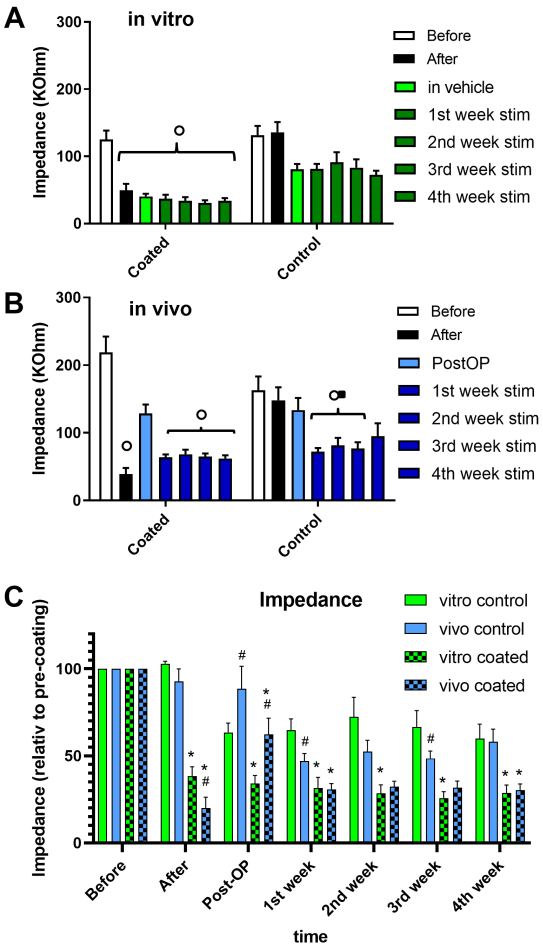

Figure 3: Impedance of electrodes after NP-coating or immersion into NP solution as control and subsequent immersion into (A) vehicle solution or (B) intracranial implantation in rats. Significant differences to pre-coating data are depicted as a circle (°), and to post-coating data as a square (X; $p < 0.05$). (C) The relative impedance of all groups for all times with significant differences between uncoated and coated electrodes as asterisks ($*$) and between in vivo and in vitro data as number sign (#; $p < 0.05$).

In addition, we applied Levene's test to assess whether coated and uncoated electrode impedance would differ in their variance. According to Levene, comparative statistics of the dispersion of pooled impedance values of coated and uncoated control electrodes under stimulation in vitro and in vivo showed that the variances during four weeks of stimulation were not equal. Likewise, Bartlett's test of homogeneity of variances showed that the variances of electrode impedances differ during four weeks of stimulation (see Table 1).

Table 1: Statistics of the dispersion of pooled impedance values of coated and uncoated control electrodes under stimulation in vitro and in vivo

	In vitro	**In vivo**
Mean ± SD, impedance in kΩ coated/uncoated (ctrl)	33.8 ± 12.7 / 82.0 ± 29.9	64.8 ± 13.2 / 81.3 ± 31.9
Levene	F(1,58)=12.126, p=0.0010	F(1,54)=5.521, p=0.0225
Bartlett	χ^2=18.050, p<0.0001	χ^2=18.342, p<0.0001

4 Discussion

We showed that pulsed DC EPD of laser-generated PtNPs reduces impedance and stabilizes impedance during long-term stimulation in saline and after intracranial implantation into the rat brain with subsequent long-term stimulation.

In a previous study, we already demonstrated that NP coating stabilizes the impedance of electrodes after intracranial implantation and long-term stimulation[12]. In that study, however, the electrode's impedance was increased after NP-coating via DC-EPD. In contrast, in the present study pulsed DC EPD was used for coating based on our more recent work[14], which resulted in a reduced impedance. This finding is most likely attributed to the higher coating homogeneity achievable by pulsed DC EPD, which also reduced impedance in an in vitro setting[14]. This reduced impedance in more homogeneous coatings was attributed to a higher active surface area not driven by the geometric surface area but by an enhanced chemical activity and oxidation state of the surface atoms[18]. However, in the case of nanoparticles arranged as assemblages (agglomerates and aggregates) on the electrode surface, which is most pronounced in DC EPD, electrical contacts may be impaired and impedance is reduced[14]. The in vivo environment is complex, and various factors can influence the electrode's surface structure. Biological interactions, immune responses, and the presence of bodily fluids and tissues can all play a role in altering the electrode's surface properties. It is postulated that geometry and area affect charge-injection capacity (CIC) measurements because of the non-uniform current distribution that localizes the charge-injection reactions to the perimeter or tip of an electrode[20]. Further analysis through, for example, cyclic voltammetry is an excellent way to assess the electrochemical properties of the electrodes and we used it to characterize our electrodes

in multiple studies to determine the electrocatalytic surface area and we found pronounced changes due to surface coverage[18], used EPD pulse mode (DC vs. pulsed DC[14]) and solvent[21]. However, cyclic voltammetry can be informative about the electrode's performance and response to electrical stimulation, but it may not directly reveal all the detailed changes in the surface structure induced by in vivo stimulation. Advanced techniques like X-ray photoelectron spectroscopy (XPS), or in-situ imaging techniques can be used to study these changes, although due to the frequent contamination with cell residue and damage of the electrodes utilization of these techniques was not possible in the in vivo samples after 4 weeks of stimulation.

In animal models, conducting chronic deep brain stimulation (DBS) over a four-week period can be challenging due to various limitations. However, a preclinical study in non-human primates has shown that the major changes in DBS electrode impedance occur after electrode implantation and during stimulation. These impedance changes could be an important issue for DBS patients implanted with voltage-controlled stimulators[22]. Notably, right after implantation into the rat's brain, the impedance in NP-coated electrodes increased temporarily. This observation corroborates our previous measures of elevated impedance after implantation into the rat brain[12], a finding also reported by other groups[23,24,25]. This finding is most likely attributed to the acute response of the neural tissue around the electrode contact[26,27,28,29,30] and is visualized as a spike in the impedance measurements[24,30]. This acute postoperative tissue reaction is followed by a chronic one, which is characterized by moderate gliosis[24,31], and roughly corresponds to the reduced impedance measure at the time of the onset of our electrostimulation period, two weeks after intracranial implantation. Notably, our parallel in vitro measures in saline do not show enhanced impedance, confirming our hypothesis that acute postoperative tissue reaction leads to enhanced electrode impedance in our in vivo setting. Interestingly, immersion of uncoated electrodes into saline reduced impedance, which is likely due to differences in the chemical composition of the different environments[32].

Increased impedance values of electrodes after intracranial implantation were statistically not different in coated and uncoated electrodes. We showed that glial reaction and neuronal loss do not differ between NP-coated and uncoated electrodes[12]. The three-electrode arrangement, comprising a working electrode, a reference electrode, and an auxiliary electrode, offers benefits in terms of establishing a steady baseline, reducing the risk of unwanted shifts or disruptions, and addressing electrode polarization concerns[33,34]. However, in our measurements, we've also incorporated a control electrode that lacks a nanoparticle coating, serving as a means of comparison. With the onset of stimulation, however, impedance decreased in NP-coated and uncoated electrodes, possibly due to intrinsic changes in the electrode. Nevertheless, this effect was more substantial in NP-coated electrodes, most likely, as the electric field stimulation leads to a surface restructuring, with the more fortunate ordering of the nanoparticles or – as controls are likewise affected – just all atoms on the surface. Another explanation would be a rearrangement and restructuring of the surface coatings upon multiple electrochemical stimulation rounds. A similar phenomenon was observed when we cycled the coatings multiple times in an electrochemical cell[15]. Nonetheless, although the impedance of coated electrodes is reduced during four weeks of stimulation as compared to uncoated control electrodes, there is no difference in the impedance between in vivo and in vitro settings, indicating that tissue reaction and scar formation seem to have no pronounced effect on the stimulation effi-

ciency in the chronic setting. Nevertheless, a chronic response can affect the stimulation outcome in ways that are not correlated with changes in impedance. It is plausible that chronic DBS responses could affect neural network behavior or tissue responsiveness to stimulation, altering stimulation efficacy even if impedance remains unchanged. This could mean that the electrodes are stable and well-suited for use in the biological tissue in question. Experimental studies have shown that the change in electrode impedance, and histological analysis revealed an increase in astrocyte density and the extent of astrocytosis around the stimulated electrodes[35]. In general, a rise in impedance is expected as time progresses, due to tissue deposition or microglial interaction. However, continuous stimulation may prevent the buildup of tissue and protein on the electrode surface, maintaining better electrical contact and signal delivery, and reducing the impedance. However, clinical studies in Parkinson's disease patients have shown that impedance decreases gradually over time, even when DBS settings are kept constant[36,37]. Noteworthy, previous work showed that NP-coating does not affect glial reaction or the number of neural cells in the vicinity of the electrode's tip[12].

In the clinical context, with electrophoretic deposition of NP from the same material derived by laser ablation in liquid, a homogenous coating can be achieved without the use of chemical precursors and ligands that may trigger tissue response[38,39,40,41]. Although water-ethanol mixtures can lead to even more homogeneous coatings and more favorable electrochemical properties[21], we deliberately used samples from pulsed DC EPD synthesis in water for the present experiments, as utilization of solvents should be avoided in *in vivo* or clinical settings. Moreover, the mechanical stability of pulsed DC EPD of PtNPs onto Pt-based neural electrodes has already been demonstrated using agarose gel, adhesive tape, and ultrasonication-based stress tests that simulated brain environments. In addition, it has been evidenced that NPs can still be found on an exemplarily explanted electrode's surface after the in vivo stimulation experiments. In addition, the mechanical force during the implantation may have affected the nanoparticles on the surface, though a full delamination of the coating could not be observed as reported[15].

In conclusion, pulsed DC EPD of colloidal, ligand-free PtNPs on neural electrodes reduces impedance, favoring stimulation efficiency and may prolong the battery life of the pulse generator. As the coating and the implant material are identical, adverse effects concerning the biocompatibility of the electrode are unlikely, and thus clinical approval would be less complicated. From the viewpoint of medical application, pulsed DC EPD of PtNPs may be a helpful approach to generate an optimized nano-coating, which would reduce and stabilize the overall impedance in vivo and enhance the quality and durability of chronic recording and stimulation in patients with electrical implants for therapeutic use over decades.

5 Ethics approval and consent to participate

All methods described were carried out in compliance with guidelines and regulations at the Hannover Medical School. All experimental protocols followed the German Animal Welfare Act, including approval of the Niedersächsisches Landesamt für Verbraucherschutz und Lebensmittelsicherheit, Dezernat 33/Tierschutz; AZ 18/2837. Additionally, animal experiments were conducted and reported

here in accordance with ARRIVE guidelines.

6 Consent for publication

All co-authors have seen and agree with the contents of the manuscript and there is no financial interest to report.

7 Availability of data and materials

All data and material are presented in the main manuscript and additional supporting files are available from the corresponding author on reasonable request.

8 Competing interests

The authors declare that they have no conflict of interest.

9 Funding

This work is supported by the German Research Foundation (DFG) through the grants KR 2931-3-1 and BA 3580-8-1.

10 Authors Contributions

SA, KS, CR, SB, and JK took part in the study concept and design. SA performed the in vivo experiments, and histochemistry statistical analysis of the collected data, and wrote the first draft of the manuscript. SA, MA, and HH did the impedance measurements. KS participated in the statistical analysis and manuscript drafting. CR and VR carried out the laser ablation and electrophoretic deposition of nanoparticles. KS, CR, SB, and JK supervised and coordinated the study and also took part in the critical revision of the manuscript. All authors read and approved the final manuscript to be published.

11 Acknowledgement

The authors thank Jürgen Wittek for his expert technical assistance.

References

[1] Michael Schulder, Akash Mishra, Antonios Mammis, Andres Horn, Alexandre Boutet, Patric Blomstedt, Stephan Chabardes, Oliver Flouty, Andres M Lozano, Joseph S Neimat, et al. Advances in technical aspects of deep brain stimulation surgery. *Stereotactic and Functional Neurosurgery*, 101(2):112–134, 2023.

[2] Andres M Lozano, Nir Lipsman, Hagai Bergman, Peter Brown, Stephan Chabardes, Jin Woo Chang, Keith Matthews, Cameron C McIntyre, Thomas E Schlaepfer, Michael Schulder, et al. Deep brain stimulation: current challenges and future directions. *Nature Reviews Neurology*, 15(3):148–160, 2019.

[3] Joachim K Krauss, Nir Lipsman, Tipu Aziz, Alexandre Boutet, Peter Brown, Jin Woo Chang, Benjamin Davidson, Warren M Grill, Marwan I Hariz, Andreas Horn, et al. Technology of deep brain stimulation: current status and future directions. *Nature Reviews Neurology*, 17(2):75–87, 2021.

[4] Megan S Lord, Morten Foss, and Flemming Besenbacher. Influence of nanoscale surface topography on protein adsorption and cellular response. *Nano Today*, 5(1):66–78, 2010.

[5] Bengt Kasemo. Biological surface science. *Surface science*, 500(1-3):656–677, 2002.

[6] Adam Curtis and Chris Wilkinson. Nantotechniques and approaches in biotechnology. *TRENDS in Biotechnology*, 19(3):97–101, 2001.

[7] Adam Curtis and Chris Wilkinson. Topographical control of cells. *Biomaterials*, 18(24):1573–1583, 1997.

[8] C Boehler, T Stieglitz, and M Asplund. Nanostructured platinum grass enables superior impedance reduction for neural microelectrodes. *Biomaterials*, 67:346–353, 2015.

[9] Christian Boehler, Diego M Vieira, Ulrich Egert, and Maria Asplund. Nanopt—a nanostructured electrode coating for neural recording and microstimulation. *ACS applied materials & interfaces*, 12(13):14855–14865, 2020.

[10] Isaac R Cassar, Chunxiu Yu, Jaydeep Sambangi, Curtis D Lee, John J Whalen III, Artin Petrossians, and Warren M Grill. Electrodeposited platinum-iridium coating improves in vivo recording performance of chronically implanted microelectrode arrays. *Biomaterials*, 205:120–132, 2019.

[11] Kostas N Fountas, Joseph R Smith, Anthony M Murro, Jeffrey Politsky, Yong D Park, and Patrick D Jenkins. Implantation of a closed-loop stimulation in the management of medically refractory focal epilepsy. *Stereotactic and functional neurosurgery*, 83(4):153–158, 2005.

[12] Svilen D Angelov, Sven Koenen, Jurij Jakobi, Hans E Heissler, Mesbah Alam, Kerstin Schwabe, Stephan Barcikowski, and Joachim K Krauss. Electrophoretic deposition of ligand-free platinum nanoparticles on neural electrodes affects their impedance in vitro and in vivo with no negative effect on reactive gliosis. *Journal of nanobiotechnology*, 14(1):1–11, 2016.

[13] WD Ristenpart, Ilhan A Aksay, and DA Saville. Electrohydrodynamic flow around a colloidal particle near an electrode with an oscillating potential. *Journal of Fluid Mechanics*, 575:83–109, 2007.

[14] Vaijayanthi Ramesh, Christoph Rehbock, Brian Giera, John J Karnes, Jean-Baptiste Forien, Svilen D Angelov, Kerstin Schwabe, Joachim K Krauss, and Stephan Barcikowski. Comparing direct and pulsed-direct current electrophoretic deposition on neural electrodes: deposition mechanism and functional influence. *Langmuir*, 37(32):9724–9734, 2021.

[15] Vaijayanthi Ramesh, Nadine Stratmann, Viktor Schaufler, Svilen D Angelov, Ilona D Nordhorn, Hans E Heissler, Ricardo Martínez-Hincapié, Viktor Čolić, Christoph Rehbock, Kerstin Schwabe, et al. Mechanical stability of nano-coatings on clinically applicable electrodes, generated by electrophoretic deposition. *Advanced Healthcare Materials*, page 2102637, 2022.

[16] George Paxinos and Charles Watson. The rat brainin stereotaxic coordinates. 1997.

[17] William T Nichols, Takeshi Sasaki, and Naoto Koshizaki. Laser ablation of a platinum target in water. i. ablation mechanisms. *Journal of Applied Physics*, 100(11):114912, 2006.

[18] Sven Koenen, Christoph Rehbock, Hans E Heissler, Svilen D Angelov, Kerstin Schwabe, Joachim K Krauss, and Stephan Barcikowski. Optimizing in vitro impedance and physicochemical properties of neural electrodes by electrophoretic deposition of pt nanoparticles. *ChemPhysChem*, 18(9):1108–1117, 2017.

[19] Carmen Streich, Sven Koenen, Marco Lelle, Kalina Peneva, and Stephan Barcikowski. Influence of ligands in metal nanoparticle electrophoresis for the fabrication of biofunctional coatings. *Applied Surface Science*, 348:92–99, 2015.

[20] Stuart F Cogan. Neural stimulation and recording electrodes. *Annu. Rev. Biomed. Eng.*, 10:275–309, 2008.

[21] Vaijayanthi Ramesh, Brian Giera, John J Karnes, Nadine Stratmann, Viktor Schaufler, Yao Li, Christoph Rehbock, and Stephan Barcikowski. Solvent composition during electrophoretic deposition of platinum nanoparticles on neural electrode surfaces influences their electrochemical behavior. *Journal of the Electrochemical Society*, 169(LLNL-JRNL-826684), 2022.

[22] Scott F Lempka, Svjetlana Miocinovic, Matthew D Johnson, Jerrold L Vitek, and Cameron C McIntyre. In vivo impedance spectroscopy of deep brain stimulation electrodes. *Journal of neural engineering*, 6(4):046001, 2009.

[23] Mohammad Reza Abidian, Joseph M Corey, Daryl R Kipke, and David C Martin. Conducting-polymer nanotubes improve electrical properties, mechanical adhesion, neural attachment, and neurite outgrowth of neural electrodes. *small*, 6(3):421–429, 2010.

[24] Kip A Ludwig, Nicholas B Langhals, Mike D Joseph, Sarah M Richardson-Burns, Jeffrey L Hendricks, and Daryl R Kipke. Poly (3, 4-ethylenedioxythiophene)(pedot) polymer coatings facilitate smaller neural recording electrodes. *Journal of neural engineering*, 8(1):014001, 2011.

[25] Pouria Fattahi, Guang Yang, Gloria Kim, and Mohammad Reza Abidian. Biomaterials: a review of organic and inorganic biomaterials for neural interfaces. *Advanced Materials*, 26(12):1793–1793, 2014.

[26] Christopher R Butson, Christopher B Maks, and Cameron C McIntyre. Sources and effects of electrode impedance during deep brain stimulation. *Clinical Neurophysiology*, 117(2):447–454, 2006.

[27] Xindong Liu, Douglas B McCreery, Randy R Carter, Leo A Bullara, Ted GH Yuen, and William F Agnew. Stability of the interface between neural tissue and chronically implanted intracortical microelectrodes. *IEEE transactions on rehabilitation engineering*, 7(3):315–326, 1999.

[28] Miguel AL Nicolelis, Dragan Dimitrov, Jose M Carmena, Roy Crist, Gary Lehew, Jerald D Kralik, and Steven P Wise. Chronic, multisite, multielectrode recordings in macaque monkeys. *Proceedings of the National Academy of Sciences*, 100(19):11041–11046, 2003.

[29] Vadim S Polikov, Patrick A Tresco, and William M Reichert. Response of brain tissue to chronically implanted neural electrodes. *Journal of neuroscience methods*, 148(1):1–18, 2005.

[30] Jennie Leach, Anil Kumar H Achyuta, and Shashi K Murthy. Bridging the divide between neuroprosthetic design, tissue engineering and neurobiology. *Frontiers in neuroengineering*, page 18, 2010.

[31] Martin Kronenbuerger, Kay Wilhelm Nolte, Volker Arnd Coenen, Jean-Marc Burgunder, Joachim K Krauss, and Joachim Weis. Brain alterations with deep brain stimulation: new insight from a neuropathological case series. *Movement Disorders*, 30(8):1125–1130, 2015.

[32] Xuefeng F Wei and Warren M Grill. Impedance characteristics of deep brain stimulation electrodes in vitro and in vivo. *Journal of neural engineering*, 6(4):046008, 2009.

[33] Alexander R Harris, David B Grayden, and Sam E John. Electrochemistry in a two-or three-electrode configuration to understand monopolar or bipolar configurations of platinum bionic implants. *Micromachines*, 14(4):722, 2023.

[34] Giuseppe Schiavone, Xiaoyang Kang, Florian Fallegger, Jérôme Gandar, Grégoire Courtine, and Stéphanie P Lacour. Guidelines to study and develop soft electrode systems for neural stimulation. *Neuron*, 108(2):238–258, 2020.

[35] J Evers, K Sridhar, J Liegey, J Brady, H Jahns, and M Lowery. Stimulation-induced changes at the electrode–tissue interface and their influence on deep brain stimulation. *Journal of Neural Engineering*, 19(4):046004, 2022.

[36] David Satzer, Huiyan Yu, Meredith Wells, Mahesh Padmanaban, Matthew R Burns, Peter C Warnke, and Tao Xie. Deep brain stimulation impedance decreases over time even when stimulation settings are held constant. *Frontiers in Human Neuroscience*, 14:584005, 2020.

[37] Joshua Wong, Aysegul Gunduz, Jonathan Shute, Robert Eisinger, Stephanie Cernera, Kwo Wei David Ho, Daniel Martinez-Ramirez, Leonardo Almeida, Christina A Wilson, Michael S Okun, et al. Longitudinal follow-up of impedance drift in deep brain stimulation cases. *Tremor and Other Hyperkinetic Movements*, 8, 2018.

[38] Jennifer A Dahl, Bettye LS Maddux, and James E Hutchison. Toward greener nanosynthesis. *Chemical reviews*, 107(6):2228–2269, 2007.

[39] Niko Bärsch, Jurij Jakobi, Sascha Weiler, and Stephan Barcikowski. Pure colloidal metal and ceramic nanoparticles from high-power picosecond laser ablation in water and acetone. *Nanotechnology*, 20(44):445603, 2009.

[40] Jurij Jakobi, Ana Menéndez-Manjón, Venkata Sai Kiran Chakravadhanula, Lorenz Kienle, Philipp Wagener, and Stephan Barcikowski. Stoichiometry of alloy nanoparticles from laser ablation of ptir in acetone and their electrophoretic deposition on ptir electrodes. *Nanotechnology*, 22(14):145601, 2011.

[41] Alexander Heinemann, Sven Koenen, Kerstin Schwabe, Christoph Rehbock, and Stephan Barcikowski. How electrophoretic deposition with ligand-free platinum nanoparticles affects contact angle. In *Key engineering materials*, volume 654, pages 218–223. Trans Tech Publ, 2015.

7 In vitro and In vivo Mechanical stability of EPD-generated Nano-coatings

Published in Advanced Healthcare Materials (2022) 2102637

Mechanical Stability of Nano-Coatings on Clinically Applicable Electrodes, Generated by Electrophoretic Deposition

Vaijayanthi Ramesh[1], Nadine Stratmann[1], Viktor Schaufler[1], Svilen D. Angelov[2], Ilona D. Nordhorn[3], Hans E Heissler[2], Ricardo Martínez-Hincapié[4], Victor Čolić[4], Christoph Rehbock[1], Kerstin Schwabe[2], Uwe Karst[3], Joachim K. Krauss[2] and Stephan Barcikowski[1,*]

[1] Institute of Technical Chemistry I, University of Duisburg-Essen and Center for Nanointegration Duisburg-Essen (CENIDE), Essen, Germany

[2] Department of Neurosurgery, Hannover Medical School, Hannover, Germany

[3] Institute of Inorganic and Analytical Chemistry, University of Münster, Münster, Germany

[4] Electrochemistry for Energy Conversion, Max-Planck-Institute for Chemical Energy Conversion, Mülheim an der Ruhr, Germany

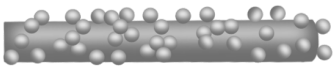

Least impedance increase in vitro

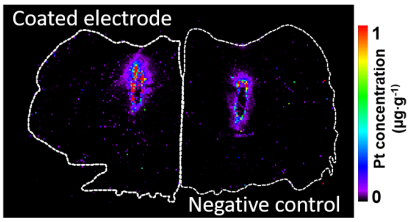

Stable impedance throughout in vivo stimulation

Summary:

In the previous section, the PtNP-coated neural electrodes were stimulated in vitro and in vivo in Parkinson's rat models, and the electrode impedances were monitored. However, to implement these nano-coatings clinically their mechanical stability has to be tested. Therefore in the forthcoming section, the mechanical stability of EPD-generated coatings, both in vitro and in vivo, is investigated to determine the coating's clinical applicability. The stability of EPD-generated Nano-coatings was analyzed in vitro (agarose gel, ultrasonication, and adhesive tape) and in vivo (rat models). In vitro, the nano-coatings were found to be mechanically stable in simulated brain environments (agarose gel). Electrochemically, the coatings were stable revealing a statistically significant 17.5% reduction in electrode impedance after 1000 CV cycles. Quantification of Pt in the stimulated brain sections via LA-ICP-MS reveals a significantly higher amount of Pt in the region stimulated with PDC-coated electrodes, in comparison to the uncoated electrode region, however below any toxicologically relevant levels.

Author contributions:

Design and supervision of the experiments on the mechanical stability of EPD-coated electrodes and their characterization were performed by VR. Data collection was carried out by NS and VS. Electrochemical measurements were supported by RMH and VC. IN and UK assisted in the analysis of explanted brain sections via LA-ICP-MS. Implantation of the coated electrodes in rat brains was performed by SDA. The original manuscript draft was prepared by VR. The review and editing of the manuscript were carried out by VR, CR, SDA, IN, RMH, VC, KS, JKK, and SB. SB and CR designed the study, supervised, obtained funding support, and promoted collaborations between the institutions.

ADVANCED HEALTHCARE MATERIALS
www.advhealthmat.de

Mechanical Stability of Nano-Coatings on Clinically Applicable Electrodes, Generated by Electrophoretic Deposition

Vaijayanthi Ramesh, Nadine Stratmann, Viktor Schaufler, Svilen D. Angelov, Ilona D. Nordhorn, Hans E. Heissler, Ricardo Martínez-Hincapié, Viktor Čolić, Christoph Rehbock, Kerstin Schwabe, Uwe Karst, Joachim K. Krauss, and Stephan Barcikowski**

The mechanical stability of implant coatings is crucial for medical approval and transfer to clinical applications. Here, electrophoretic deposition (EPD) is a versatile coating technique, previously shown to cause significant post-surgery impedance reduction of brain stimulation platinum electrodes. However, the mechanical stability of the resulting coating has been rarely systematically investigated. In this work, pulsed-DC EPD of laser-generated platinum nanoparticles (PtNPs) on Pt-based, 3D neural electrodes is performed and the in vitro mechanical stability is examined using agarose gel, adhesive tape, and ultrasonication-based stress tests. EPD-generated coatings are highly stable inside simulated brain environments represented by agarose gel tests as well as after in vivo stimulation experiments. Electrochemical stability of the NP-modified surfaces is tested via cyclic voltammetry and that multiple scans may improve coating stability could be verified, indicated by higher signal stability following highly invasive adhesive tape stress tests. The brain sections post neural stimulation in rats are analyzed via laser ablation-inductively coupled plasma-mass spectrometry (LA-ICP-MS). Measurements reveal higher levels of Pt near the region stimulated with coated electrodes, in comparison to uncoated controls. Even though local concentrations in the vicinity of the implanted electrode are elevated, the total Pt mass found is below systemic toxicologically relevant concentrations.

1. Introduction

Neural electrodes are employed for various treatments including deep brain stimulation (DBS) in Parkinson's disease, epilepsy, depression, deafness, spinal cord injuries, blindness, advanced tremors, etc.[1,2] Although these electrodes have long been used in clinics, a drawback lies in the increased electrode impedance (Z) due to gliosis, reducing the efficiency of stimulation/recording.[3] To address this issue, researchers try to increase the electrode's electrochemical surface area (ECSA) utilizing various surface modification techniques.[4–9]

Platinum (Pt) based electrodes are considered to be one of the best materials to act as a neural implant.[10] Their surfaces have been widely modified using metals, metal oxides, conductive polymers and nanoparticles, for improving the electrochemical characteristics.[11–16] Established techniques used to modify platinum electrode surfaces include anisotropic etching,[17,18] two-photon lithography,[19] laser-induced

V. Ramesh, N. Stratmann, V. Schaufler, C. Rehbock, S. Barcikowski
Institute of Technical Chemistry I
University of Duisburg-Essen and Center for NanoIntegration Duisburg-Essen (CENIDE)
45141 Essen, Germany
E-mail: stephan.barcikowski@uni-due.de

The ORCID identification number(s) for the author(s) of this article can be found under https://doi.org/10.1002/adhm.202102637

DOI: 10.1002/adhm.202102637

S. D. Angelov, H. E. Heissler, K. Schwabe, J. K. Krauss
Department of Neurosurgery
Hannover Medical School
30625 Hannover, Germany
E-mail: krauss.joachim@mh-hannover.de

I. D. Nordhorn, U. Karst
Institute of Inorganic and Analytical Chemistry
University of Münster
48149 Münster, Germany

R. Martínez-Hincapié, V. Čolić
Electrochemistry for Energy Conversion
Max-Planck-Institute for Chemical Energy Conversion
45470 Mulheim an der Ruhr, Germany

forward transfer (LIFT).[20] as well as focused electron/ion beam induced deposition (FEBID/FIBID).[21,22] Particularly, studies, where the coating and the implant material are identical, are highly interesting, as they do not adversely affect the biocompatibility of the device and clinical approval is less complicated. However, if the coating delaminates from the implant surface and gets released into the organism, these advantages become invalid. Thereto, it is highly important to guarantee that the coatings are mechanically stable under in vivo conditions. Boehler et al. electrodeposited Pt on Pt–Ir electrodes and observed stable nanostructured coatings after 1 billion stimulation pulses that were biocompatible in vivo and efficient during stimulation.[23] In another study, they deposited Pt nanograss on Pt microelectrodes through a chemical reduction method, which resulted in an increased ECSA and reduced Z of about two orders of magnitude.[6] Pt–Ir has been electrodeposited on rectangular Pt cochlear electrodes[24] and Pt–Ir microwire arrays[25] resulting in a 91–93% reduction of polarization Z and low noise, high signal-to-noise ratio, and low Z, respectively. Zátonyi et al. deposited Pt black coatings on Pt ECoG microelectrode arrays (MEAs) and observed a reduction in thermal noise, enhanced signal-to-noise ratio, and increased ECSA.[26] An alternate surface modification technique to nanostructure Pt-based neural electrode surfaces is the electrophoretic deposition (EPD) of laser-generated ligand-free PtNPs.[13,15,27] These purely electrostatically stabilized NPs are advantageous over their ligand-coated counterparts, as they facilitate linear scaling of the deposition process concerning concentration and electric field strength, due to the absence of ligand-induced electrostatic repulsion at the particle-electrode interface.[28] Using this method, we previously reported process parameter optimization for 2D target surfaces, and the in vivo functionality of 3D electrodes when coated with direct current (DC) EPD.[15] In our recent work, we deposited PtNPs on 3D Pt–Ir surfaces and studied the electrode performances by applying DC and pulsed-DC (PDC) electric fields,[14] and further evaluated the impact of the solvent (ethanol–water mixtures) on coating quality.[16] However, for a coating aimed at clinical application, its mechanical stability is one of the most critical factors to be studied. If the developed coatings are not stable enough, the detached particles may undergo biodispersion inside the body after implantation and can become toxic to the local tissue. Furthermore, coating delamination frequently goes along with impairment of electrode functionality. Boehler et al. chemically deposited nano-Pt on Pt microelectrodes and tested the coating stability by dipping the modified electrodes in a 0.6% agar dummy. They found that the charge storage capacity (CSC) decreased by 4% and Z increased by 6%.[7] Pt black coatings were deposited on various neural electrode surfaces, after which their durability was studied via ultrasonic agitation. Strong forces generated by ultrasonication deteriorated the electrochemical properties of Pt black modified surfaces: 77% decrease in ECSA,[29] 21%,[30] and 20%[31] loss in CSC, and 63% increase in Z.[8] Minev et al. produced stretchable composite coating (mixture of Pt powder and silicone) on MEAs and tested the mechanical integrity using a tensile stretcher and found that the coatings deformed with the applied strain but retained their electrical contact with the MEAs.[32] Wang et al. performed ultrasonic agitation of their Pt-black:PEDOT/PSS coated microelectrodes inside agarose gel to simulate brain tissue micromotions. They found a Z-increase of 9.5% after 100 min of mechanical agitation and hence concluded that the coatings were durable for long-term usage.[33] In addition, material adhesion tests were also performed on modified neural electrode surfaces following the American Society for Testing and Materials (ASTM D3359),[34] wherein a pattern (usually an X or a crosshatch) was scratched on the coatings, after which a pressure-sensitive adhesive tape was pressed on the pattern and removed at an angle to observe coating delamination.[35–38] Another important assay concept for evaluation of electrode mechanical stability is a standardized bending fatigue test, for example, based on a sliding-plate assay, where correlations between bending angle and resistivity are recorded.[39] Here, Kim et al. could show that in hybrid structures where the Cu thin films were deposited on polyimine supports, bending strain is a direct function of film thickness.[40] However, this method is primarily applicable to flexible electrode thin films on polymer support and difficult to apply to free metal wires with micrometer diameter in direct contact with tissue.

Nevertheless, to the best of our knowledge, a comprehensive and exclusive study on the mechanical stability of neural electrode surface coatings with several complementary testing methods, and detailed electrochemical analysis, including correlation with in vivo stability is rare. In this work, we present a systematic investigation of the stability of PtNP EPD on 3D Pt–Ir (90:10) neural electrode surfaces. Pt–Ir wires were coated with DC- and PDC-EPD and their coating stabilities were tested via three approaches: dipping in 0.6 wt% agarose gel, adhesion test, and ultrasonic agitation. In addition, the electrochemical stability of the coatings was evaluated by cycling the samples multiple times in cyclic voltammetry (CV). Please note that optimization of coating parameters has been addressed in previous studies. Here, we aimed to evaluate the quality of an EPD-coating synthesized under conditions optimized for optimum performance (low impedance) based on the following previous works.[14–16]

The surfaces were electrochemically characterized before and after performing stability tests via CV and electrochemical impedance spectroscopy (EIS). In addition, the rat brain slices post-DBS were quantified for the presence of Pt using laser ablation-inductively coupled plasma-mass spectrometry[41] (LA-ICP-MS) (**Figure 1**). Furthermore, qualitative characterization of the coated surfaces was performed using scanning electron microscopy (SEM).

2. Results and Discussion

To evaluate the mechanical stability of EPD coatings, microscale (76 µm diameter) Pt–Ir ($Pt_{90}Ir_{10}$ molar ratio) wire surfaces with dimensions and composition comparable to commercially available brain electrodes were modified using laser-generated, ligand-free colloidal Pt NPs. Particles were synthesized via a two-step laser-based approach starting with pulsed laser ablation of a Pt target in Milli-Q water followed by a consecutive laser fragmentation in liquid (LFL) step for size control yielding a final mean particle diameter of 14 nm. Consecutively, the Pt NPs (100 µg mL^{-1}, pH11) were deposited on the wires by EPD utilizing DC (5 V cm^{-1}, 5 min) and PDC (5 V cm^{-1}, 1 µs period, 50% duty cycle, 10 min) electric fields as previously reported.[14] The coating stability was assessed via three methods: dipping the coated samples in agarose gel (0.6 wt%), adhesion test using 3M Scotch

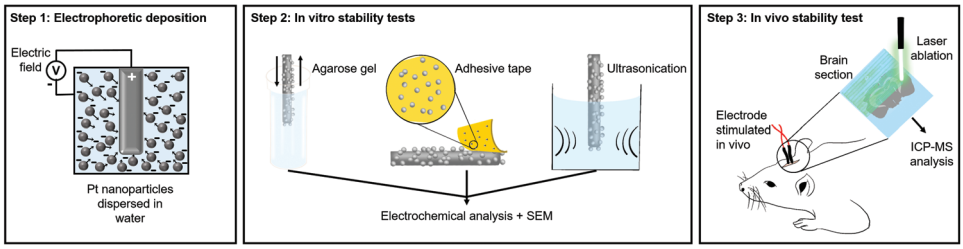

Figure 1. Schematic representation of the experimental workflow: Step 1 shows the EPD of negatively charged PtNPs on positively charged Pt neural electrode surfaces; Step 2 represents the three in vitro stability testing methods; and Step 3 shows the analysis of rat brain sections via LA-ICP-MS.

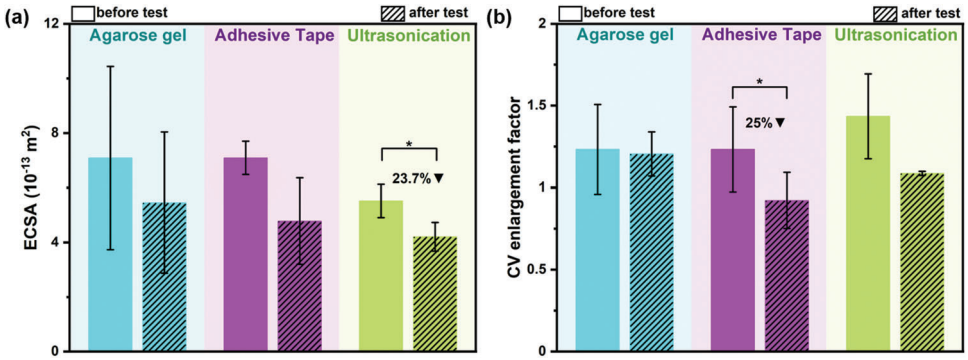

Figure 2. Electrode surface chemistry before and after mechanical stress testing. a) Average ECSA values of PDC-coated neural electrodes, measured by applying 20 CV cycles ($N = 4$, $\alpha = 0.05$). b) Average CV enlargement factor (CSC) values of PDC-coated neural electrodes ($N = 3$, $\alpha = 0.05$). Bar plots represent mean values and error standard deviations.

tape, and ultrasonication in Milli-Q water for 5 min. Before and after the mechanical tests, the samples were characterized using CV, EIS, and SEM. Since in our previous work, PDC-EPD was reported to significantly reduce the neural electrode's Z compared to the DC-EPD,[14] we focused our study on the PDC-EPD coatings while DC-EPD results are presented in Section S4, Supporting Information. **Figure 2** demonstrates the decrease in ECSA, **Figure 3** shows the increase in Z and **Figure 4** shows the neural electrode surfaces, after the stability tests performed on PDC-coated samples. Their corresponding cyclic voltammograms and EIS spectra are shown in Figure S6, Supporting Information. To achieve sufficient signal stability all samples were cycled 20 times in the electrochemical setup before measurements.

From Figure 2a, it is observed that the ECSA of all the samples that underwent stability tests, decreased. Among them, the decrease in ECSA was the least in samples tested using an agarose gel. Similarly, the CSC also showed the least decrease in agarose gel compared to the other two tests (Figure 2b). Figure 3a,b shows the increase in Z values at both of the medically relevant frequencies after the stability tests, revealing an insignificant increase in Z after the agarose gel test at 150 Hz. It is well known from the literature that the ECSA and Z are inversely proportional to each other.[8,42] Therefore, the obtained results are in good agreement with each other. The significant levels of delamination, represented by Z increase, after adhesion test or ultrasonication are due to the high mechanical stress induced on the particle coatings, which causes them to peel off. During the agarose gel test, however, much lower friction forces of ≈5 μN were applied. Additionally, from the SEM images, it is clear that the adhesive tape removes more particles from the surface than ultrasonication (Figure 4e,f). This could be due to the distributed coatings produced by PDC-EPD,[14] which can be observed in Figure 4a–c. Here, since the NP coverage is less clustered in comparison to the DC-EPD (Figure S5a–c, Supporting Information), the force generated by the adhesive tape was strong enough to remove a large number of monolayer particles from the surface than the force induced during ultrasonication, which probably has only removed the agglomerated particles that are loosely bound. SEM images from Figure 4 support this explanation, where after the tests the particles are not entirely removed from the electrode surfaces, however, more particles seem to have been removed after the tape test (Figure 4e). Boehler et al. found a 4% decrease in their CSC,[7] however, our samples show no statistically significant decrease in CSC after the agarose gel test. Therefore, the mechanical stability tests confirm that the EPD-generated coatings are more stable in an agarose gel (simulated brain density and viscosity) environment, compared to the other two in vitro stability tests.

To investigate the electrochemical stability of the EPD-generated coatings, Pt–Ir wires coated with Pt NPs using PDC-EPD were scanned in CV for multiple cycles: 100, 500, 1000, and 2000. Before and after CV scanning, the Z-values of the samples were measured. **Figure 5** shows the CV analysis and **Figure 6** shows the EIS analysis of the samples. The corresponding EIS spectra are shown in Figure S7a, Supporting Information.

Figure 5 shows that the ECSA and CSC of the samples gradually increase with an increasing number of CV cycles up to 1000 cycles. This finding may be attributed to the fact that repeated CV scanning of Pt surfaces in sulfuric acid helps to maximize the exposure of surface Pt sites for hydrogen adsorption,[43] in turn

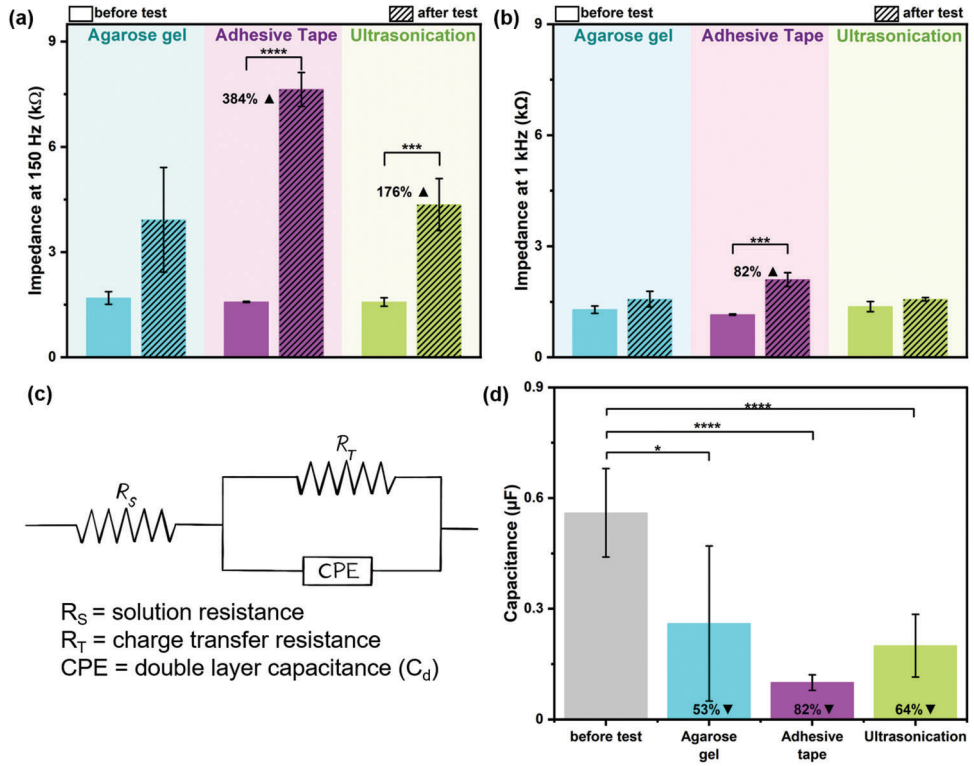

Figure 3. Average impedance values of PDC-coated neural electrodes, before and after stability tests at a) 150 Hz and b) 1 kHz ($N = 4$, $\alpha = 0.05$). c) Equivalent circuit model comprising an R(RC) circuit is used for fitting the EIS data. d) Average fitted capacitance values of the samples, before and after stability tests ($N = 4$, $\alpha = 0.05$). Bar plots represent mean values and error standard deviations.

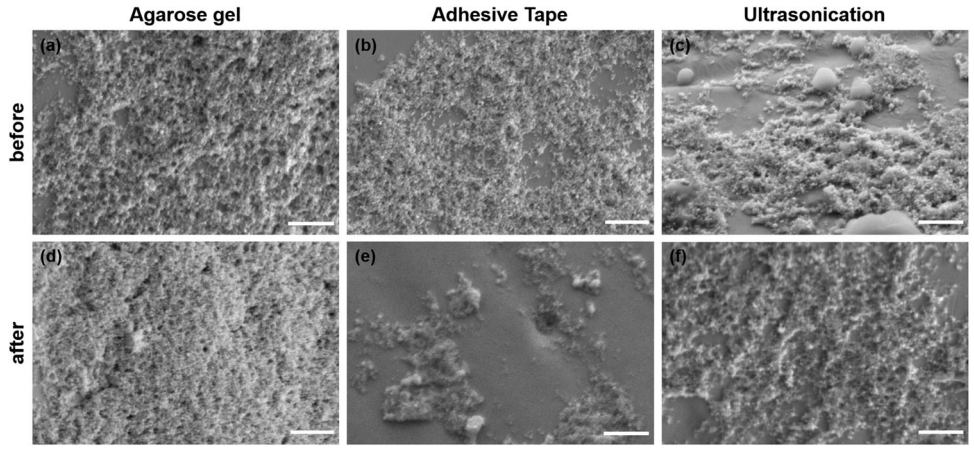

Figure 4. Exemplary SEM images from the sides of the PDC-coated neural electrodes a–c) before and d–f) after the mechanical stability tests. Scale bars are 500 nm.

activating the surface and increasing the ECSA and CSC[43,44] of the electrodes (Figure 5b,c). Interestingly, for longer cycling at 2000 cycles, the trend seems to decrease and no differences between the samples before and after cycling is available, which may point to more extensive particle delamination at a higher number of cycles, which seems to counter the observed activation effect at lower cycle numbers. EIS analysis on the samples before and after multiple CV cycles, reveals a significant decrease in Z at 150 Hz after 1000 cycles and no significant differences at longer cycling after 2000 cycles, which points to a saturation effect. (Figure 6a). At 1 kHz, the decreasing trend starts already after 500 cycles (Figure 6b), although not statistically significant, and here as well, saturation seems to occur after 2000 cycles. Upon fitting the EIS data with an equivalent circuit, the capacitance also shows an increasing though non-significant trend after 1000 cycles and saturation at 2000 cycles. Wang et al. found that after 10 000 CV cycles the Z increased,[33] representing coating instability. However, it should be noted that Wang et al.

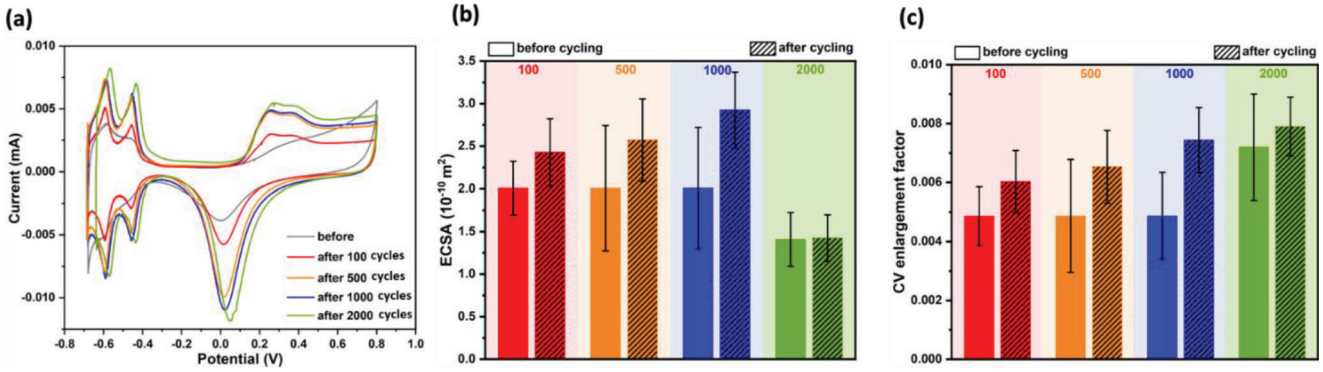

Figure 5. a) Exemplary cyclic voltammograms of PDC-coated electrodes before and after electrochemical stability test, b) average ECSA values of the electrodes before and after electrochemical stability test ($N = 3$, $\alpha = 0.05$), and c) average CSC values of the electrochemical stability tested electrodes ($N = 3$, $\alpha = 0.05$). Bar plots represent mean values and error standard deviations.

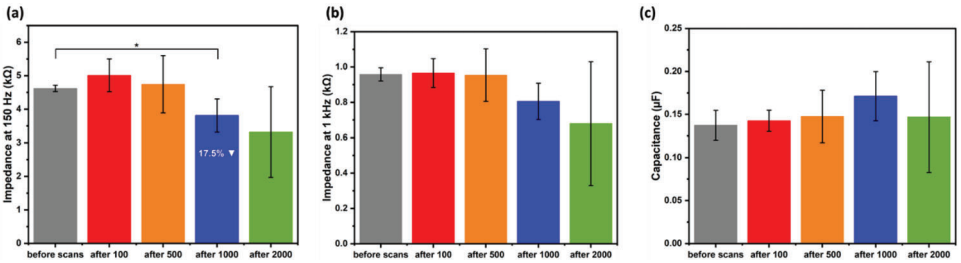

Figure 6. Average impedance values of electrochemical stability tested electrodes at a) 150 and b) 1 kHz. c) Average fitted capacitance values of the electrodes obtained after EIS equivalent circuit fitting. Bar plots represent mean values and errors standard deviations ($N = 3$, $\alpha = 0.05$).

evaluated the performances of electrodes with a completely different design. In their case layered electrodes consisting of a platinum black/conductive polymer sandwich structure were analyzed, while in our work coatings composed of Pt-electrode Pt-nanoparticle metal-metal interfaces were evaluated.

Our samples showed a statistically significant 17.5% reduction in Z after 1000 cycles at 150 Hz, revealing an improvement in their stability at intermediate cycles and saturation in impedance at 2000 cycles. Based on these findings it may be concluded that cycling a coated electrode in an electrochemical setup for 500–1000 cycles can improve certain properties like higher ECSA or lower impedance, though this effect is negated when more cycles are used, probably due to more pronounced coating delamination with more cycles.

To additionally test whether the extended CV cycling influences the mechanical stability of the deposited particles, adhesion tape tests were performed on the samples after CV cycling. **Figure 7** shows the EIS analysis and SEM images, before and after the tape test, respectively. Please note that the controls used here are not derived from values without cycles as in Figure 6 (before scan) but had also undergone limited cycling (20 cycles) to allow comparability to previous stability assays. This fact accounts for inconsistencies in starting impedance at 150 Hz between Figures 6 and 7, though the massive differences occurring here cannot be explained based on the current experimental design.

Since the adhesion test induced the highest force on the particles and resulted in the highest levels of delamination previously, we were interested to investigate the strength of particle adherence after repeated CV cycles via the tape test. Figure 7a,b reveals a significant increase in Z after the test in all samples, at both frequencies with similar final impedance values independent of the previous cycling. However, the percentage increase in Z was lower in those samples that underwent multiple CV cycling. Also, the least increase in impedance can be observed after 500 CV cycles at both 150 Hz and 1 kHz. Figure 7c–g shows the corresponding coated surfaces after the tape test, indicating that the adhesive tape led to the expected pronounced delamination of the particles in the coatings, though particle detachment was not quantitative. Furthermore, multiple cycling before the tape test influenced the final morphology of the coating. Here more homogeneous coatings after multiple cycles were found pointing toward surface restructuring, while in the controls, coatings were primarily composed of multilayer assemblages though the images seem to indicate higher surface coverage. However, please note that in assemblage-like multilayers, the contact between electrode and coating is less pronounced, which may explain why the final impedance in the multi-cycled and control samples were similar even though surface coverage with particles in the controls was higher.

Therefore, for Pt-based neural electrode fabrication, we demonstrate a surface coating technique using PDC-EPD of laser-generated Pt NPs, which decreases electrode Z significantly in comparison to their DC counterparts.[14] Concerning the mechanical stability of these coatings, we note that additional multiple cycling of the electrode has a significant impact on coating stability with a minimum impedance change after 500 cycles. This went along with substantial differences in coating

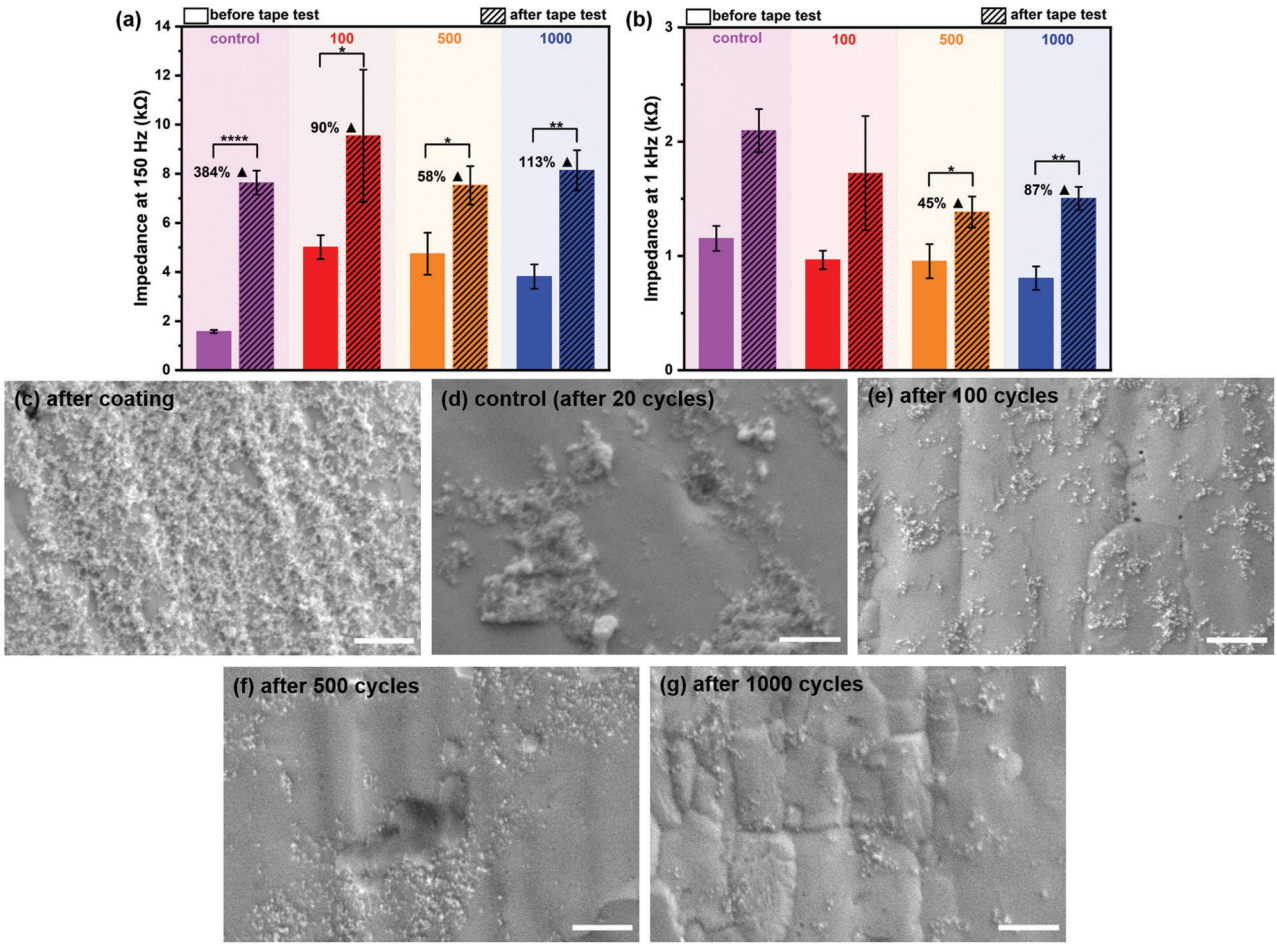

Figure 7. Average impedance values of the electrodes before and after adhesion test at a) 150 and b) 1 kHz, after electrochemical stability testing ($N = 3$, $\alpha = 0.05$). The control samples are previously described in Figure 3, which were tested for adhesion with 20 previous CV scans. Bar plots represent mean values and error standard deviations. Exemplary SEM images of the PDC-coated, adhesion tested samples: c) after coating; d) control (after 20 cycles); e) after 100 cycles; f) after 500 cycles; and g) after 1000 cycles. Scale bars are 500 nm.

morphology, which retained assemblage-based coatings in the controls, whereas more homogeneous coatings were found after continuous cycling. This could lead to an improved particle-electrode electrical contact, lowering the overall impedance increase.

Another relevant kind of mechanical stress on a nanoparticle-coated micrometer-sized neural electrode would be bending. To examine this, we bent a 76 µm diameter Pt–Ir wire coated via PDC-EPD with a tweezer assuming a final angle of ≈90°. The wires before and after the bending test were examined using SEM (Figure S9, Supporting Information). We could observe no further delamination or significant changes in nanoscale coating geometry due to macroscopic bending, which seems to indicate coating stability upon macroscopic electrode deformation.

To analyze the stability of coated NPs inside an in vivo environment, coating stability was evaluated by SEM after 4 weeks of in vivo DBS and the brain sections of rats that underwent 4-week DBS as previously described in our work,[15] which were mounted on glass slides, and Pt content in the tissue surrounding the implantation site was quantified using LA-ICP-MS. In this previous work, we already demonstrated a pronounced stabilization of impedance in vivo for 4 weeks, while the impedance in the uncoated controls increased in the corresponding period verifying the beneficial properties of the analyzed coatings. Hence, this work focuses on coating degradation and dissolution in vivo and does not aim to reproduce the functionality assays. Please note that the electrodes used for in vivo studies in this work were not pre-treated by multiple cycling. **Figure 8**a depicts SEM images of neural electrodes after removal from the rat's brain after a 4-week stimulation period. While many of the electrodes were contaminated with organic residues (Figure 8a, right), a minor fraction of the examined electrodes remained uncontaminated (Figure 8a, left). Here the presence of a partially intact nanoparticle surface coating can be verified (Figure 8a) and qualitatively only minor differences between the coatings before stability tests (Figure 4, top row) and those after in vivo stimulation are observable. Based on this finding we conclude that neither the long-term in vivo stimulation period nor the physical strain during electrode removal substantially degraded the electrodes' coatings. Figure 8b shows the amount of Pt present in the stimulated brain region using PDC-coated electrodes, uncoated negative control, and colloid injected positive control. Pt quantified in brain regions

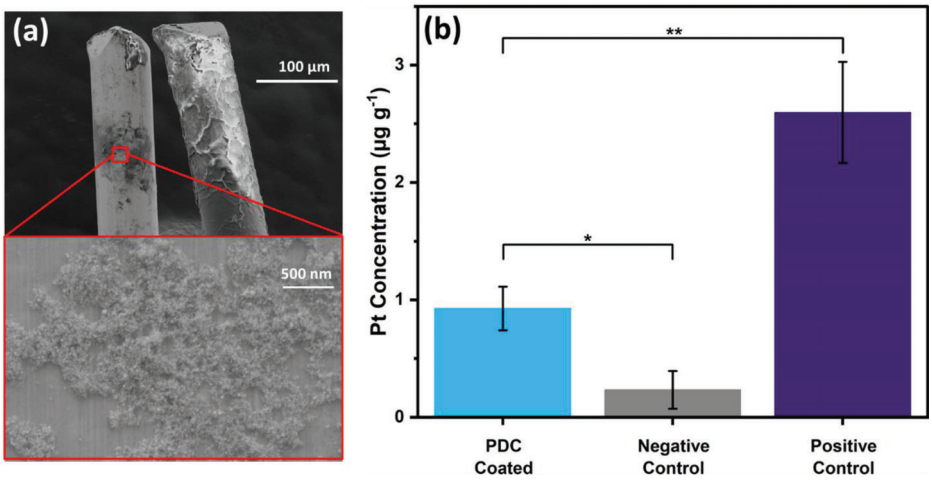

Figure 8. a) In vivo coating stability: SEM image of electrode coatings after 4 weeks in vivo stimulation in rat's brain. b) In vivo functionality of biodispersed Pt mass: average Pt concentration found in the brain slices stimulated with PDC-coated electrodes ($N = 3$, $\alpha = 0.05$), uncoated electrodes ($N = 3$, $\alpha = 0.05$), and in the ex vivo brain slices injected with Pt NP colloid solution (positive control) ($N = 2$, $\alpha = 0.05$). Bar plots represent mean values and error standard deviations.

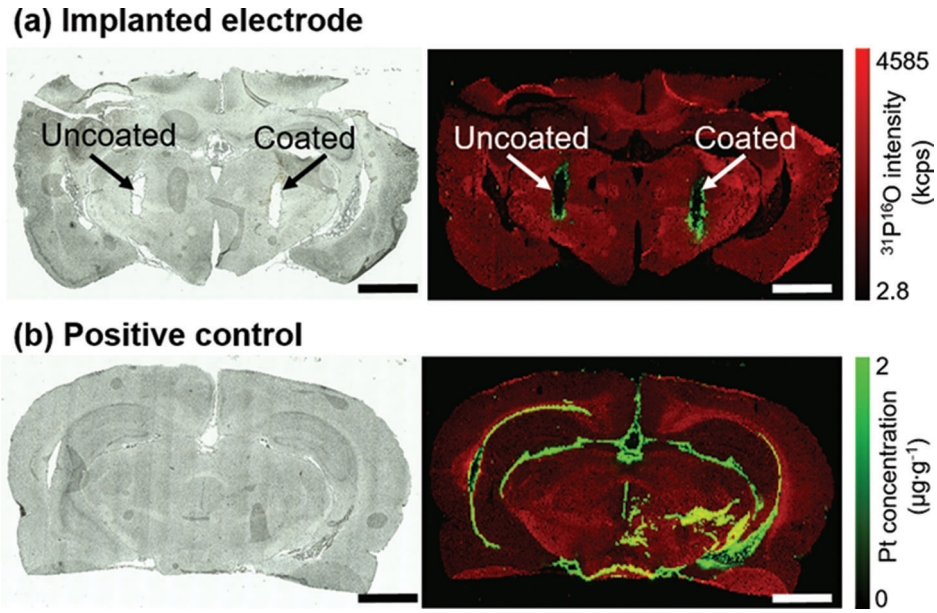

Figure 9. Pt biodistribution after 4-week DBS in rat brain: a) optical microscopic and LA-ICP-MS overlay images of brain sections stimulated with uncoated and PDC-coated electrodes; and b) Optical microscopic and LA-ICP-MS overlay images of brain sections injected with Pt NPs. Scale bars are 2 mm. In the overlay pictures, red signals represent the intensity of phosphorus, and green signals represent the Pt concentration.

stimulated with coated electrodes was significantly higher than the negative control and significantly lower than the positive control. **Figure 9**a represents the distribution of Pt inside the brain sections that were implanted with uncoated and PDC-coated electrodes. The intensity of the green color (Pt) is higher in the coated side of the brain in comparison to the negative control (uncoated electrode). It should be noted that the insertion holes in Figure 9a are caused by the electrode housing. Due to the friction forces during implantation, Pt from the electrode tips could have diffused to the inner sides of the brain tissues revealing the presence of Pt. Furthermore, the green signals are the highest in the positive control (NP solution injected) brain slices (Figure 9b). Since the amount of NP injected in the positive control was higher (50 µL), it is likely that the colloidal NP solution migrated out of the tissue and entered the surrounding fluid, revealing the Pt signal in the arachnoidal space. Interestingly, Pt signals were distributed along the implantation tracks of the uncoated and PDC-coated electrodes and not solely where the electrode tip was located. Robblee et al. have observed a similar behavior after stimulation of Pt electrodes and proposed diffusion processes and fluid exchanges as explanations.[45] In the case of the PDC-coated electrode, also a detachment of Pt NP from the

surface during electrode insertion or removal could be an explanation, but this would not apply to the uncoated electrode. To further investigate these findings, two additional experiments were performed and the LA-ICP-MS results are presented in Figure S8, Supporting Information. By analyzing a brain sample with only steel casing implantation (without PtIr electrode) (Figure S8d, Supporting Information) a release of Pt from surgical equipment or an introduction of Pt from other sources than the implanted electrodes was ruled out. Furthermore, an unstimulated brain sample after short-term implantation of a PDC-coated electrode and an electrode immersed in Pt NP were analyzed (Figure S8b, Supporting Information). Here, Pt is detected for both electrodes revealing that Pt is also released from the electrodes without stimulation, while immersed and coated electrodes release about the same amount of Pt. This is surprising though probably attributed to an overlay of two effects: I) particle release from the immersed electrode is more likely as they are only loosely bound to the electrode; and II) particles from the PDC-EPD-coated electrodes are more tightly bound but on the other side higher total deposition yields are reached. Hence, the interplay between these effects will result in similar amounts of Pt release in both samples. Nonetheless, the release is significantly lower than in electrodes exposed to long-term in vivo stimulation (Figure S8a, Supporting Information). Overall, the results suggest that the broader distribution of Pt after stimulation cannot be entirely attributed to the detachment of Pt NPs during electrode insertion and removal, but that stimulation leads to the dissolution of Pt from the electrodes, regardless of the coating. Please note that isolated Pt signals located millimeters away from the insertion site, for example, in Figure 9a, are either the electronic noise of the ICP-MS system or artifacts from the laser ablation process of the tissue sample. In particular, the fact that these particles are isolated and no gradual Pt change is visible makes their transport by a biological process highly unlikely.

Pt NPs are widely used in various biomedical applications, such as for drug delivery, medical implants, cancer cell detection and many more, and their toxicological nature was investigated by some researchers.[46] Adeyemi and peers administered Pt NPs (10, 50, and 100 mg kg^{-1}) orally in Wistar rats for 30 consecutive days, which resulted in organ weight alterations, inflammation-induced lesions, and cellular degeneration.[47] They performed another study, where the highest dosage was 50 mg kg^{-1} body weight, which resulted in oxidative stress induction in rat plasma.[47] In another study, Pt NPs (15 mg kg^{-1}) were introduced intravenously into BALB/c mice, resulting in acute hepatic injury along with increased levels of liver enzymes. However, NPs of 15 nm sizes showed no significant change in the enzyme levels.[48] Yamagishi and peers also studied the effects of Pt NPs size via intraperitoneal injection and found that 8 nm particles did not cause nephrotoxic reactions.[49] Various other studies confirm that the Pt NPs are non-cytotoxic and can be used in anticancer therapies.[50,51] Pt NP solutions (1–20 μg ml^{-1}) were injected into chicken embryos and their results indicated no adverse effect on their growth and development.[52] In a recent study, researchers found that the FDA-approved Pt-based drugs such as cisplatin turned into Pt NPs in vivo in human blood, and it was biocompatible and hindered the growth of chemotherapy-resistant tumors.[53] As our findings reveal the presence of 1 μg Pt per gram of brain, for a rat brain weighing an average of 2 g,[54] ≈2 μg of Pt would have been biodispersed. In comparison to the total weight of a rat (≈335 g), ≈0.006 mg kg^{-1} body weight of Pt would have been systematically released. As this is at least four orders of magnitude lower than any systemic Pt concentration used in the literature for biocompatibility assays, systemic adverse effects are unlikely, however high local concentrations in the brain are to be considered as well. Thereto, in our previous work, we studied the neuronal cell counts and glial scar formation around the implantation site after neural electrode removal and found no differences between coated and uncoated electrodes.[15] However, in the course of potential clinical approval of the coated electrodes more sophisticated biocompatibility assays, for example, monitoring of inflammatory markers would be useful though these studies are beyond the scope of this work.

3. Conclusion

The mechanical stability of implant coatings greatly influences their applicability in vivo. Herein, we performed a surface modification technique, EPD of laser-generated Pt NPs, on Pt-based 3D neural electrode surfaces. Due to a lack of a comprehensive study investigating exclusively the mechanical stability of neural electrode nano-coatings, we evaluated the same using agarose gel, adhesive tape and ultrasonication. EPD-generated coatings were more stable in agarose gel (mimicking brain tissue) compared to the other two complementary methods and stability was retained during in vivo stimulation in rat brains. A subsequent electrochemical stability test through multiple CV cycling reveals a further, statistically significant, 17.5% reduction in Z after 1000 cycles probably due to surface restructuring and activation. However, more cycles negated these effects probably due to further delamination, pointing at an optimum intermediate cycle number for maximum performance of the electrodes. Further, quantification of Pt in brain sections after DBS via LA-ICP-MS reveals a significantly higher amount of Pt in the brain region stimulated with PDC-coated electrodes, in comparison to that of the control region. However, the body mass-specific Pt dose released was four times lower in magnitude than those reported in Pt-nanotoxicity literature. Based on these results, we conclude that a good way to fabricate high-performance Pt neural electrodes with the least coating delamination is to electrophoretically deposit laser-generated PtNPs on their surfaces followed by cycling the substrates for 500–1000 times in CV, which additionally activates the surface Pt sites and in turn improves electrode performance. Therefore, the demonstrated coating fabrication and stability testing could be applied to all relevant 3D implant manufacturing, while particularly the "activation" of the nano-coating by the cycling of the electrode in an electrochemical cell constitutes an underexplored approach to improve electrode performance and coating stability.

4. Experimental Section

Nanoparticle Generation: Ligand-free Pt NPs were synthesized in Milli-Q water via laser processing in liquids as previously described elsewhere.[14] In brief, a Pt bulk target (10 × 10 × 1 mm^3) was ablated in Milli-Q water using an Nd:YAG laser (Ekspla, Atlantic series, 10 ps,

1064 nm, 9.6 mJ, 100 kHz), and subsequently laser fragmentation in liquid environment (LFL) using a nanosecond laser (Innolas, Spitlight, 9 ns, 532 nm, 84 mJ, 100 Hz, 1.5 J cm^{-2}) in a passage reactor. This synthesis route yields particles with an average hydrodynamic diameter of 14 nm and a total mass concentration of ≈500 µg mL^{-1}. These concentrated colloids were diluted to a concentration of 100 µg mL^{-1} using Milli-Q water and their pH was adjusted to a value of 11 using NaOH solution (0.1 M), before EPD. The zeta potential value of the Pt NP colloids was determined to be −62 mV.

Target Substrate Preparation: PTFE coated Pt–Ir (90:10) wires (Science Products GmbH, Germany) with a diameter of 76 µm were used as coating substrates for the stability tests. These wires had the same geometry and composition as the neural electrodes that were used for in vivo stimulations. The wires were cut into lengths of 20 mm and on both ends, the isolation was removed exposing 4 mm of Pt–Ir surface. One end of the wires was soldered to electrical plug pins and the other end was thoroughly rinsed with ethanol and introduced into Pt colloid for EPD. Bipolar electrodes for in vivo experiments were made of two parallel Pt–Ir (90:10%) wires insulated with Teflon ($d = 0.0055''$ with insulation and $d = 0.003''$ uninsulated; Science-Products GmbH, Hofheim, Germany), placed in a 0.55 × 17 mm stainless steel tube cut from a 24G syringe needle. At the contact end, both wires were uninsulated leaving a 500 µm long bare surface with ≈250 µm intercontact distance. Contact pins were soldered to the other end. The electrode tip was cleaned and conditioned before coating by immersing it in 65% nitric acid for 15 min and then rinsing it thoroughly with distilled water. The first impedance measurement was done before coating, but after cleaning, to exclude changes induced by the cleaning procedure.

Electrophoretic Deposition: A custom-made EPD chamber for 3D wires was used for coating.[15] For all the stability tests, the samples were coated using DC and PDC electric fields. The target substrates were connected to the positive pole of the electrical source and the surrounding metal counter electrode in the chamber was connected to the negative terminal. Pt colloid (600 µL) was filled into the chamber and the depositions were carried out. An electric field strength of 5 V cm^{-1} was applied for both DC- and PDC-EPD. In addition, for PDC-EPD a period of 1 µs and pulse width of 500 ns was applied. The deposition time was set to 5 min for DC and 10 min for PDC-EPD. The colloids were magnetically stirred during deposition to avoid sedimentation. Before and after coating, the colloids were characterized via UV–Vis extinction spectroscopy (Evolution 201, Thermo Scientific) in the wavelength range of 190–900 nm using a quartz cuvette with a path length of 10 mm to determine the deposited mass of NPs on each sample (Figure S2a, Supporting Information). The area under the curve (AUC) of the whole spectra was integrated and quantified against known Pt NP mass concentrations (Figure S2b, Supporting Information).

To characterize the coated surfaces, the electrode samples were mounted on aluminum holders and imaged via SEM (operating voltage: 5 kV, Apreo S LoVac, Thermo Fisher Scientific). It should be noted that the qualitative SEM analysis suffers from poor statistics and it is difficult to measure the same spot on the wires before and after stability testing. Therefore, after mounting the samples on aluminum holders, the images for "before stability testing" were performed. The mechanical stresses as described below were then applied to the samples, without removing them from the holders. Subsequently, the "after stability testing" images were taken. In this way, it could be made sure that the areas of the images are the regions where the stresses were applied.

Mechanical Stability Tests: The mechanical stability of DC- and PDC-coated wires were evaluated using three exemplary testing methods: dipping in agarose gel, ultrasonic agitation, and standard adhesion test (ASTM D3359–17). All the samples were characterized in CV and EIS, before and after stability testing. Additionally, SEM images were taken before and after the tests.

Agarose Gel Test: DC- and PDC-coated Pt–Ir wires were dipped into a simulated brain environment[7,55] (0.6 wt% agarose gel). For the gel preparation, agarose powder (0.6 g) was added to Milli-Q water (100 mL) and stirred continuously at 95 °C until a transparent solution was obtained. The mixture was cooled down to 35 °C and transferred to plastic cuvettes and left to set overnight.[56] The average dipping speed was calculated to be 2 ± 0.5 mm s^{-1} and the friction force was calculated to be ≈5 µN using Stokes equation (compare Section S3, Supporting Information).

Ultrasonic Agitation: EPD-coated samples were ultrasonicated (PTIC-30-ES, ALLPAX GmbH & Co. KG, Germany) in Milli-Q water at a frequency of 40 kHz for 5 min,[8,31,32] after which they were characterized using CV, EIS and SEM. The energy applied to the samples was measured to be 864 kJ (refer to Section S3, Supporting Information).

Adhesion Test: A slightly modified nano-adhesion tape test was performed according to the American Society for Testing and Materials (ASTM D3359-17).[40–43] 10 × 10 mm^2 of 3M Scotch pressure-sensitive tape was stuck on the coated wire surfaces and peeled off. Since the wires had a diameter of 0.076 mm and the coatings were presumed to be monolayer packing, an X was not scratched before applying the tape.

Electrochemical Characterization: To evaluate the electrochemical properties of the depositions, the samples were characterized before and after stability tests using a three-electrode setup potentiostat (VersaSTAT 3F, AMETEK Scientific Instruments, USA). A Pt wire was used as a counter electrode, Ag/AgCl or $Hg/HgSO_4$ as reference electrodes and the coated or uncoated Pt–Ir wires as a working electrode. The electrochemical cell and all components in contact with the working electrode were soaked overnight in a mixture of ca. 3 g L^{-1} $KMnO_4$ in 0.5 M H_2SO_4. After the permanganate solution is recovered, the pieces were rinsed with a diluted piranha solution and then boiled at least six times with ultrapure water. Here, a homemade RHE electrode, and Suprapur sulfuric acid were used.

Cyclic Voltammetry: CV measurements were carried out in sulfuric acid (1 M). The potential window was set from −0.2 to 1.2 V versus RHE at a scan rate of 0.2 V s^{-1}. Before measurements, the electrolyte was purged with nitrogen for 45 min and thereafter for 5 min between consecutive measurements. Twenty cycles were performed for each sample and the ECSA was calculated from the voltammogram using the following equation:[57,58]

$$ECSA = Q_H / Q_a \quad (1)$$

where Q_H is the charge associated with hydrogen adsorption peak and Q_a = 210 µC cm^{-2}, the theoretical charge density of a polycrystalline Pt surface.[43,59–61]

For testing the electrochemical stability of the coatings, the PDC-coated samples were "cleaned" by sweeping for a varying number of CV cycles: 100, 500, 1000, and 2000. A three-electrode setup potentiostat (VSP-3e Potentiostat, BioLogic Sciences Instruments) was used. The potential window was set from −0.2 to 1.5 V versus RHE at a scan rate of 0.5 V s^{-1}. Sulfuric acid (0.5 M) was used as the electrolyte and purged with argon before the measurements. The CV enlargement factors were calculated to determine the CSC values, by integrating the area under the curve (AUC) of one full CV cycle.[6,62]

Electrochemical Impedance Spectroscopy: Z measurements were performed in potentiostatic EIS mode from 1 Hz to 100 kHz by applying an AC_{rms} value of 10 mV and using NaCl (0.9%) as the electrolyte. The measured values were plotted in Bode format (Z_{mag} versus frequency) and the Z_{mag} values at medically relevant frequencies (150 Hz and 1 kHz) were studied. In addition, the values of electrolyte resistance (R_S), charge transfer resistance (R_T), and double layer capacitance (constant phase element, CPE) were obtained by fitting the measured data to a one-time constant equivalent circuit (OTC-EC) model[30,63] (Figure 3c) using the software ZView (AMETEK Scientific Instruments, USA). The capacitance values were calculated from the obtained fitting results using the formula:[64,65]

$$\text{Capacitance} = Rs^{(1-n)/n} \bullet Q^{(1/n)} \quad (2)$$

where Q is the pseudo capacitance and n is the CPE order, both extracted from the CPE used in the EC.

In Vivo Experiments: For the in vivo study electrodes were bilaterally implanted in the STN of 3 male Sprague-Dawley rats as follows: Coated electrodes were always implanted in the left hemisphere; uncoated, in the right hemisphere. After two weeks of postoperative recovery, the animals received chronic electrical stimulation for 4 weeks (100 µA, 130 Hz sym-

metric, biphasic, and rectangular waves with a duration of 160 µs and polarization change after 80 µs were used. More details can be found in the authors' previous work.[15] After the stimulation period, the rats were deeply anesthetized with an overdose of chloral hydrate and transcardially perfused with paraformaldehyde (4%) solution. The brains were removed from the cranial cavity, placed in sucrose/phosphate-buffered saline (30%) solution for at least 12 h, and cut on a freezing microtome (coronal plane) with a section thickness of 20 µm. For the positive control Pt NP microinjections, cadavers were fixed on the stereotaxic frame. After incision and defining the bregma, two burr holes were drilled bilaterally above the targets and 50 µL of Pt NP colloid (100 µg mL^{-1}) was injected into the subthalamic nucleus with a Hamilton syringe, using the following coordinates (in mm) relative to Bregma: anteroposterior: −3.8, mediolateral: ±2.5; dorsoventral: +8. The brain slices were mounted on glass slides and later analyzed via an LA-ICP-MS device.

LA-ICP-MS Analysis: Experiments were carried out in accordance with the EU Directive 2010/63/EU for animal experiments, including approval by the Lower Saxony State Office for Consumer Protection and Food Safety (LAVES, AZ 18/2837). LA-ICP-MS measurements were carried out using an ImageBIO266 laser ablation system (Elemental Scientific Lasers, Bozeman, USA) coupled to an iCAP TQ ICP-MS system (Thermo Fisher Scientific, Bremen, Germany) via a Dual Concentric Injector (DCI, Elemental Scientific Lasers). For the quantification of Pt in the brain tissue sections, an external calibration with matrix-matched standards based on gelatin (10% w/w) was used.[66] Ten calibration points in a concentration range from 0 to 80 µg g^{-1} of Pt were prepared. The validation of Pt concentration in the gelatin standards was carried out by bulk analysis via ICP-MS after digestion with nitric acid. Gelatin standards were cut into 20 µm thick sections with a cryomicrotome (Cryostar NX70, Thermo Fisher Scientific) and mounted on microscopic glass slides. Brain samples and gelatin standards were ablated in a line-by-line scan with a laser spot size of 60 µm, a scan speed of 180 µm s^{-1}, a space between the lines of 0 µm, and a laser repetition rate of 100 Hz. A helium gas flow of 1 l min^{-1} was applied to transport the ablated material into the ICP-MS. An additional argon gas flow of 1.1 l min^{-1} was introduced after the ablation cell for plasma stabilization purposes. The ICP-MS was equipped with a quartz injector tube with an inner diameter of 3.5 mm, a nickel sampler, and a skimmer cone. The ICP-MS parameters were set to 1550 W RF power, 14 l min^{-1} cool gas flow, and 0.8 l min^{-1} auxiliary gas flow. The ICP-MS was used in the triple quadruple mode with oxygen as a reaction gas. The isotopes ^{31}P (detected as $^{31}P^{16}O$), ^{194}Pt, and ^{195}Pt were monitored. ^{195}Pt was used for data visualization, whereas ^{194}Pt was used for validation purposes. It should be noted that the form of Pt (chemical species, NP, or ionic) could not be determined based on the results obtained. Bright-field microscopic images were obtained before LA-ICP-MS analysis with a BZ-9000 inverted fluorescence/bright field microscope (Keyence, Osaka, Japan). Data evaluation and visualization were performed using in-house developed software (Robin Schmid, WWU Muenster, Muenster, Germany).

Statistical Analysis: All data points are presented as mean values ± standard deviation the sample size was $n = 3$–4 and details for each experimental series are depicted in the figure captions. The statistical analysis was performed using OriginLab (v. 2020b) software. One-way ANOVA evaluations were performed on the data with Tukey's test as a post-hoc comparison. The α value was set to 0.05, and the levels of statistical significance are represented as $*p \leq 0.05$, $**p \leq 0.01$, $***p \leq 0.001$, and $****p \leq 0.0001$. All the presented data was tested for significance, but only those with a significant difference are explicitly depicted in the graphs.

Supporting Information

Supporting Information is available from the Wiley Online Library or from the author.

Acknowledgements

The authors gratefully acknowledge the German Research Foundation (DFG) for their financial support under project numbers BA 3580/24-1 and KR 2931/3-3. V.R. thanks Barbara Urbano for her support in data collection and Tobias Bochmann for the SEM measurements. Sandra Zwiehoff is acknowledged for assistance with the preparation of in vivo electrodes for SEM.

Open access funding enabled and organized by Projekt DEAL.

Conflict of Interest

The authors declare no conflict of interest.

Data Availability Statement

The data that support the findings of this study are available from the corresponding author upon reasonable request.

Keywords

biocompatibility, biomaterials, colloids, deep brain stimulation, impedance, laser ablation in liquids

Received: December 3, 2021
Revised: September 8, 2022
Published online:

[1] J. K. Krauss, N. Lipsman, T. Aziz, A. Boutet, P. Brown, J. W. Chang, B. Davidson, W. M. Grill, M. I. Hariz, A. Horn, M. Schulder, A. Mammis, P. A. Tass, J. Volkmann, A. M. Lozano, *Nat. Rev. Neurol.* **2021**, *17*, 75.
[2] A. M. Lozano, N. Lipsman, H. Bergman, P. Brown, S. Chabardes, J. W. Chang, K. Matthews, C. C. Mcintyre, T. E. Schlaepfer, M. Schulder, Y. Temel, J. Volkmann, J. K. Krauss, *Nat. Rev. Neurol.* **2019**, *15*, 148.
[3] M. Kronenbuerger, K. W. Nolte, V. A. Coenen, J.-M. Burgunder, J. K. Krauss, J. Weis, *Mov. Disord.* **2015**, *30*, 1125.
[4] J. H. Shin, G. B. Kim, E. J. Lee, T. An, K. Shin, S. E. Lee, W. Choi, S. Lee, C. Latchoumane, H.-S. Shin, G. Lim, *Adv. Healthcare Mater.* **2014**, *3*, 245.
[5] M. Ferguson, D. Sharma, D. Ross, F. Zhao, *Adv. Healthcare Mater.* **2019**, *8*, 1900558.
[6] C. Boehler, T. Stieglitz, M. Asplund, *Biomaterials* **2015**, *67*, 346.
[7] C. Boehler, F. Oberueber, T. Stieglitz, M. Asplund, *IEEE* **2017**, 1058.
[8] S. A. Desai, J. D. Rolston, L. Guo, S. M. Potter, *Front. Neuroeng.* **2010**, *3*, 5.
[9] S. Carli, M. Bianchi, E. Zucchini, M. Di Lauro, M. Prato, M. Murgia, L. Fadiga, F. Biscarini, *Adv. Healthcare Mater.* **2019**, *8*, 1900765.
[10] X. S. Zheng, C. Tan, E. Castagnola, X. T. Cui, *Adv. Healthcare Mater.* **2021**, *10*, 2100119.
[11] S. F. Cogan, *Annu. Rev. Biomed. Eng.* **2008**, *10*, 275.
[12] Y. J. Lee, H.-J. Kim, J. Y. Kang, S. H. Do, S. H. Lee, *Adv. Healthcare Mater.* **2017**, *6*, 1601022.
[13] J. Jakobi, A. Menéndez-Manjón, V. S. K. Chakravadhanula, L. Kienle, P. Wagener, S. Barcikowski, *Nanotechnology* **2011**, *22*, 145601.
[14] V. Ramesh, C. Rehbock, B. Giera, J. J. Karnes, J.-B. Forien, S. D. Angelov, K. Schwabe, J. K. Krauss, S. Barcikowski, *Langmuir* **2021**, *37*, 9724.
[15] S. D. Angelov, S. Koenen, J. Jakobi, H. E. Heissler, M. Alam, K. Schwabe, S. Barcikowski, J. K. Krauss, *J. Nanobiotechnol.* **2016**, *14*, 3.
[16] V. Ramesh, B. Giera, J. J. Karnes, N. Stratmann, V. Schaufler, Y. Li, C. Rehbock, S. Barcikowski, *J. Electrochem. Soc.* **2022**, *169*, 022504.
[17] Y. Terasawa, H. Tashiro, Y. Nakano, J. Ohta, *Sens. Mater.* **2019**, *31*, 1957.

[18] T. J. P. Hersbach, A. I. Yanson, M. T. M. Koper, *Nat. Commun.* **2016**, *7*, 12653.
[19] M. Luitz, M. Lunzer, A. Goralczyk, M. Mader, S. Bhagwat, A. Warmbold, D. Helmer, F. Kotz, B. E. Rapp, *Adv. Mater.* **2021**, *33*, 2101992.
[20] J. Luo, R. Pohl, L. Qi, G.-W. Römer, C. Sun, D. Lohse, C. W. Visser, *Small* **2017**, *13*, 1602553.
[21] J. D. Fowlkes, R. Winkler, B. B. Lewis, M. G. Stanford, H. Plank, P. D. Rack, *ACS Nano* **2016**, *10*, 6163.
[22] G. Pakeltis, Z. Hu, A. G. Nixon, E. Mutunga, C. P. Anyanwu, C. A. West, J. C. Idrobo, H. Plank, D. J. Masiello, J. D. Fowlkes, P. D. Rack, *ACS Appl. Nano Mater.* **2019**, *2*, 8075.
[23] C. Boehler, D. M. Vieira, U. Egert, M. Asplund, *ACS Appl. Mater. Interfaces* **2020**, *12*, 14855.
[24] C. D. Lee, E. M. Hudak, J. J. Whalen, A. Petrossians, J. D. Weiland, *J. Electrochem. Soc.* **2018**, *165*, G3015.
[25] I. R. Cassar, C. Yu, J. Sambangi, C. D. Lee, J. J. Whalen, A. Petrossians, W. M. Grill, *Biomaterials* **2019**, *205*, 120.
[26] A. Zátonyi, F. Fedor, Z. Borhegyi, Z. Fekete, *J. Neural Eng.* **2018**, *15*, 054003.
[27] S. Koenen, C. Rehbock, H. E. Heissler, S. D. Angelov, K. Schwabe, J. K. Krauss, S. Barcikowski, *ChemPhysChem* **2017**, *18*, 1108.
[28] C. Streich, S. Koenen, M. Lelle, K. Peneva, S. Barcikowski, *Appl. Surf. Sci.* **2015**, *348*, 92.
[29] R. Tang, W. Pei, S. Chen, H. Zhao, Y. Chen, Y. Han, C. Wang, H. Chen, *Sci. China Inf. Sci.* **2014**, *57*, 1.
[30] Y.-F. Rui, J.-Q. Liu, B. Yang, K.-Y. Li, C.-S. Yang, *Biomed. Microdevices* **2012**, *14*, 367.
[31] Q. Zeng, K. Xia, B. Sun, Y. Yin, T. Wu, M. S. Humayun, *Electrochim. Acta* **2017**, *237*, 152.
[32] I. R. Minev, N. Wenger, G. Courtine, S. P. Lacour, *APL Mater.* **2015**, *3*, 014701.
[33] L.-C. Wang, M.-H. Wang, C.-F. Ge, B.-W. Ji, Z.-J. Guo, X.-L. Wang, B. Yang, C.-Y. Li, J.-Q. Liu, *Biosens. Bioelectron.* **2019**, *145*, 111661.
[34] A. I. D3359-17, *American Society for Testing and Materials* **2017**, https://www.pcbase.cn/wp-content/uploads/2020/04/ASTM-D3359-2017.pdf.
[35] T. M. Gwon, J. H. Kim, G. J. Choi, S. J. Kim, *J. Mater. Sci.* **2016**, *51*, 6897.
[36] T. Ware, D. Simon, D. E. Arreaga-Salas, J. Reeder, R. Rennaker, E. W. Keefer, W. Voit, *Adv. Funct. Mater.* **2012**, *22*, 3470.
[37] N. Chou, S. Yoo, S. Kim, *IEEE Trans. Neural Syst. Rehabil. Eng.* **2012**, *21*, 544.
[38] R. A. Green, N. H. Lovell, L. A. Poole-Warren, *Biomaterials* **2009**, *30*, 3637.
[39] Y. J. Lee, Y. U. Lee, H. W. Yeon, H. A. S. Shin, L. A. Evans, Y. C. Joo, *Appl. Phys. Lett.* **2013**, *103*, 241904.
[40] T. W. Kim, J. S. Lee, Y. C. Kim, Y. C. Joo, B. J. Kim, *Materials* **2019**, *12*, 2490.
[41] P. A. Doble, R. G. de Vega, D. P. Bishop, D. J. Hare, D. Clases, *Chem. Rev.* **2021**, *121*, 11769.
[42] T. Boretius, T. Jurzinsky, C. Koehler, S. Kerzenmacher, H. Hillebrecht, T. Stieglitz, in 2011 Annu. Int. Conf. IEEE Eng. Med. Biol. Soc., IEEE, Piscataway, NJ **2011**, pp. 5404–5407.
[43] E. M. Hudak, D. W. Kumsa, H. B. Martin, J. T. Mortimer, *J. Neural Eng.* **2017**, *14*, 046012.
[44] M. Leber, R. Bhandari, J. Mize, D. J. Warren, M. M. H. Shandhi, F. Solzbacher, S. Negi, *Biomed. Microdevices* **2017**, *19*, 62.
[45] L. S. Robblee, J. McHardy, W. F. Agnew, L. A. Bullara, *J. Neurosci. Methods* **1983**, *9*, 301.
[46] E. Czubacka, S. Zerczak, *Med. Pr.* **2019**, *70*, 487.
[47] O. S. Adeyemi, F. A. Sulaiman, M. A. Akanji, H. O. B. Oloyede, A. A. Sulaiman, A. Olatunde, S. T. Salman, A. R. Aransiola, A. G. Ajayi, M. M. Ekundayo, F. A. Abubakar, S. A. Olaoye, *Comp. Clin. Pathol.* **2016**, *25*, 855.
[48] O. S. Adeyemi, I. O. Olajide, A. A. Adeyanju, O. J. Awakan, D. A. Otohinoyi, *Biointerface Res. Appl. Chem.* **2018**, *8*, 3364.
[49] Y. Yamagishi, A. Watari, Y. Hayata, X. Li, M. Kondoh, Y. Tsutsumi, K. Yagi, *Die Pharm. - Int. J. Pharm. Sci.* **2013**, *68*, 178.
[50] Y. Yamagishi, A. Watari, Y. Hayata, X. Li, M. Kondoh, Y. Yoshioka, Y. Tsutsumi, K. Yagi, *Nanoscale Res. Lett.* **2013**, *8*, 395.
[51] J. Pelka, H. Gehrke, M. Esselen, M. Türk, M. Crone, S. Bräse, T. Muller, H. Blank, W. Send, V. Zibat, P. Brenner, R. Schneider, D. Gerthsen, D. Marko, *Chem. Res. Toxicol.* **2009**, *22*, 649.
[52] P. Asharani, N. Xinyi, M. P. Hande, S. Valiyaveettil, *Nanomedicine* **2010**, *5*, 51.
[53] M. Prasek, E. Sawosz, S. Jaworski, M. Grodzik, T. Ostaszewska, M. Kamaszewski, M. Wierzbicki, A. Chwalibog, *Nanoscale Res. Lett.* **2013**, *8*, 251.
[54] X. Zeng, J. Sun, S. Li, J. Shi, H. Gao, W. S. Leong, Y. Wu, M. Li, C. Liu, P. Li, J. Kong, Y.-Z. Wu, G. J. Nie, Y. M. Fu, G. Zhang, *Nat. Commun.* **2020**, *11*, 567.
[55] Y. Piao, Y. Liu, X. Xie, *J. Toxicol. Pathol.* **2013**, *26*, 29.
[56] F. Pervin, W. W. Chen, in *Dynamic Behavior of Materials*, Springer, New York **2011**, Vol. *1*, pp. 9–13.
[57] S.-A. Sheppard, S. A. Campbell, J. R. Smith, G. W. Lloyd, F. C. Walsh, T. R. Ralph, *Analyst* **1998**, *123*, 1923.
[58] E. P. Lee, Z. Peng, D. M. Cate, H. Yang, C. T. Campbell, Y. Xia, *J. Am. Chem. Soc.* **2007**, *129*, 10634.
[59] S. Trasatti, O. A. Petrii, *J. Electroanal. Chem.* **1992**, *327*, 353.
[60] D. W. Kumsa, N. Bhadra, E. M. Hudak, S. C. Kelley, D. F. Untereker, J. T. Mortimer, *J. Neural Eng.* **2016**, *13*, 052001.
[61] M. Ganji, A. C. Paulk, J. C. Yang, N. W. Vahidi, S. H. Lee, R. Liu, L. Hossain, E. M. Arneodo, M. Thunemann, M. Shigyo, A. Tanaka, S. B. Ryu, S. W. Lee, Y. Tchoe, M. Marsala, A. Devor, D. R. Cleary, J. R. Martin, H. Oh, V. Gilja, T. Q. Gentner, S. I. Fried, E. Halgren, S. S. Cash, S. A. Dayeh, *Nano Lett.* **2019**, *19*, 6244.
[62] A. Petrossians, J. J. Whalen, J. D. Weiland, F. Mansfeld, in *2011 Annu. Int. Conf. IEEE Eng. Med. Biol. Soc.*, IEEE, Piscataway, NJ **2011**, pp. 3001–3004.
[63] C. M. Gore, J. O. White, E. D. Wachsman, V. Thangadurai, *J. Mater. Chem. A* **2014**, *2*, 2363.
[64] Z. Yan, L. Zhu, Y. C. Li, R. J. Wycisk, P. N. Pintauro, M. A. Hickner, T. E. Mallouk, *Energy Environ. Sci.* **2018**, *11*, 2235.
[65] A.-C. Niehoff, J. Grünebaum, A. Moosmann, D. Mulac, J. Söbbing, R. Niehaus, R. Buchholz, S. Kröger, A. Wiehe, S. Wagner, M. Sperling, H. von Briesen, K. Langer, U. Karst, *Anal. Chim. Acta* **2016**, *938*, 106.
[66] A. Capon, R. Parsons, *J. Electroanal. Chem. Interfacial Electrochem.* **1973**, *45*, 205.

8 Summary and Outlook

The development of application-specific surface modification on neural electrodes to improve their stimulation and recording efficiencies is in high demand. Although nanocoatings based on carbon nanotubes, polymers, silicon, quantum dots, diamond, etc. are widely investigated, modifying the surfaces using materials that are minimally different from the base material leads to fewer complications and rejections later during manufacturing and clinical approvals.

When starting this thesis, open questions around the coating transferability onto 3D neural electrode surfaces, formation of submonolayer homogeneous depositions, and reduction of electrode impedance both in vitro and in vivo existed. Therefore in this work, Pt neural electrodes are coated with laser-generated Pt and Pt-alloy NPs to improve the electrode's electrochemical performance. In LAL, the generated PtNPs have a negative surface charge, which electrostatically stabilizes the colloids in dilute aqueous media. This eliminates the need for adding external stabilizing ligands to maintain their colloidal nature. Previously, the electrophoretic mobility of the laser-generated NPs, its relationship with field strength, the stoichiometry of PtIr NPs during EPD, the influence of contact angle, and stabilizer ligands were studied. The laser-generated NPs of 10 nm and 50 nm sizes were used to nanostructure the neural electrode surfaces and a 3-week in vitro and in vivo stimulations in rats were performed. It was observed that the 10 nm particles produced a stable in vivo impedance. Further optimization of the coating parameters on 2D substrates, and the relationship between various process parameters such as impedance, electric field strength, surface coverage, ECSA, and surface oxidation were studied.

When these pure and spherical PtNPs were deposited onto 3D neural electrode surfaces via DC EPD, a large number of agglomerates were produced with less homogeneous surface coverage. This was believed to be due to the electric field-induced flows such as the EOF and EHD that form due to the movement of polar liquids under the influence of a constant electric current. Therefore to eliminate clustering issues, PDC EPD was chosen as a suitable method in this work. Even though PDC EPD was also performed in an aqueous medium similar to DC EPD, the non-constant applied field relaxes the clustered particles when the electric field is in the OFF state. During this OFF state, the weakly bound particles in the clusters break off and get suspended in the surrounding medium. When the field is again switched ON, these floating particles adhere to a different spot on the surface. This phenomena eventually produced more homogeneously distributed sub-monolayer depositions which went along with a significant reduction in electrode impedance.

When the solvent composition was modified by mixing water and ethanol instead of pure water, the homogeneity of the deposits became better. The 30% ethanol-water ratio eventually produced the most homogeneous deposits among all other ratios, which increased the ECSA seven times more than that of a pure water deposit. This optimum was most likely associated with an interplay between two opposing forces. For once, water-splitting reactions and bubble formation were reduced when the ethanol content increased, which led to a more homogeneous coating. On the other hand, at higher ethanol content viscosity effects inhibited the coating homogeneity. Since tungsten and iridium are often used in the manufacturing of neural electrodes, PtW and PtIr NPs were also additionally used

for EPD. Here, the Pt90Ir10 NPs were found to be a highly interesting combination as they increased the ECSA and capacitance of the electrodes thereby significantly decreasing the impedance values. The Pt50W50 NPs on the other hand showed less particle deposition and consequently increased electrode impedance. This could be due to the fact that the tungsten NPs oxidize in the presence of water and hence reduce the electrophoretic mobility of the particles. This phenomenon hinders particle motion and subsequent depositions.

To investigate if the lowering of impedances prevails even in the in vivo environments, PtNP-coated neural electrodes were implanted into the STN of rats and stimulated for a period of 4 weeks. These NP-coated electrodes were successfully able to maintain low impedance throughout the stimulation period without fluctuations. When a surface-modified implant is to be used clinically, the most relevant and deciding factor is the mechanical stability of the deposited coatings. If the coating delaminates internally after implantation, it could increase the risk to the patients, doctors, and eventually also to the manufacturers. Therefore, the mechanical stability of the PtNP coatings was studied by applying minimal, moderate, and maximal mechanical stresses. It was found that the delamination of the coating was minimal in the simulated brain environment conditions. Upon analyzing the explanted brain sections, the levels of PtNPs found in them were much lower than the relevant toxicological values. Therefore, these coatings demonstrate their potential in clinical applications.

In summary, the EPD coatings prove to be versatile, low cost, and a simple method for surface modifications. It could be transferable onto target electrodes of any shape and size, hence applicable in a broad spectrum of research fields. Any scientist irrespective of their area of interest, working on surface modifications aiming to develop sub-monolayer nanostructures can highly benefit from the coatings developed in this thesis. Here, the coatings performed using ethanol-water mixtures and PtIr alloy NPs were found to enhance the electrochemical properties of the neural electrodes. Based on these results, further investigations are necessary by using PtIr NPs as coating materials and ethanol-water mixture as the dispersion medium. Future studies should investigate this combination's coating homogeneity, electrochemical performance, and in vivo behavior.

References

[1] DB Clane. Treatment of parkinson disease. *New England J. Med*, pages 1021–1027, 1993.

[2] S Fahn. Adverse effects of levodopa in parkinson's disease. In *Drugs for the Treatment of Parkinson's Disease*, pages 385–409. Springer, 1989.

[3] Stephen T Gancher, John G Nutt, and William R Woodward. Peripheral pharmacokinetics of levodopa in untreated, stable, and fluctuating parkinsonian patients. *Neurology*, 37(6):940–940, 1987.

[4] Svjetlana Miocinovic, Suvarchala Somayajula, Shilpa Chitnis, and Jerrold L Vitek. History, applications, and mechanisms of deep brain stimulation. *JAMA neurology*, 70(2):163–171, 2013.

[5] Paul Krack, P Limousin, AL Benabid, and Pierre Pollak. Chronic stimulation of subthalamic nucleus improves levodopa-induced dyskinesias in parkinson's disease. *The Lancet*, 350(9092):1676, 1997.

[6] Abdelhamid Benazzouz, Sorin Breit, Adnan Koudsie, Pierre Pollak, Paul Krack, and Alim-Louis Benabid. Intraoperative microrecordings of the subthalamic nucleus in parkinson's disease. *Movement disorders: official journal of the Movement Disorder Society*, 17(S3):S145–S149, 2002.

[7] Paul Krack, Alina Batir, Nadège Van Blercom, Stephan Chabardes, Valérie Fraix, Claire Ardouin, Adnan Koudsie, Patricia Dowsey Limousin, Abdelhamid Benazzouz, Jean François LeBas, et al. Five-year follow-up of bilateral stimulation of the subthalamic nucleus in advanced parkinson's disease. *New England Journal of Medicine*, 349(20):1925–1934, 2003.

[8] Svilen D Angelov, Sven Koenen, Jurij Jakobi, Hans E Heissler, Mesbah Alam, Kerstin Schwabe, Stephan Barcikowski, and Joachim K Krauss. Electrophoretic deposition of ligand-free platinum nanoparticles on neural electrodes affects their impedance in vitro and in vivo with no negative effect on reactive gliosis. *Journal of nanobiotechnology*, 14(1):1–11, 2016.

[9] Saida Khan and Golam Newaz. A comprehensive review of surface modification for neural cell adhesion and patterning. *Journal of Biomedical Materials Research Part A: An Official Journal of The Society for Biomaterials, The Japanese Society for Biomaterials, and The Australian Society for Biomaterials and the Korean Society for Biomaterials*, 93(3):1209–1224, 2010.

[10] Geon Hwee Kim, Kanghyun Kim, Eunji Lee, Taechang An, WooSeok Choi, Geunbae Lim, and Jung Hwal Shin. Recent progress on microelectrodes in neural interfaces. *Materials*, 11(10):1995, 2018.

[11] Stuart F Cogan. Neural stimulation and recording electrodes. *Annu. Rev. Biomed. Eng.*, 10:275–309, 2008.

[12] Chong Xie, Ziliang Lin, Lindsey Hanson, Yi Cui, and Bianxiao Cui. Intracellular recording of action potentials by nanopillar electroporation. *Nature nanotechnology*, 7(3):185–190, 2012.

[13] Ju-Hyun Kim, Gyumin Kang, Yoonkey Nam, and Yang-Kyu Choi. Surface-modified microelectrode array with flake nanostructure for neural recording and stimulation. *Nanotechnology*, 21(8):085303, 2010.

[14] Hong-Bo Zhou, Gang Li, Xiao-Na Sun, Zhuang-Hui Zhu, Qing-Hui Jin, Jian-Long Zhao, and Qiu-Shi Ren. Integration of au nanorods with flexible thin-film microelectrode arrays for improved neural interfaces. *Journal of microelectromechanical systems*, 18(1):88–96, 2009.

[15] TSN Sankara Narayanan, Il-Song Park, and Min-Ho Lee. Surface modification of magnesium and its alloys for biomedical applications: opportunities and challenges. *Surface modification of magnesium and its alloys for biomedical applications*, pages 29–87, 2015.

[16] S Anil, J Venkatesan, MS Shim, EP Chalisserry, and S-K Kim. Bone response to calcium phosphate coatings for dental implants. In *Bone Response to Dental Implant Materials*, pages 65–88. Elsevier, 2017.

[17] Luigi Denardo, Giuseppina Raffaini, Fabio Ganazzoli, and Roberto Chiesa. Metal surface oxidation and surface interactions. In *Surface modification of biomaterials*, pages 102–142. Elsevier, 2011.

[18] S Bonnas, J Tabellion, H-J Ritzhaupt-Kleissl, and J Haußelt. Systematic interaction of sedimentation and electrical field in electrophoretic deposition. In *4M 2006-Second International Conference on Multi-Material Micro Manufacture*, pages 187–190. Elsevier, 2006.

[19] S Barcikowski, V Amendola, M Lau, G Marzun, C Rehbock, S Reichenberger, D Zhang, and B Gökce. Handbook of laser synthesis & processing of colloids, 2019.

[20] Ana Menendez-Manjon, Jurij Jakobi, Kerstin Schwabe, Joachim K Krauss, and Stephan Barcikowski. Mobility of nanoparticles generated by femtosecond laser ablation in liquids and its application to surface patterning. *JLMN-Journal of Laser Micro/Nanoengineering*, 4(2):95–99, 2009.

[21] Jurij Jakobi, Ana Menéndez-Manjón, Venkata Sai Kiran Chakravadhanula, Lorenz Kienle, Philipp Wagener, and Stephan Barcikowski. Stoichiometry of alloy nanoparticles from laser ablation of ptir in acetone and their electrophoretic deposition on ptir electrodes. *Nanotechnology*, 22(14):145601, 2011.

[22] Alexander Heinemann, Sven Koenen, Kerstin Schwabe, Christoph Rehbock, and Stephan Barcikowski. How electrophoretic deposition with ligand-free platinum nanoparticles affects contact angle. In *Key engineering materials*, volume 654, pages 218–223. Trans Tech Publ, 2015.

[23] Carmen Streich, Sven Koenen, Marco Lelle, Kalina Peneva, and Stephan Barcikowski. Influence of ligands in metal nanoparticle electrophoresis for the fabrication of biofunctional coatings. *Applied Surface Science*, 348:92–99, 2015.

[24] Sven Koenen, René Streubel, Jurij Jakobi, Kerstin Schwabe, Joachim K Krauss, and Stephan Barcikowski. Continuous electrophoretic deposition and electrophoretic mobility of ligand-free, metal nanoparticles in liquid flow. *Journal of The Electrochemical Society*, 162(4):D174, 2015.

[25] Svilen D Angelov, Sven Koenen, Jurij Jakobi, Hans E Heissler, Mesbah Alam, Kerstin Schwabe, Stephan Barcikowski, and Joachim K Krauss. Electrophoretic deposition of ligand-free platinum nanoparticles on neural electrodes affects their impedance in vitro and in vivo with no negative effect on reactive gliosis. *Journal of nanobiotechnology*, 14(1):1–11, 2016.

[26] Sven Koenen, Christoph Rehbock, Hans E Heissler, Svilen D Angelov, Kerstin Schwabe, Joachim K Krauss, and Stephan Barcikowski. Optimizing in vitro impedance and physicochemical properties of neural electrodes by electrophoretic deposition of pt nanoparticles. *ChemPhysChem*, 18(9):1108–1117, 2017.

Appendix

A1 Supporting Information: Comparing Direct and Pulsed-Direct Current Electrophoretic Deposition on Neural Electrodes: Deposition Mechanism and Functional Influence

Available at: https://pubs.acs.org/doi/10.1021/acs.langmuir.1c01081

Supporting Information

Comparing direct and pulsed-direct current electrophoretic deposition on neural electrodes: Deposition mechanism and functional influence

Vaijayanthi Ramesh[1], Christoph Rehbock[1], Brian Giera[2], John J. Karnes[2], Jean-Baptiste Forien[2], Svilen D. Angelov[3], Kerstin Schwabe[3], Joachim K. Krauss[3] and Stephan Barcikowski[1]

[1] Technical Chemistry I, University of Duisburg-Essen and Center for Nanointegration Duisburg-Essen (CENIDE), Universitaetsstr. 7, 45141 Essen, Germany.

[2] Center for Engineered Materials and Manufacturing, Lawrence Livermore National Laboratory, California, USA.

[3] Department of Neurosurgery, Hannover Medical School, Carl-Neuberg-Str. 1, 30625 Hannover, Germany.

S1. Hydrodynamic size distributions

Hydrodynamic size distributions of colloidal platinum nanoparticles (PtNPs) were measured using analytical disc centrifuge (ADC) at 22000 rpm. LAL and LFL colloid samples were measured against a sucrose gradient for 20 minutes using a gold NP calibration standard (d = 7.4 nm). Picosecond laser ablation produced colloids with more than one size mode. Upon laser fragmentation, the larger particles were broken down to form monomodal particles. The colloids and their corresponding scanning transmission electron microscopy (STEM) images are shown in Figure S1.

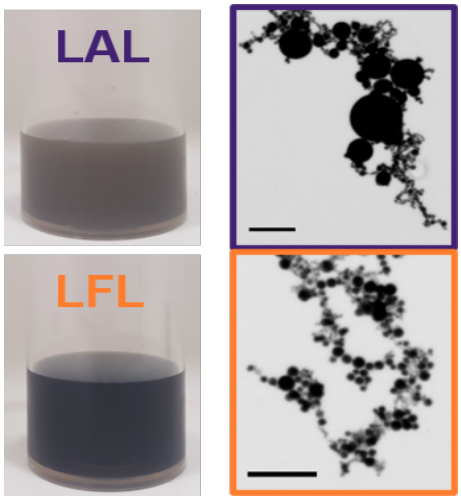

Figure S1: PtNP colloids and their corresponding STEM images after LAL (top) and LFL (bottom). Scale bar: 100 nm.

Figure S2 shows the number-weighted hydrodynamic size distributions of two different batches of PtNPs, whose ADC measurements were performed after 1 day and 60 days of LFL. The results indicate no significant growth in particles even after long storage period.

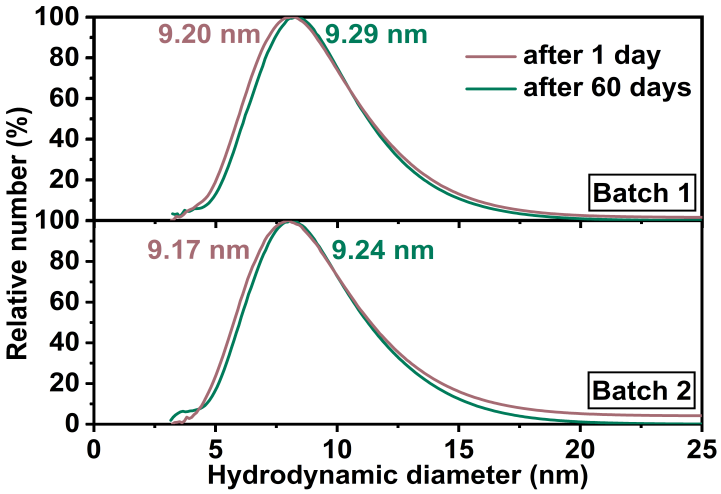

Figure S2: Hydrodynamic number distribution of two Pt colloid batches, after day 1 and day 60 of LFL.

S2. EPD yield

To measure the mass deposited on electrode samples, concentration gradient measurements on generated colloid were performed using UV-Vis spectroscopy. The area under the curve values (AUC) (integrated from 190 nm to 900 nm) were plotted against the corresponding mass concentration dilutions (Figure S3). Linear fitting was performed to the obtained gradient and the AUC values of the samples were correlated with the fit equation to find their mass concentrations. These mass concentrations were then subtracted from the original mass before EPD to obtain the yield.

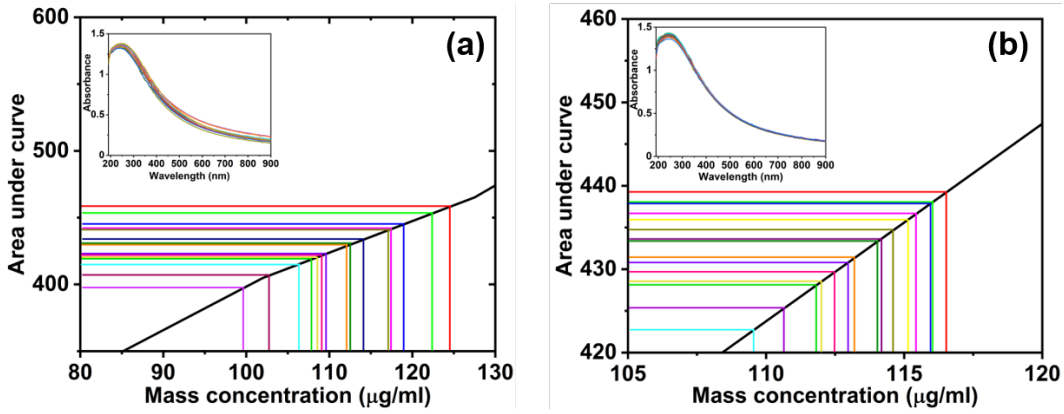

Figure S3: Mass concentrations of Pt colloid supernatants after (a) DC and (b) pulsed-DC EPD, correlated with known mass concentration gradient in order to determine the yield (N = 15).

S3. Furlong slope calculations

As explained in the manuscript, Furlong curves were obtained by plotting −log(absorbance) vs. log(wavelength) from UV-Vis spectra (Figure S4). These Furlong curves were linearly fitted (avoiding the peak region) to obtain slope values. Furlong slope values are indirectly proportional to the particle size changes. Therefore, when the absolute Furlong slope value

increases, it indicates a decrease in the particle size (or decrease in aggregation fraction) and vicé versa [1].

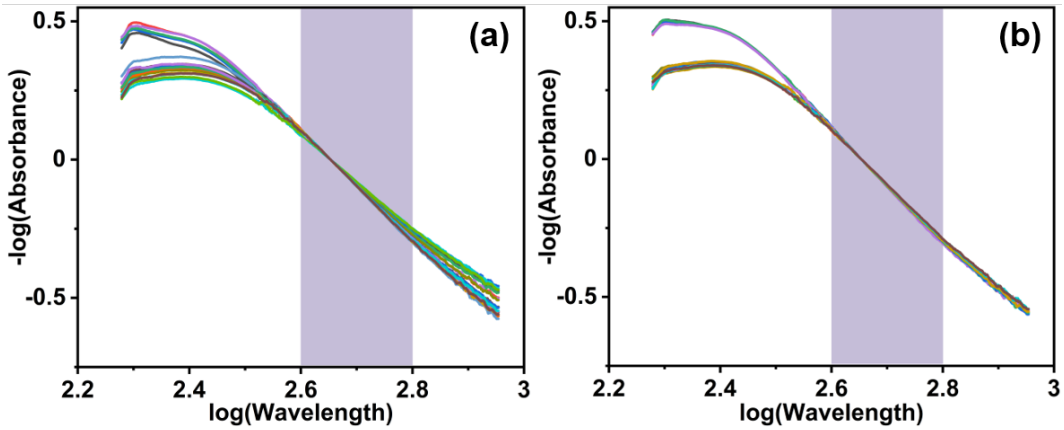

Figure S4: Furlong curves of Pt colloid supernatant after (a) DC and (b) pulsed-DC EPD to determine the Furlong slopes (N = 20). Fitted region is highlighted.

S4. Reproducibility of EPD coatings

In general, EPD in aqueous medium is known to be non-reproducible because of the poor coating quality due to water splitting, bubble formations and other adverse effects [2, 3]. In our experiments too, we observed similar effects. In comparison with DC-EPD, the samples with pulsed-DC EPD were better reproducible. The representative images below (Figure S5) show the reproducibility of coatings we observed after DC and pulsed-DC depositions.

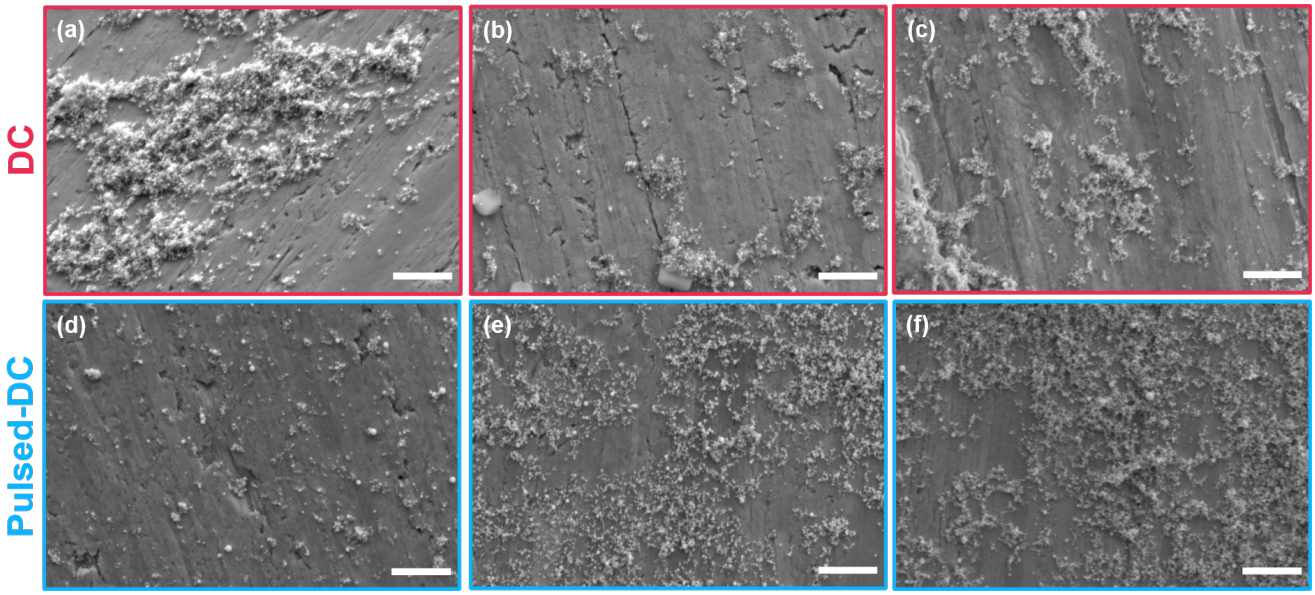

Figure S5: Representative SEM images of samples coated using (a,b,c) DC and (d,e,f) pulsed-DC fields (N = 3). Scale bar: 500 nm.

S5. Particle coordinate analysis with controls

Control experiments were performed using the following EPD parameters and image analysis was performed to generate radial distribution functions (RDFs) and nearest neighbor (NN) distribution curves. During the control experiments, the colloid concentration was maintained constant at around 100 µg/ml.

Table S1: EPD parameters used for control experiments

Sample	Period	Pulse width	Duty cycle	t_{ON}/t_{OFF}	δ/d_p	Cluster
Parameter in main text	1 µs	500 ns	50%	1	1.2	YES
Control 1	1 µs	50 ns	5%	0.05	1.72	NO
Control 2	10 µs	5 µs	50%	1	3.95	YES
Control 3	100 µs	50 µs	50%	1	12.5	YES
Immersed	–	–	–	0	43267	NO

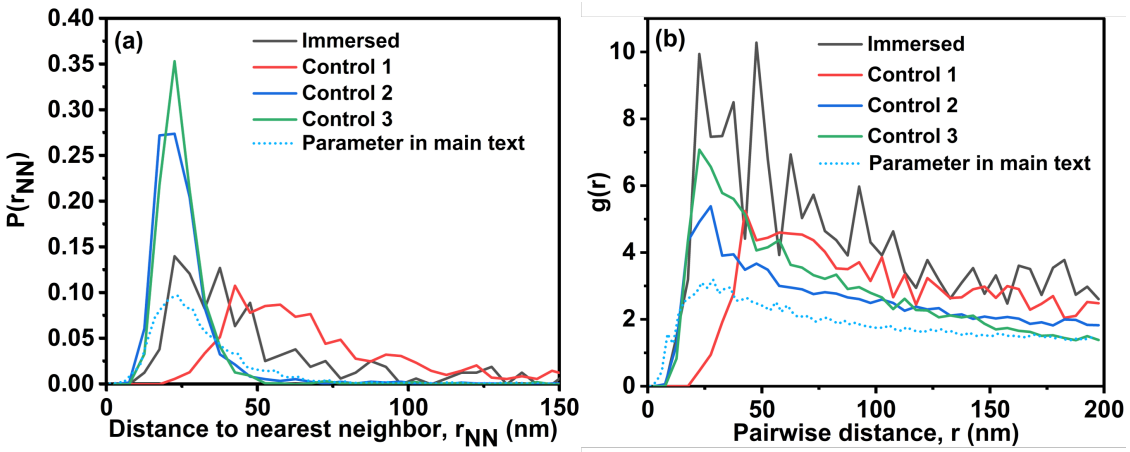

Figure S6: (a) Nearest neighbor distributions and (b) RDFs of control samples coated with varying electric fields, revealing cluster formation when both $\delta/d_p \ll 1$ and $t_{ON}/t_{OFF} = 1$.

References

[1] Furlong et al. Colloidal Platinum Sols — Preparation, Characterization and Stability towards Salt. *J. Chem. SOC., Faraday Trans. I*, 1984, 80, 571–588.

[2] Besra, L and Liu, M. A review on fundamentals and applications of electrophoretic deposition (EPD). *Progress in Materials Science*, 2007, 52(1), 1–61.

[3] Neirinck et al. A Current Opinion on Electrophoretic Deposition in Pulsed and Alternating Fields. *The Journal of Physical Chemistry B*, 2013, 117, 1516–1526.

A2 Supporting Information: Electrophoretic Deposition of Platinum Nanoparticles using Ethanol-Water Mixtures Significantly Reduces Neural Electrode Impedance

Available at: https://iopscience.iop.org/article/10.1149/1945-7111/ac51f8

Supporting Information

Electrophoretic Deposition of Platinum Nanoparticles using Ethanol-water mixtures significantly reduces Neural Electrode Impedance

Vaijayanthi Ramesh[1], Brian Giera[2], John J. Karnes[2], Nadine Stratmann[1], Viktor Schaufler[1], Yao Li[1], Christoph Rehbock[1] and Stephan Barcikowski[1]

[1] Institute of Technical Chemistry I, University of Duisburg-Essen and Center for Nanointegration Duisburg-Essen (CENIDE), 45141 Essen, Germany

[2] Center for Engineered Materials and Manufacturing, Lawrence Livermore National Laboratory, 94550 California, USA

S1. Determination of deposited nanoparticle mass on the samples

Mass deposited on Pt-Ir wires after electrophoretic deposition (EPD) was determined using UV-Vis extinction spectroscopy (Figure S1). Area under curve (AUC) values of the sample spectra before and after EPD were correlated with the known mass concentration gradients of platinum nanoparticles (PtNPs) (Figure S2). The mass remaining in supernatants after EPD were then subtracted from the mass of the colloid before EPD, to obtain the deposited mass on each sample[1].

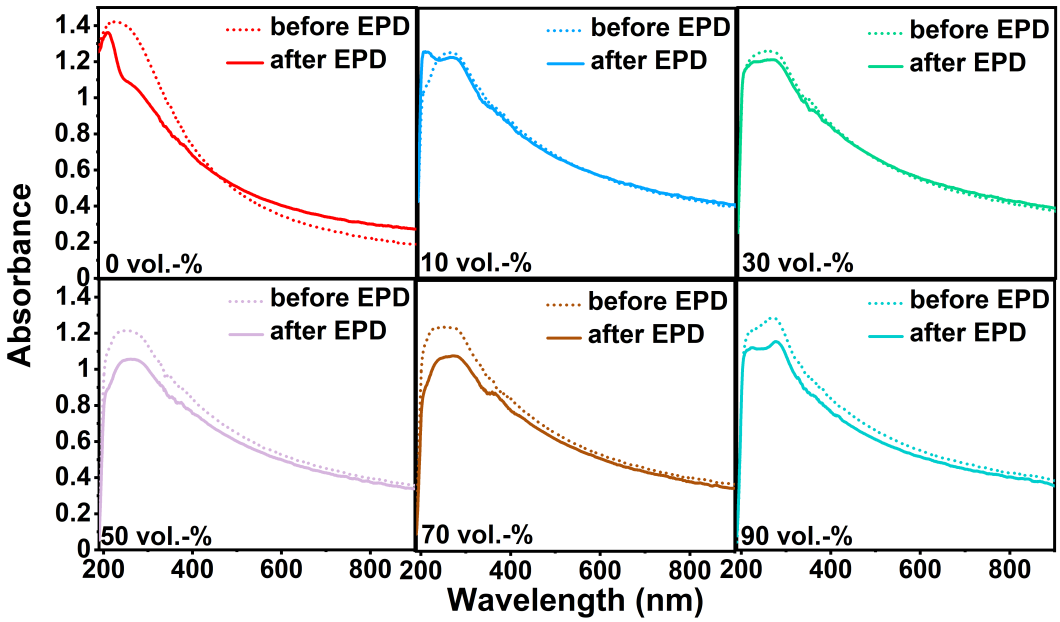

Figure S1: Exemplary UV-Vis spectra of PtNPs before and after EPD performed using varying concentrations of ethanol-water mixtures as solvent.

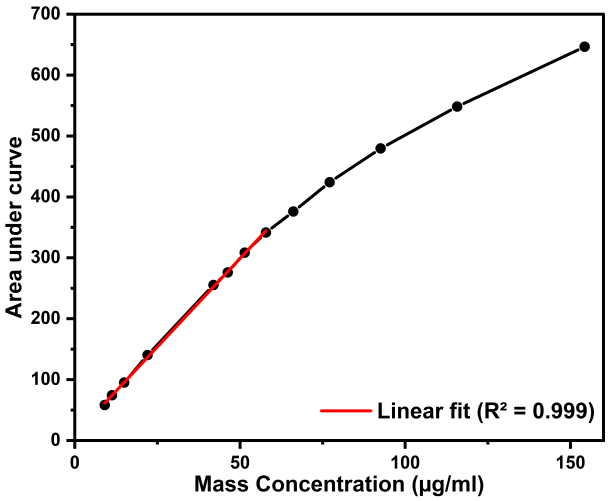

Figure S2: Mass concentration gradient of PtNPs dilutions, measured using UV-Vis spectroscopy.

S2. Electrochemical Impedance Spectroscopy

Figure S3 shows exemplary electrochemical impedance spectra of the samples coated with PtNPs dispersed in pure water, 10 vol.% through 90 vol.% (in steps of 20 vol.%) of ethanol concentrations and an uncoated sample. The graph confirms the U-shaped parabolic trend of the impedance values (as observed in the main text) with increasing ethanol concentration.

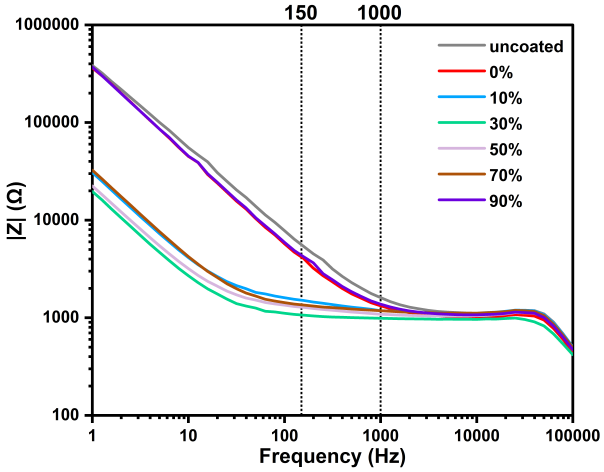

Figure S3: Electrochemical impedance spectra of Pt-Ir wires coated with PtNPs dispersed in varying concentrations of ethanol-water mixtures.

S3. Charge storage capacity calculation

Figure S4 shows an exemplary cyclic voltammogram (CV) of a coated Pt-Ir sample. The AUC of one full CV cycle was integrated to obtain the charge storage capacity (CSC) factors of the samples.

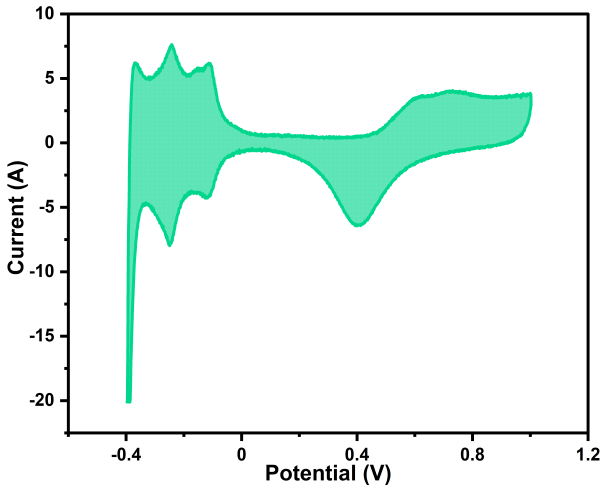

Figure S4: A cyclic voltammogram showing the integrated AUC used for calculating CSCs.

S4. Surface coverage of PtNPs after EPD

Figure S5 shows the SEM images of Pt-Ir samples - uncoated and coated with PtNPs in varying ethanol concentrations. Although the SEM has poor statistics, the images still comply with the trend observed in other analytical methods.

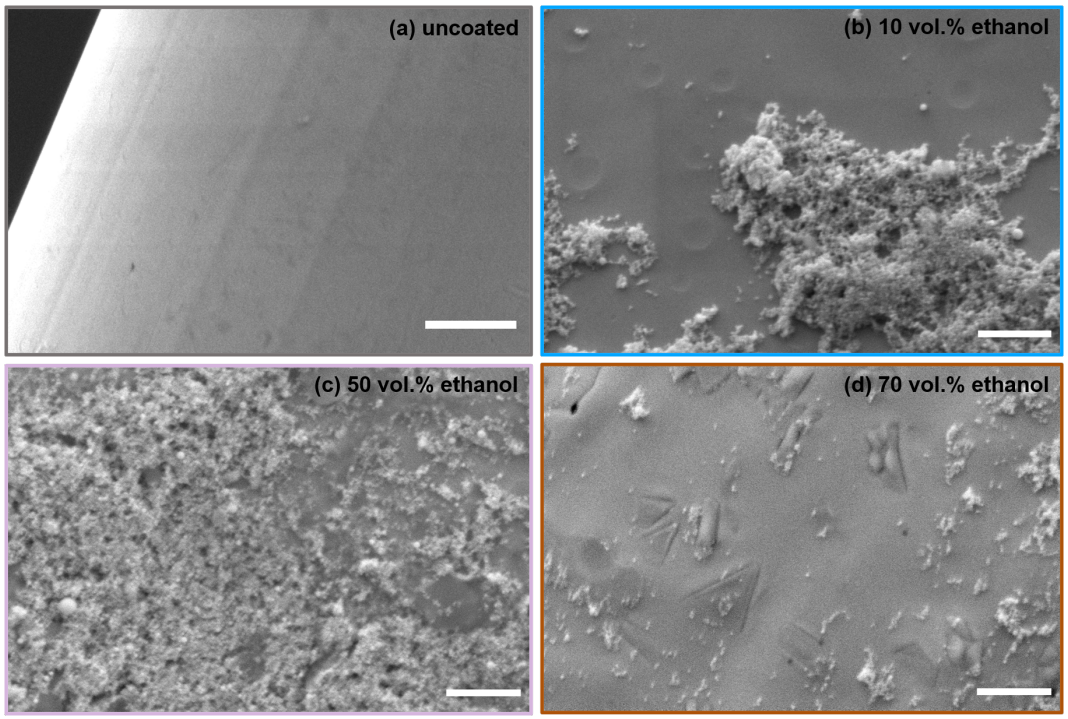

Figure S5: Exemplary SEM images of (a) uncoated sample, PtNP-coated Pt-Ir wires in (b) 10 vol.% ethanol, (c) 50 vol.% ethanol and (d) 70 vol.% ethanol mixtures.

S5. Platinum loading and surface roughness after EPD

The surface roughness factor is calculated using electrochemical surface area (ECSA) divided by geometric surface area (GSA, 1.2 cm^2). For this purpose, the ECSA is calculated

by taking into account the Pt mass loading using the formula[2],

$$\mathrm{ECSA} = Q_H/[\mathit{mass\ loading}\ (\mu g) \times Q_a] \tag{S1}$$

where Q_H is the charge associated with the hydrogen adsorption peak and Q_a is the theoretical charge density of polycrystalline Pt surface, 210 $\mu C/cm^2$.[3,4]
Figure S6 shows the ECSA calculated using the above equation. Due to high variations in Pt mass loadings because of the fact that microscopic electrodes were coated with sub-monolayer nanoscopic particles, the ECSA calculated by this method leads to high error bars. Therefore, a better and more reliable ECSA calculation is used in the main manuscript, in order to correlate with the impedance change. Table S1 shows the average roughness factor values calculated.

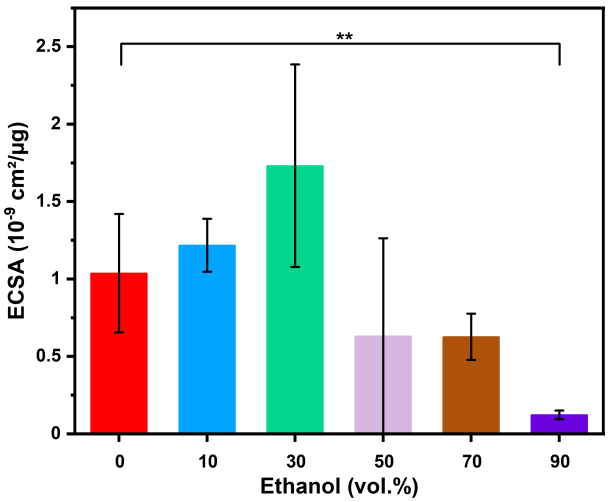

Figure S6: Average ECSA values calculated by taking Pt mass loading into account using the Equation S1 (N = 4, α = 0.05).

Table S1: Average roughness factor values of coated electrode surfaces

Ethanol (vol.%)	Roughness factor (10^{-9})
0	0.864
10	1.014
30	1.442
50	0.526
70	0.522
90	0.101

S6. Particle-based simulations

For clarity, only a subset of the radial distributions (RDFs) from the simulations were shown in the main text. Figure S7 shows all RDFs together. Collectively, this analysis indicates that the particles are more closely spaced as ethanol concentration increases. This

supports the results and discussion of the main text and is explained by the decreasing Debye length and reduced range of electrostatic interactions, as shown in Figure 3(b).

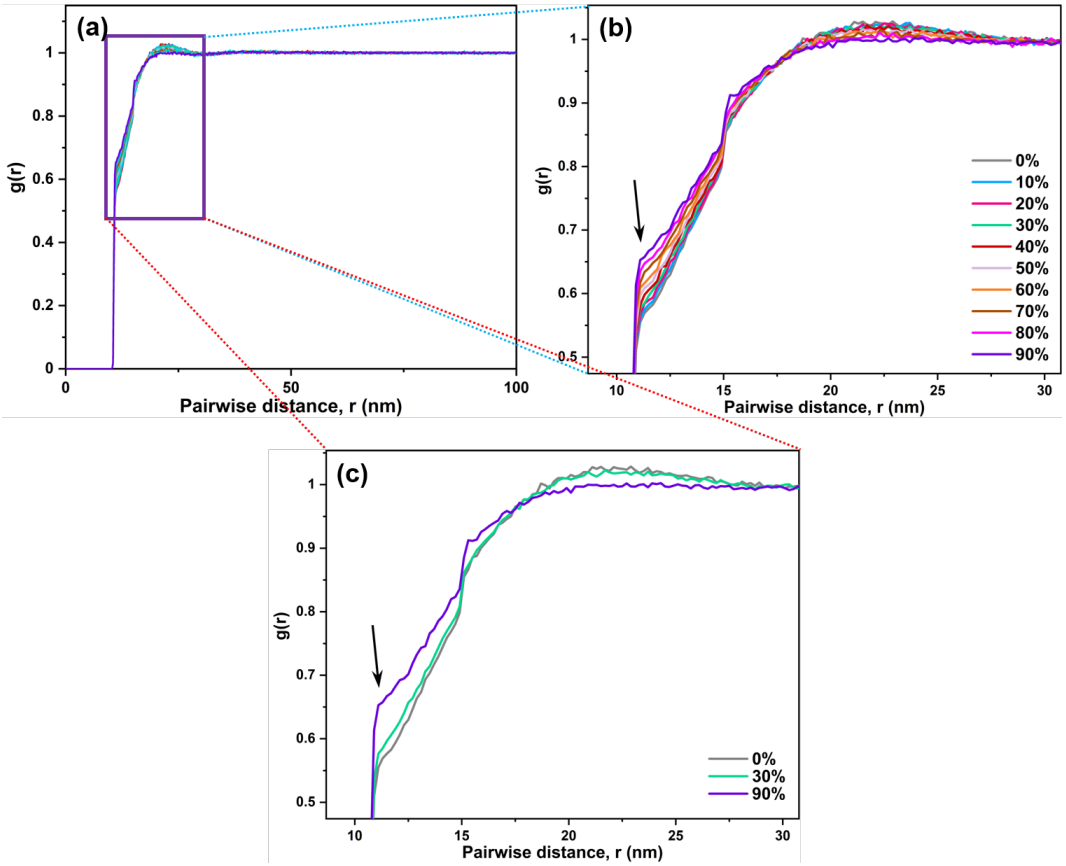

Figure S7: (a) RDFs of all simulations from Figure 3(a). (b,c) Within close separation distances 10 nm $<$ r $<$ 35 nm, the differences in the radial distribution function are most apparent, indicating that the particles are more closely spaced as ethanol concentrations increase.

References

[1] Ramesh et al. Comparing Direct and Pulsed-Direct Current Electrophoretic Deposition on Neural Electrodes: Deposition Mechanism and Functional Influence. *Langmuir*, 2021, 37(32), 9724–9734.

[2] Sun et al. A highly durable platinum nanocatalyst for proton exchange membrane fuel cells: multiarmed starlike nanowire single crystal *Angewandte Chemie*, 2011, 123(2), 442–446.

[3] Boretius et al. High-porous platinum electrodes for functional electrical stimulation *Annual International Conference of the IEEE Engineering in Medicine and Biology Society*, 2011, 5404–5407.

[4] Kumsa et al. Electron transfer processes occurring on platinum neural stimulating

electrodes: a tutorial on the i(Ve) profile *Journal of Neural Engineering*, 2016, 13, 052001.

Acknowledgement

We gratefully acknowledge the German Research Foundation (DFG) for their financial support under the project number BA 3580/24-1 and B.G. thanks DFG for Mercator Fellowship. This work was performed in part under the auspices of the U.S. Department of Energy by Lawrence Livermore National Laboratory under contract DE-AC52-07-NA27344, release number LLNL-JRNL-826684. V.R. thanks Tobias Bochmann (for the SEM measurements) and Johannes Wolter (for his support in the preliminary optimization experiments).

A3 Supporting Information: Influence of Platinum Alloy Nanoparticle EPD on Neural Electrode Impedance Reduction

Unpublished results under submission

Supporting Information

Platinum-Iridium Alloy Nanoparticle Coatings Produced by Electrophoretic Deposition Reduce Impedance in 3D Neural Electrodes

Vaijayanthi Ramesh[1], Jacob Johny[1], Jurij Jakobi[1], Christoph Rehbock[1] and Stephan Barcikowski[1,*]

[1] Institute of Technical Chemistry I, University of Duisburg-Essen and Center for Nanointegration Duisburg-Essen (CENIDE), 45141 Essen, Germany

S1. EDX of the metal targets used for nanoparticle synthesis

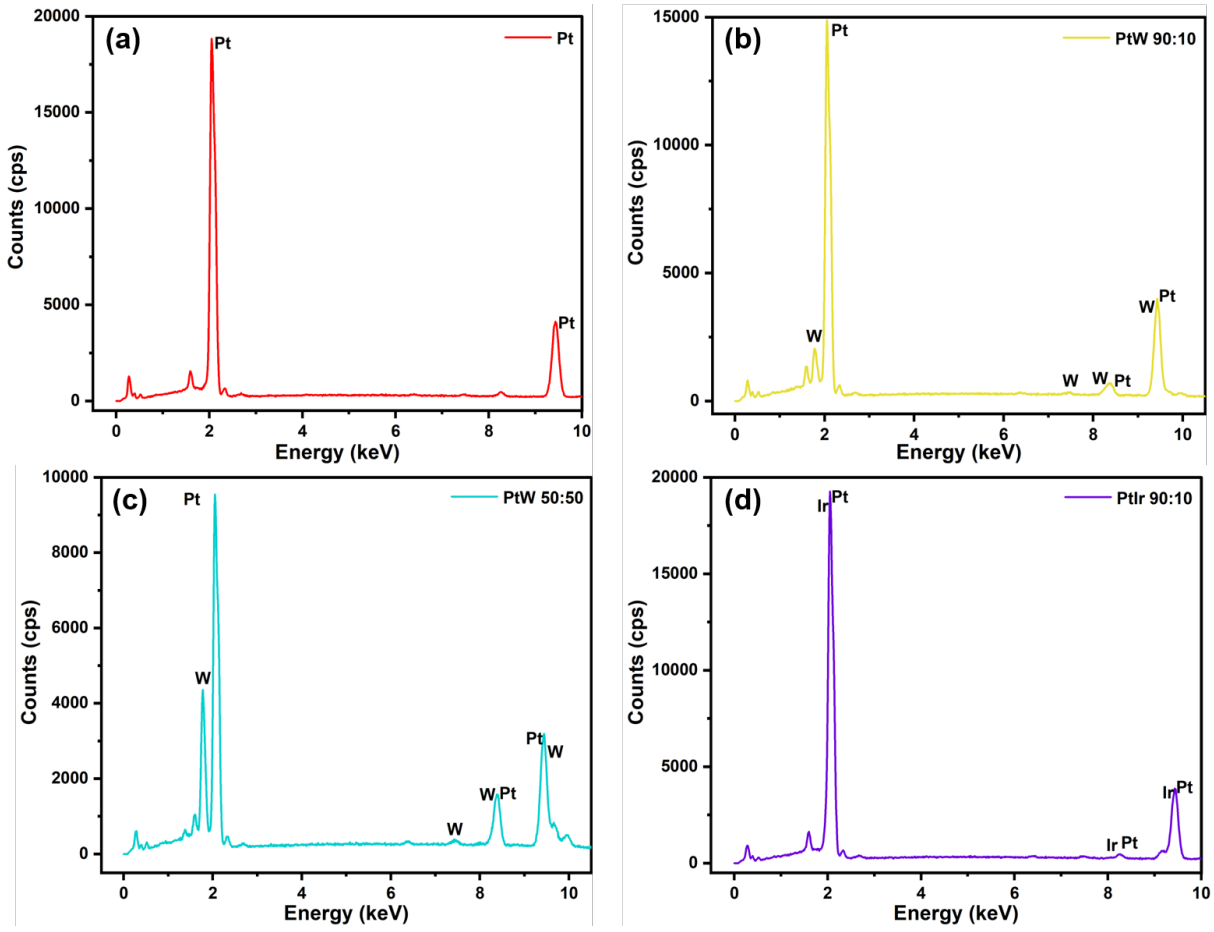

Figure 1: Exemplary EDX spectra of the metal targets used for the generation of NP colloids: (a) Pt, (b) Pt90W10, (c) Pt50W50, and (d) Pt90Ir10.

S2. HRTEM-EDX of Pt alloy nanoparticles

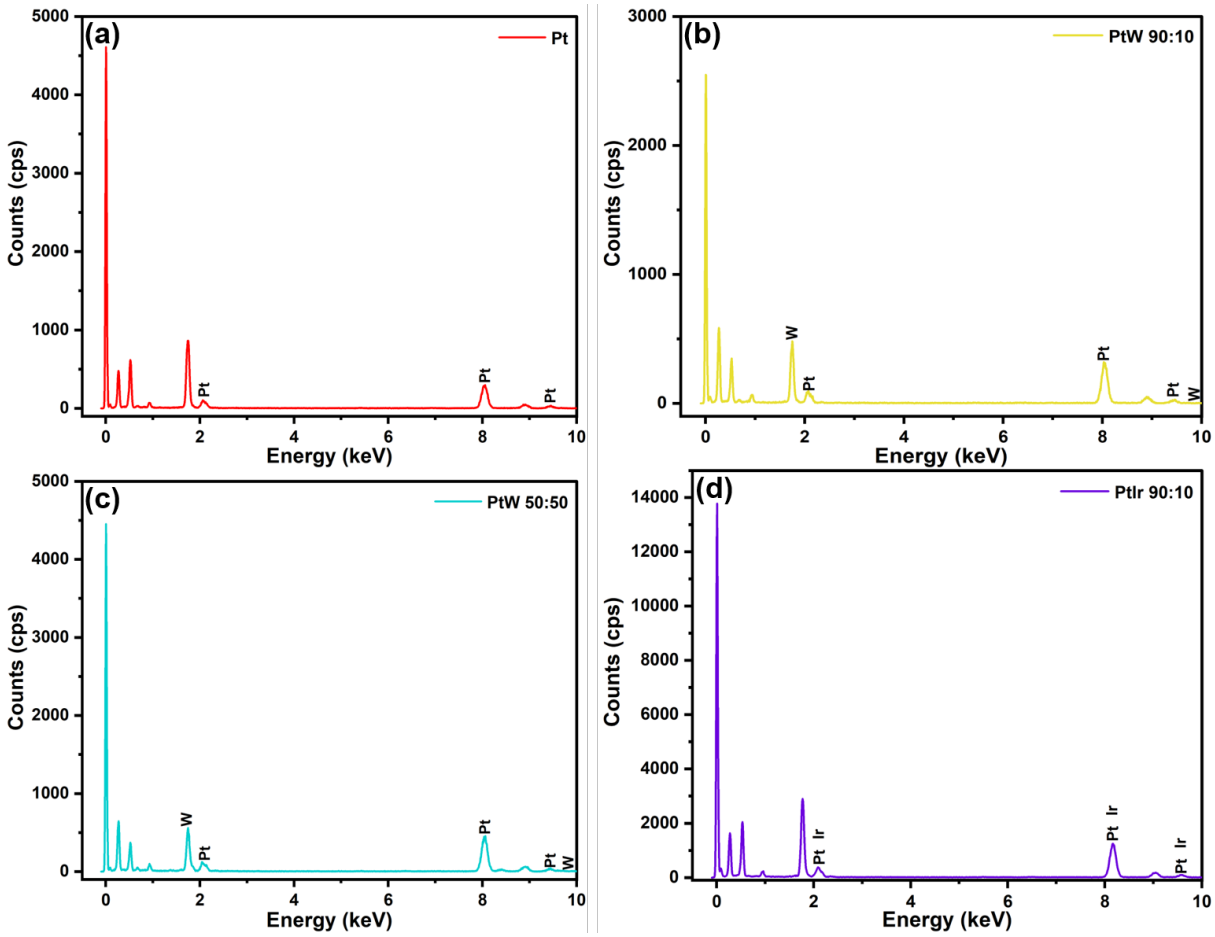

Figure 2: Exemplary EDX spectra of the Pt-alloy NP colloids measured using HR-TEM/EDX after drop-casting: (a) Pt, (b) Pt90W10, (c) Pt50W50, and (d) Pt90Ir10.

S3. Particle size distribution measured by ADC

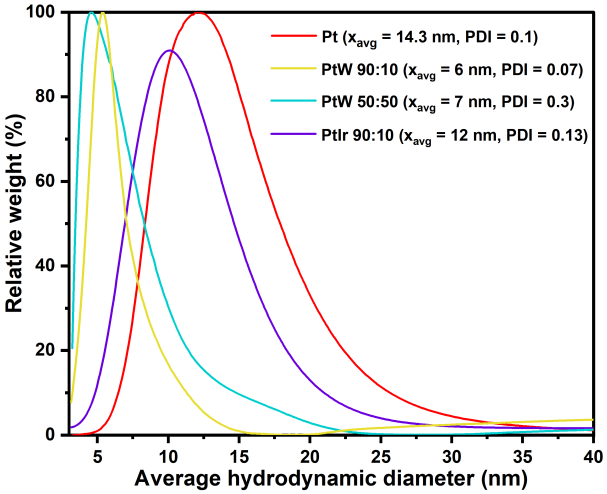

Figure 3: Average hydrodynamic mass-weighted particle size distribution of the laser-synthesized NPs, measured by ADC.

S4. Nanoparticle mass deposited on the electrode surface

Mass deposited on Pt-Ir wires after electrophoretic deposition (EPD) was determined using UV-Vis extinction spectroscopy (Figure 4). The area under the curve (AUC) values of the sample spectra before and after EPD were measured and correlated with a calibration curve based on platinum nanoparticle (PtNP) colloids with known mass concentrations (Figure 5). The mass remaining in supernatants after EPD was then subtracted from the mass of the colloid before EPD, to obtain the deposited mass on each sample[1].

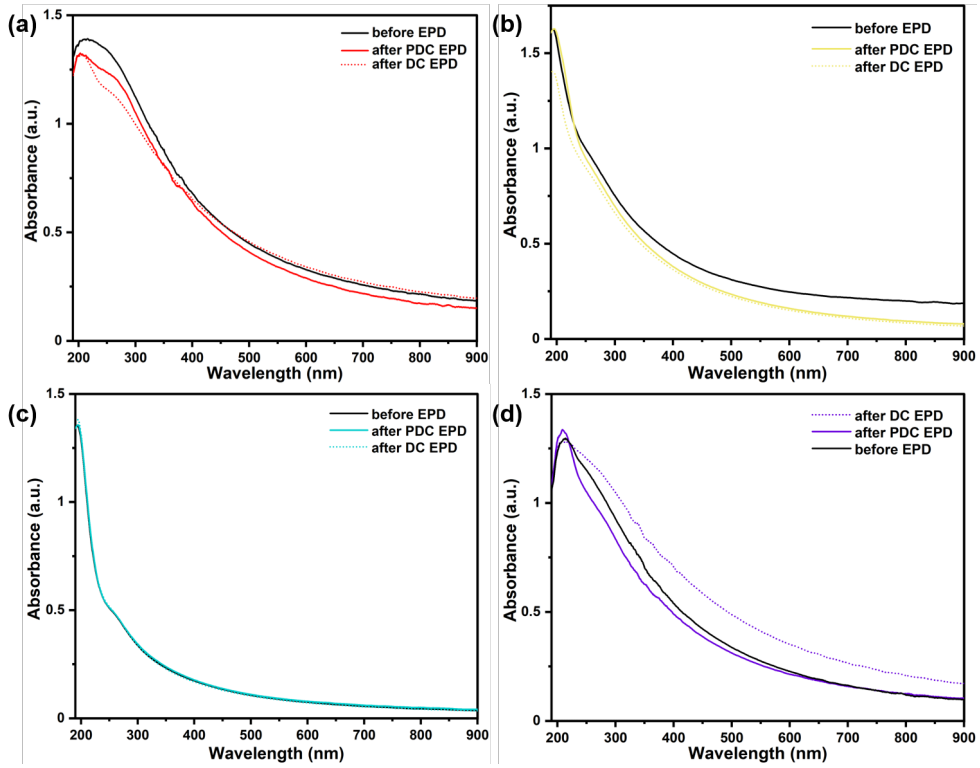

Figure 4: Exemplary UV-Vis extinction spectra of NPs before and after EPD: (a) Pt, (b) Pt90W10, (c) Pt50W50, and (d) Pt90Ir10.

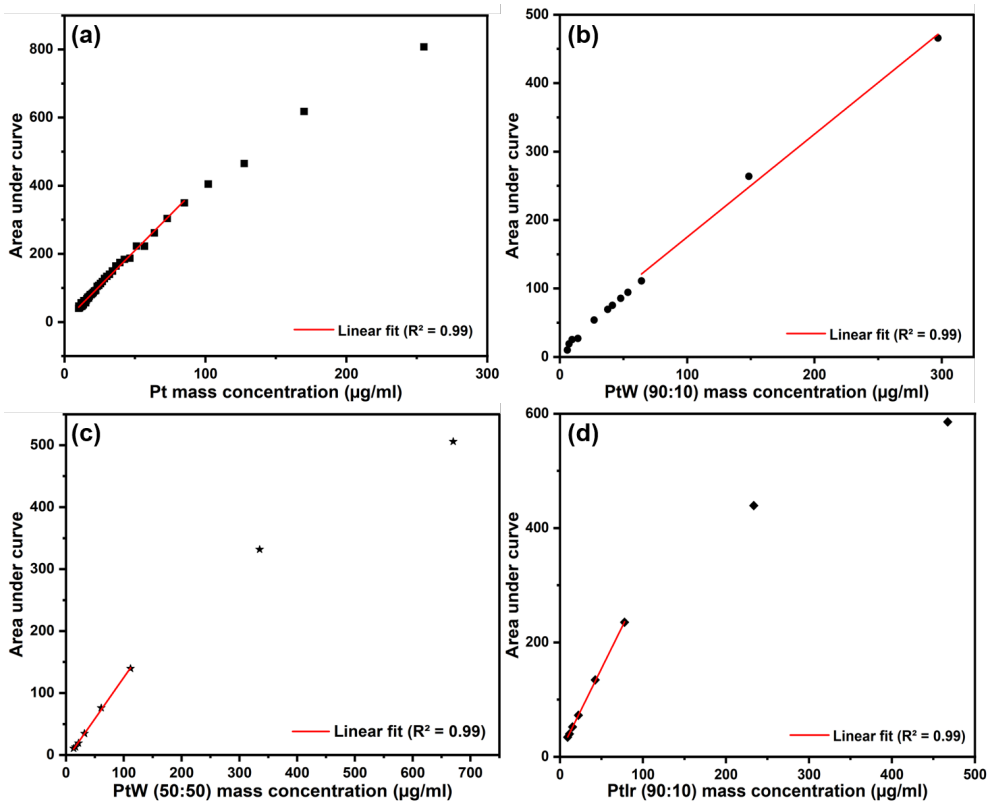

Figure 5: Mass concentration gradient of NPs dilutions, measured using UV-Vis extinction spectroscopy: (a) Pt, (b) Pt90W10, (c) Pt50W50, and (d) Pt90Ir10.

S5. CV and EIS curves of PDC-coated electrodes

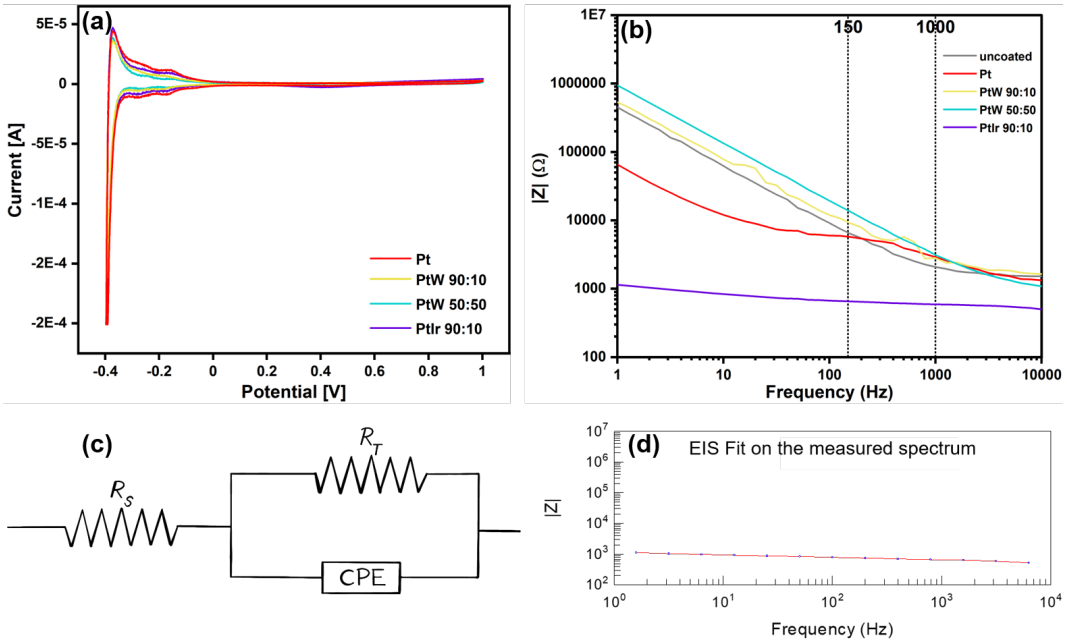

Figure 6: Electrochemical functionality of neural electrodes coated using Pt and Pt-based alloy nanoparticles: (a) Exemplary cyclic voltammograms, (b) Exemplary EI spectra, (c) EIS equivalent circuit model used for fitting the EIS data, and (d) Exemplary EIS fit performed on one of the measured data.

S6. EPD of Pt alloy NPs using DC-EPD

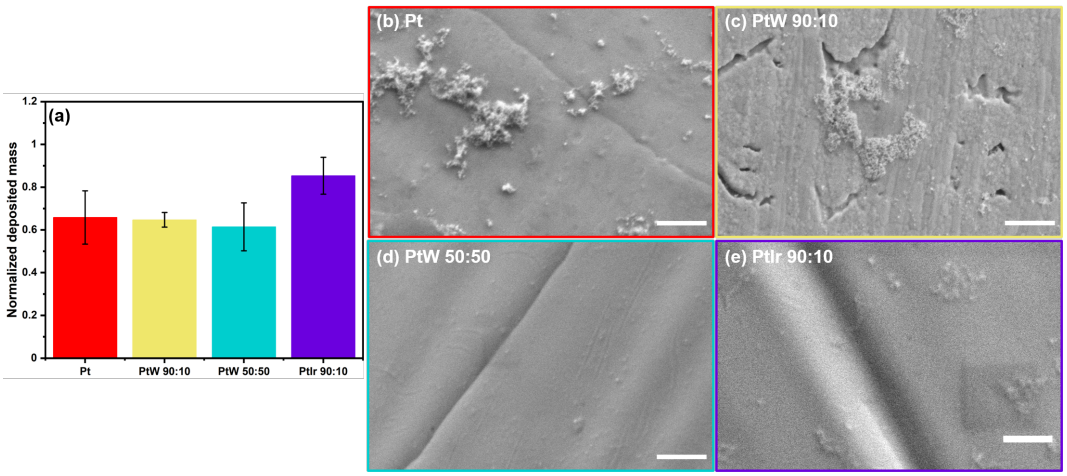

Figure 7: DC-EPD of Pt-based alloy NPs: (a) Average mass deposited (normalized to 1) on the electrodes (N = 3, α = 0.05), and (b–e) Exemplary SEM images taken from the sides of the electrodes. Scale bars are 500 nm.

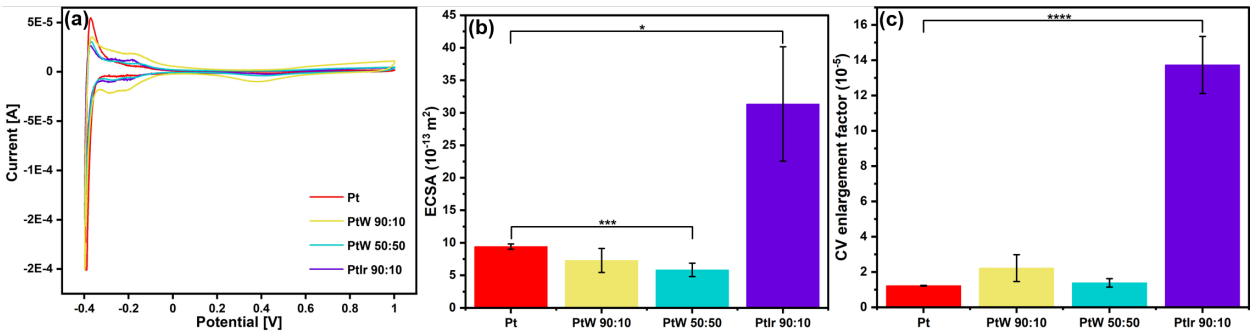

Figure 8: Cyclic voltammetry analysis of neural electrodes coated using Pt-based alloy NPs via DC-EPD: (a) Exemplary cyclic voltammograms, (b) Average ECSA values (N = 3, $\alpha = 0.05$), (c) Average CV enlargement factor values (CSC, N = 3, $\alpha = 0.05$).

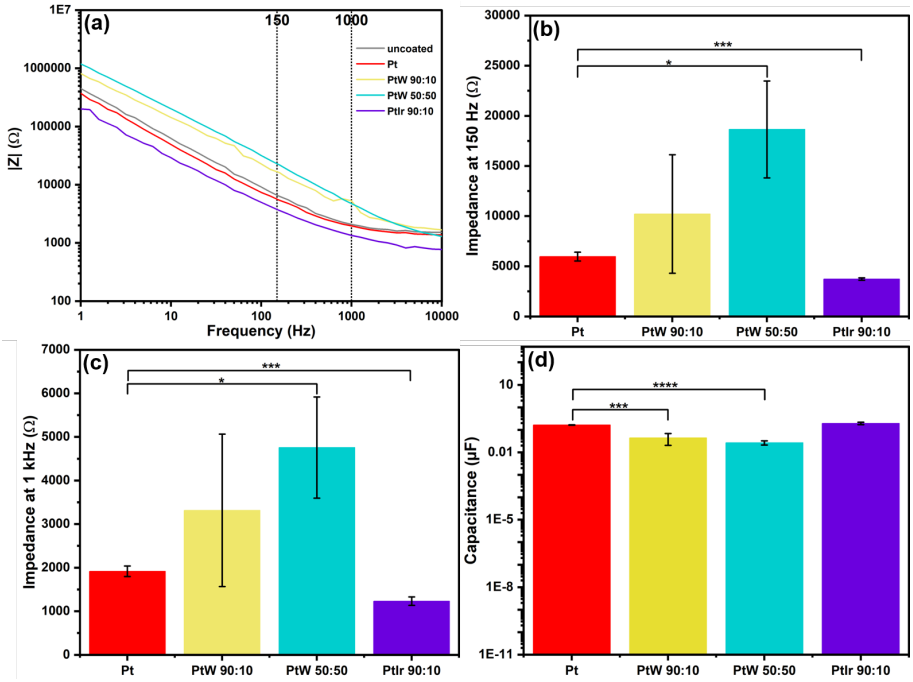

Figure 9: Electrochemical impedance of neural electrodes coated using Pt-based alloy NPs via DC-EPD: (a) Exemplary EIS spectra, (b) Average Z values at 150 Hz (N = 3, $\alpha = 0.05$), (c) Average Z values at 1 kHz (N = 3, $\alpha = 0.05$) and (d) Average capacitance values obtained after fitting EIS data with equivalent circuit model (N = 3, $\alpha = 0.05$).

References

[1] Ramesh et al. Comparing Direct and Pulsed-Direct Current Electrophoretic Deposition on Neural Electrodes: Deposition Mechanism and Functional Influence. *Langmuir*, 2021, 37(32), 9724–9734.

A4 Supporting Information: Influence of Platinum Nanoparticle Coatings on the In vivo Behaviour of Neural Electrodes

Unpublished results under review

Supporting Information

Coating of neural electrodes with platinum nanoparticles reduces and stabilizes impedance in vitro and in vivo in a rat model

Svilen D. Angelov[1], Christoph Rehbock[2], Vaijayanthi Ramesh[2], Hans E. Heissler[1], Mesbah Alam[1], Stephan Barcikowski[2], Kerstin Schwabe[1], Joachim K. Krauss[1,*]

[1] Department of Neurosurgery, Hannover Medical School, Carl-Neuberg-Str. 1, 30625 Hannover, Germany.

[2] Technical Chemistry I, University of Duisburg-Essen and Center for Nanointegration Duisburg-Essen (CENIDE), Universitaetsstr. 7, 45141 Essen, Germany.

S1. Mass Concentration curve of the laser-generated Platinum Nanoparticles

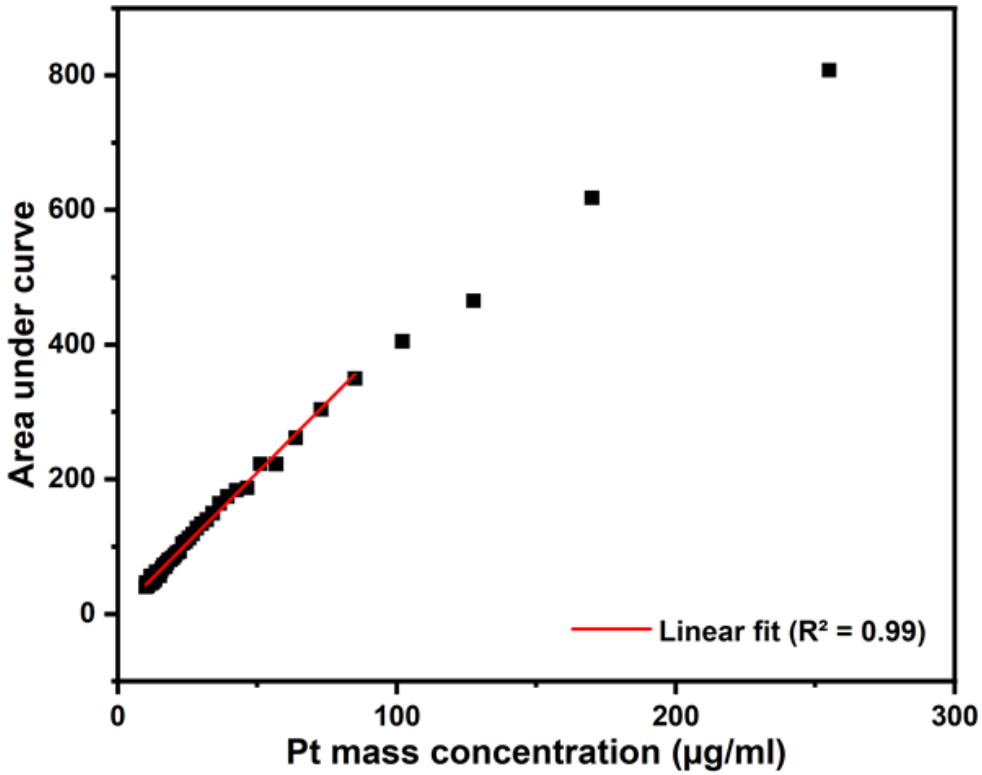

Figure 1: Calibration curve based on UV-Vis extinction spectra of the laser-generated, aqueous Pt nano-colloids at different mass concentrations. Area under curve (AUC) values were determined by integration of the absorbance values in a spectral range 190 - 900 nm.

A5 Supporting Information: Mechanical Stability of Nano-Coatings on Clinically Applicable Electrodes, Generated by Electrophoretic Deposition

Available at: https://onlinelibrary.wiley.com/doi/10.1002/adhm.202102637

ADVANCED HEALTHCARE MATERIALS

Supporting Information

for *Adv. Healthcare Mater.*, DOI 10.1002/adhm.202102637

Mechanical Stability of Nano-Coatings on Clinically Applicable Electrodes, Generated by Electrophoretic Deposition

Vaijayanthi Ramesh, Nadine Stratmann, Viktor Schaufler, Svilen D. Angelov, Ilona D. Nordhorn, Hans E. Heissler, Ricardo Martínez-Hincapié, Viktor Čolić, Christoph Rehbock, Kerstin Schwabe, Uwe Karst, Joachim K. Krauss and Stephan Barcikowski**

Supporting Information

Mechanical Stability of Nano-Coatings on Clinically Applicable Electrodes, Generated by Electrophoretic Deposition

Vaijayanthi Ramesh[1], Nadine Stratmann[1], Viktor Schaufler[1], Svilen D. Angelov[2], Ilona D. Nordhorn[3], Hans E. Heissler[2], Ricardo Martínez-Hincapié[4], Victor Čolić[4], Christoph Rehbock[1], Kerstin Schwabe[2], Uwe Karst[3], Joachim K. Krauss[2] and Stephan Barcikowski[1,*]

[1] Institute of Technical Chemistry I, University of Duisburg-Essen and Center for NanoIntegration Duisburg-Essen (CENIDE), Essen, Germany.

[2] Department of Neurosurgery, Hannover Medical School, Hannover, Germany.

[3] Institute of Inorganic and Analytical Chemistry, University of Muenster, Muenster, Germany

[4] Electrochemistry for Energy Conversion, Max-Planck-Institute for Chemical Energy Conversion, Muelheim an der Ruhr, Germany

S1. Particle size distribution

Figure S1 shows the average hydrodynamic number and weight distribution of laser fragmented platinum nanoparticles (Pt NPs) used for electrophoretic deposition (EPD).

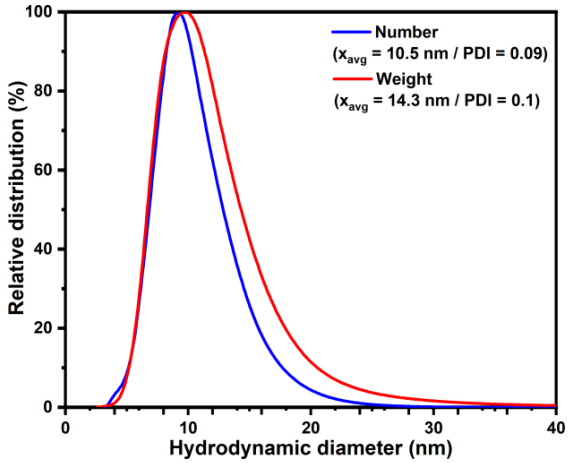

Figure S1: Average hydrodynamic size distributions of laser fragmented PtNPs, showing average diameters at 14 nm (weight %) and 10 nm (number %).

S2. Mass of Pt NP deposited on the samples

Mass deposited on the samples after direct current (DC) and pulsed DC (PDC) EPD was determined using UV-Vis extinction spectroscopy (Figure S2(a)). Area under curve (AUC) values of the spectra before and after EPD, were correlated with the known mass concentration gradients of Pt NPs (Figure S2(b)). The mass remaining in supernatants after EPD was subtracted from the mass of the colloid before EPD, to obtain the deposited mass on each

sample[1] (Figure S2(c)).

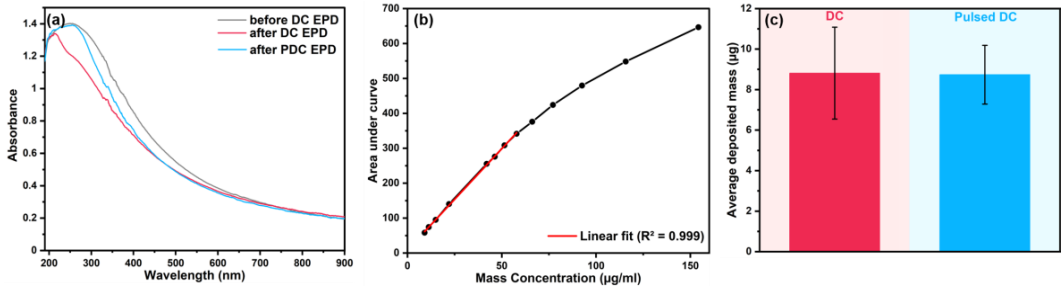

Figure S2: (a) Exemplary UV-Vis spectra of Pt NPs before EPD and after DC- and PDC- EPD, (b) mass concentration gradient of Pt NP dilutions, measured using UV-Vis spectroscopy, and (c) average mass of Pt NPs deposited on the electrode samples after DC- and PDC-EPD (N = 7).

S3. Force and energy generated during stability tests

Agarose gel test:

Frictional force during the agarose gel test was calculated using Stoke's law (Equation 1). Here, the sample radius was 38 µm, the viscosity of agarose gel was 5.6 Pa.s[2], and the manually measured push-pull rate was 1.33 mm s^{-1}.

$$F = 6\pi \cdot r \cdot \eta \cdot v \quad (1)$$

Upon calculation, the friction force was equal to **5.35 µN**.

Ultrasonication test:

Energy developed during ultrasonic agitation was calculated using Equation 2.

$$E = P \cdot t \quad (2)$$

Here, the power (P) of the ultrasonicator was 2880 W[3] and time (t) is equal to 300 s. The calculated energy applied to the samples was **864 kJ**.

S4. Mechanical stability of DC-coated Pt-Ir samples

Figure S3(a,b,c) shows exemplary cyclic voltammograms of DC-coated samples, before and after the stability tests: dipping in agarose gel, adhesion test according to ASTM D3359–17, and ultrasonication for 5 min in Milli-Q water. Figure S3(d) shows the average electrochemical surface areas (ECSA) and Figure S3(e) shows the charge storage capacities (CSC) of the samples, before and after stability tests. It can be seen that, since DC-EPD produces more agglomerated deposits[1], upon stability testing all the samples showed a significant reduction in ECSA. However, the least amount of disintegration was seen in agarose gel (20% ECSA decrease). This could be because the clustered deposits are loosely bound to one another and are easily removable by ultrasonic waves. If the adhesive tape would have stuck onto an agglomerated deposit, it also in turn removed a high number of

particles from the surface.

Figure S4(a,b,c) shows exemplary electrochemical impedance (EIS) spectra of DC-coated samples, before and after the stability tests. Figures S4(d) and (e) show the average impedance values at 150 Hz and 1 kHz respectively, before and after the tests. Since the impedance and ECSA are inversely proportional to each other, the EIS analysis conforms with the ECSA analysis, where the ultrasonication shows the highest statistically significant increase (264% at 150 Hz and 98% at 1 kHz) in impedance and the agarose gel test shows the least increase (13% at 150 Hz and 26% at 1 kHz), which is significant at 1 kHz. Figure S5 shows exemplary SEM images of the Pt-Ir surfaces before and after stability tests. It should be noted that the SEM analysis suffers from bad statistics and it is difficult to image the same area before and after the test. Nevertheless, the after-test images still reveal the presence of NPs on them confirming that in no testing method, the NPs are completely removed.

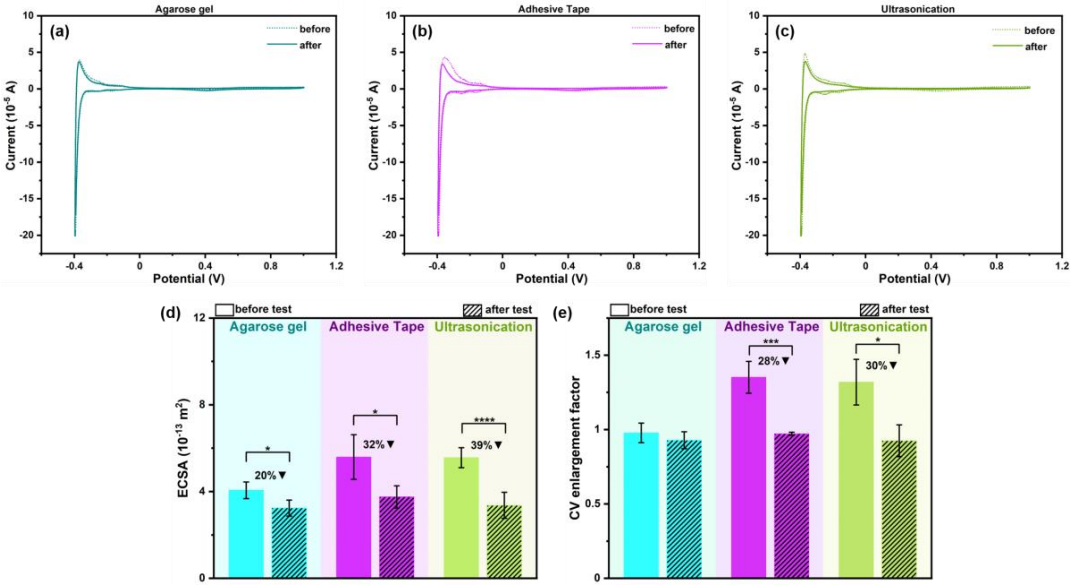

Figure S3: (a,b,c) Exemplary cyclic voltammograms of DC-coated Pt-Ir wires, before and after stability tests. Average (d) ECSA (N = 4, α = 0.05) and (e) CV enlargement factor (CSC, N = 3, α = 0.05) of the DC-coated samples before and after the stability tests.

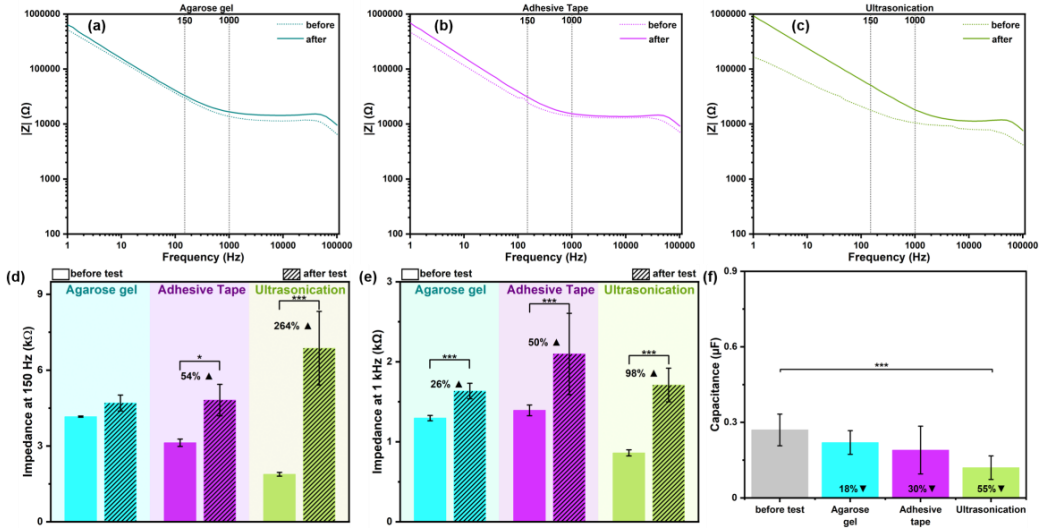

Figure S4: (a,b,c) Exemplary EIS spectra of DC-coated Pt-Ir wires, before and after stability tests. Average impedance values at (d) 150 Hz (N = 4, α = 0.05), (e) 1 kHz (N = 4, α = 0.05). (f) Average capacitance values of the DC-coated samples before and after the stability tests, showing significant capacitance reduction after ultrasonication (N = 3, α = 0.05).

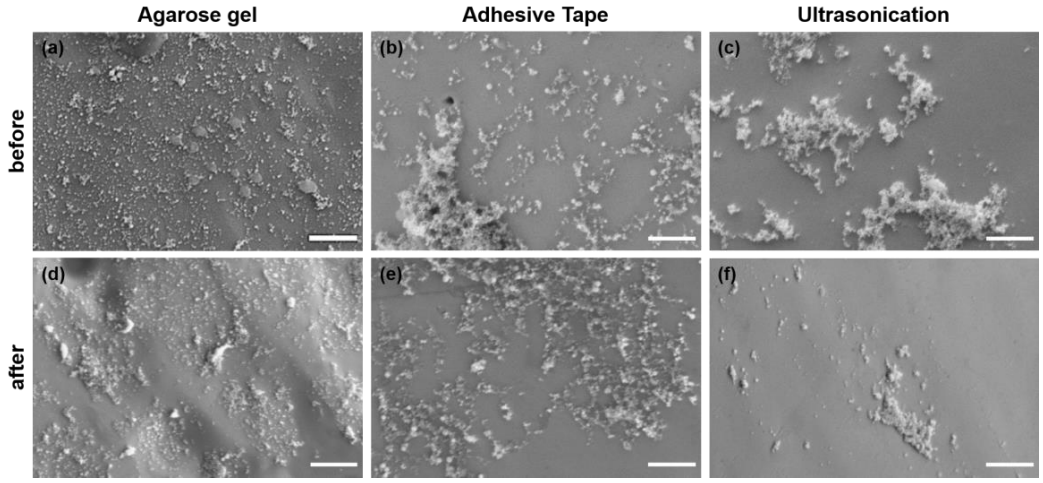

Figure S5: Exemplary SEM images of the DC-coated samples (a,b,c) before and (d,e,f) after the stability tests. Scale bars are 500 nm.

S5. Cyclic voltammograms and EIS spectra of PDC-coated samples

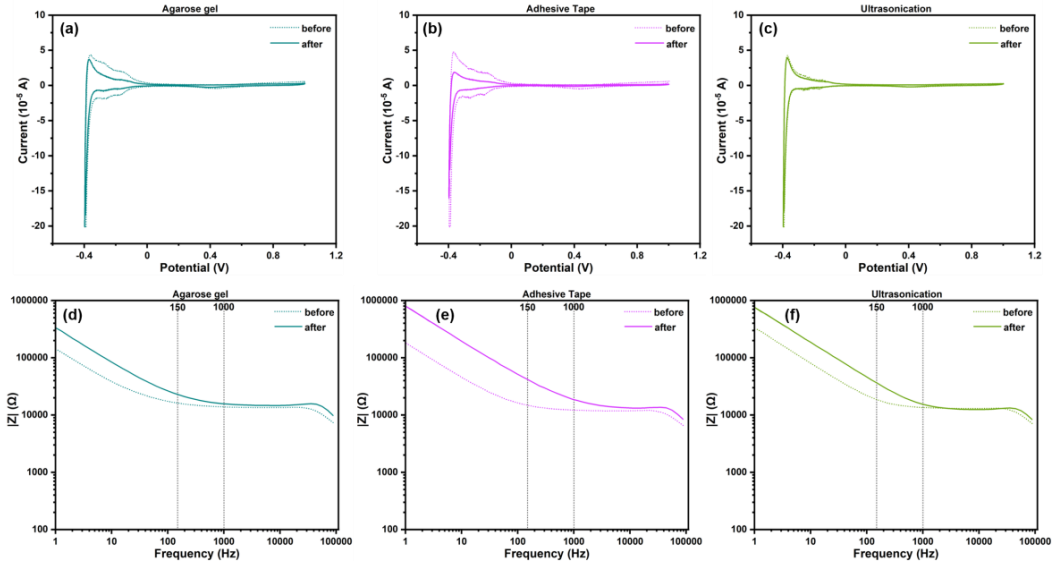

Figure S6: (a,b,c) Exemplary cyclic voltammograms of PDC-coated Pt-Ir wires, before and after stability tests, and (d,e,f) exemplary EIS spectra of PDC-coated Pt-Ir wires, before and after stability tests.

S6. EIS analysis of electrochemical stability tested samples

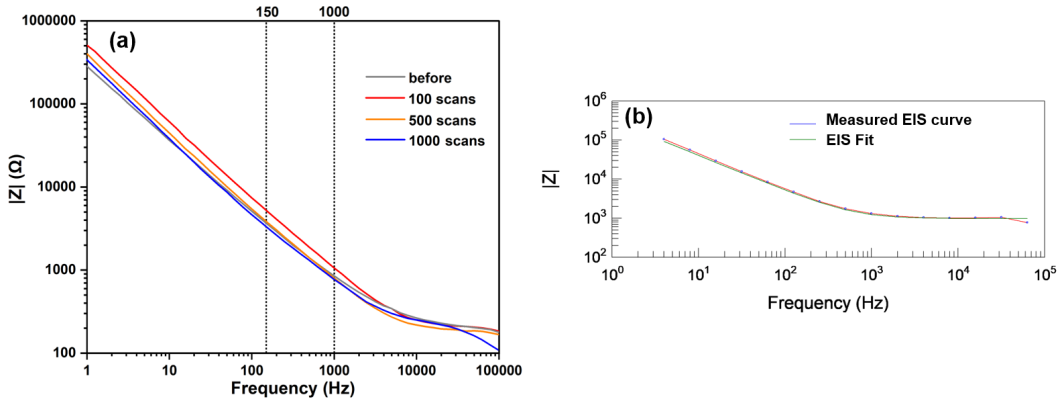

Figure S7: (a) Exemplary EIS spectra of PDC-coated Pt-Ir wires, before and after electrochemical stability tests, and (b) an exemplary EIS fit performed on one of the measured spectra.

S7. LA-ICP-MS controls with rat brain sections

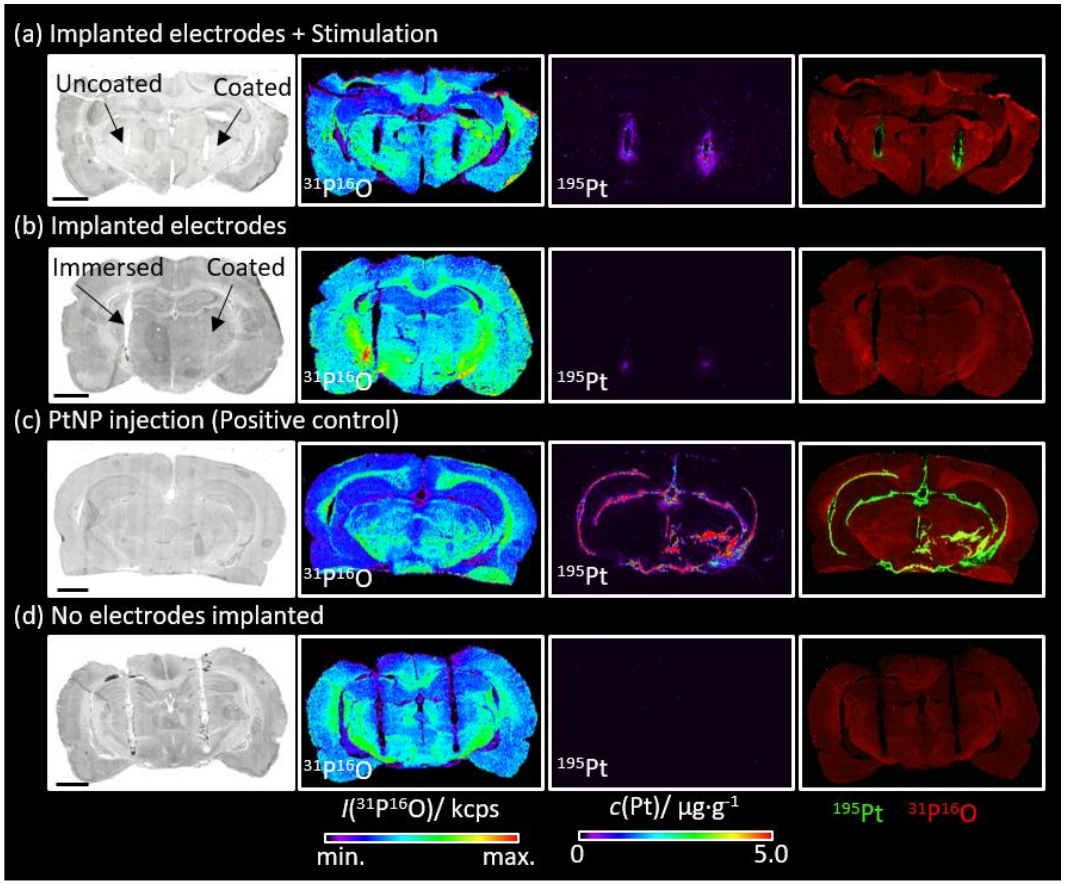

Figure S8: Pt biodistribution in rat brain sections visualized by LA-ICP-MS: (a) Brain section stimulated with uncoated and PDC-coated electrodes. (b) Brain section with implantation of immersed and PDC-coated electrodes removed after one hour without stimulation. (c) Brain section after injection of Pt NPs. (d) Brain section without electrode implantation. Shown are the optical microscopic images, LA-ICP-MS distribution

images of $^{31}P^{16}O$ and ^{195}Pt as well as overlay images of $^{31}P^{16}O$ (red) and ^{195}Pt (green). The scale bar indicates 2 mm.

S8. Bending Assay

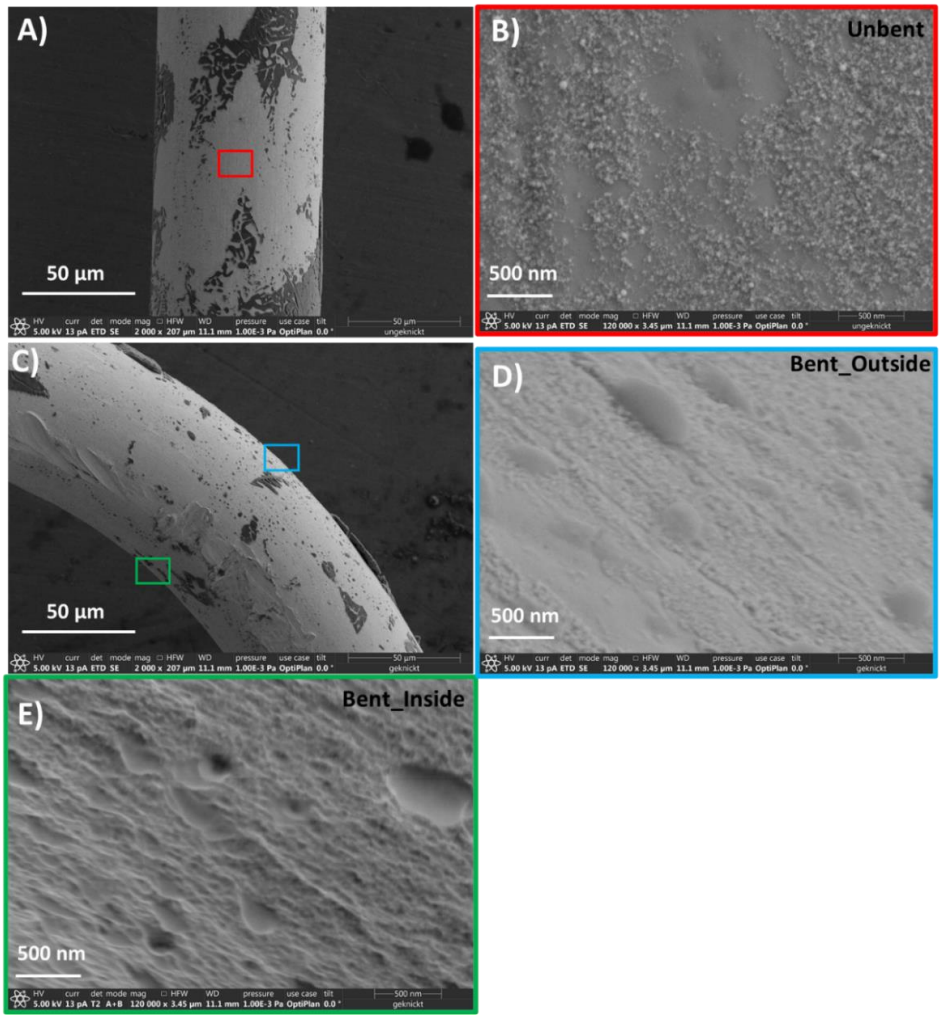

Figure S9: Bending Assay. A) Coated Pt-Ir wire (unbent control) 2,000x magnification. B) Coated Pt-Ir wire (unbent control) 120,000 x magnification. C) Coated Pt-Ir wire bent by ~90° 2,000 x magnification. D) Coated Pt-Ir wire bent by ~90°, Outside, 120,000 x magnification. E) Coated Pt-Ir wire bent by ~90°, Inside, 120,000 x magnification.

References

[1] Ramesh et al. Comparing Direct and Pulsed-Direct Current Electrophoretic Deposition on Neural Electrodes: Deposition Mechanism and Functional Influence. *Langmuir*, 2021, 37(32), 9724-9734.

[2] Fallenstein et al. Dynamic mechanical properties of human brain tissue. *Journal of Biomechanics*, 2.3, 1969, 217-226.

[3] Allpax GmbH & Co. KG, ‘‘https://www.allpax.de/index.php/cat/c22227_Ultraschallreinigungsgeraete-Standard.html’’, 14.09.2021.

Curriculum Vitae

The curriculum vitae is not included in the online version for data protection reasons.

List of Publications

Peer-reviewed Journals (* = equal contribution; underlined = students supervised)

1. **Vaijayanthi Ramesh**, Christoph Rehbock, Brian Giera, John J. Karnes, Jean-Baptiste Forien, Svilen D. Angelov, Kerstin Schwabe, Joachim K. Krauss, and Stephan Barcikowski, *Comparing Direct and Pulsed-Direct Current Electrophoretic Deposition on Neural Electrodes: Deposition Mechanism and Functional Influence*, Langmuir 37(32) (2021) 9724–9734.

2. **Vaijayanthi Ramesh**, Brian Giera, John J. Karnes, Nadine Stratmann, Viktor Schaufler, Yao Li, Christoph Rehbock, and Stephan Barcikowski, *Electrophoretic Deposition of Platinum Nanoparticles using Ethanol-Water Mixtures Significantly Reduces Neural Electrode Impedance*, The Journal of Electrochemical Society 169 (2022) 022504.

3. Yaya Li*, **Vaijayanthi Ramesh***, Faina Bider, Nathan Bradshaw, Christoph Rehbock, Aldo R. Boccaccini and Stephan Barcikowski, *Co-doping of Iron and Copper ions in nanosized 45S5 bioactive glass produced by one-step laser fragmentation*, Journal of Biomedical Materials Research Part A (2022) 1–14.

4. **Vaijayanthi Ramesh**, Nadine Stratmann, Viktor Schaufler, Svilen D. Angelov, Ilona D. Nordhorn, Hans E Heissler, Ricardo Martínez-Hincapié, Victor Čolić, Christoph Rehbock, Kerstin Schwabe, Uwe Karst, Joachim K. Krauss and Stephan Barcikowski, *Mechanical Stability of Nano-Coatings on Clinically Applicable Electrodes, Generated by Electrophoretic Deposition*, Advanced Healthcare Materials (2022) 2102637.

5. **Vaijayanthi Ramesh**, Jacob Johny, Jurij Jakobi, Christoph Rehbock and Stephan Barcikowski, *Platinum-Iridium Alloy Nanoparticle Coatings Produced by Electrophoretic Deposition Reduce Impedance in 3D Neural Electrodes*, under submission.

6. **Vaijayanthi Ramesh**, Christoph Rehbock and Stephan Barcikowski, *A State-of-the-Art Review on Neural Electrode Nano-Coatings*, under preparation.

7. Svilen D. Angelov, Christoph Rehbock, **Vaijayanthi Ramesh**, Hans E Heissler, Mesbah Alam, Stephan Barcikowski, Kerstin Schwabe and Joachim K. Krauss, *Coating of neural electrodes with platinum nanoparticles reduces and stabilizes impedance in vitro and in vivo in a rat model*, under review.

8. John J. Karnes, Andrew J. Pascal, Christoph Rehbock, **Vaijayanthi Ramesh**, Marcus A. Worsley, Stephan Barcikowski, Elaine Lee, and Brian Giera, *Beyond the Standard Theory: Particle-Based Simulations of Electrophoretic Deposition with Adaptive Physics Models*, under submission.

9. Pichaporn Sutthavas, Matthias Schumacher, Martyna Nikody, Elizabeth Rosado Balmayor, Pamela Habibovic, **Vaijayanthi Ramesh**, Jurij Jakobi, Christoph Rehbock, Stephan Barcikowski and Sabine van Rijt, *Laser-based ion doping is a suitable alternative to dope biologically active ions into colloidal bioglass nanoparticles*, Materials Advances, in press.

10. Lisa Gamrad, Carmen Streich, **Vaijayanthi Ramesh**, Andreas Schielke, Christoph Rehbock, Steffen Franzka, Sabine Klein, Wilfried A. Kues, Detlef Rath and Stephan Barcikowski, *Striped Sperm Heads — Confocal Microscopy and Fluorescence Lifetime Imaging of Bio-conjugated Gold Clusters' Membrane Adsorption and Distribution inside Spermatozoa*, under review.

Book Chapter

1. Bilal Gökce, Christoph Rehbock, **Vaijayanthi Ramesh**, Sebastian Kohsakowski, Tim Hupfeld, Sven Reichenberger and Stephan Barcikowski, *Laser synthesis of colloids: applications. Handbook of Laser Micro-and Nano-Engineering*, Springer (2020) 1–25.

List of Conference Contributions

(* = presenting author)

1. **Vaijayanthi Ramesh**, Christoph Rehbock*, Svilen D. Angelov, Hans E. Heissler, Kerstin Schwabe, Joachim K. Krauss, Stephan Barcikowski. *In vivo applications of neuronal electrodes structured with laser-generated platinum nanoparticles by electrophoretic deposition*, 57^{th} Annual Conference on Biomedical Engineering (DGBMT), Rhein-Ruhr, September 2023.

2. Christoph Rehbock*, **Vaijayanthi Ramesh**, Brian Giera, John J. Karnes, Svilen D. Angelov, Hans E. Heissler, Kerstin Schwabe, Joachim K. Krauss, Stephan Barcikowski. *In vivo applications of neuronal electrodes structured with laser-generated platinum nanoparticles by electrophoretic deposition*, ECI: Electrophoretic Deposition VII: Fundamentals and Applications, Online, November 2022.

3. Svilen D. Angelov, **Vaijayanthi Ramesh**, Christoph Rehbock, Hans E. Heissler, Massabah Alam, Kerstin Schwabe*, Stephan Barcikowski, Joachim K. Krauss. *Coating of neural electrodes with platinum nanoparticles reduces and stabilizes impedance in vitro and in vivo in a rat model*, 73^{rd} Annual Meeting of the German Society for Neurosurgery, Cologne, May/June 2022.

4. **Vaijayanthi Ramesh***, Christoph Rehbock, Svilen D. Angelov, Kerstin Schwabe, Joachim K. Krauss, and Stephan Barcikowski, *Mechanical stability of electrophoretically deposited Platinum Nanoparticles on Neural electrode surfaces*, Annual Meeting of the German Society for Biomaterials (DGBM), Online, October 2021.

5. **Vaijayanthi Ramesh***, Christoph Rehbock, Svilen D. Angelov, Kerstin Schwabe, Joachim K. Krauss, and Stephan Barcikowski, *Neural electrode Impedance reduction via Pulsed-DC Electrophoretic Deposition*, 55^{th} Annual Conference on Biomedical Engineering (DGBMT), Hannover, October 2021.

6. **Vaijayanthi Ramesh***, Christoph Rehbock, Svilen D. Angelov, Kerstin Schwabe, Joachim K. Krauss, and Stephan Barcikowski, *Pulsed-DC Electrophoretic Deposition of Platinum Nanoparticles on neural electrodes significantly lower their Impedance*, European Congress and Exhibition on Advanced Materials and Processes (EUROMAT), Online, September 2021.

7. **Vaijayanthi Ramesh***, Christoph Rehbock, Svilen D. Angelov, Kerstin Schwabe, Joachim K. Krauss, and Stephan Barcikowski, *Surface modification of neural electrodes via Pulsed-DC Electrophoretic Deposition and their in-vivo application*, 31^{st} Annual Conference of the European Society for Biomaterials (ESB), Online, September 2021.

8. **Vaijayanthi Ramesh***, Christoph Rehbock, Brian Giera, John J. Karnes, Svilen D. Angelov, Kerstin Schwabe, and Stephan Barcikowski, *Electrophoretic deposition of laser-generated Platinum Nanoparticles on neural prostheses*, 6^{th} International Conference on Advanced Nanoparticle Generation & Excitation by Lasers in Liquids (ANGEL), Online, June 2021.

9. **Vaijayanthi Ramesh***, Christoph Rehbock, Brian Giera, John J. Karnes, Svilen D. Angelov, Kerstin Schwabe, and Stephan Barcikowski, *Comparing the influence of DC and Pulsed-DC Electrophoretic Depositions on Neural Electrode Impedance*, 9^{th} NRW Nano Conference – Innovations in Materials and Applications, Online, April 2021.

List of Publications included in this Thesis and Author Contributions

1. **Vaijayanthi Ramesh**, Christoph Rehbock, Brian Giera, John J. Karnes, Jean-Baptiste Forien, Svilen D. Angelov, Kerstin Schwabe, Joachim K. Krauss, and Stephan Barcikowski, *Comparing Direct and Pulsed-Direct Current Electrophoretic Deposition on Neural Electrodes: Deposition Mechanism and Functional Influence*, Langmuir 37(32) (2021) 9724–9734.

   Conceptualization: VR, CR, SB; Methodology: VR, BG, JJK, SDA; Formal analysis: VR, BG, SB; Investigation: VR, BG; Data curation: VR, BG; Original draft preparation: VR; Review and editing: VR, CR, BG, JJK, SDA, KS, SB; Visualization: VR, BG; Supervision: CR, SB; Funding acquisition: CR, SB.

2. **Vaijayanthi Ramesh**, Brian Giera, John J. Karnes, Nadine Stratmann, Viktor Schaufler, Yao Li, Christoph Rehbock, and Stephan Barcikowski, *Electrophoretic Deposition of Platinum Nanoparticles using Ethanol-Water Mixtures Significantly Reduces Neural Electrode Impedance*, The Journal of Electrochemical Society 169 (2022) 022504.

   Conceptualization: VR, CR, BG, SB; Methodology: VR, BG, JJK, NS, VS; Formal analysis: VR, BG, SB; Investigation: VR, BG; Data curation: VR, BG; Original draft preparation: VR, BG; Review and editing: VR, CR, BG, JJK, SB; Visualization: VR, BG; Supervision: CR, SB; Funding acquisition: CR, SB.

3. **Vaijayanthi Ramesh**, Nadine Stratmann, Viktor Schaufler, Svilen D. Angelov, Ilona D Nordhorn, Hans E Heissler, Ricardo Martínez-Hincapié, Victor Čolić, Christoph Rehbock, Kerstin Schwabe, Uwe Karst, Joachim K. Krauss, and Stephan Barcikowski, *Mechanical Stability of Nano-Coatings on Clinically Applicable Electrodes, Generated by Electrophoretic Deposition*, Advanced Healthcare Materials (2022) 2102637.

   Conceptualization: VR, CR, SB; Methodology: VR, NS, VS, SDA, IDN, RMH; Formal analysis: VR, SB; Investigation: VR; Data curation: VR; Original draft preparation: VR; Review and editing: VR, CR, SDA, KS, RMH, VC, JJK, UK, SB; Visualization: VR; Supervision: CR, SB; Funding acquisition: CR, SB.

4. **Vaijayanthi Ramesh**, Christoph Rehbock and Stephan Barcikowski, *A State-of-the-Art Perspective on Neural Electrode Nano-Coatings*, under preparation.

   Conceptualization: VR, CR, SB; Methodology: VR; Formal analysis: VR, SB; Investigation: VR; Data curation: VR; Original draft preparation: VR; Review and editing: VR, CR, SB; Visualization: VR; Supervision: CR, SB; Funding acquisition: CR, SB.

5. **Vaijayanthi Ramesh**, Jacob Johny, Jurij Jakobi, Christoph Rehbock and Stephan Barcikowski, *Platinum-Iridium Alloy Nanoparticle Coatings Produced by Electrophoretic Deposition Reduce Impedance in 3D Neural Electrodes*, under submission.

   Conceptualization: VR, CR, SB; Methodology: VR, JaJ, JJ; Formal analysis: VR, SB; Investigation: VR; Data curation: VR; Original draft preparation: VR; Review and editing: VR, CR, SB; Visualization: VR; Supervision: CR, SB; Funding acquisition: CR, SB.

6. Svilen D. Angelov, Christoph Rehbock, **Vaijayanthi Ramesh**, Hans E. Heissler, Mesbah Alam, Stephan Barcikowski, Kerstin Schwabe, Joachim K. Krauss, *Coating of neural electrodes with platinum nanoparticles reduces and stabilizes impedance in vitro and in vivo in a rat model*, under review.

   Conceptualization: SDA, KS, JKK; Methodology: SDA, HEH, MA, VR; Formal analysis: KS, JKK; Investigation: SDA, KS; Data curation: SDA; Original draft preparation: KS; Review and editing: SDA, KS, JKK, VR, CR, SB; Visualization: KS; Supervision: KS, JKK; Funding acquisition: KS, JKK.

List of Student Works

The student works listed below was carried out in the context of the present thesis in the Institute of Technical Chemistry I at the University of Duisburg-Essen. The objective definition, planning, and conduction of experiments as well as the evaluation, interpretation, and visualization of the results took place under the scientific guidance of Vaijayanthi Ramesh. The results have been used in the following practical/bachelor/master theses.

1. Johannes Wolter, *Optimisation of electrophoretic deposition parameters: Effect of applied voltage and colloid solution*, Master Thesis (23.03. – 03.06.2020)
2. Anne Krause, Barbara Urbano and Mena-Alexander Kraeenbring, *Surface modification of implants and electrophoretic coating stability*, Master Project (11.05. – 21.08.2020)
3. Nadine Stratmann and Viktor Schaufler, *Elektrochemische Charakterisierung von elektrophoretisch beschichteten Platin-Iridium-Drähten*, Analytical Internship (28.04. – 09.06.2021)
4. Joman Barakeh, *Electrophoretic deposition of platinum alloy nanoparticles and their electrochemical characterization*, Bachelor Thesis (01.05. – 31.07.2021)

Declaration

I hereby declare that I am the sole author of this thesis and that I have not used any sources other than those listed in the bibliography and identified as references. All figures have been created exclusively for this work and do not violate any copyright provision. The results used in this thesis have been partly published in peer-reviewed journals as well as in bachelor and master theses of supervised students, as described in the previous sections.

I further declare that I have neither successfully nor unsuccessfully participated in any other doctoral program. Consequently, I have not submitted and will not submit this work in this form or in any similar form to other institutions.

I am aware that making any false declarations in this statement can cause me to be excluded from the doctoral proceedings or, at a later date, result in the termination of the proceedings or revocation of an already awarded doctoral degree.

Nuremberg, 02. Sep. 2023

_____

(Vaijayanthi Ramesh)